

DTIC FILE COPY

GL-TR-90-0067

ENVIRONMENTAL RESEARCH PAPERS, NO. 1059

AD-A223 568

PROCEEDINGS OF THE SEVENTEENTH ANNUAL GRAVITY
GRADIOMETER CONFERENCE
12-13 OCTOBER 1989

Editors:

CHRISTOPHER JEKELI

GERALD L. SHAW, Lt Col, USAF



28 March 1990



DTIC
ELECTE
JUL 05 1990
S E D

Approved for public release; distribution unlimited.

EARTH SCIENCES DIVISION
GEOPHYSICS LABORATORY

PROJECT 7600

HANSCOM AFB, MA 01731-5000

"This technical report has been reviewed and is approved for publication"



(Signature)

GERALD L. SHAW
Deputy Director

FOR THE COMMANDER



(Signature)

DONALD H. ECKHARDT
Division Director

This report has been reviewed by the ESD Public Affairs Office (PA) and is releasable to the National Technical Information Service (NTIS).

Qualified requestors may obtain additional copies from the Defense Technical Information Center. All others should apply to the National Technical Information Service.

If your address has changed, or if you wish to be removed from the mailing list, or if the addressee is no longer employed by your organization, please notify GL/IMA, Hanscom AFB, MA 01731. This will assist us in maintaining a current mailing list.

Do not return copies of this report unless contractual obligations or notices on a specific document requires that it be returned.

REPORT DOCUMENTATION PAGE			Form Approved OMB No. 0704-0188	
<small>Public reporting burden for this collection of information is estimated to average 1 hour per response, including the time for reviewing instructions, searching existing data sources, gathering and maintaining the data needed, and completing and reviewing the collection of information. Send comments regarding this burden estimate or any other aspect of this collection of information, including suggestions for reducing this burden, to Washington Headquarters Services, Directorate for Information Operations and Reports, 1215 Jefferson Davis Highway, Suite 1204, Arlington, VA 22202-4302, and to the Office of Management and Budget, Paperwork Reduction Project (0704-0188), Washington, DC 20503.</small>				
1. AGENCY USE ONLY (Leave blank)	2. REPORT DATE 28 March 1990	3. REPORT TYPE AND DATES COVERED Scientific Interim Mar 88 - Oct 89		
4. TITLE AND SUBTITLE Proceedings of the Seventeenth Annual Gravity Gradiometer Conference		5. FUNDING NUMBERS PE - 62101F PR - 7600 TA - 06 WU - 07		
6. AUTHOR(S) Edited by Christopher Jekeli Gerald L. Shaw, Lt Col, USAF				
7. PERFORMING ORGANIZATION NAME(S) AND ADDRESS(ES) Geophysics Laboratory (LWG) Hanscom AFB Massachusetts, MA 01731-5000		8. PERFORMING ORGANIZATION REPORT NUMBER GL-TR-90-0067 ERP, No. 1059		
9. SPONSORING / MONITORING AGENCY NAME(S) AND ADDRESS(ES)		10. SPONSORING / MONITORING AGENCY REPORT NUMBER		
11. SUPPLEMENTARY NOTES				
12a. DISTRIBUTION / AVAILABILITY STATEMENT Approved for Public Release; Distribution Unlimited		12b. DISTRIBUTION CODE y		
13. ABSTRACT (Maximum 200 words) Fourteen papers were presented at this conference, reviewing the status of terrestrial gravity gradiometers, applications of gravity gradiometry and cryogenic gradiometer technology. The status of the Gravity Gradiometer Survey System (GGSS) was reviewed and the future of gradiometry was projected in terms of instrumentation and applications. The technical papers covered test program results, applications to gravity field mapping, gravity signal processing, geophysical interpretation, space applications, inertial navigation aiding, new instrumentation and application to strategic arms reduction treaty verification. This report consists of viewgraphs of the presentations. Keywords;				
14. SUBJECT TERMS Gravity Gradiometry Navigation, Gravity Mapping;		> Superconducting Gradiometers; Cryogenic Inertial Instruments, (EDC)		15. NUMBER OF PAGES 314
				16. PRICE CODE
17. SECURITY CLASSIFICATION OF REPORT UNCLASSIFIED	18. SECURITY CLASSIFICATION OF THIS PAGE UNCLASSIFIED	19. SECURITY CLASSIFICATION OF ABSTRACT UNCLASSIFIED	20. LIMITATION OF ABSTRACT SAR	

17th GRAVITY GRADIOMETRY CONFERENCE

12-13 October 1989

Sponsored By:

Geophysics Laboratory
Earth Sciences Division

Accession For	
NTIS GRA&I	<input checked="" type="checkbox"/>
DTIC TAB	<input type="checkbox"/>
Unannounced	<input type="checkbox"/>
Justification	
By	
Distribution/	
Availability Codes	
Dist	Avail and/or Special
A-1	

ABOUT THE GRAVITY GRADIOMETRY CONFERENCE.....

The First Gravity Gradiometry Conference was held at the Air Force Cambridge Research Laboratory (AFCRL, now GL) in 1973. Its purpose was to provide a forum to evaluate and compare the efforts of three vendors (Charles Stark Draper Lab, Hughes Research Lab and Bell Aerospace Textron) in still-emerging areas of gravity gradiometry. About 15 people attended, most of them from the companies mentioned above or the Terrestrial Sciences Division at AFCRL. In contrast, the 1988 Conference had a guest list of 60 plus attendees, with participation from academia (foreign and domestic), private industry and Government. The papers presented were not restricted to gradiometry alone. Indeed, the scope of this annual event has broadened considerably since 1973.

In 1988, a major milestone was achieved with the delivery of the Gravity Gradiometer Survey System (GGSS) to DMA. This one-of-a-kind moving base gravity gradiometer was manufactured for DMA by Bell Aerospace Textron of Buffalo, NY under GL management.

The Geodesy and Gravity Branch of the Earth Sciences Division of the Geophysics Laboratory, Hanscom AFB, Massachusetts, has always organized the Conference. With the exception of the first two conferences, all the others had been held at the US Air Force Academy in Colorado Springs, Colorado. In 1989, however, the 17th conference returned to Hanscom AFB at the recently completed GL Science Center. This conference reviewed the status of the GGSS and projected the future of gradiometry in terms of instrumentation and applications. Technical papers covered test program results, applications to gravity field mapping, gravity signal processing geophysical interpretation, space applications, inertial navigation aiding, new instrumentation and application to strategic arms reduction treaty verification.

If you are not already on our mailing list and would like to attend future conferences, or if you have any questions, please write to:

GL/LWG
Hanscom AFB, MA 01731-5000
USA

Copies of conference proceedings for prior years are not available. Also, we appreciate any comments or suggestions you may have regarding this document.

17th GRAVITY GRADIOMETRY CONFERENCE

12-13 October 1989

Sponsored By:

Geophysics Laboratory
Earth Sciences Division

ACKNOWLEDGEMENTS

We'd like to recognize the efforts of some outstanding individuals without whose hard work the Conference could not have been a success.

First of all we thank Ms Joan Beaulieu, Nancy Fleming, Joanne Michael and Jo Ann Patti, who did a superb job handling the registration and administrative job of keeping the conference running smoothly.

Many thanks go out to Mr Bob Ziegler at DMA, Mr Albert Jircitano and Mr Bryant Everard of Bell Aerospace Textron and Mr Maurice Aubrey and Ms Suzanne Banacos at Geophysics Laboratory Support Services Division, whose collective diligence and determination on short notice made possible the GGSS presence at the Conference. Also, SMSgt Roger Sands and Mr Anestis Romaides of the Geophysics Laboratory's Earth Sciences Division, who orchestrated the delicate off loading - storage - and on loading of the GGSS at Hanscom. And finally, M. Neil Stark for providing a safe haven for the GGSS in the high bay.

Next, we thank all the speakers for taking the time to compile and present their papers for the benefit of the Conference attendees. As in the past, the broad mix and high quality of topics went a long way towards making the Conference a stimulating scientific forum.

Finally, we thank Colonel Robert J. Hovde, Commander, GL, Dr Donald H. Eckhardt, Director, Earth Sciences Division and Dr Thomas P. Rooney, Chief, Geodesy and Gravity Branch, without whose continued support and guidance this Conference could not have been held.

The 17th Gravity Gradiometer Conference
12-13 October 1989
Attendees

Clive Affleck
Bell Aerospace Textron
Post Office Box One
Buffalo, New York 14240

Mario Cosmo
Smithsonian Astrophysical Observatory
60 Garden Street, M/S 59
Cambridge, MA 02138

Ronald Beard
Naval Research Laboratory
Space Systems Technology Dept.
Space Applications Branch, (Code 8320)
4555 Overlook Avenue, S.W.
Washington, DC 20375-5000

Donald Eckhardt
Geophysics Laboratory
Earth Sciences Division
Hanscom AFB, MA 01731-5000

Don Benson
Dynamics Research Corp.
60 Frontage Road
Andover, MA 01810

Cyril Edwards
Physics Department
The Univ of Western Australia
Nedlands
Western, Australia 6009

Srinivas V. Bettadpur
Center for Space Research
Dept of Aerospace Engineering
University of Texas at Austin
Austin, TX 78712

Fannie Gee
OSWR
c/o Jack Neilson
P.O. Box 1925
Washington, DC 20505

Carl Bowin
Dept of Geology and Geophysics
Woods Hole Oceanographic Institution
Woods Hole, MA 02543

David Gleason
Geophysics Laboratory
Earth Sciences Division
Hanscom AFB, MA 01731-5000

Paul Branagan
CER Corporation
950 Grier Drive
Las Vegas, NV 89119

Jake Goldstein
TASC
55 Walkers Brook Drive
Reading, MA 01867

Edgar Canavan
Department of Physics and Astronomy
University of Maryland
College Park, MD 20742

Luke Gournay
HY-Tech Services Inc
P.O. Box 1145
Granbury, TX 76048

Oscar Colombo
University of Maryland
Astronomy Program
NASA Goddard SFC, Code 626
Greenbelt, MD 20904

John Graham
DMA Systems Center
3200 South Second Street
St. Louis, MO 63118-3399

Andrew Grierson
Bell Aerospace Textron
Post Office Box One
Buffalo, New York 14240

J. C. Harrison
Geodynamics Corporation
5520 Ekwill St., Suite A
Santa Barbara, CA 93111

Warren Heller
The Analytic Science Corportaion (TASC)
55 Walkers Brook Drive
Reading, MA 01867

Boyd Holsapple
USAF
WRDC/AAAN-1
Wright-Patterson AFB, OH 45433-6543

J. R. Huddle
Litton Guidance & Control Systems
5500 Canoga Avenue
MS 67/35
Woodland Hills, CA 91367-6698

James Impastato
Rockwell International
Space Transportation Systems Division
12214 Lakewood Blvd.
Downey, CA 90241

Barry Irwin
U.S.G.S.
Quissett Campus
Woods Hole, MA 02543

Christopher Jekeli
Geophysics Laboratory
Earth Sciences Division
Hanscom AFB, MA 01731

Albert Jircitano
Bell Aerospace Textron
Post Office Box One
Buffalo, New York 14240

J. Edward Jones
HQ AFIA/INTB
Bldg 5681
Bolling AFB, DC 20332-5000

Seymor Kant
NASA/Goddard Space Flight Center
Code 701
Greenbelt, MD 20771

Jerry Kisabeth
4457 RDW
Exploration Research and Services
Conoco, Inc.
1000 Pine
Ponca City, OK 74603

Stepehn Lichten
Jet Propulsion Lab
M/S 238/640
4800 Oak Grove Drive
Pasadena, CA 91109

Enrico Lorenzini
Smithsonian Astrophysical Observatory
60 Garden St., M/S 59
Cambridge, MA 02138

John Lundberg
Center for Space Research
Dept of Aerospace Engineering
The University of Texas
Austin, TX 78712

Andre Mainville
Geodetic Survey of Canada
615 Booth Street
Ottawa, Ontario
CANADA K1A 0E9

Charles Martin
University of Research Foundation
6411 Ivy Lane
Greenbelt, MD 20770

Alan Rufty
NSWC/DL
Code K41
Dahlgren, Virginia 22448-5000

James Matthews
Raytheon Company, Box 1K9
528 Boston Post Road
Sudbury, MA 01776

Lt Col Gerald Shaw
Geophysics Laboratory
Earth Sciences Division
Hanscom AFB, MA 01731-5000

Jim McCullough
U.S.G.S.
Woods Hole, MA 02543

Richard Shi
McDonnell Douglas Space Systems
5301 Bolsa Avenue
Huntington Beach, CA 92647

M. Vol Moody
Department of Physics and Astronomy
University of Maryland
College Park, MD 20742

David Sonnabend
CALTECH/JPL
MS 301-125J
4800 Oak Grove Road
Pasadena, CA 91109

Ho Jung Paik
Department of Physics and Astronomy
University of Maryland
College Park, MD 20742

Charles Taylor
Geophysics Laboratory
Earth Sciences Division
Hanscom AFB, MA 01731-5000

John Parmentola
Center for Science and International
Affairs
John F. Kennedy School of Government
74 JFK Street
Harvard University
Cambridge, MA 02138

Milton Trageser
9 North Gateway
Winchester, MA 01890

George Priovolos
Mayflower Communications Company, Inc.
80 Main Street
Reading, MA 01867

Peter Ugincius
Code K-405
NSWC
Dahlgren, VA 22448

Anestis Romaides
Geophysics Laboratory
Earth Sciences Division
Hanscom AFB, MA 01731-5000

Jerome Vetter
Applied Physics Laboratory
John Hopkins Road
Laurel, MD 20707

Thomas Rooney
Geophysics Laboratory
Earth Sciences Division
Hanscom AFB, MA 01731-5000

J. V. White
TASC
55 Walkers Brook Drive
Reading, MA 01867

Leonard Wilk
C.S. Draper Labs, Inc.
555 Technology Square, M/S 6E
Cambridge, MA 02139

Richard Wold
GWR Instruments
11404 Sorronto Valley Road
Suite 117
San Diego, CA 92121

Alan Zorn
Dynamics Research Corporation
60 Frontage Road
Andover, MA 01810

Paul Zucker
Johns Hopkins Applied Physics Laboratory
Johns Hopkins Road
Laurel, MD 20707

Andrew Lazarewicz
Geo-Centers, Inc.
7 Wells Avenue
Newton Centre, MA 02159

Tom Taylor
TASC
55 Walkers Brook Drive
Reading, MA 01867

Don Vasco
CCS
Earth Sciences Division/Bldg 50E
Lawrence Berkeley Lab
1 Cyclotron Road
Berkeley, CA 94720

4. Srinivas Bettadpur, Bob Schuz, and John Lundberg (University of Texas at Austin): "Results on the Estimation of Geopotential Coefficients from a Simulation of a Satellite Gravity Gradiometer Mission"
5. Oscar Colombo (NASA Goddard SFC): "The Use of Gradiometers in Space to Monitor Changes in the Earth's Gravity Field"

FRIDAY, 13 October 1989

8:30 - 12:00 Session III: CRYOGENIC GRADIOMETER TECHNOLOGY
Chairman: Lt Col Gerry Shaw
Geophysics Laboratory (ASFC)

1. Don Vasco and Charles Taylor (Geophysics Laboratory): "Inversion of Airborne Gravity Gradient Data, South-Western Oklahoma"
2. F.J. VanKann, M.J. Buckingham, M.H. Dransfield, A.G. Mann, P.J. Turner, R.D. Penny, and Cyril Edwards: "Development of a Mobile Gravity Gradiometer for Geophysical Exploration"
3. M. Vol Moody, Q. Kong, and H.J. Paik (University of Maryland): "The Development of the Model III Superconducting Gravity Gradiometer"

BREAK

4. Edgar Canavan, H.J. Paik, and J.W. Parke (University of Maryland): "Development of a Superconducting Six-Axis Accelerometer"
5. Ho Jung Paik (University of Maryland): "Superconducting Gravity Gradiometer Mission - An Overview"

ADJOURN

ABSTRACT

By

ANDREW D. GRIERSON

BELL AEROSPACE TEXTRON
Division of Textron, Inc.
P.O. Box One
Buffalo, New York 14240-0001

GGSS RAIL GARRISON AND VAN SURVEY EXPERIENCE

Operational problems are described with observations and results relating to the acceleration environment on the rail car. Techniques used to identify and compensate for sensitivities are covered. Survey results are presented.

**GGSS RAIL GARRISON AND WNY
ROAD SURVEY EXPERIENCE**

**CLIVE AFFLECK
ANDY GRIERSON**

OCTOBER 12, 1989

GRAVITY GRADIOMETER SURVEY SYSTEM (GGSS)

- SYSTEM DEVELOPMENT WAS INITIATED IN 1983 FOR THE DMA THROUGH AFGL WITH THE OBJECTIVE OF SURVEYING ON THE LAND AND IN THE AIR FOR THE GRAVITY DISTURBANCE VECTOR TO AN ACCURACY OF 1MGAL.
- LAND VEHICLE TESTS WERE CONDUCTED ON ROADS IN WY AND OKLAHOMA IN 1986 AND 1987 AND MORE RECENTLY IN 1989.
- AIRBORNE TESTS WERE CONDUCTED IN OKLAHOMA IN 1987.
- RAILROAD TESTS FOR THE RAIL GARRISON APPLICATION WERE RUN IN 1988/1989.

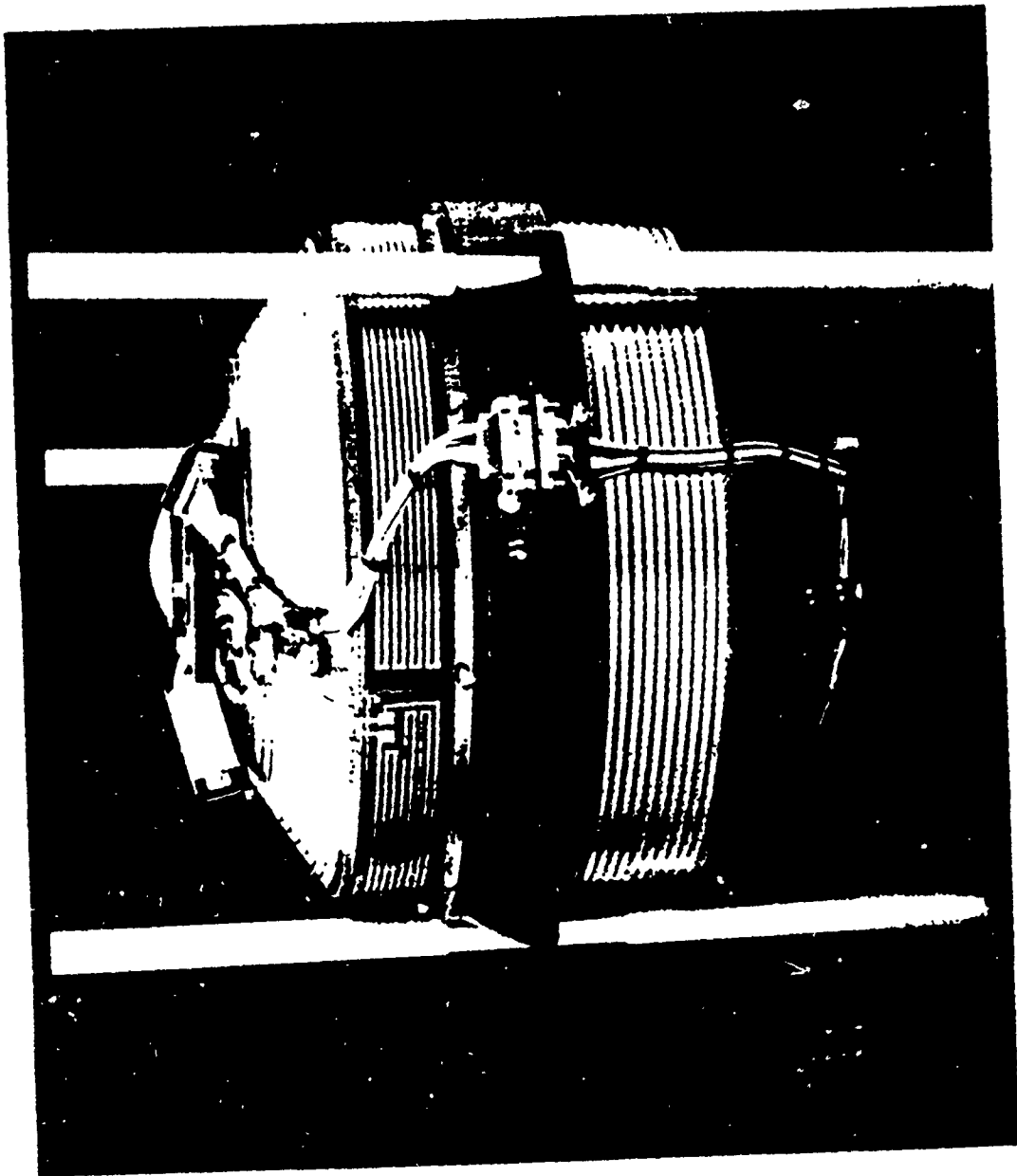
GRAVITY SENSOR SYSTEMS (GSS)

- 9 OPERATIONAL SYSTEMS BUILT.
- 64 GRADIOMETERS BUILT.
- SYSTEMS OPERATING SUCCESSFULLY ABOARD.
 - USNS VANGUARD (NTV)
 - USNS TENNESSEE
 - USNS PENNSYLVANIA

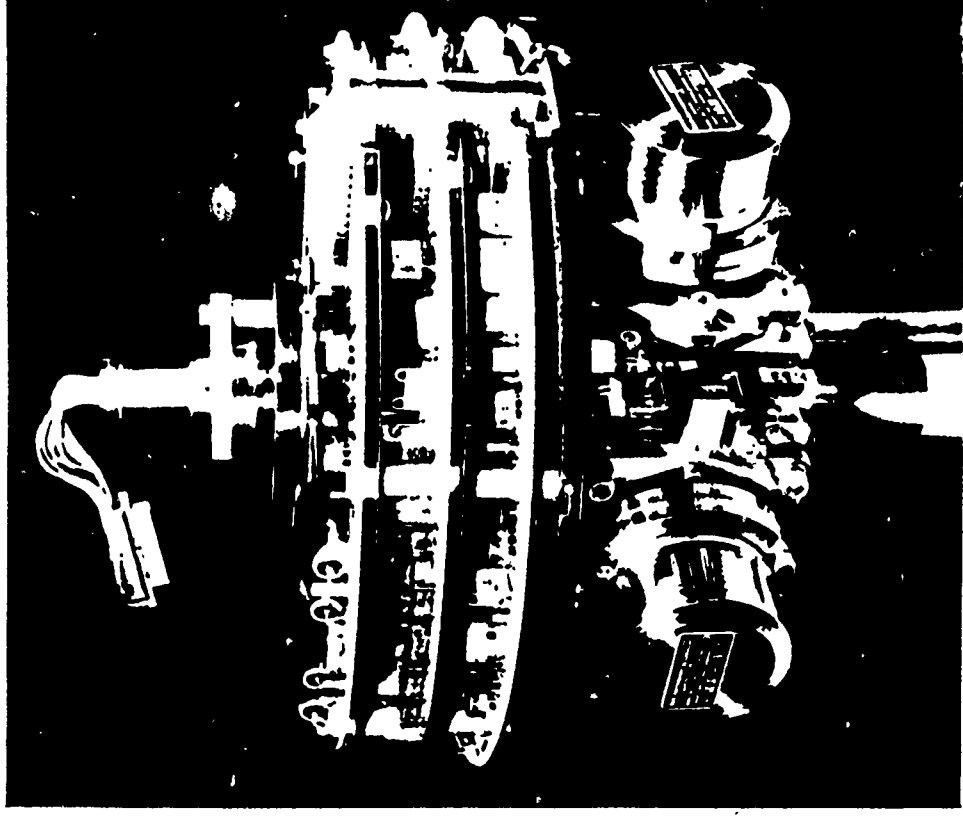
GGSS EQUIPMENT SUMMARY DESCRIPTION

- MODIFIED VERSION OF THE TRIDENT II ADM SYSTEM.
- GPS RECEIVER FOR AIRBORNE NAVIGATION AND A 5TH WHEEL FOR ROAD NAVIGATION.
- POWER SUPPLIES AND VAN AIR-CONDITIONING.
- AIRBORNE COMPUTER
- KEY COMPONENT: BELL ROTATING ACCELEROMETER GRAVITY
GRADIOMETER INSTRUMENT (GGI).

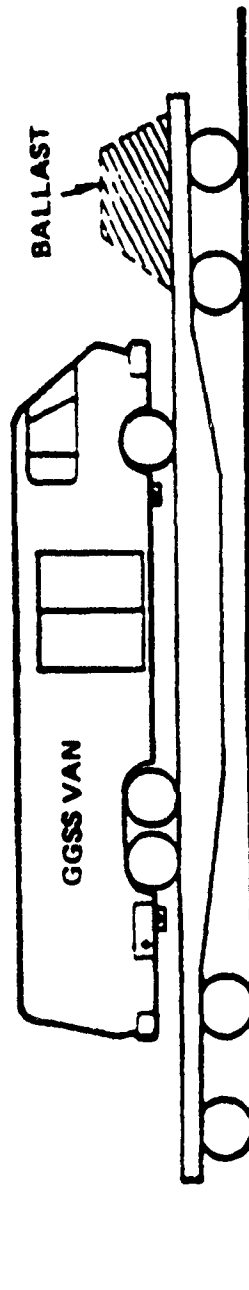
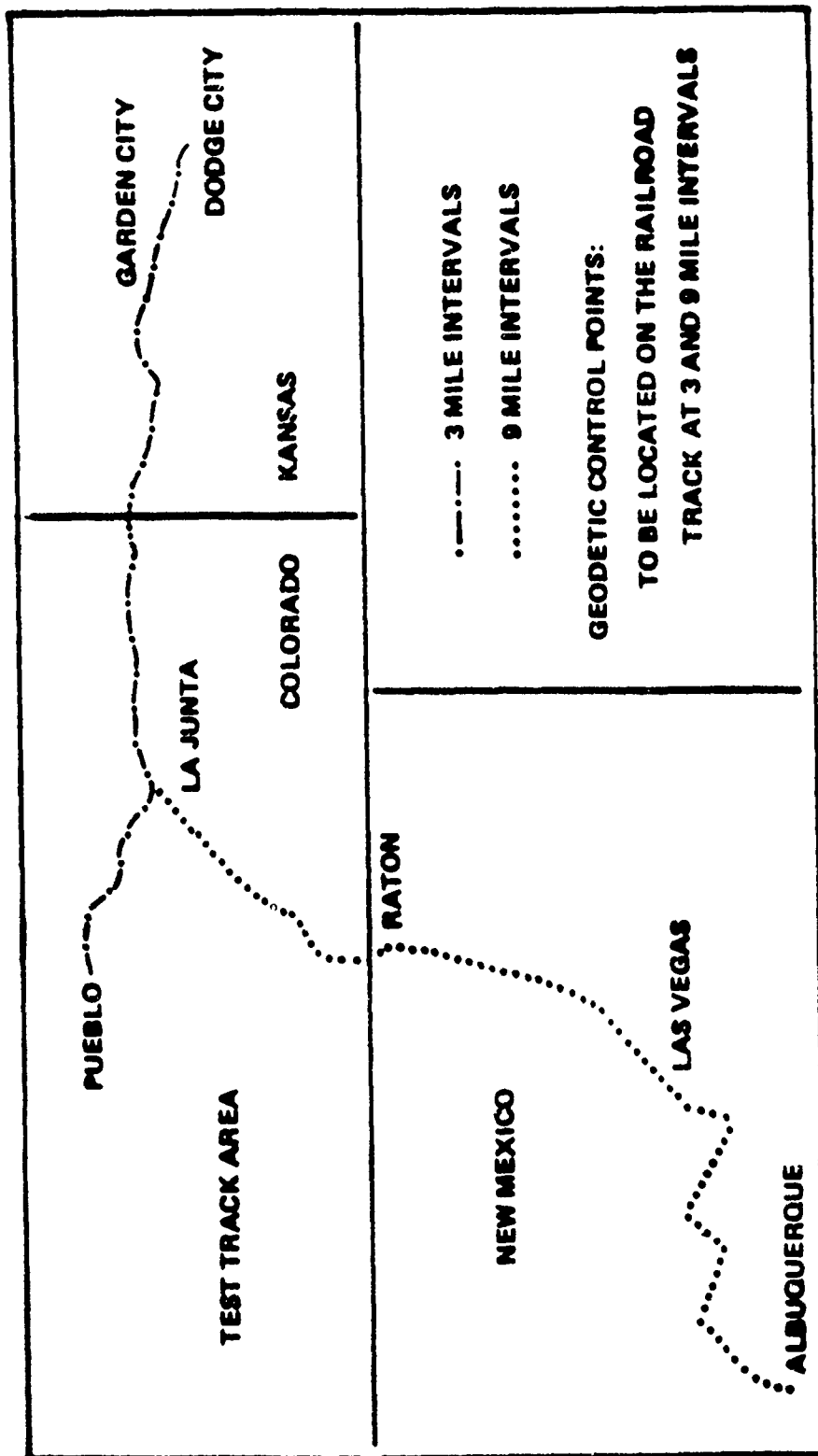
Bell Gravity Gradient Instrument (GGI) Assembly



Bell Gravity Gradient Instrument (GGI) Accelerometers and Electronics (Uncovered)



BMO/DMA Rail Garrison Test



SYSTEM CONFIGURATION CHANGES
FOR RAIL GARRISON SURVEY

- GRADIOMETER INSTRUMENTS (GGI) CHANGED TO TRIDENT II ADM UNITS.
- GGI OPERATING ROTATION SPEED CHANGED FROM 1/4 Hz TO 1/8 Hz.
- PLATFORM CONTROL MODE CHANGED FROM NED TO CONSTANT CAROUSEL AT 500°/HR.
- HIGHER DATA RATE ACCELERATION RECORDING IMPLEMENTED (FROM 16 PER SEC TO 126 PER SEC).
- A SECOND PLATFORM VIBRATION ISOLATION SYSTEM ADDED.
- MECHANISM IMPLEMENTED TO FACILITATE A TEST SHAKING OF THE VAN BOTH HORIZONTALLY AND VERTICALLY FOR CALIBRATION PURPOSES.
- 5TH WHEEL ODOMETER TAKEOFF ON RAIL CAR WHEEL.
- DIGITRAC SYSTEM FOR "FLYING" UPDATES FROM KFP'S ALONG TRACKS.

GRADIOMETER INSTRUMENT CHANGE

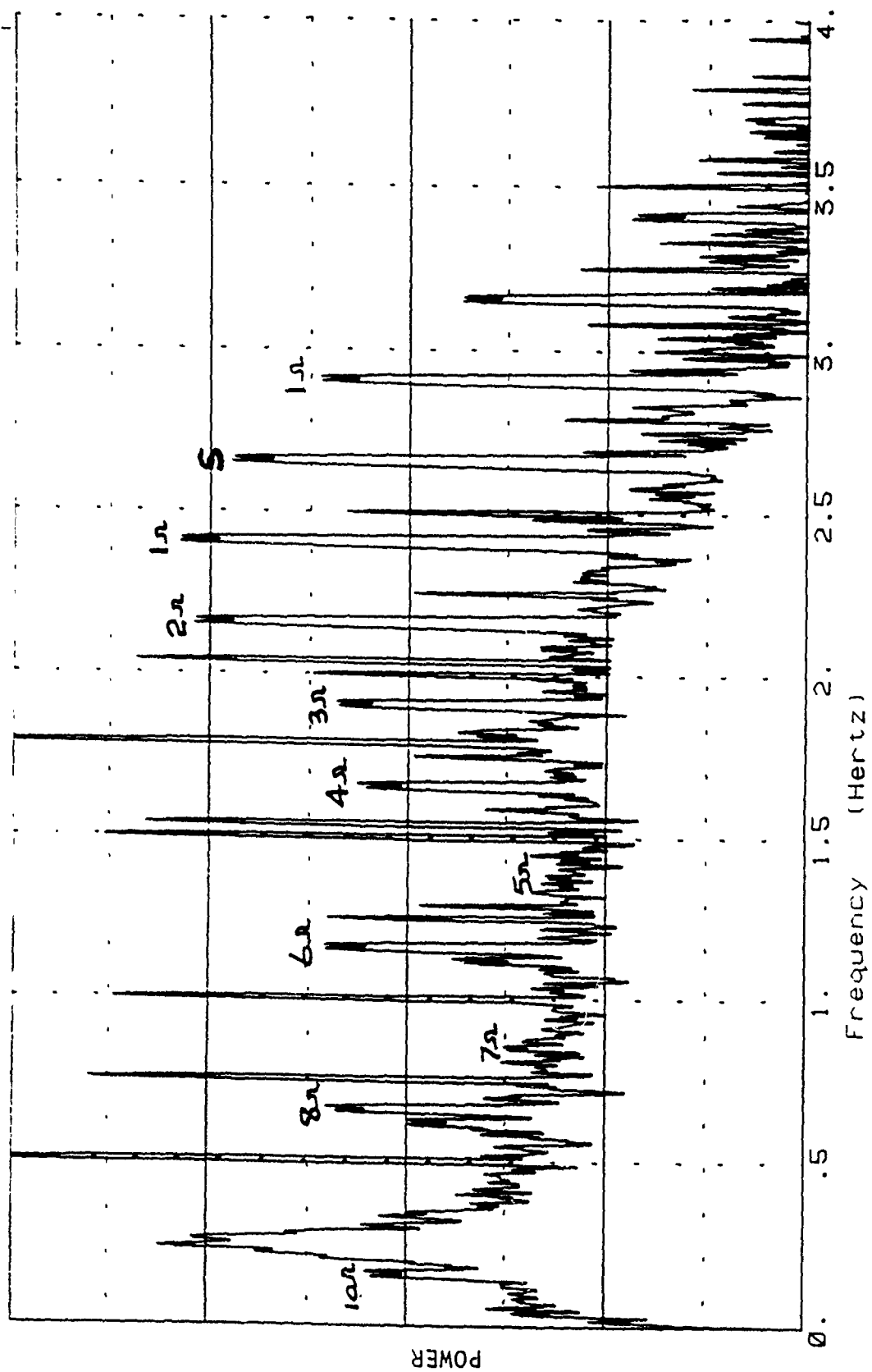
- GGI "RMS ACCELERATION SENSITIVITY" DETERMINED AND TESTS ON AVAILABLE INSTRUMENT ASSETS INDICATED THAT THREE ADM GGIs HAD THE LOWEST SENSITIVITY.

GGI "RMS ACCELERATION SENSITIVITY"

- GGI's EXHIBIT A SENSITIVITY TO LINEAR ACCELERATIONS AT FREQUENCIES NOT SYNCHRONOUSLY RELATED TO SPIN RATE.
- TESTS INDICATE THAT THIS SENSITIVITY HAS A PREDOMINATELY LINEAR RELATIONSHIP TO INPUT AMPLITUDE, AND IS INDEPENDENT OF FREQUENCY OVER THE TESTED RANGE 2 TO 8 Hz.
- IN RAIL AND ROAD ENVIRONMENTS THIS SENSITIVITY HAS TO BE COMPENSATED IN POST MISSION DATA ANALYSIS.
- AT THIS TIME NO DEVELOPMENT WORK HAS BEEN CONDUCTED TO ISOLATE THE CAUSE AND MINIMIZE THE SENSITIVITY IN THE GGI ITSELF.

GGI ROTATION RATE CHANGE

- VAN VERTICAL SHAKE TESTS SHOWED THAT THE GGI BANDPASS AMPLIFIER OUTPUT CONTAINED A HARMONIC STRING OF MODULATION OF THE SHAKE FREQUENCY AT HARMONICS OF SPIN RATE.
- A SIGNIFICANT REDUCTION IN THE POWER OF THE HARMONIC MODULATION APPEARING AT OR NEAR THE GRADIOMETER SIGNAL FREQUENCY IS REDUCED BY LOWERING THE SPIN RATE.



GGI 2 SHAKE 24 JUNE 88

PLATFORM CONTROL MODE CHANGE

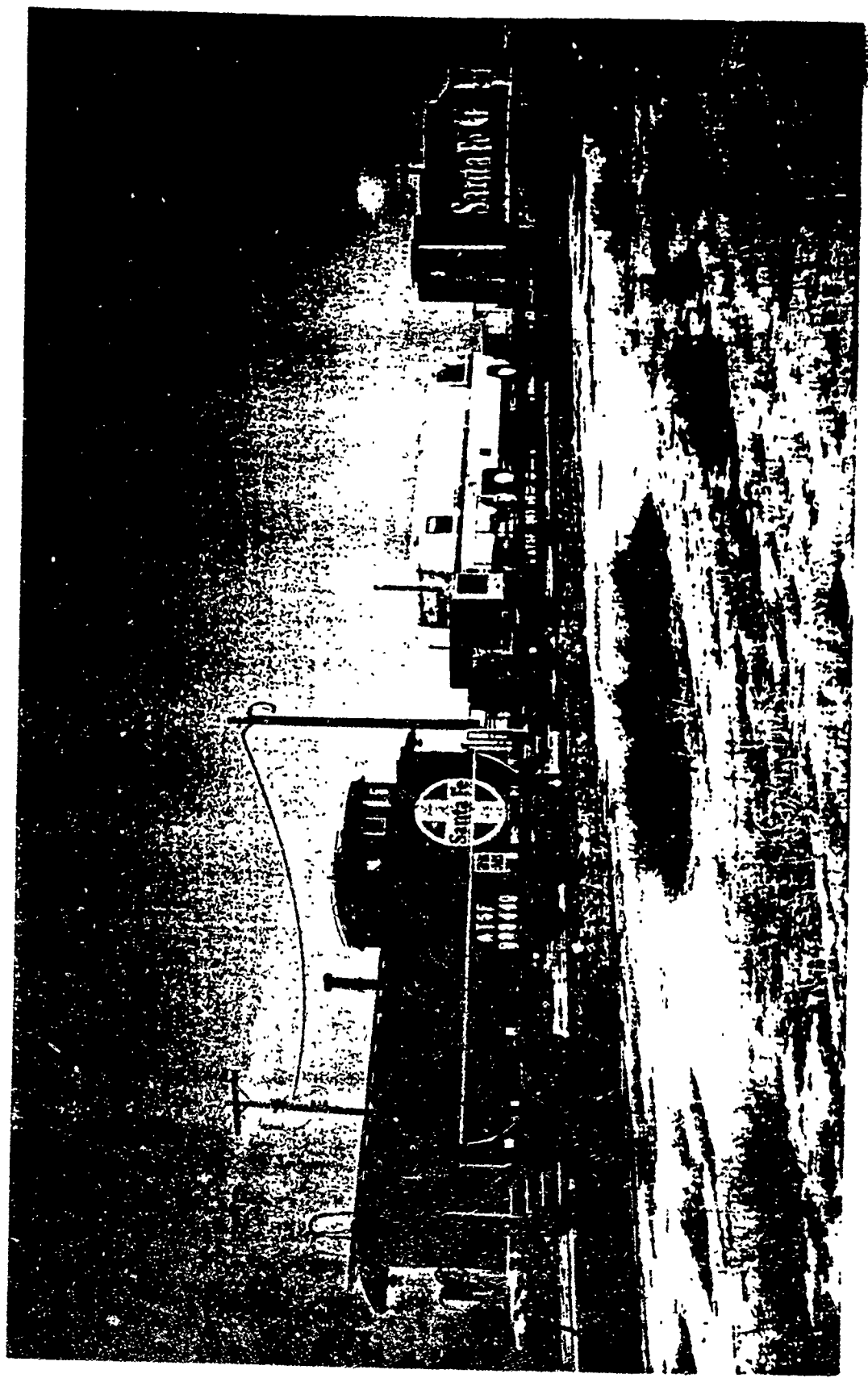
BENEFITS OF CAROUSELLING

- ABILITY TO EXTRACT MOST GGI BIASES - BIAS CAN BE EXTRACTED WHEN STATIONARY AT ANY POINT IN THE SURVEY.
- AUTOMATICALLY CALIBRATES GYRO BIASES.
- PERMITS SYSTEM HEALTH TO BE ASSESSED BY GGI COMPARISON WHEN STATIONARY.
- PROVIDES AN AVERAGING ACTION ON ANY LOCAL THERMAL GRADIENTS.

DISADVANTAGES

- MAKES INTERPRETATION OF QUICK LOOK DATA MORE DIFFICULT.

Rail Garrison Train

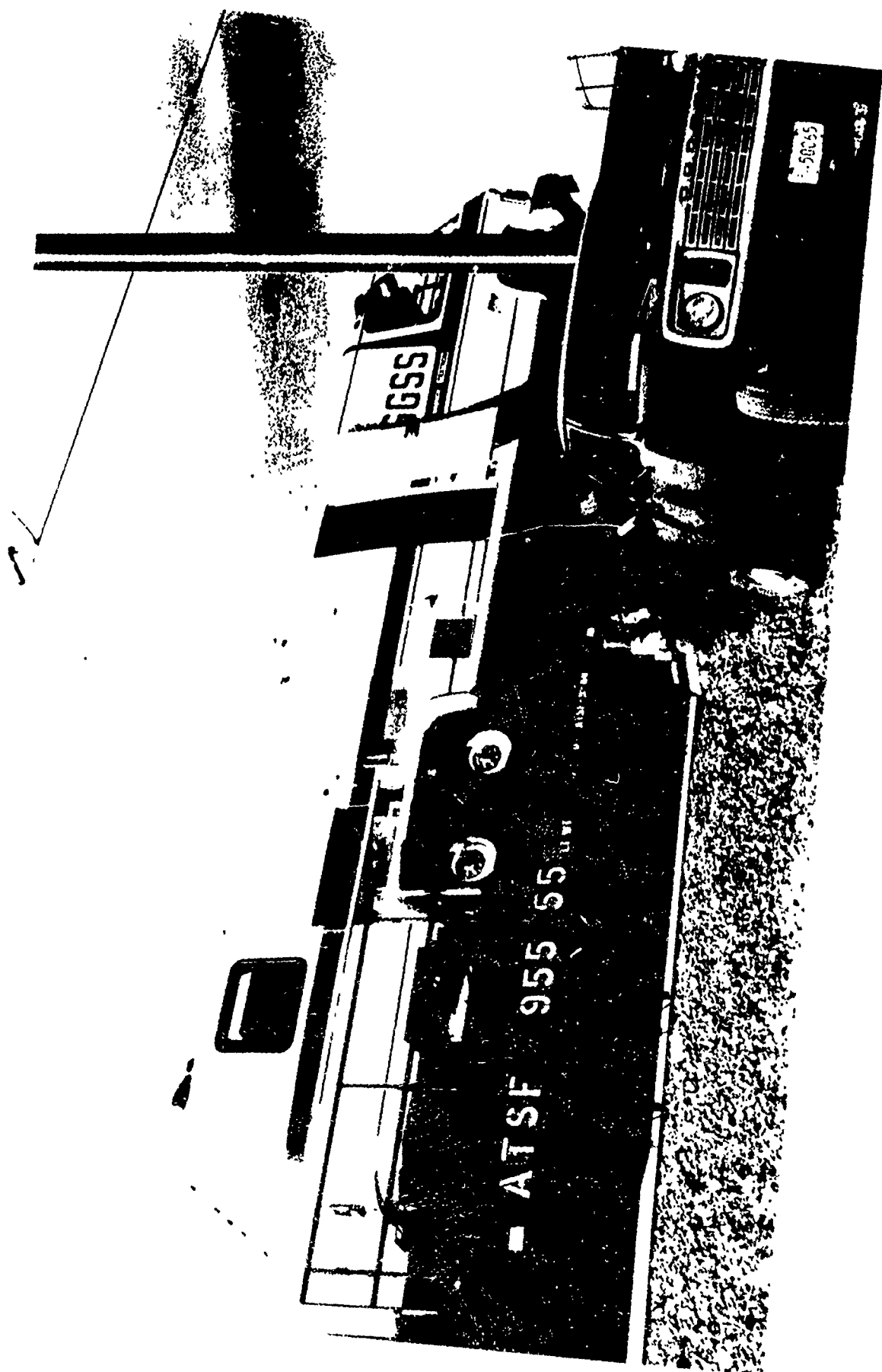


EXPERIENCE IN THE CONDUCT OF THE RAIL GARRISON DEMO

- THE ACCELERATION ENVIRONMENT WAS SIGNIFICANTLY MORE SEVERE THAN EXPECTED -- FLAT BED RAIL CAR WAS NOT AN APPROPRIATE CHOICE.
- PART WAY THROUGH SURVEY SYSTEM MODIFICATIONS WERE IMPLEMENTED TO REDUCE ACCELERATION LEVELS SEEN BY GGIs.
 - IMPROVED VAN TO RAIL CAR HOLD DOWN.
 - ADDITION OF DAMPERS TO PLATFORM VIBRATION ISOLATION SYSTEM.

	PRE MOD.	AFTER MOD.
PEAK G LEVEL	1.0	0.5
RMS G LEVEL	>100MG	60 TO 70MG

- PLANS FOR SELF GRADIENT CALIBRATION WERE THWARTED BY THE RAIL CAR DERAILING ON THE 600 FT. DIA. RAIL LOOP IN THE TEST AREA.



SYSTEM DEFICIENCIES IDENTIFIED AFTER RAIL GARRISON DEMO

- ANGULAR JITTER RATES WERE BEING IMPOSED ON THE PLATFORM
 - GROUND CONNECTION LOST CAUSING HIGH FREQUENCY NOISE IN STABILIZATION LOOPS.
 - BEAT FREQUENCY PROBLEM BETWEEN HARMONICS OF THE PLATFORM ACCELEROMETERS AND GYRO EXCITATION FREQUENCIES.
 - LESS THAN ADEQUATE FILTERING OF THE HIGHER FREQUENCIES IN THE STABILIZATION LOOPS.
- INSUFFICIENT GAIN IN THE PLATFORM STABILIZATION LOOPS TO ADEQUATELY REJECT IMPOSED ANGULAR RATES IN THE RAIL CAR ENVIRONMENT.
- CORRECTIVE ACTION TAKEN PRIOR TO TEST RUNS IN WNY.

GGSS DATA REDUCTION TECHNIQUES AND RESULTS

- STAGE 1 DATA REDUCTION TO COMPENSATE GRADIENT DATA FOR ALL ENVIRONMENTALLY INDUCED ERRORS.
- STAGE 2 DATA REDUCTION TO COMPUTE THE GRAVITY DISTURBANCE VECTOR FROM THE STAGE 1 DATA.

ABSTRACT

By

ANDREW D. GRIERSON

BELL AEROSPACE TEXTRON
Division of Textron, Inc.
P.O. Box One
Buffalo, New York 14240-0001

GRAVITY GRADIOMETER SURVEY SYSTEM

STAGE I DATA REDUCTION

Suppression of motion-induced signals and errors is vital to the measurement of gravity gradient signals on a moving vehicle. Post-mission processing of data from the Bell Gravity Gradiometer Survey System (GGSS) uses intrinsic features of the system design to accomplish this.

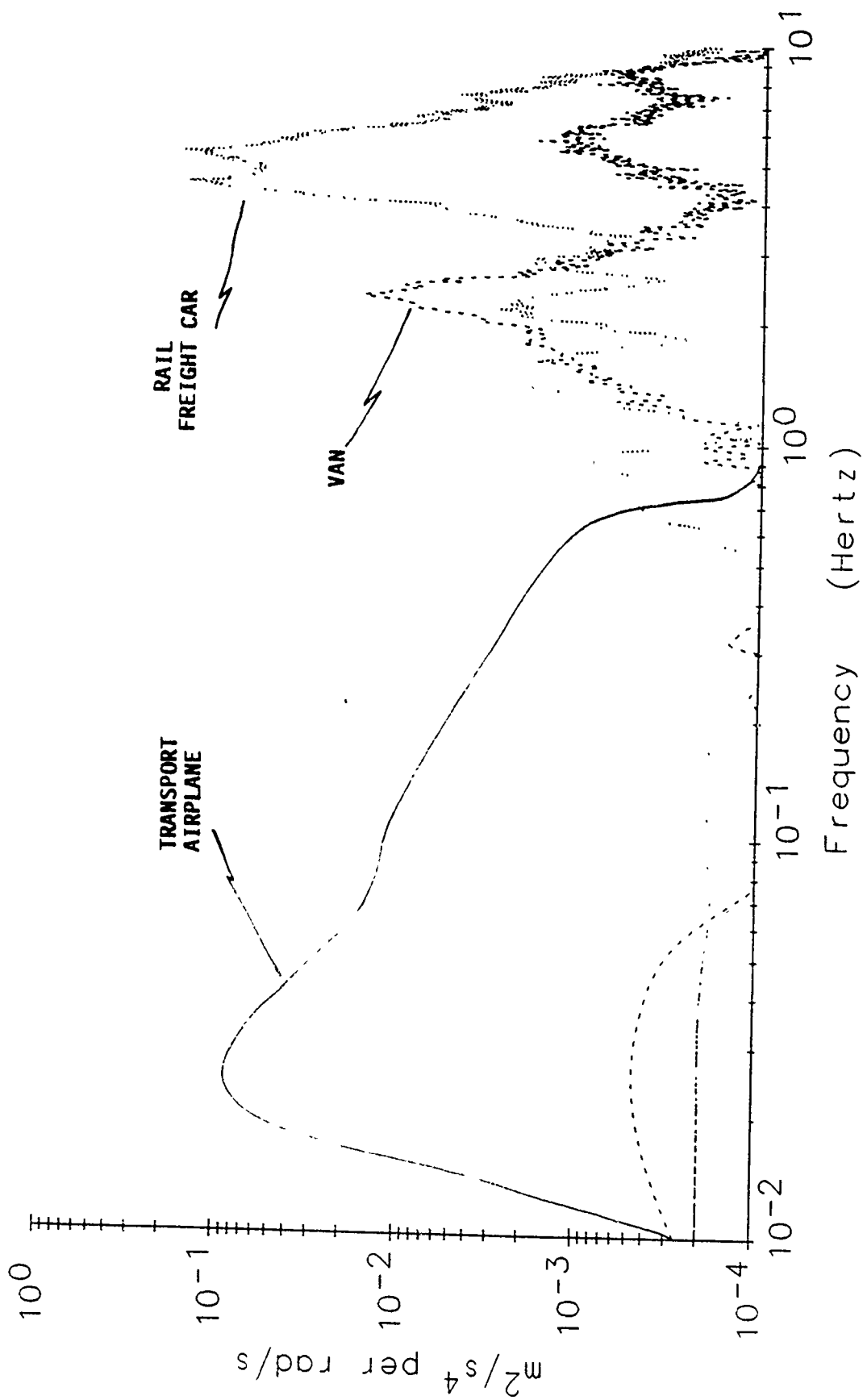
GGSS mounted on a railroad freight car experienced a high vibration environment. Post-mission compensation of the recorded data has removed much of the sensitivity to this environment.

Improvements in platform control resulted from experiences in railroad operation. Subsequent road trials have demonstrated the ability to measure gradients of local topographic features.

POST-MISSION GRADIENT EXTRACTION

MAINLY CONCERNED WITH REMOVAL OF ENVIRONMENTAL EFFECTS.

- DECODE, EDIT AND SYNCHRONIZE RAW DATA.
- COMPENSATE FOR CENTRIPETAL EFFECTS.
USE GYRO RATES AND NAVIGATION PARAMETERS.
- COMPENSATE FOR SELF-GRADIENTS.
USE VEHICLE ATTITUDE WITH RESPECT TO PLATFORM.
- COMPENSATE FOR ACCELERATION.
CORRELATE PRODUCTS OF ACCELERATIONS MEASURED ON PLATFORM
WITH INSTRUMENT OUTPUTS.
- REMOVE YAW-DEPENDENT BIAS.
USE PLATFORM ANGLE WITH RESPECT TO VEHICLE.
- DEMODULATE SYNCHRONOUSLY.
USE INSTRUMENT WHEEL ROTATION ANGLE.
- LOW FREQUENCY CONTROL.
USE CAROUSEL ANGLE WITH RESPECT TO NORTH.



VERTICAL ACCELERATION POWER SPECTRA
ROAD, RAIL AND AIR

MODIFIED PROCESSING FOR RAIL SURVEY

- HIGHER SAMPLE RATE, WIDER BANDWIDTH ACCELERATION PROCESSING.
- ALTERED MODULATION BANDS AND SIDELobe OVERLAP BECAUSE OF WHEEL RATE CHANGE.
- DIFFERENT BANDWIDTH USED IN IDENTIFICATION OF ACCELERATION SENSITIVITY DYNAMICS.
- ADDITIONAL HIGH FREQUENCY NOISE CONTROL.
- CALIBRATION OF HIGH RANK TENSOR BIAS AS A FUNCTION OF YAW.
- CALIBRATION OF DOMINANT SENSITIVITIES TO RATES OF CHANGE OF ACCELERATION AND PRODUCTS.
- RED NOISE CONTROL USING CAROUSELLING.

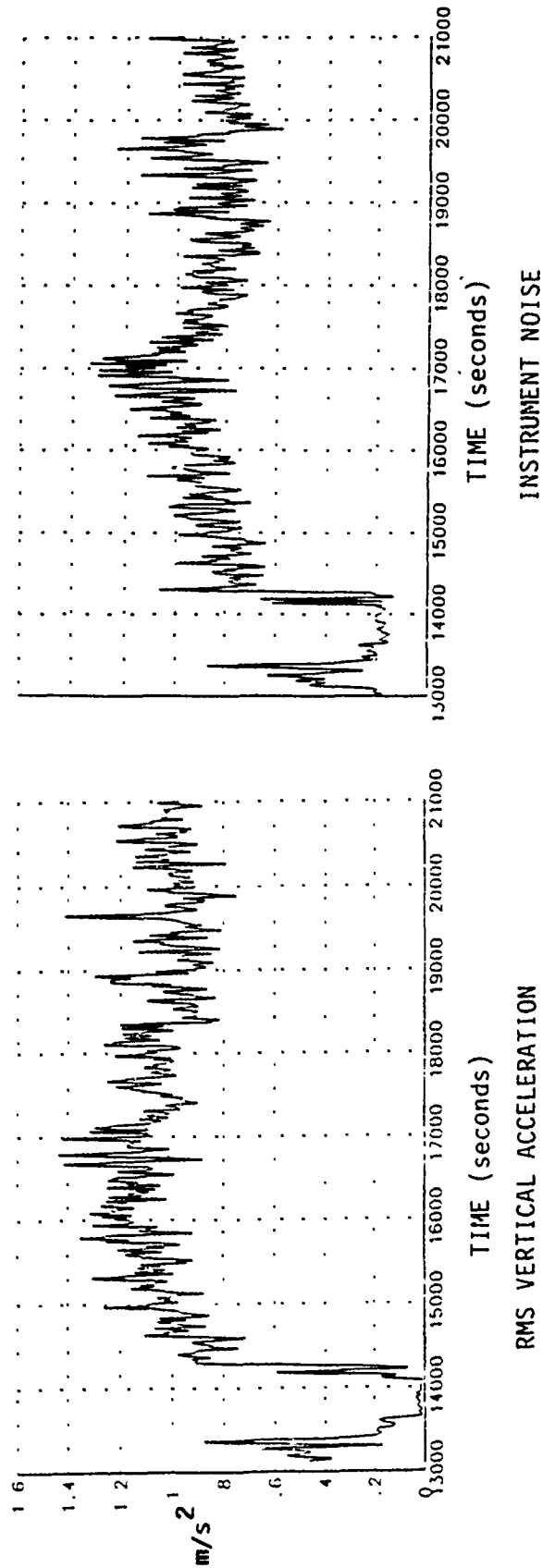
ROTATION

- THE ROTATING ACCELEROMETER DESIGN MOVES MANY ACCELEROMETER AND MOUNTING ERRORS TO FREQUENCY BANDS SEPARATE FROM GRADIENTS.

BESIDES NATURALLY REDUCING THE EFFECTS OF THESE ERRORS, THIS ALSO FACILITATES CALIBRATION OF THE RESIDUES.

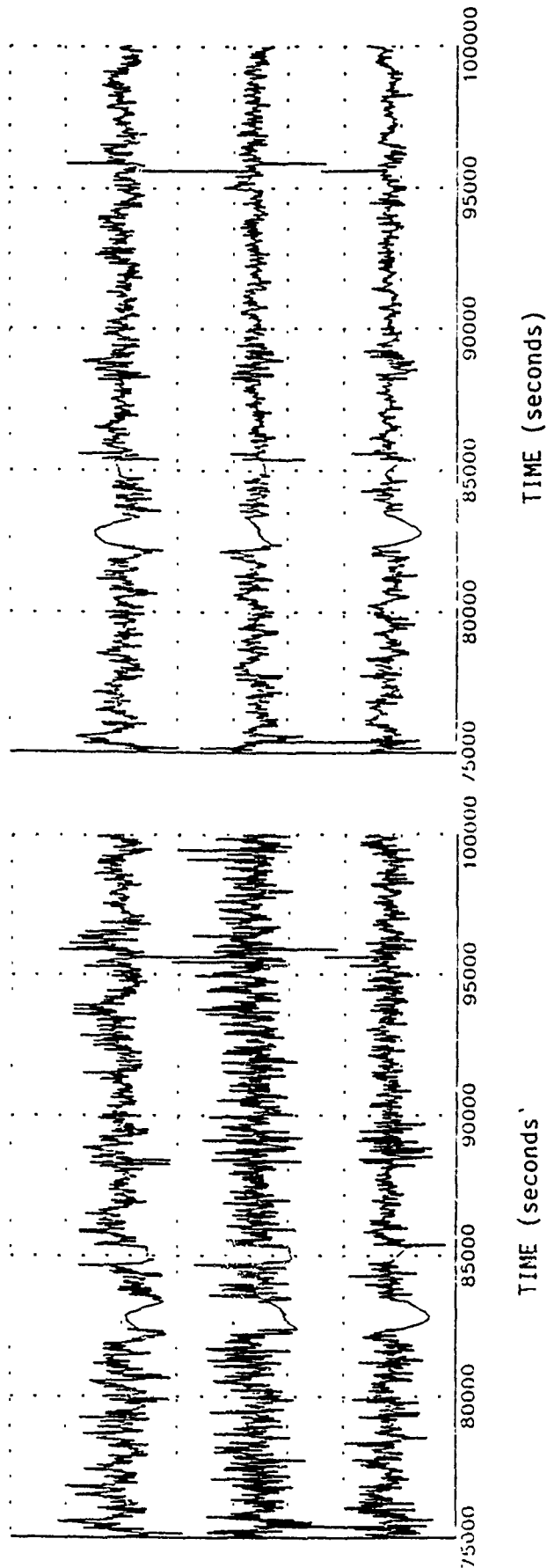
- CAROUSELLING THE COMPLETE INSTRUMENT ASSEMBLY ON ITS PLATFORM ALLOWS MANY RESIDUAL BIAS AND LOW FREQUENCY INSTRUMENT ERRORS TO BE CALIBRATED.

HOWEVER, CAROUSELLING AMPLIFIES CENTRIPETAL GRADIENTS THUS IMPOSING A TIGHTER REQUIREMENT ON PLATFORM STABILITY AND KNOWLEDGE OF ROTATION RATES.



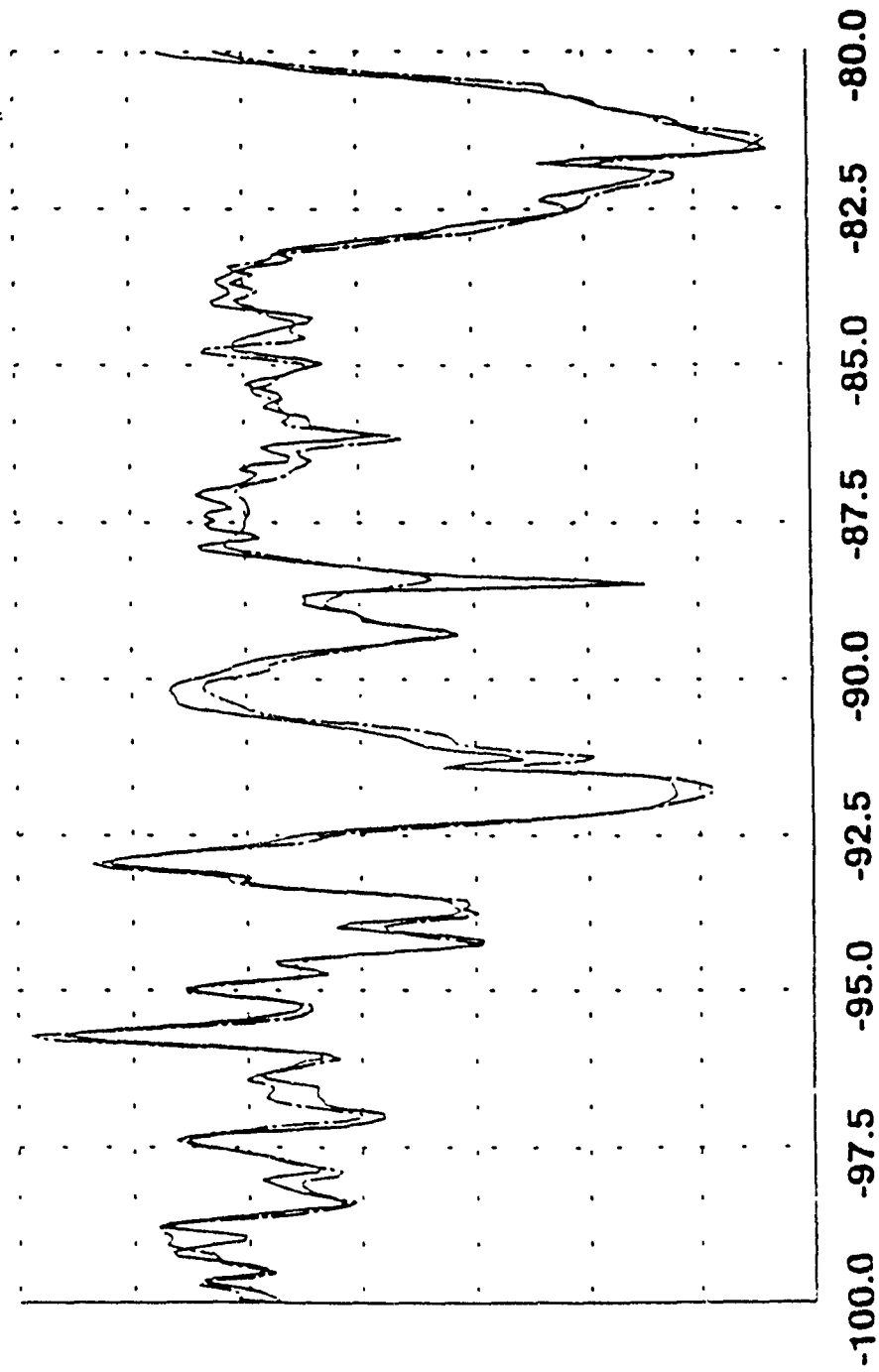
A PARTICULAR COMBINATION OF OUTPUT CHANNELS PROVIDES A MEASURE OF INSTRUMENT NOISE WHICH IS INDEPENDENT OF GRAVITY SIGNAL. CORRELATION WITH RMS VERTICAL ACCELERATION IS OBVIOUS BEFORE FULL ACCELERATION COMPENSATION IS APPLIED.

RMS ACCELERATION SENSITIVITY



COMPARISON OF 3 GRADIENT CHANNELS BEFORE AND AFTER ACCELERATION AND YAW COMPENSATION SHOWS REDUCED NOISE LEVELS IN BOTH HIGH AND MID FREQUENCIES. REMOVAL OF BIAS CHANGES IS EVIDENT IN THE CAROUSELLING SIGNALS AT STOPPING POINTS.

ACCELERATION AND YAW COMPENSATION



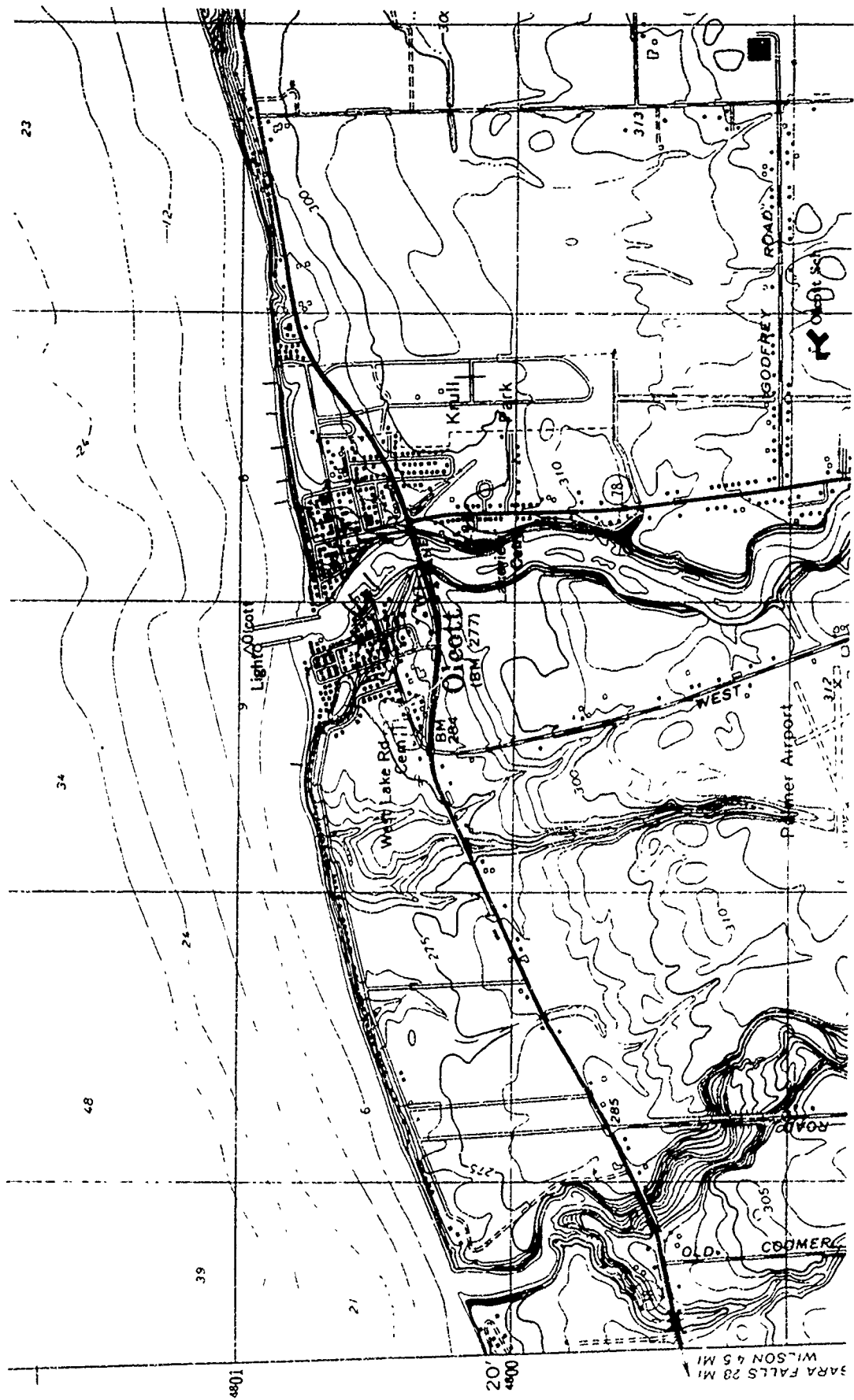
ALONG-TRACK DISTANCE (KM)

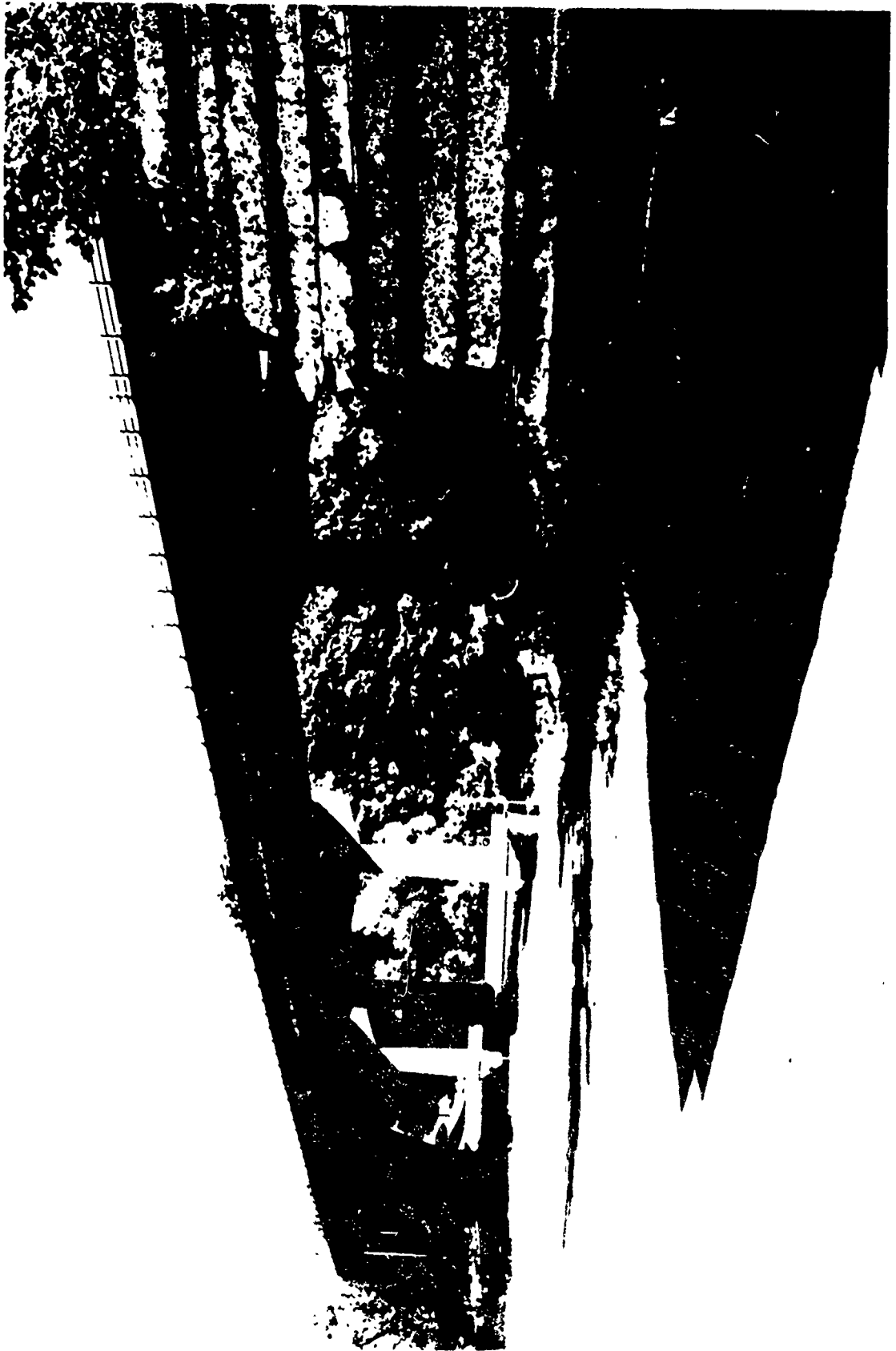
THIS GRADIENT COMPONENT WAS MEASURED ON 2 RAIL PASSES OVER AN AREA WITH A GRAVITY SIGNAL WHICH IS HIGH COMPARED TO THE ROAD SURVEY.

RAIL GRADIENTS

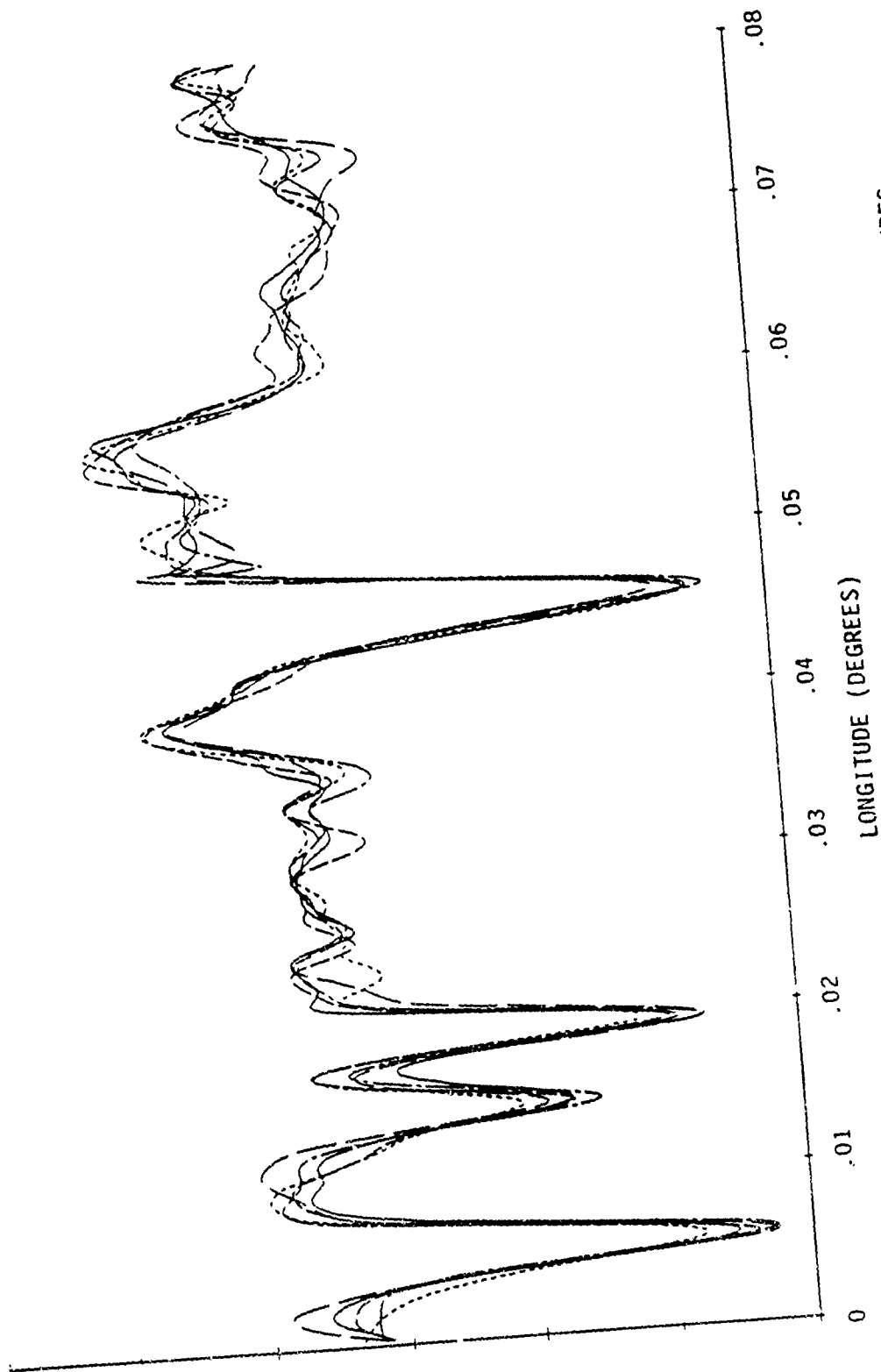
PLATFORM CONTROL IMPROVEMENTS

RECENT HARDWARE IMPROVEMENTS IN PLATFORM CONTROL HAVE DEMONSTRATED THAT YAW SENSITIVITY COMPENSATION IS NOW REDUNDANT. THIS COMPENSATION HAS, THEREFORE, BEEN REMOVED FROM RECENT ROAD TESTS.





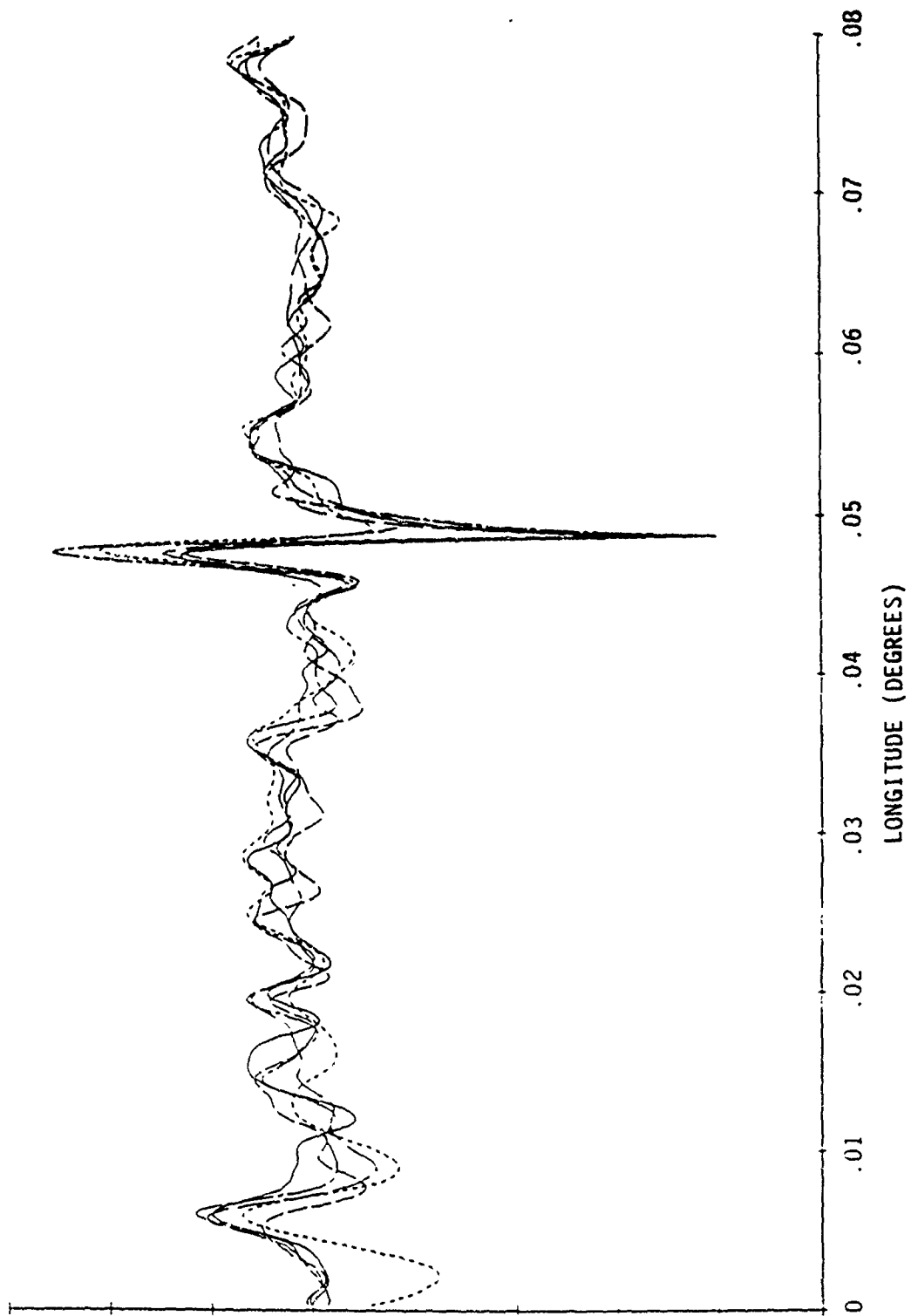




GRADIENTS MEASURED ON A SECTION OF ROAD SURVEY SHOWING LOCAL TOPOGRAPHIC FEATURES.

5 PASSES PERFORMED OVER A PERIOD OF 2 DAYS.

NORTH NORTH ROAD GRADIENT



GRADIENTS MEASURED ON A SECTION OF ROAD SURVEY SHOWING LOCAL TOPOGRAPHIC FEATURES.
5 PASSES PERFORMED OVER A PERIOD OF 2 DAYS.

EAST EAST ROAD GRADIENT

WHAT HAS THE EXPERIENCE OF OPERATION OF THE GGSS IN THE AIR AND ON THE LAND BOTH ON ROADS AND A RAILROAD INDICATED?

- CORRECTION OF HARDWARE DEFICIENCIES AND IMPLEMENTATION OF SOFTWARE COMPENSATION ROUTINES HAS RESULTED IN SIGNIFICANT PERFORMANCE IMPROVEMENT.
- GGSS IS CAPABLE OF MOVING BASE GRAVITY GRADIENT MEASUREMENTS TO THE REQUIRED ACCURACY IN THE PRESENCE OF SEVERE ENVIRONMENTAL DISTURBANCES.
- NO FUNDAMENTAL CHANGES TO THE GRADIOMETER ARE NECESSARY. A SMALLER GGI WITH ANTICIPATED REDUCED ENVIRONMENTAL SENSITIVITIES IS CURRENTLY UNDER DEVELOPMENT.

THE AGE OF MOVING BASE GRAVITY GRADIENT MEASUREMENTS

HAS BEGUN FOR

- HIGH ACCURACY, HIGH SPEED, FINE RESOLUTION AND ECONOMIC MAPPING OF THE GRAVITY DISTURBANCE VECTOR.
- PASSIVE NAVIGATION USING GRAVITY GRADIENT MAP MATCHING TECHNIQUES.
- TERRAIN FOLLOWING AND AVOIDANCE.

ABSTRACT

By

ALBERT JIRCITANO

BELL AEROSPACE TEXTRON
Division of Textron, Inc.
P.O. Box One
Buffalo, New York 14240-0001

GRAVITY BASED PASSIVE NAVIGATION

Passive covert Inertial Navigation System (INS) updating can be implemented by comparing measured gravity gradients with mapped values and using the error in an optimal filter to define in real time the INS. A parametric study is carried out showing performance as a function of;

- o Gradiometer accuracy and number of gravity gradient sensors.
- o INS - gyro and accelerometer accuracy
- o Map quality
- o Gravity field characterization (field intensity and frequency content)
- o Altitude
- o Velocity

SEVENTEENTH GRAVITY GRADIOMETER CONFERENCE

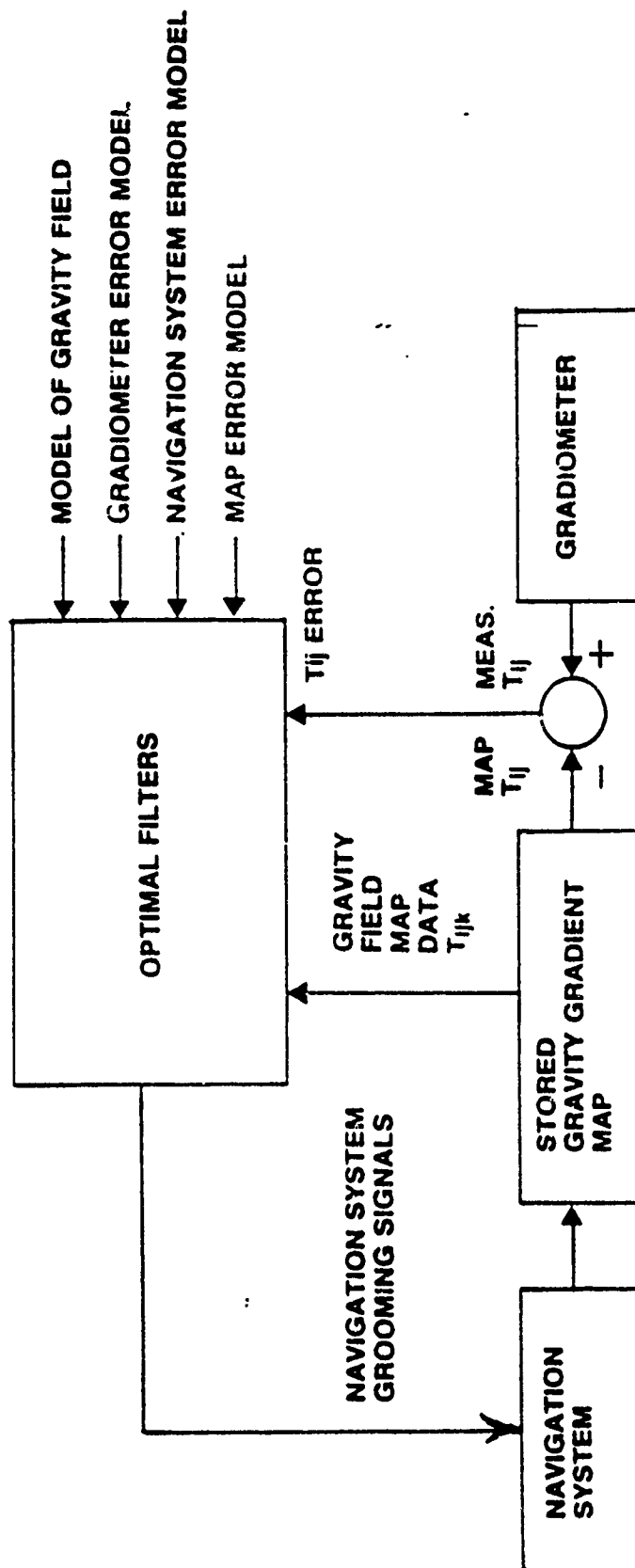
GRAVITY BASED PASSIVE NAVIGATION

OCTOBER 12-13, 1989

GRAVITY GRADIENT PASSIVE NAVIGATION

- CONCEPT AND BLOCK DIAGRAM
- ADVANTAGES
- PARAMETRIC STUDY RESULTS (GOOD MAPS).
 - AIRBORNE SYSTEM OVER LAND
 - SUBMARINE SYSTEM
- PARAMETRIC STUDY RESULTS WITH VARIABLE MAP QUALITY.
 - AIRBORNE SYSTEM WITH GRAVITY MAPS BASED ON
TERRAIN ELEVATION DATA.
 - SUBMARINE SYSTEM WITH GRAVITY MAPS BASED ON
GEOSTAT DATA MIXED WITH SHIP GRAVIMETER DATA.

Gravity Gradient Map Matching Block Diagram



GRAVITY BASED PASSIVE NAVIGATION CHARACTERISTICS

- SELF CONTAINED (NO EXTERNAL SIGNALS REQUIRED).
- COVERT (NO SIGNALS EMINATED).
- ALL WEATHER
- BOUNDED NAVIGATION ERROR WITH TIME (VERTICAL AS WELL AS HORIZONTAL POSITION ERROR CONTROLLED).
- NAVIGATION ERRORS DECREASE WITH TERRAIN PROXIMITY.
- TERRAIN ESTIMATION CAPABILITY.
- OPERATIVE OVER WATER AS WELL AS LAND.
- GRAVITY FIELD MAP REQUIREMENTS LARGELY IN HAND.
 - TERRAIN OR BATHYMETRIC DATA.
 - GEOSAT ALTIMETRY DATA (OCEAN AREAS).
 - EXTENSIVE DMA AND NOO DATA BASES.

Summary of Parametric Study Conditions

	GYRO			ACCELEROMETER
	0.01 DEG/HR	0.001 DEG/HR	0.0001 DEG/HR	
RANDOM DRIFT SIGNAL				0.485 μ G
CORRELATION TIME	0.5 HR	0.5 HR	0.5 HR	0.5 HR
BIAS DRIFT	0.01	0.001	0.0001	0.485 μ G

GRADIOMETER WHITE NOISE - 10, 100, 1000 E²/RAD/SEC

ONE AND 3 GGI SYSTEM

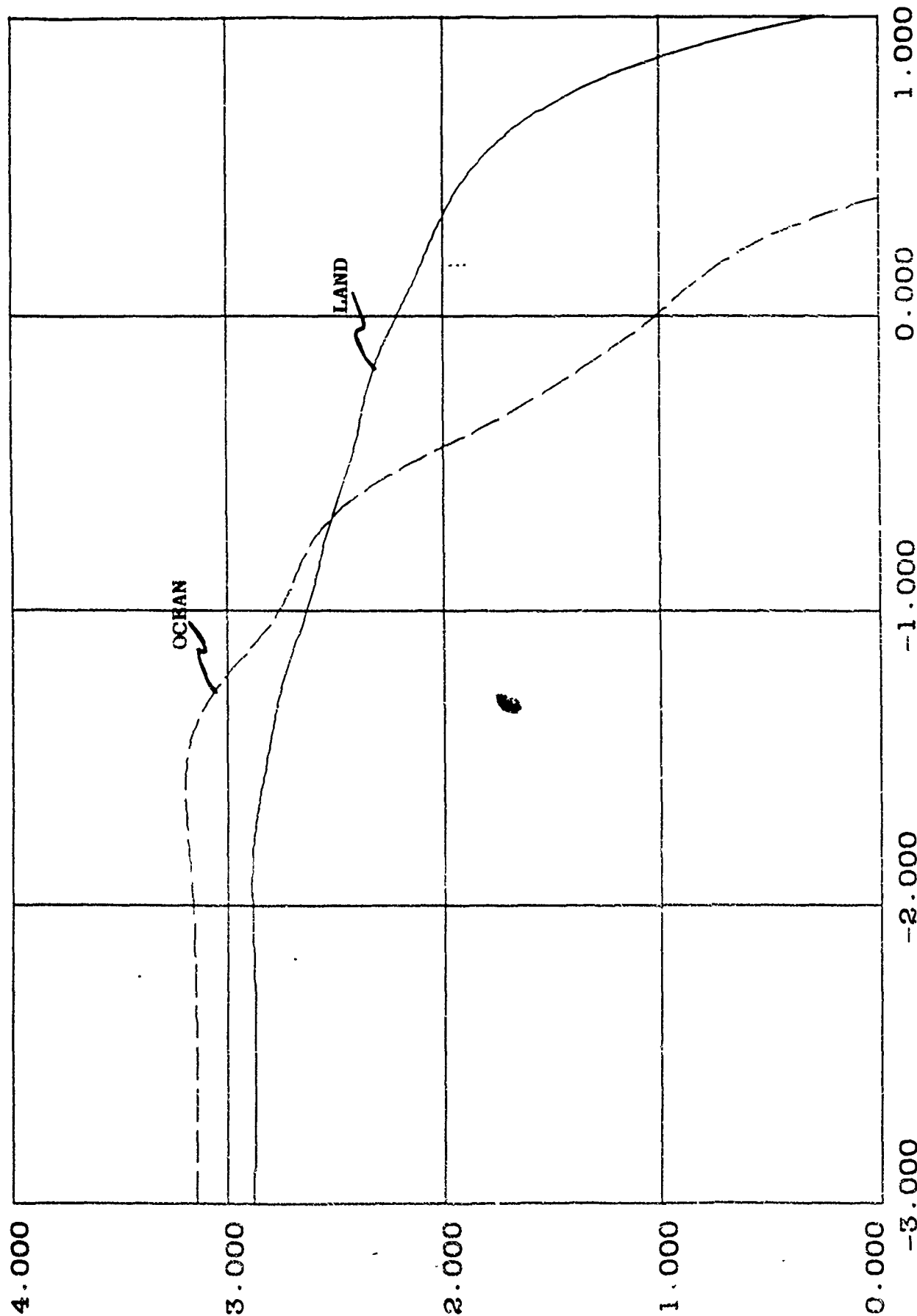
GRAVITY FIELD MODELS

ALTITUDE 100, 200, 400 M

VELOCITY 360, 720 KM/HR

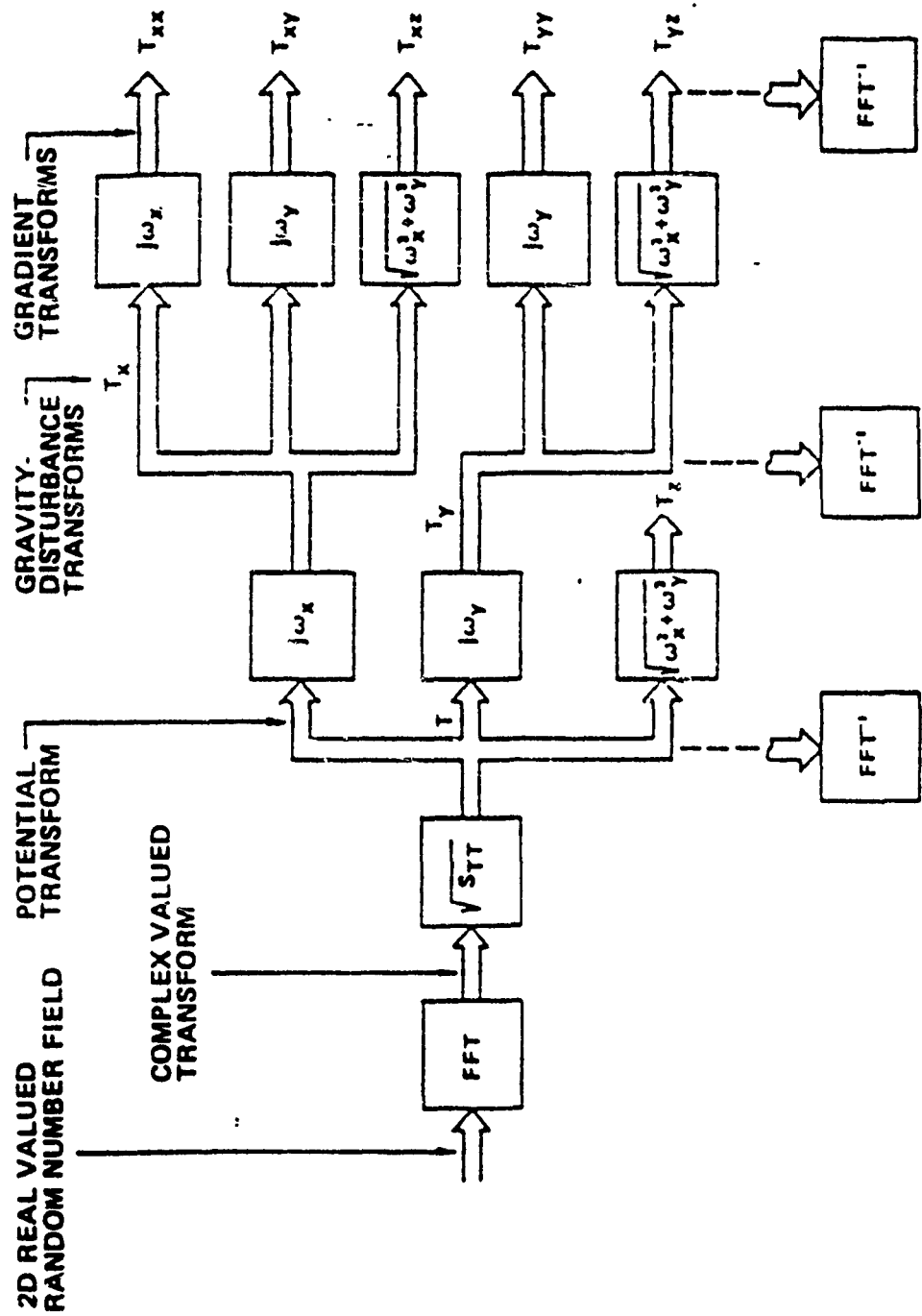
LOG $1^{1/2} \omega_s$ (RAD/KM)^{1/2}

GRAVITY FIELD MODELS

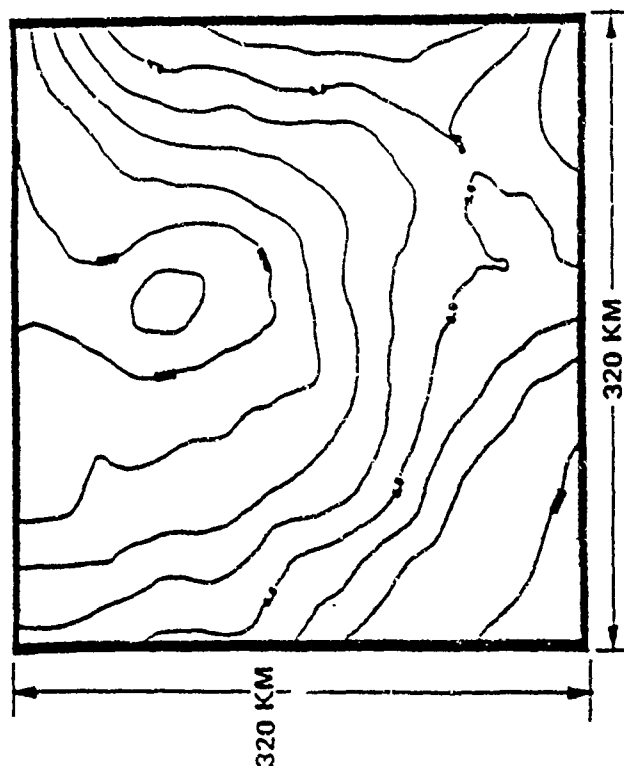


NORTH ATLANTIC AND NORTH BAKER PEAK STAG GRAVITY MODELS
LOG ONE DIMENSIONAL ZZ GRADIENT PSD'S VS. LOG FREQUENCY

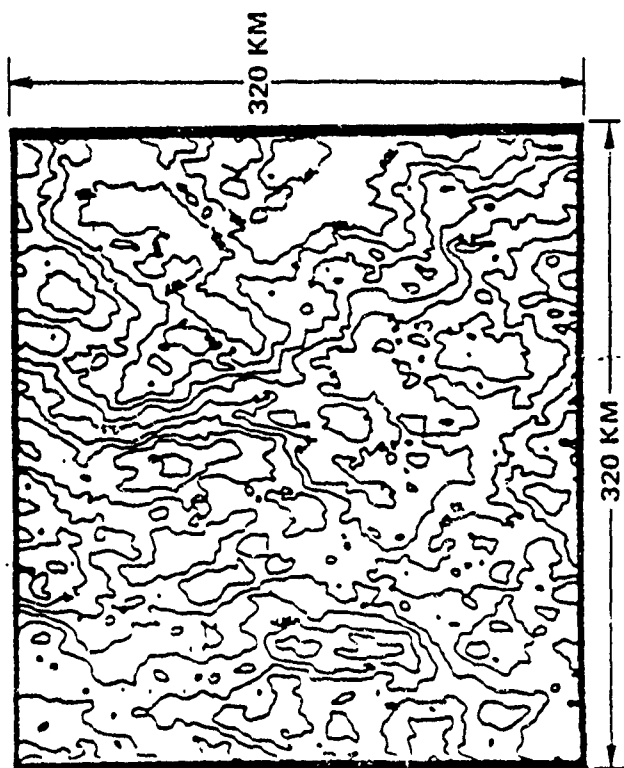
Synthetic Field Generation



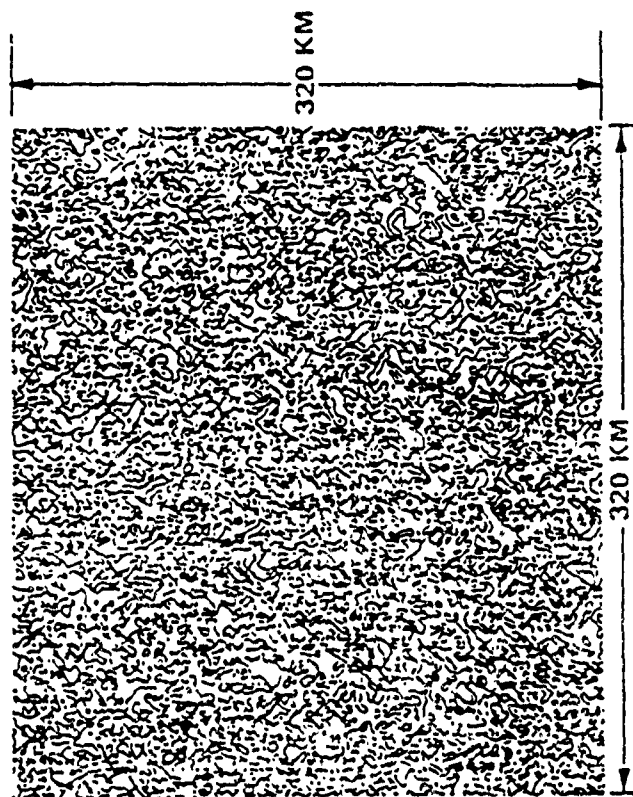
SYNTHETIC FIELD POTENTIAL CONTOUR MAP
CONTOUR INTERVAL 2000 E KM²



SYNTHETIC FIELD VERTICAL DEFLECTION (T_x) CONTOUR MAP
CONTOUR INTERVAL 1/2 SEC



SYNTHETIC FIELD GRADIENT (T_{xy}) CONTOUR MAP
CONTOUR INTERVAL 2 EOTVOS



BASELINE CONDITIONS

ALT - 200 M ABOVE TERRAIN

VEL - 360 KM/HR

3 - GGI's

**HORIZONTAL POSITION
ERROR CEP FT**

200

100

80

60

40

20

**GYRO RANDOM DRIFT
(DEG/HR RMS)**

0.001

0.0001

10

1000.0

**GRADIOMETER WHITE
NOISE (E^2 /RAD/SEC)**

100.0

10.0

VERTICAL POSITION
ERROR (FT RMS)

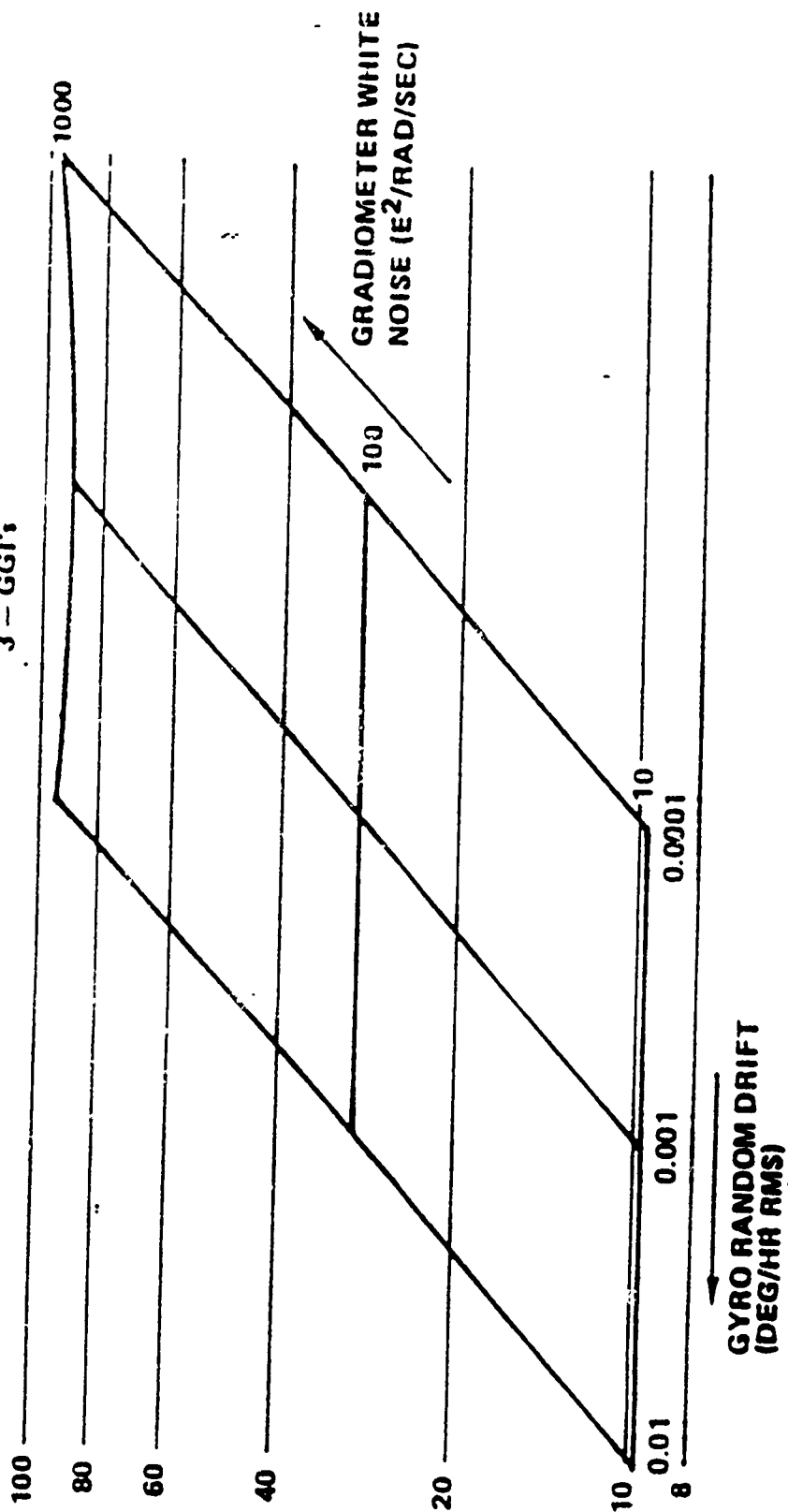
200

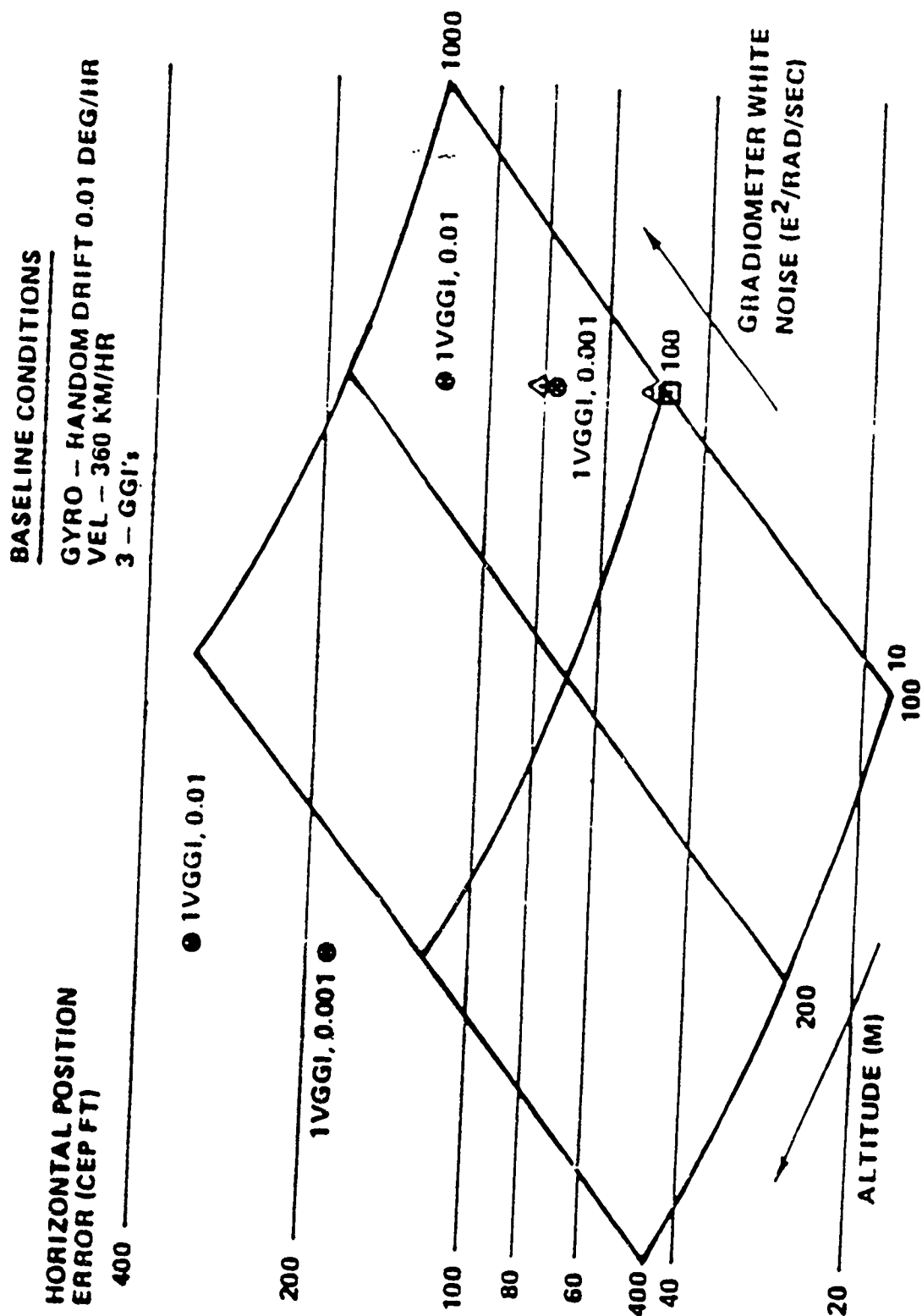
BASELINE CONDITIONS

ALT - 200 M ABOVE TERRAIN

VEL - 360 KM/HR

3 - GGI's





BASELINE CONDITIONS

GYRO - RANDOM DRIFT 0.01 DEG/HR
 VEL - 360 KM/HR
 3 - GGI's

VERTICAL POSITION
 ERROR (FT RMS)

200

● 1VGGI

100

80

60

40

20

400

1VGGI

1000

GRADIOMETER WHITE
 NOISE (E^2 /RAD/SEC)

100

200

ALTITUDE (M)

8

6

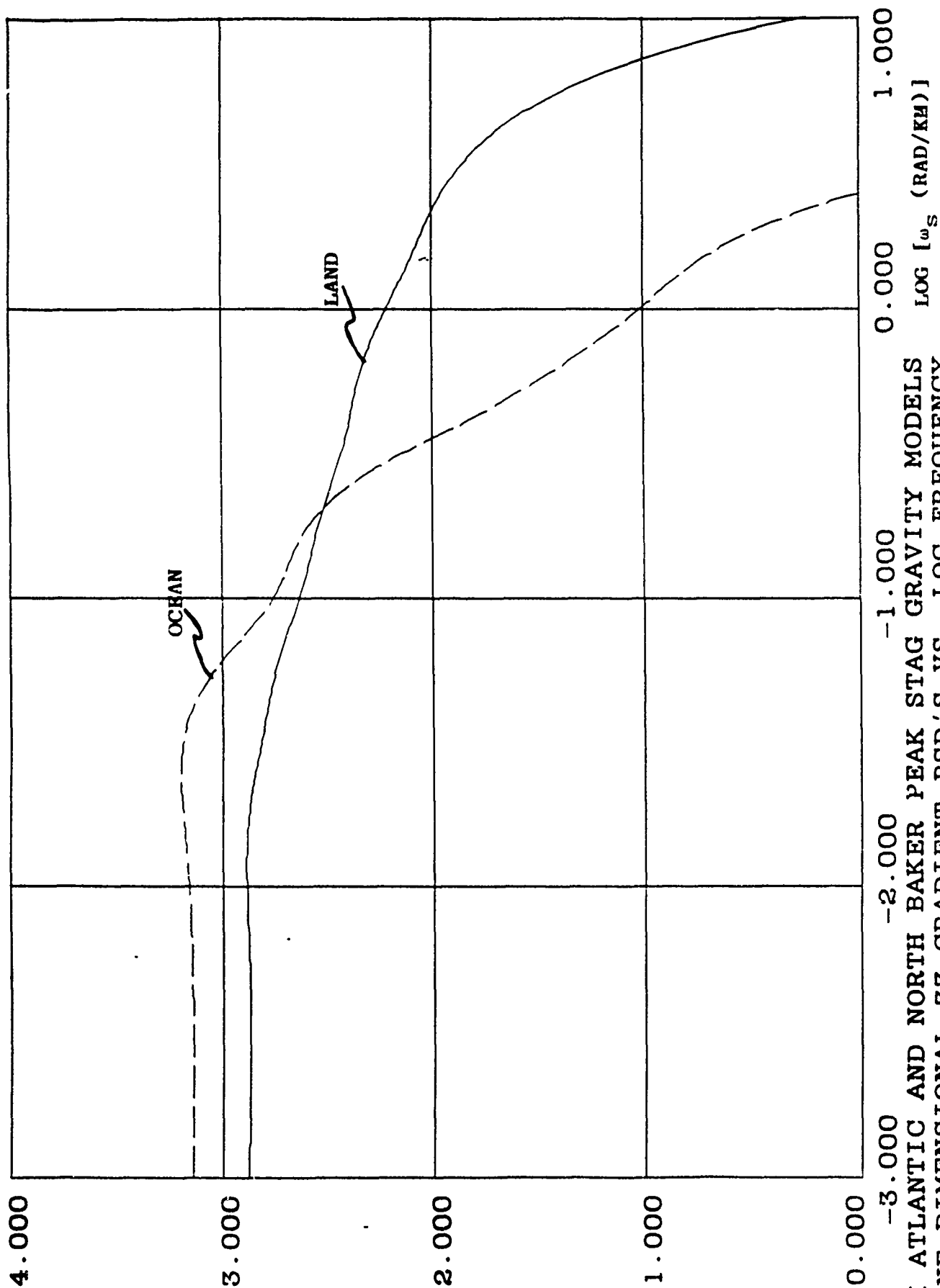
10

100

SUBMARINE PERFORMANCE RESULTS

LOG [T_{zz} ($\frac{E^2}{\text{RAD/KM}}$)]

GRAVITY FIELD MODELS



NORTH ATLANTIC AND NORTH BAKER PEAK STAG GRAVITY MODELS
LOG ONE DIMENSIONAL, 7% GRADIENT PSD'S VS. LOG FREQUENCY

Summary of Parametric Study Conditions

	GYRO	ACCELEROMETER
RANDOM GYRO DRIFT	10^{-2} TO 10^{-5} DEG/HR	0.0485 AND 0.485 μ G
CORRELATION TIME	0.5 HR	0.5 HR
BIAS DRIFT	3 X RANDOM DRIFT	3 X RANDOM DRIFT

GRADIOMETER WHITE NOISE - 10, 100, 1000 E^2 /RAD/SEC

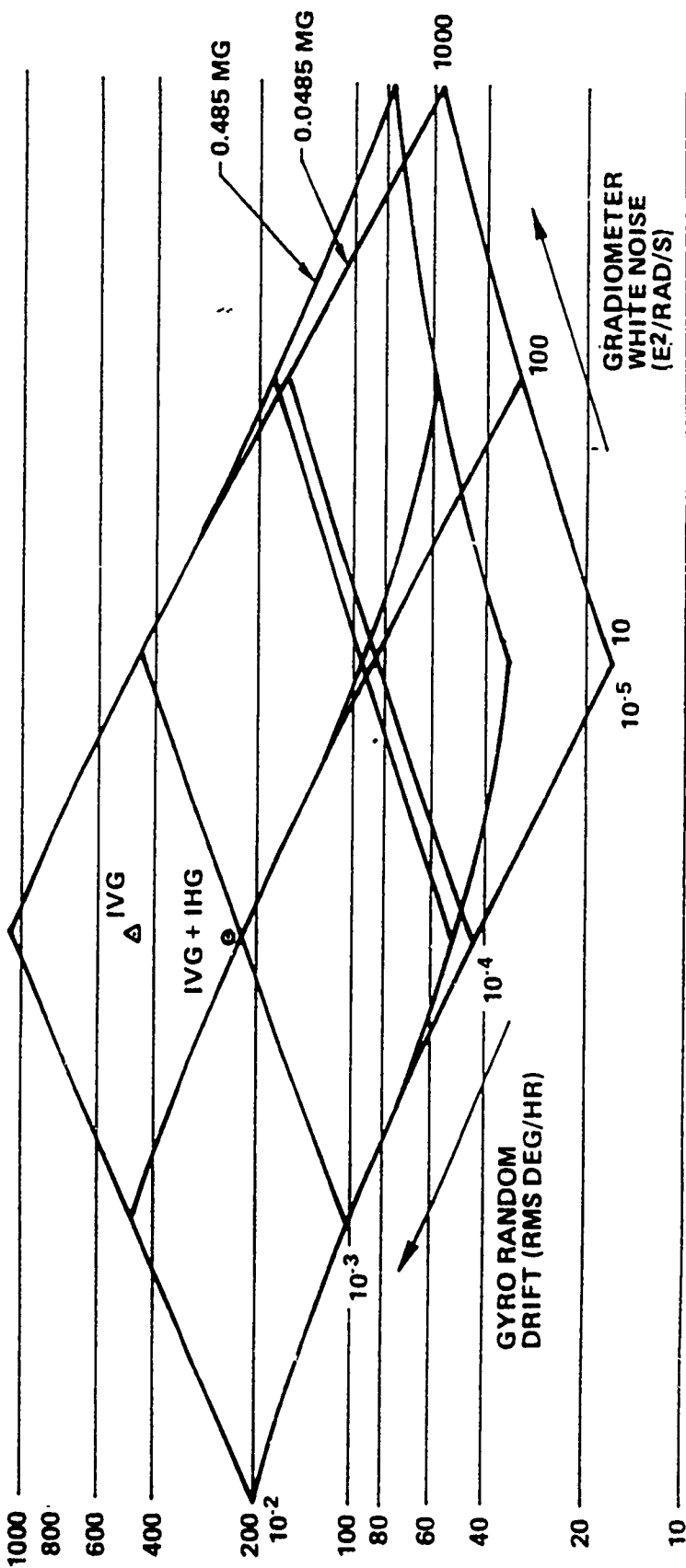
GRAVITY FIELD MODEL - NORTH ATLANTIC

Navigation Performance Analysis (Position)

BASELINE CONDITIONS

SUB. NEAR SURFACE
NORTH ATLANTIC GRAVITY MODEL
3 GGI SYSTEM
NO MAP ERROR

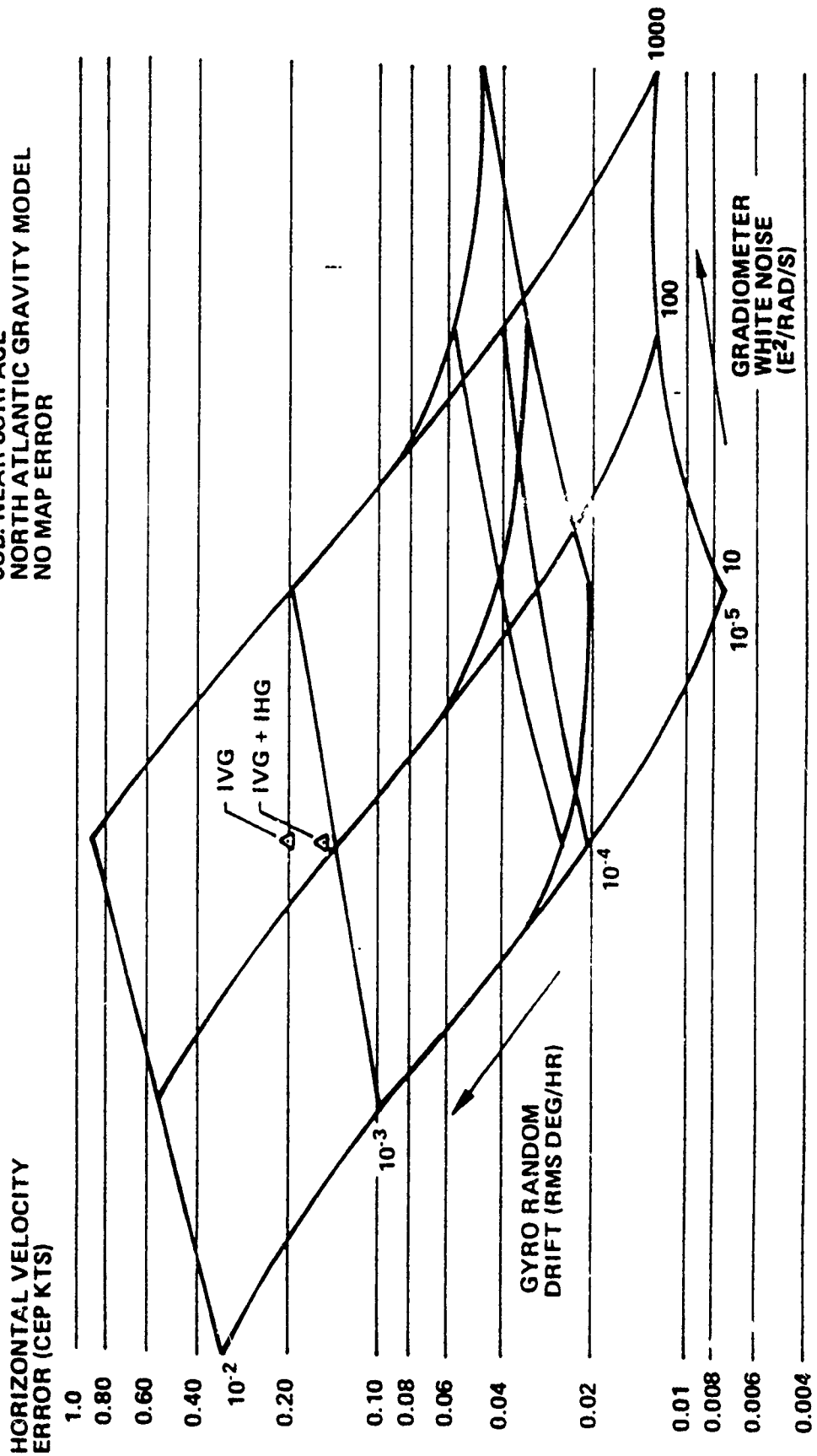
HORIZONTAL POSITION
ERROR (CEP FT)



Navigation Performance Analysis (Velocity)

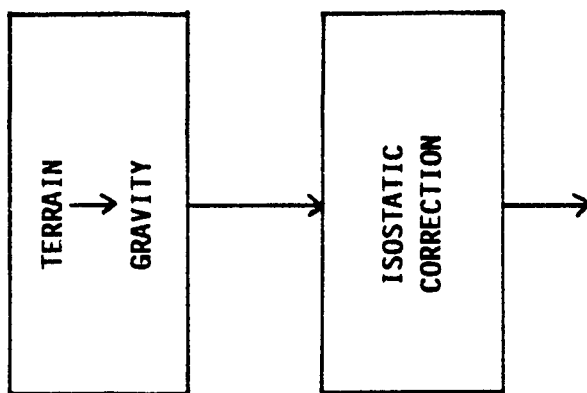
BASELINE CONDITIONS

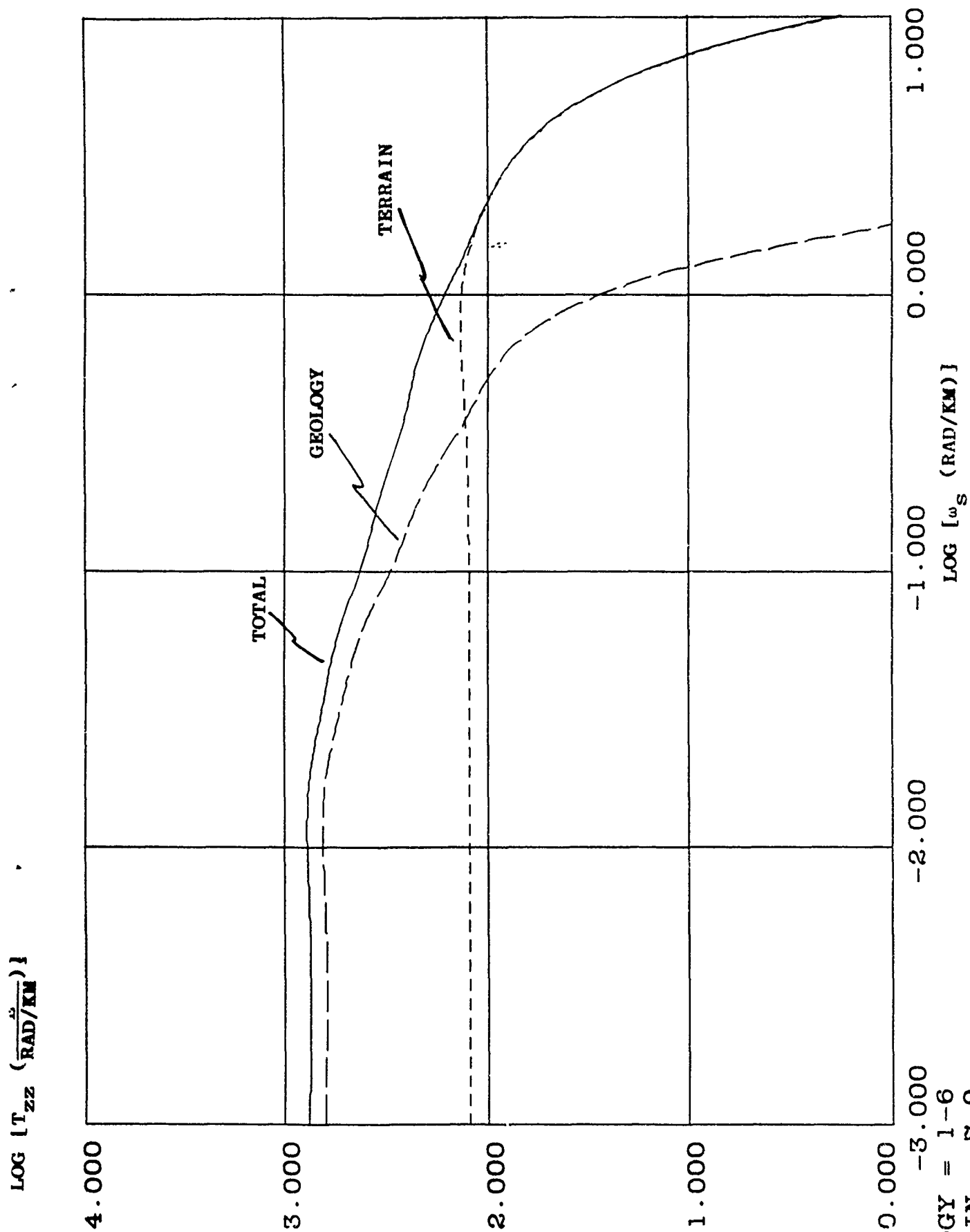
SUB. NEAR SURFACE
NORTH ATLANTIC GRAVITY MODEL
NO MAP ERROR



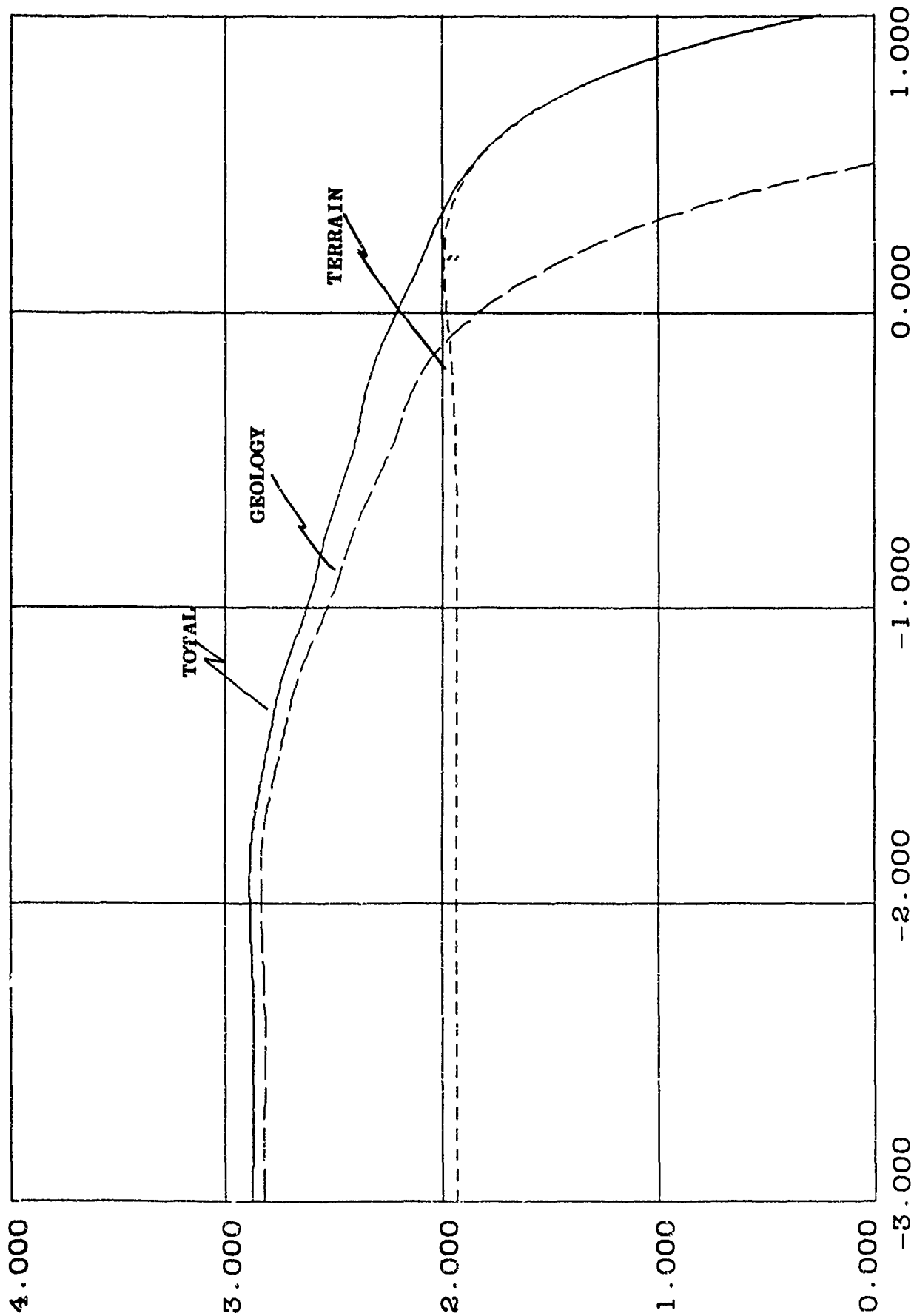
PASSIVE NAVIGATION ANALYSIS WITH VARIABLE MAP QUALITY

TERRAIN BASED GRAVITY MAP





LOG [T_{zz} ($\frac{\tilde{E}}{\text{RAD/KM}}$)]



LOG [ω_s (RAD/KM)]

-3.000

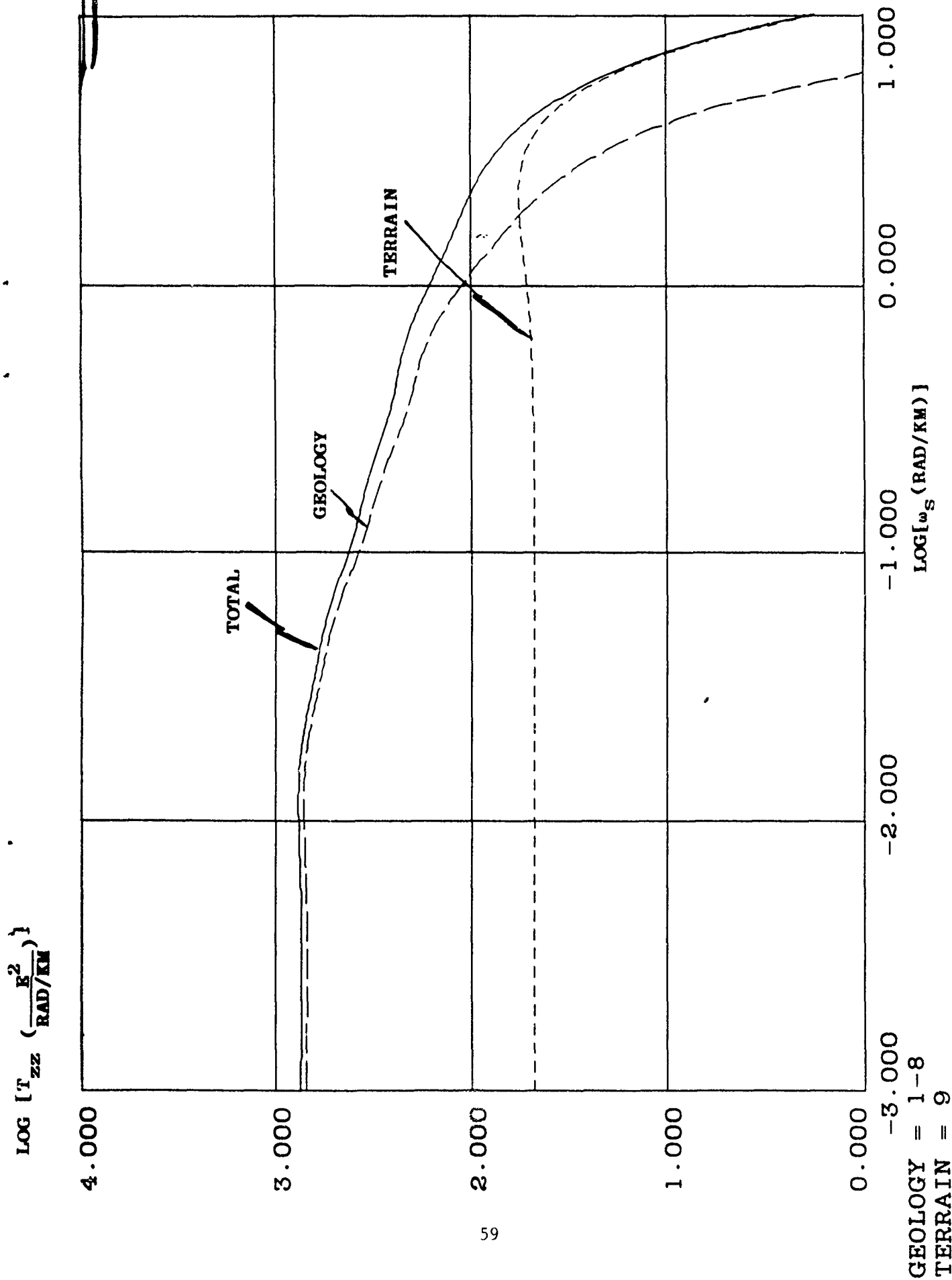
-2.000

-1.000

0.000

1.000

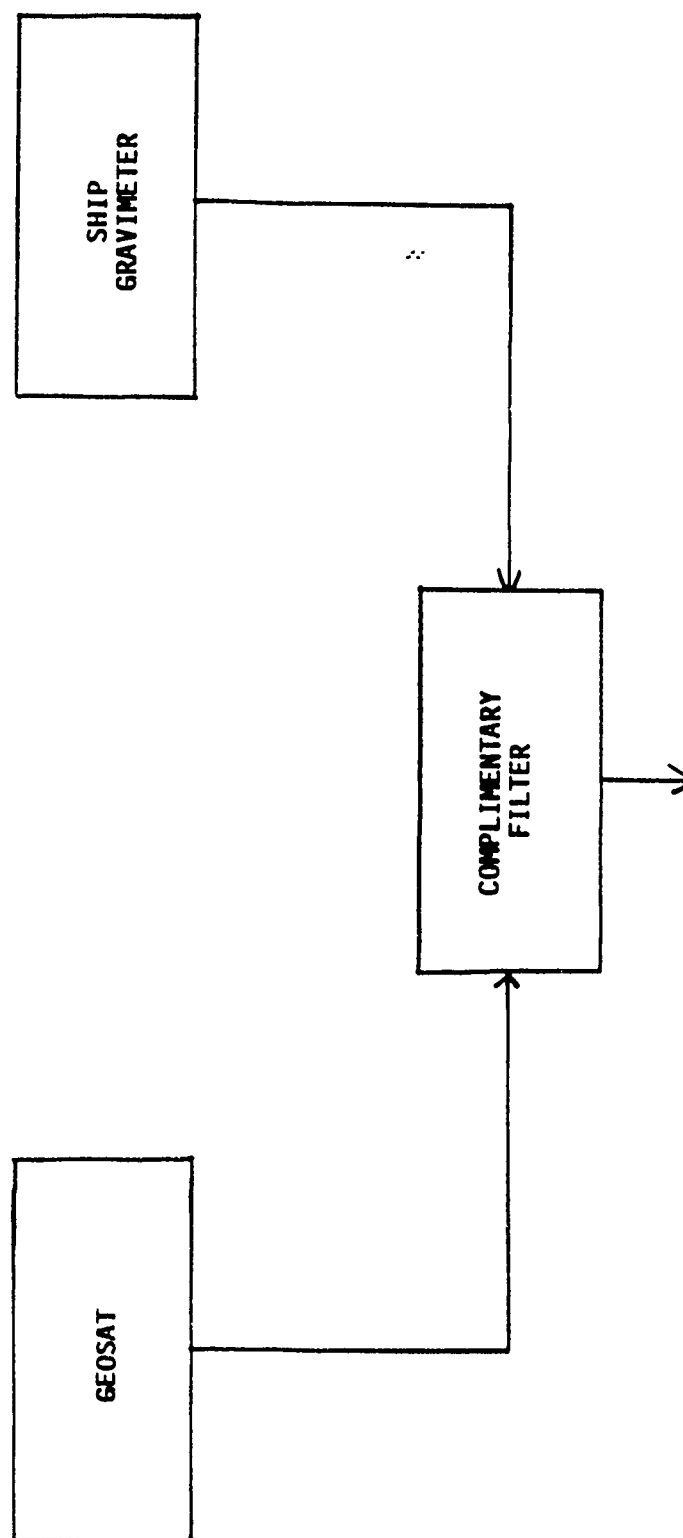
GEOLOGY = 1-7
TERRAIN = 8-9

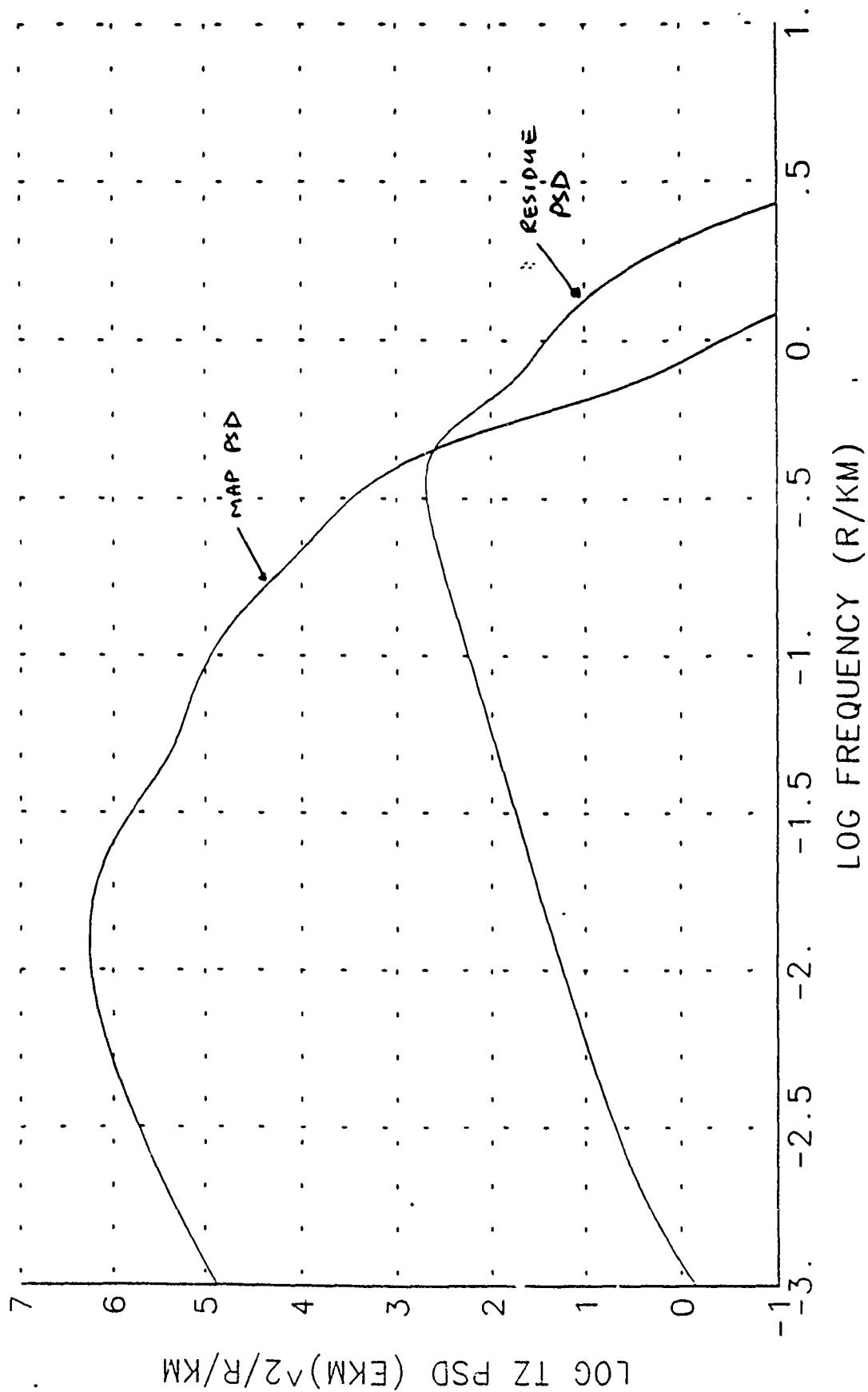


TERRAIN DERIVED MAP PERFORMANCE

CONDITIONS					
100M ALTITUDE					
720 KM/HR VELOCITY (389 KTS)					
100 E ² /r/s GGI					
.01 °/HR GYRO DRIFT, 1/2 HR. COV TIME					
MAP	HORIZONTAL POSITION ERROR (CEP FT)	VERTICAL POSITION ERROR (RMS FT)	HORIZONTAL VELOCITY ERROR (CEP FT/S)	VERTICAL VELOCITY ERROR (RMS FT/S)	
SURVEY	47	18	.22	.03	
A	47	19	.22	.04	
B	48	26	.23	.10	
C	79	45	.32	.15	

OCEAN GRAVITY MAP





NNA MODEL WITH SAT ALT AND GRAVIMETER

SIGNAL AND ERROR PSD'S

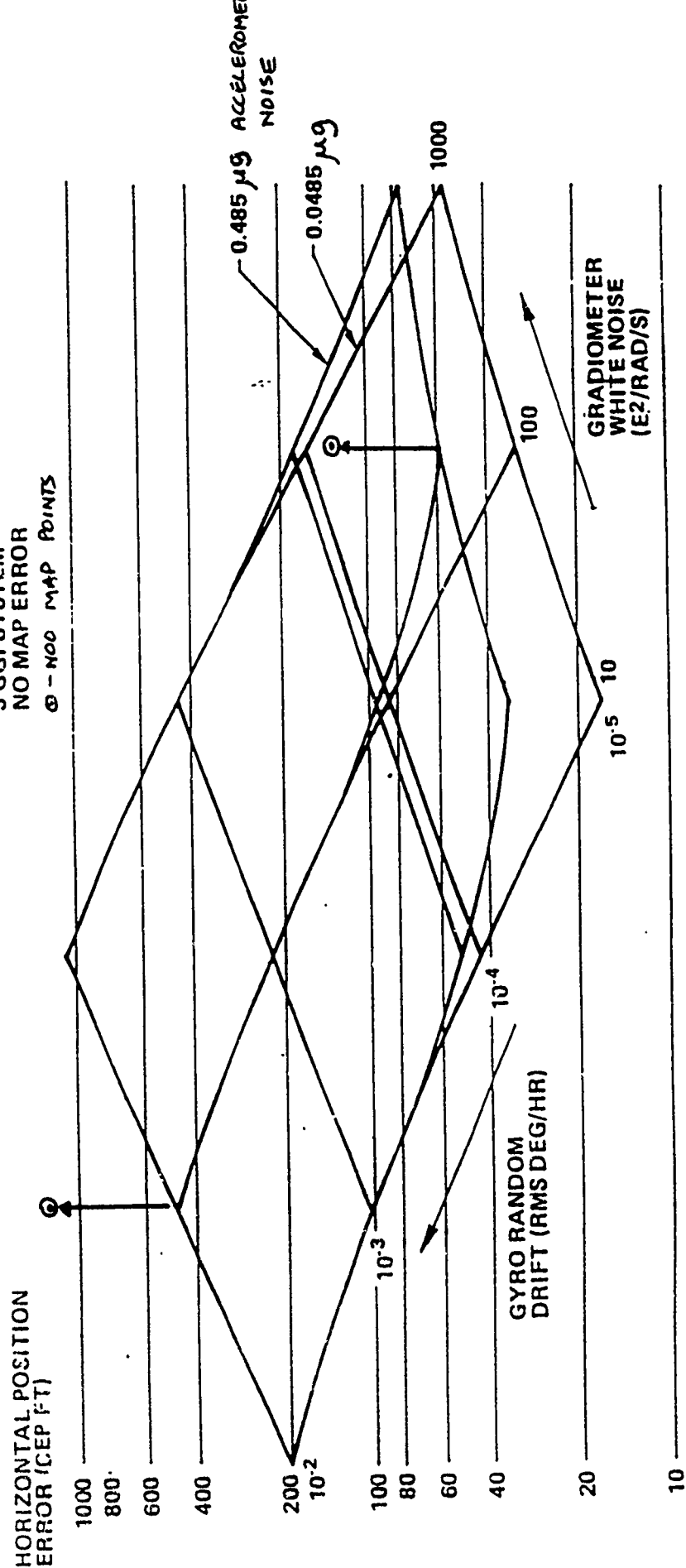
SAT ALT WN = $5E7$ (EKM²)²/R/KM GRAV WN = $1E3$ (EKM)²/R/KM

FIGURE 1.2

Navigation Performance Analysis (Position)

BASELINE CONDITIONS

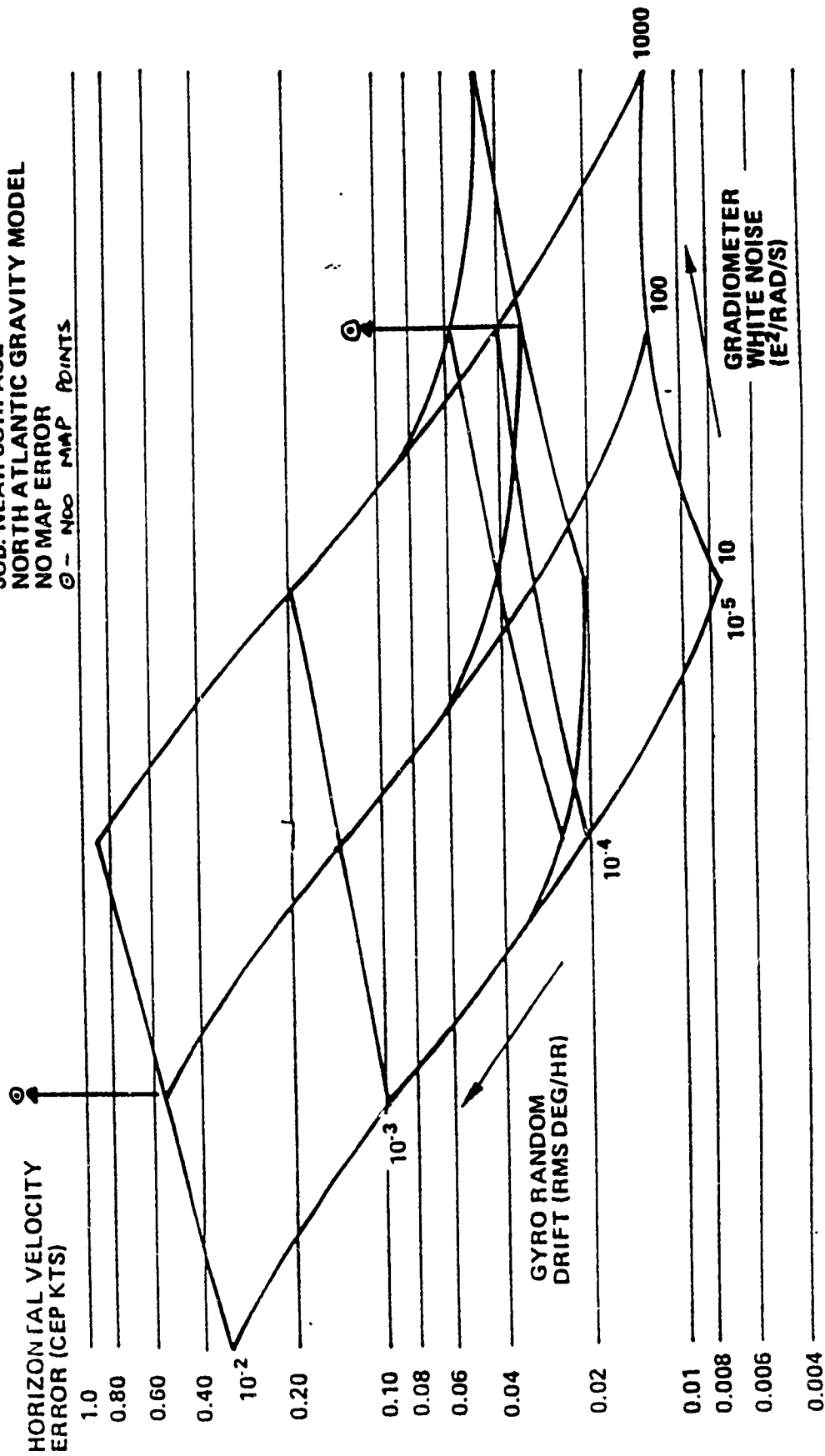
SUB. NEAR SURFACE
NORTH ATLANTIC GRAVITY MODEL
3 GGI SYSTEM
NO MAP ERROR
0 - NOO MAP POINTS



Navigation Performance Analysis (Velocity)

BASELINE CONDITIONS

SUB. NEAR SURFACE
NORTH ATLANTIC GRAVITY MODEL
NO MAP ERROR
0 - NOO MAP POINTS



SP-5362-13

**RECENT TEST RESULTS FOR
GRAVITY GRADIOMETER SURVEY
SYSTEM RAIL DATA**

12 October 1989

Prepared for:

**1989 MOVING BASE GRAVITY GRADIOMETER REVIEW
L.G. Hanscom Air Force Base
Massachusetts**

Prepared by:

**S.J. Brzezowski
J.D. Goldstein
W.G. Heller
T.H. Taylor
J.V. White**

**THE ANALYTIC SCIENCES CORPORATION
55 Walkers Brook Drive
Reading, Massachusetts 01867**

FOREWORD

This document contains material used in a presentation given by The Analytic Sciences Corporation. The material is not intended to be self-explanatory, but rather should be considered in the context of the overall presentation.

RECENT TEST RESULTS FOR GGSS RAIL DATA

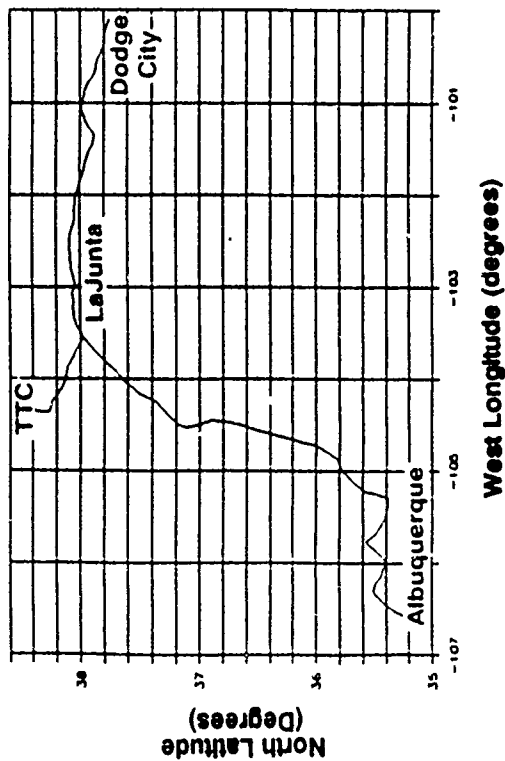
OVERVIEW

- **Summary of data collection**
- **Navigation data analysis results**
- **Gradiometer data analysis**
- **Special gravity gradient signature
along railroad tracks**
- **Comparisons with truth data**
- **Summary findings from the rail tests**

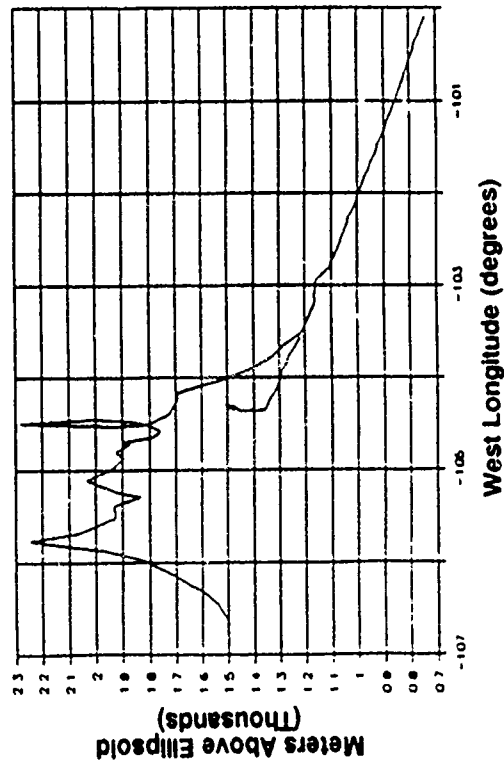
SUMMARY OF DATA COLLECTION

DATA COLLECTION SCENARIO

Track Plan

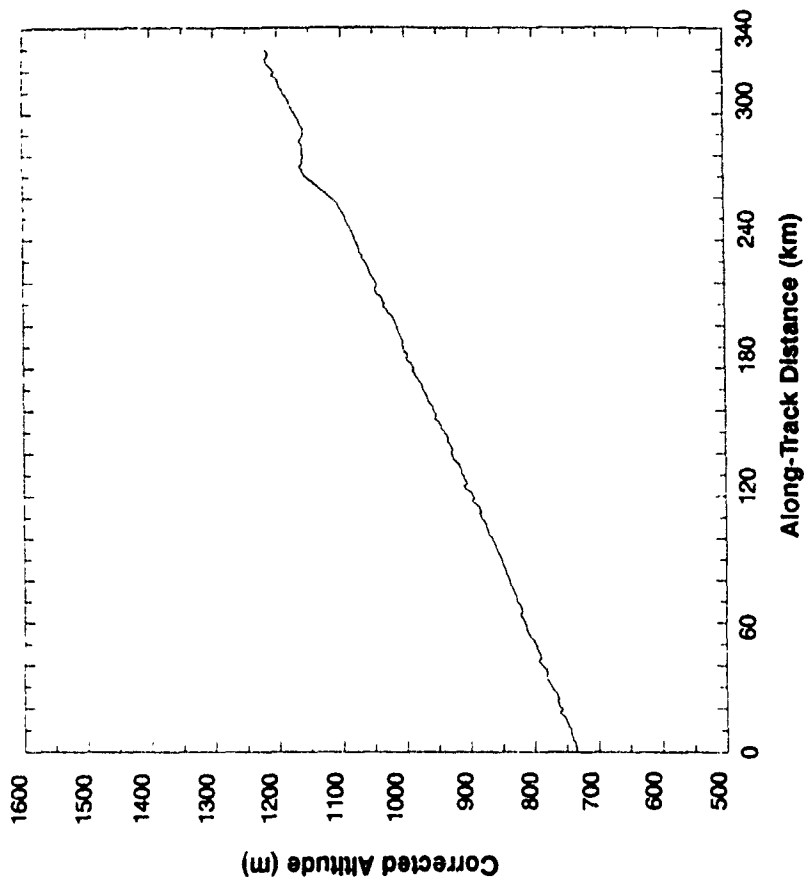
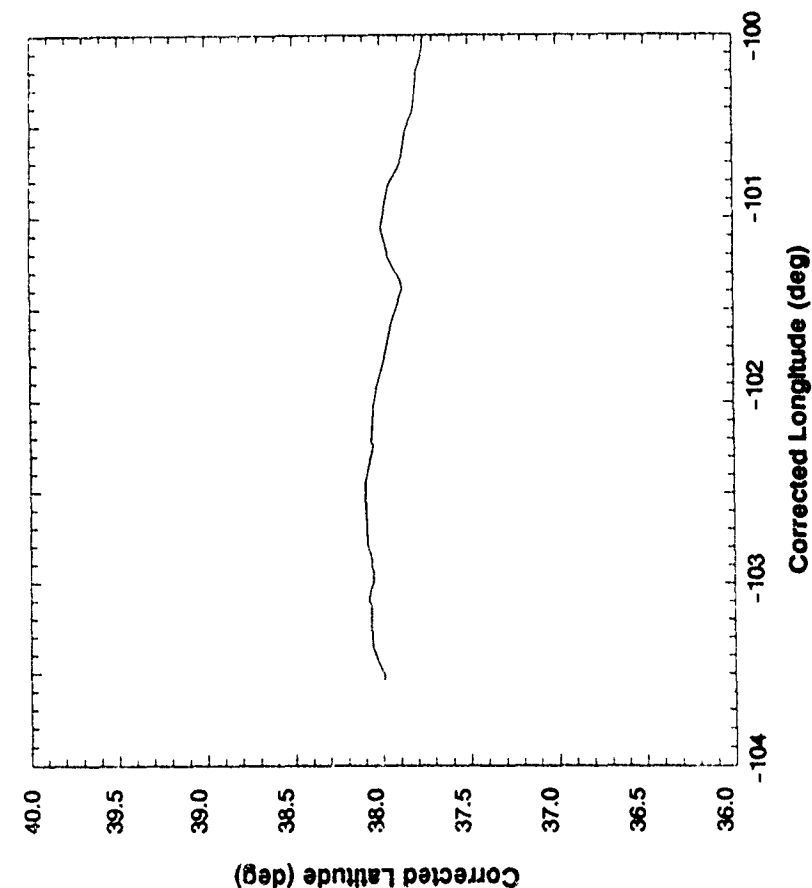


Track Elevation



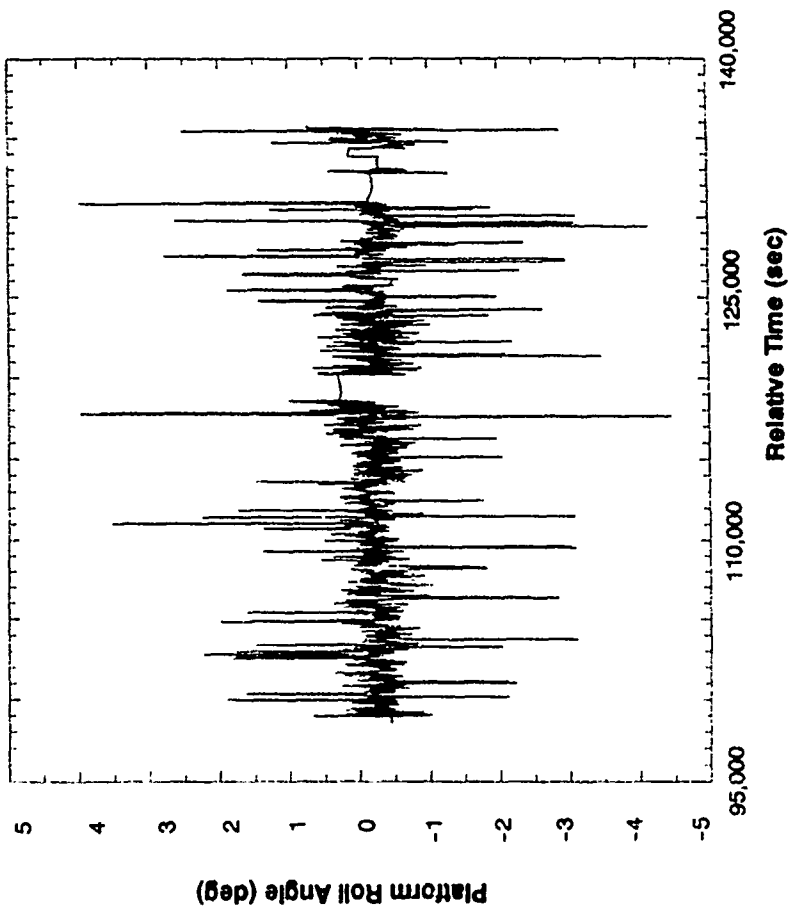
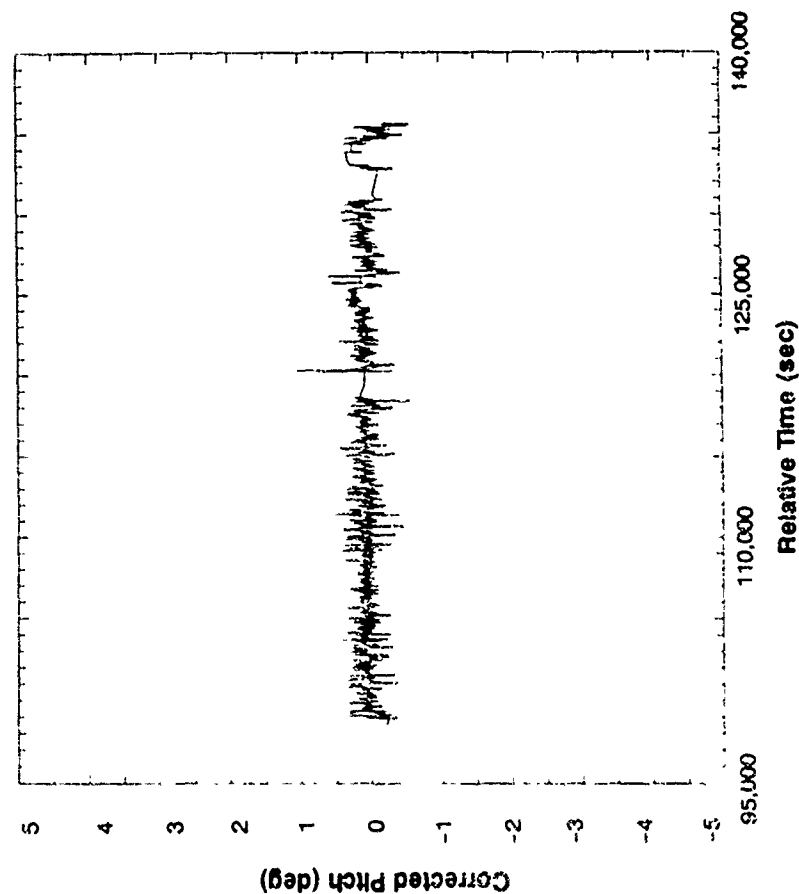
- Data collected along two round-trip routes
 - La Junta, CO to Dodge City, KS and return (325 km)
 - La Junta, CO to Albuquerque, NM and return (560 km)
- Total of 18 tracks (five Dodge trips, and four Albuquerque trips)
- Train speed = 11M/S (25 Mph) on tracks one to ten; 6 M/S (15 Mph) on tracks 11 to 18
- Transponders spaced at three mile intervals on Dodge route; nine miles on Albuquerque route
- Albuquerque route features large variability in elevation
- Five Dodge tracks and three Albuquerque tracks provided by Bell Aerospace, Inc.

TYPICAL NAVIGATION DATA (STAGE I OUTPUTS) FROM DODGE ROUTE



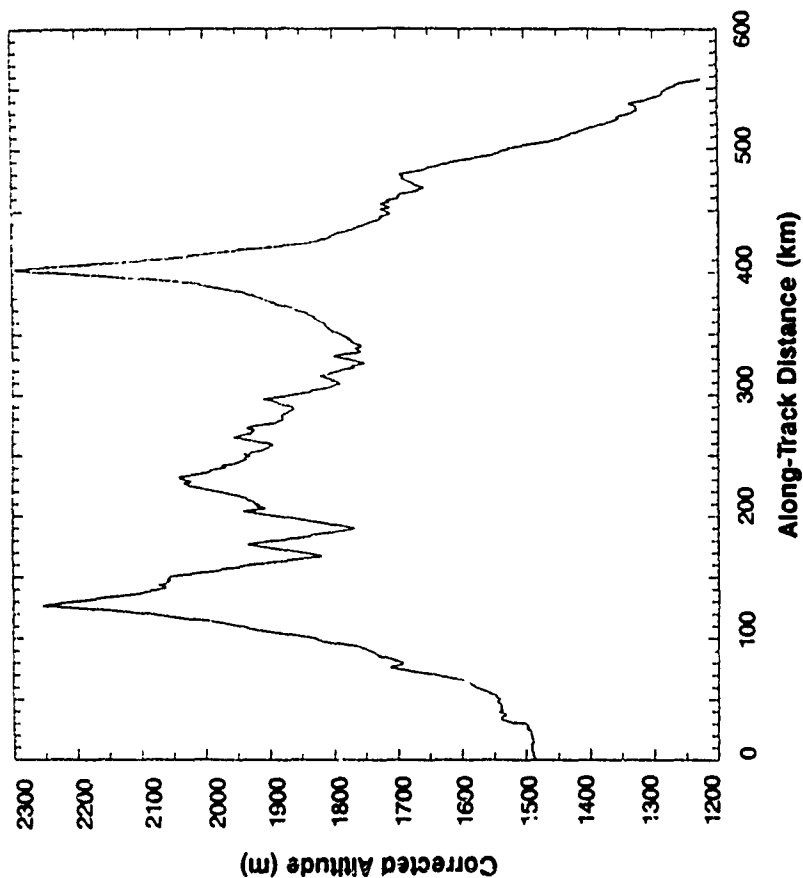
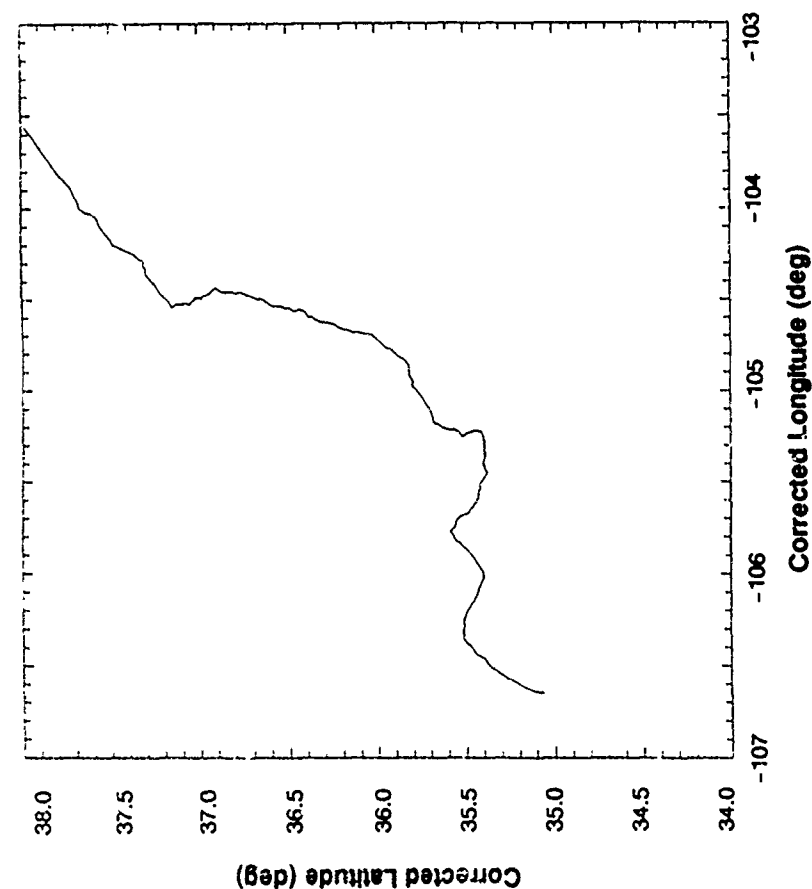
- Data are from track 6 (Dodge City to La Junta)
- Position and elevation profiles reflect use of transponder truth data
- "Corrected" scales refer to transponder smoothing of axle tachometer output

TYPICAL NAVIGATION DATA (STAGE I OUTPUTS) FROM DODGE ROUTE (cont.)



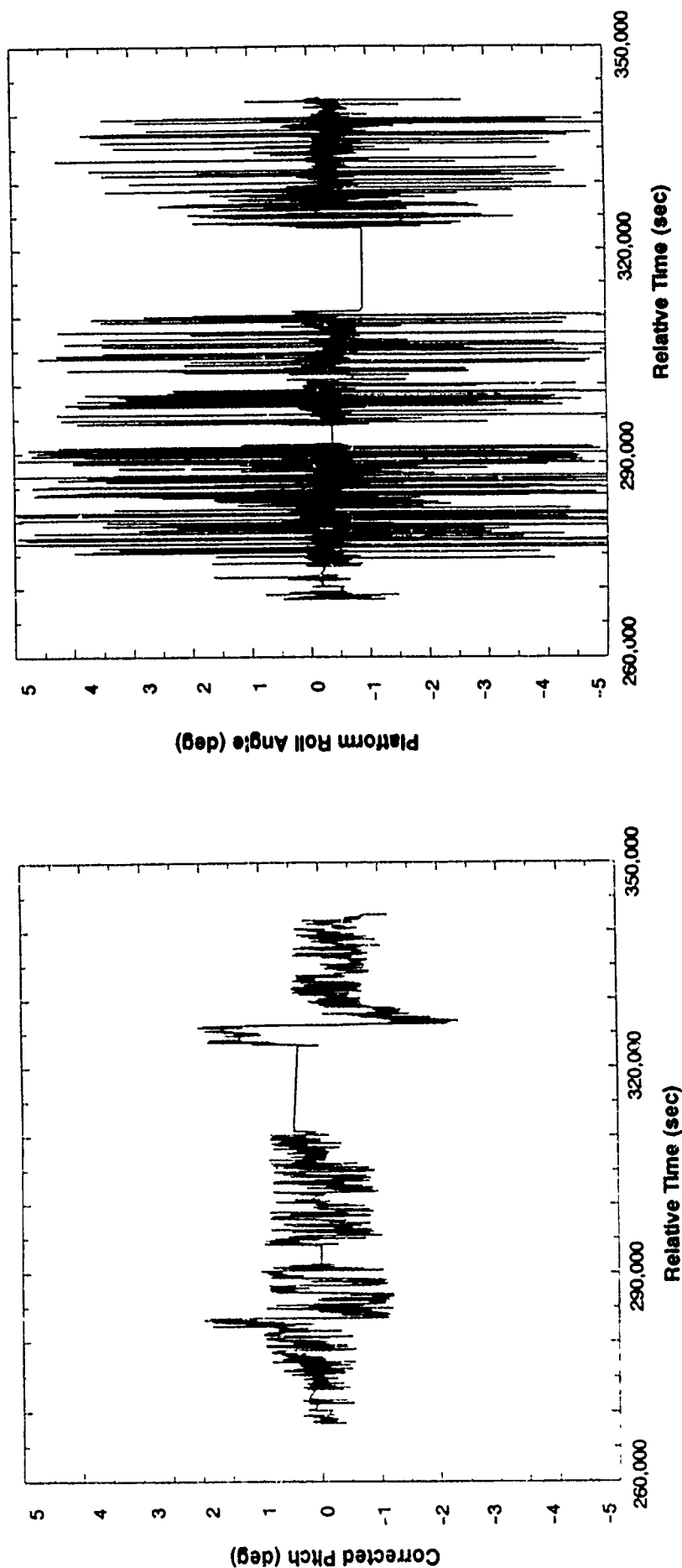
- Data are from track 6 (Dodge City to La Junta)
- "Corrected" scales refer to transponder smoothing of axle tachometer output

TYPICAL NAVIGATION DATA (STAGE I OUTPUTS) FROM ALBUQUERQUE ROUTE



- Data are from track 8 (Albuquerque to La Junta)
- Position and elevation profiles reflect use of transponder truth data
- "Corrected" scales refer to transponder smoothing of axle tachometer output

TYPICAL NAVIGATION DATA (STAGE I OUTPUTS) FROM ALBUQUERQUE ROUTE (cont.)



- Data are from track 8 (Albuquerque to La Junta)
- Pitch and roll magnitude are generally about twice as large as those for Dodge route ($\leq 4\text{deg}$)
- "Corrected" scales refer to transponder smoothing of axle tachometer output

NAVIGATION DATA ANALYSIS RESULTS

ASSESSMENT OF GGSS NAVIGATION SYSTEM PERFORMANCE

Available outputs

- Platform latitude, longitude, altitude, velocity (north, east, down), pitch, roll, yaw, carousel angle
- Axle tachometer, latitude, longitude
- Corrected latitude, longitude, elevation, pitch angle estimates derived by Bell using transponder-indicated position to smooth tachometer outputs

Assessment techniques

- Analyze outputs versus time and along-track distance
- Compare corrected and axle tachometer-derived quantities
- Compare corrected positions with corresponding transponder values
- Compare total distance covered between first and last common transponders
- Analyze position profiles along straight stretches (identified from topographic maps)

COMPARISON OF CORRECTED NAVIGATION QUANTITIES AND AXLE-TACHOMETER DERIVED VALUES INITIALIZED AT TRANSPONDER SITES

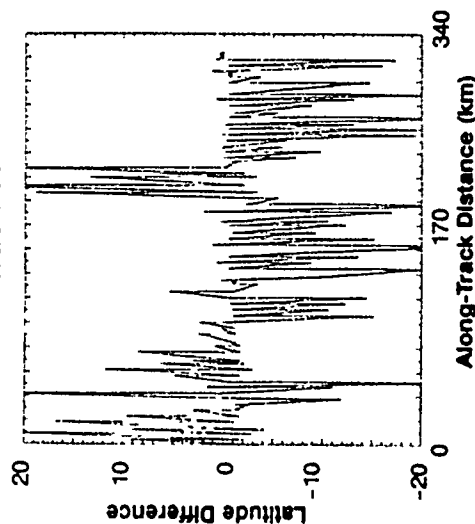
G-17139
10-11-89

Track Number	Latitude Difference		Longitude Difference		Starting Track Distance (km)
	Mean (m)	Sigma (m)	Mean (m)	Sigma (m)	
3	-4.2	8.3	4.0	4.2	10.1
5	-3.9	8.4	4.8	3.5	10.0
6	3.2	8.2	-0.16	4.5	16.6
8*	10.0	28.0	-5.6	23.0	50.0
9*	-9.0	23.0	12.0	22.0	0.0
10*	13.0	27.0	-7.3	24.0	50.0
11	-3.4	7.3	0.53	2.9	0.0
12	-0.77	17.0	4.2	4.6	0.0

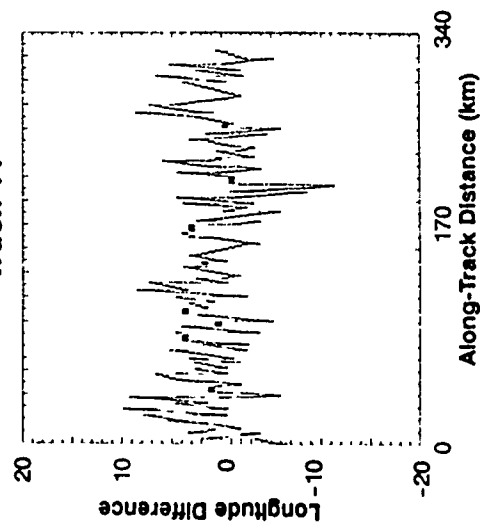
- Plots for other tracks are similar to track 11
- Differences are acceptable for registration of gravity quantities
- Larger differences associated with Albuquerque tracks reflect wider transponder spacing (9 vs. 3 miles)
- Initial portions of certain tracks exhibited differences significantly larger than the remainder of those tracks

* Albuquerque track (others are Dodge City Tracks)

Track 11



Track 11



COMPARISON OF CORRECTED POSITIONS AND APPARENT TRACK-TO-TRACK DIFFERENCES BETWEEN TRANSPONDER LOCATIONS

- Differences of transponder locations are near zero — consistent with Bell Aerospace's processing algorithm

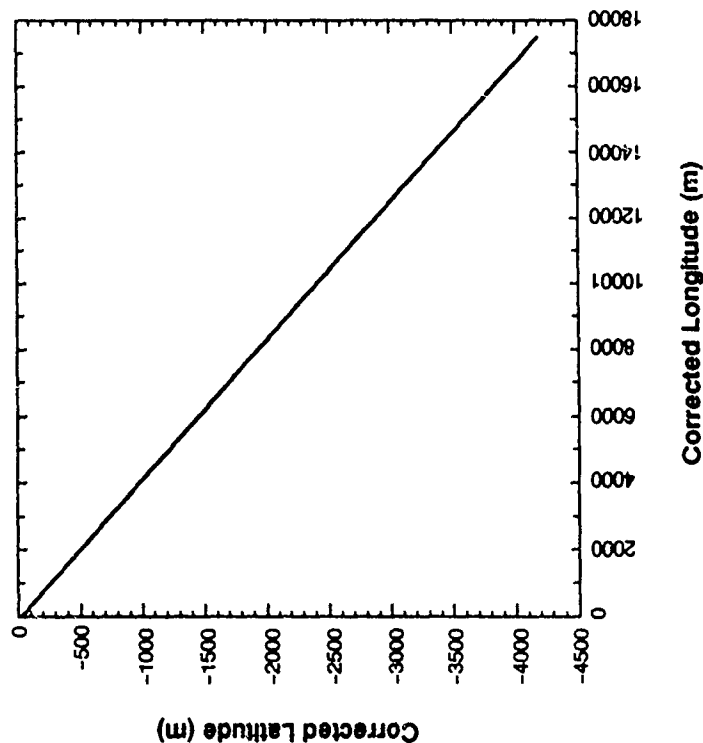
DODGE TRACK NUMBER	ALONG-TRACK DISTANCE (km) BETWEEN TRANSPONDERS 1 AND 61	ALBUQUERQUE TRACK NUMBER	ALONG-TRACK DISTANCE (km) BETWEEN TRANSPONDERS 62 AND 87
3	313.9617	8	482.4398
5	313.9470	9	484.5445
6	314.2555	10	483.3604
11	313.9690		
12	314.3449		

- Maximum track-to-track differences are about 400 m (Dodge) and 2100 m (Albuquerque)
- Because of consistency between corrected and axle tachometer outputs, these track-to-track differences are assessed as caused by temporary detours to track sidings

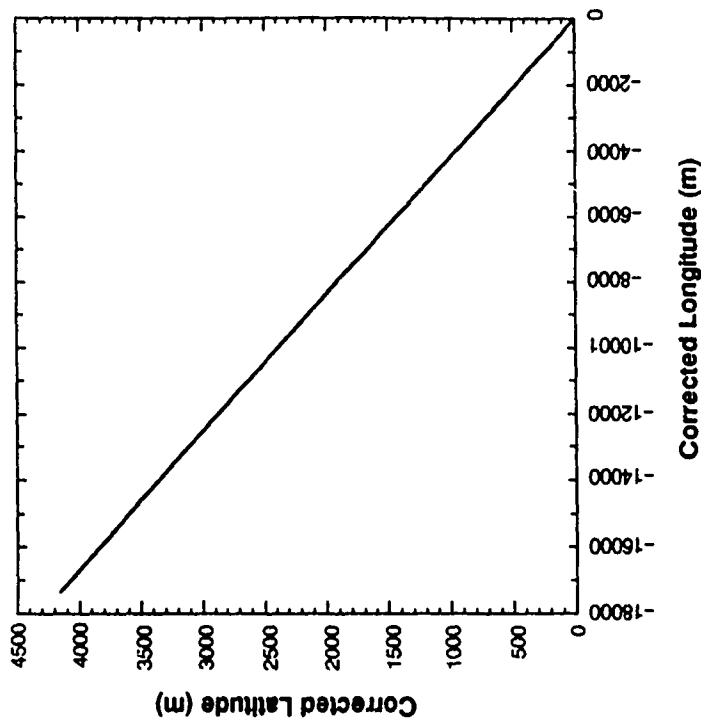
TYPICAL COMPARISON OF CORRECTED POSITIONS AND TOPOGRAPHIC MAPS

- 18-km straight section identified between ($37^{\circ}59'41''$, $101^{\circ}02'07''$) and ($37^{\circ}57'25''$, $100^{\circ}50'04''$)

Track 11



Track 12



- No significant deviations from straightness are apparent
- Implies that positions between transponders are sufficiently accurate to support registration of gravity quantities

SUMMARY OF NAVIGATION ASSESSMENT

- **Plots accurately reflect data collection scenarios**
- **Larger differences between corrected and axle transponder indicated positions for Albuquerque tracks than for Dodge City are consistent with greater transponder spacing**
- **Position data are sufficiently accurate at and between transponders for registration of gravity quantities**

GRADIOMETER DATA ANALYSIS

ANALYSIS OBJECTIVES

- **Determine power spectra of self-noise of GGIs**
- **Determine repeatability and coherence between traverses**
- **Estimate errors caused by vibrations and apply compensations**
- **Estimate errors caused by self-gradients and apply compensations**

TIME-SERIES DATA

- **Demodulated Gravity Gradiometer Instrument (GGI) outputs**

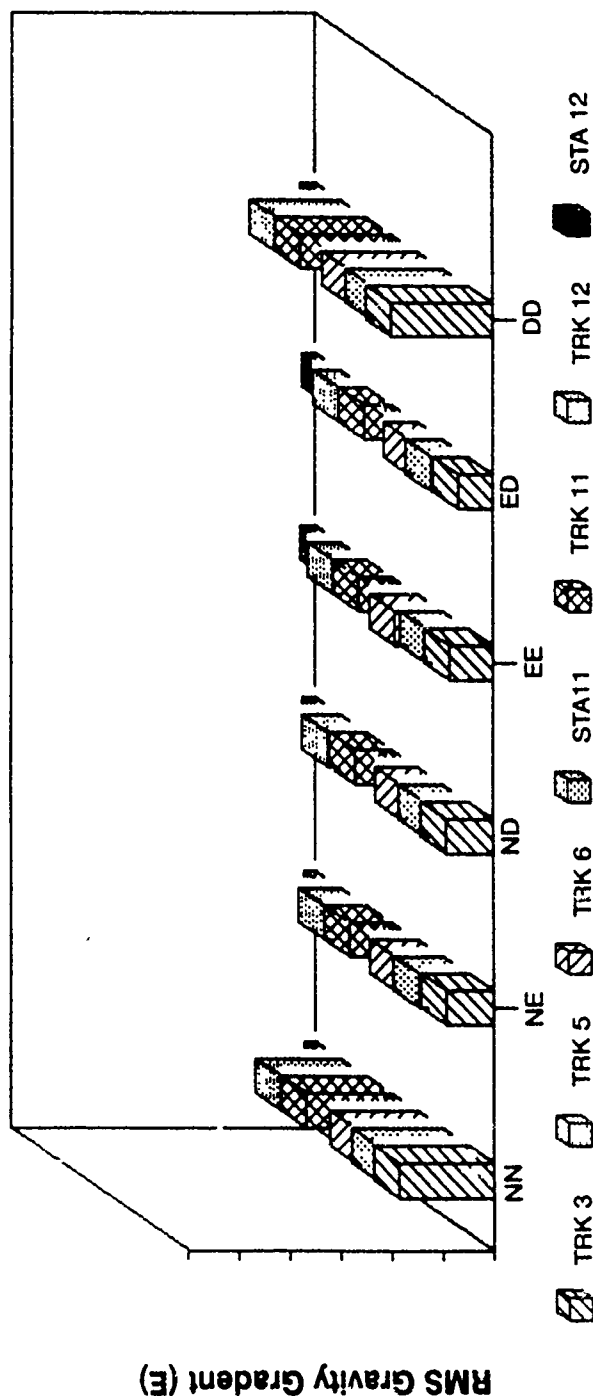
Inline and cross channel gradient element in instrument frame, sampled at 1 hertz (Hz)

Instruments carouselled on local-level platform

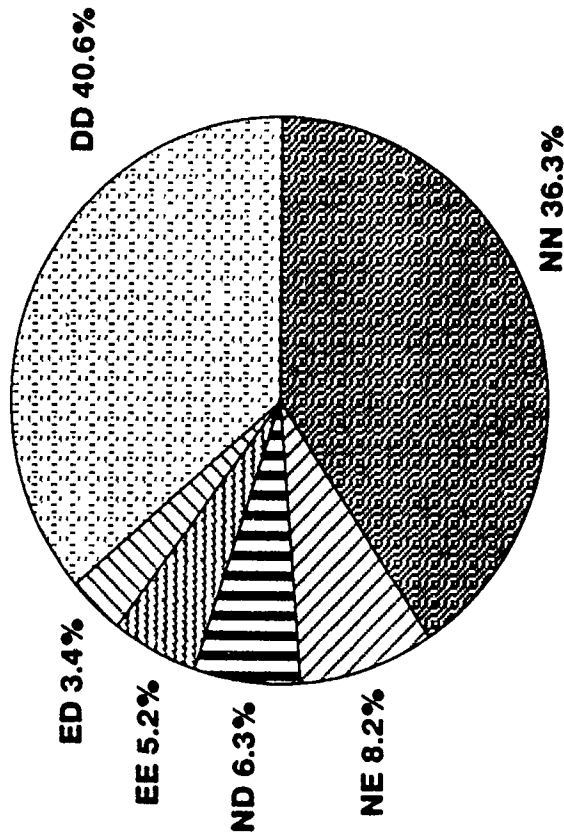
- **System time, distance traveled, carousel angle, and pitch, roll and yaw**
- **Acceleration in platform frame, three components (x, y, z) sampled at 128 Hz**

OVERVIEW OF DODGE CITY DATA

RMS GRADIENT MEASUREMENTS

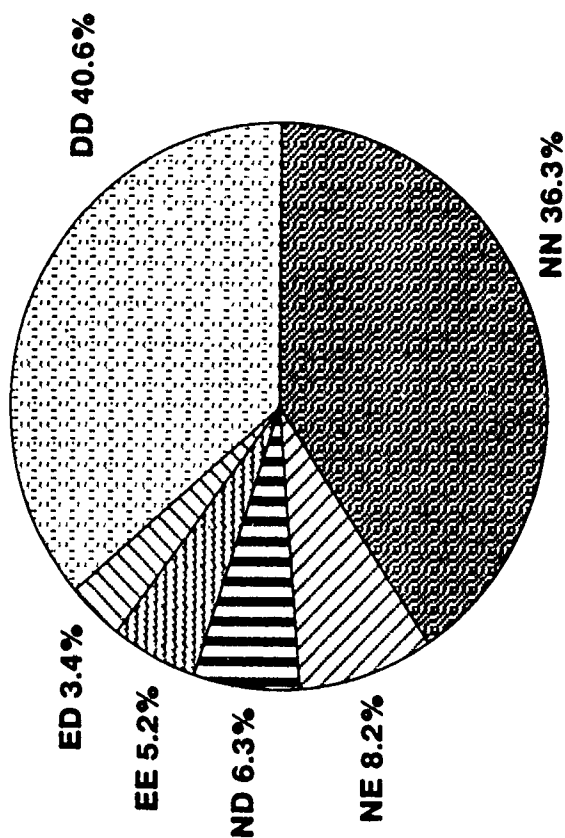


DISTRIBUTION OF VARIANCES FOR TRACK 11, DODGE CITY



- Most of variance (77%) is in DD and NN gradient measurements
- Only 17% of variance involves rates of change in east direction, which is predominantly in the along-track direction
- Anisotropic variances are result of correlation between rail-track and gravity-field geometries

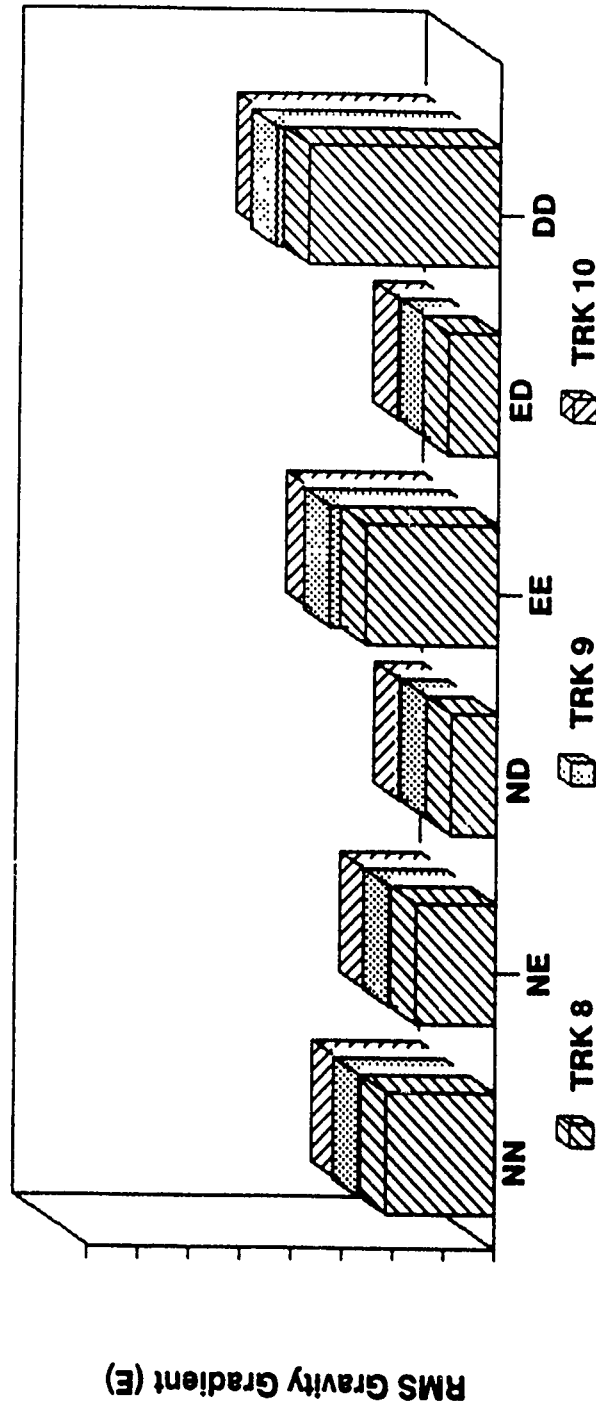
DISTRIBUTION OF VARIANCES FOR TRACK 11, DODGE CITY



- Most of variance (77%) is in DD and NN gradient measurements
- Only 17% of variance involves rates of change in east direction, which is predominantly in the along-track direction
- Anisotropic variances are result of correlation between rail-track and gravity-field geometries

OVERVIEW OF ALBUQUERQUE DATA

RMS GRADIENT MEASUREMENTS



- Consistency from track to track

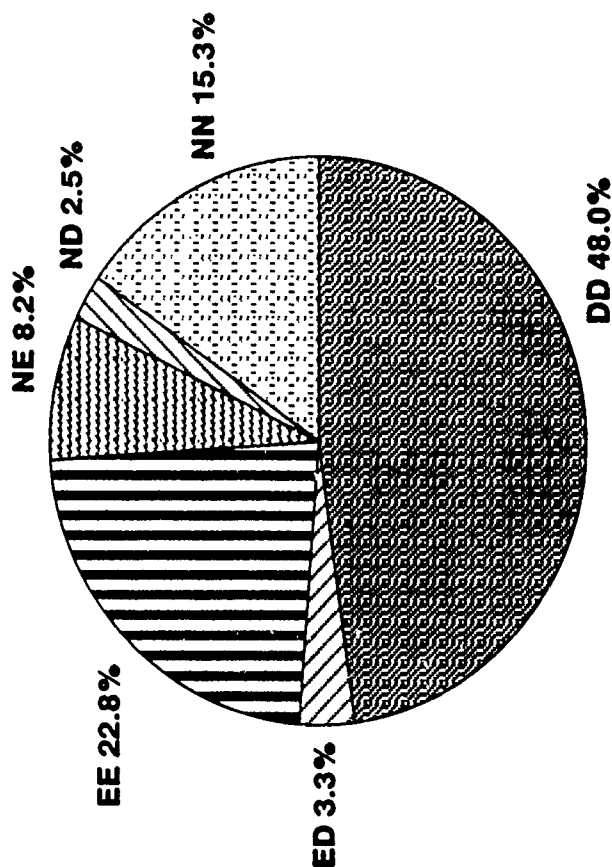
POTENTIAL BENEFIT OF SMOOTH GRAVITY FIELD ALONG-TRACK

- Data from gradiometer tests suggests that $a > 0.5$
- Foregoing analysis indicates that maximum distance over which deflection station can be transformed (at same accuracy) increases by the factor:

$$\Delta' = \frac{\Delta}{a} = 2\Delta$$

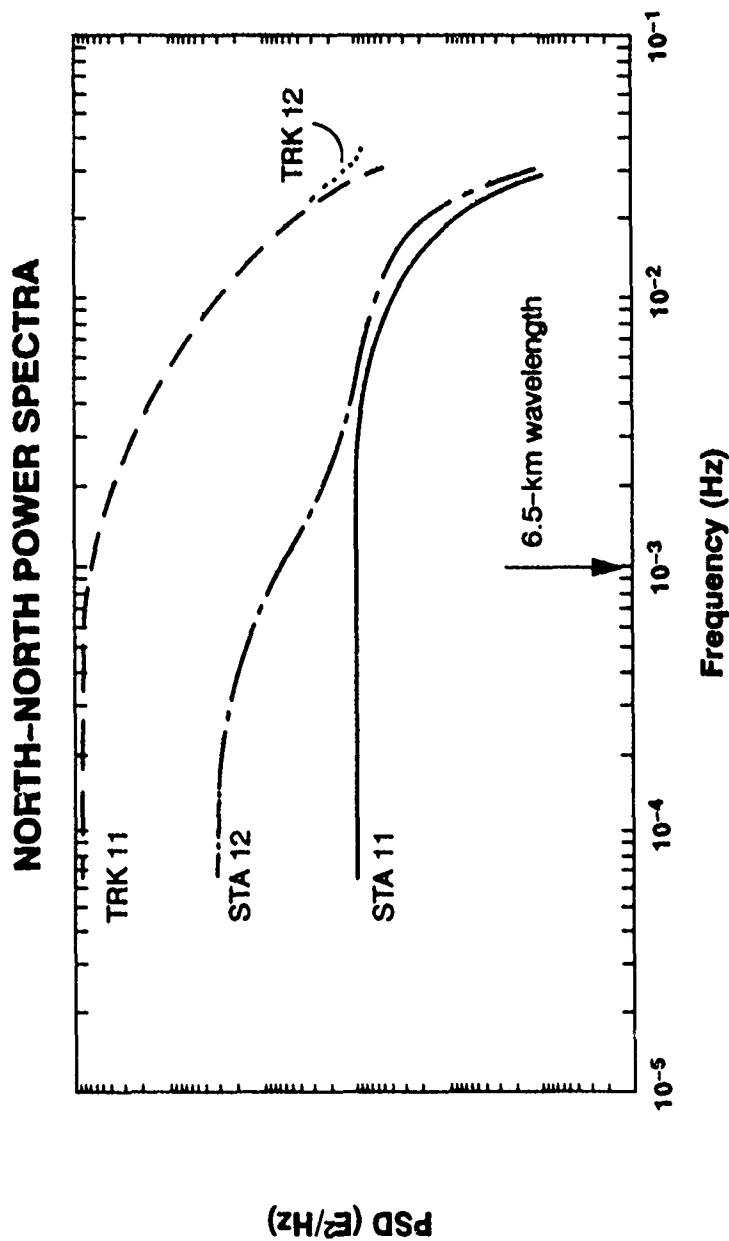
- For highly densified deflection coverage, number of astro stations required is reduced by a factor of two
- Concomitant reduction in survey cost
- Foregoing analysis needs refinement but general magnitude of benefit gained by accounting for anisotropy is quite encouraging

DISTRIBUTION OF VARIANCES FOR TRACK 8, ALBUQUERQUE



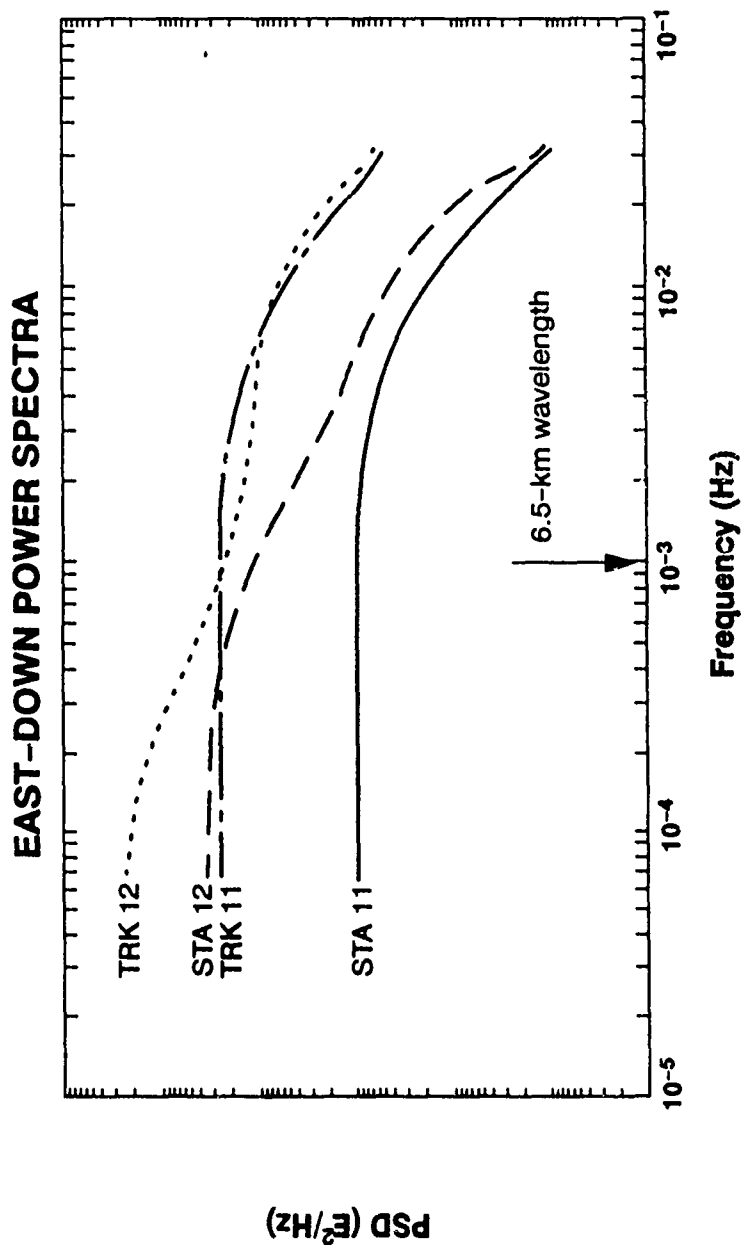
- DD variance (48%) approximately equals sum of NN, EE, and twice NE variances (54.5%); this is consistent with typical gravity-field models
- NN and EE variances are similar, because along-track direction changes significantly along Albuquerque tracks; this differs from Dodge City tracks

POWER SPECTRA FOR STATIONARY AND MOVING GGSS



- STA-11 and STA-12 data yield self-noise power spectra (PSDs) before and after tracks 11 and 12 were traversed
- Low-noise process appears in STA-12
- GGSS lowpass filter rolls-off spectra above 0.01 Hz

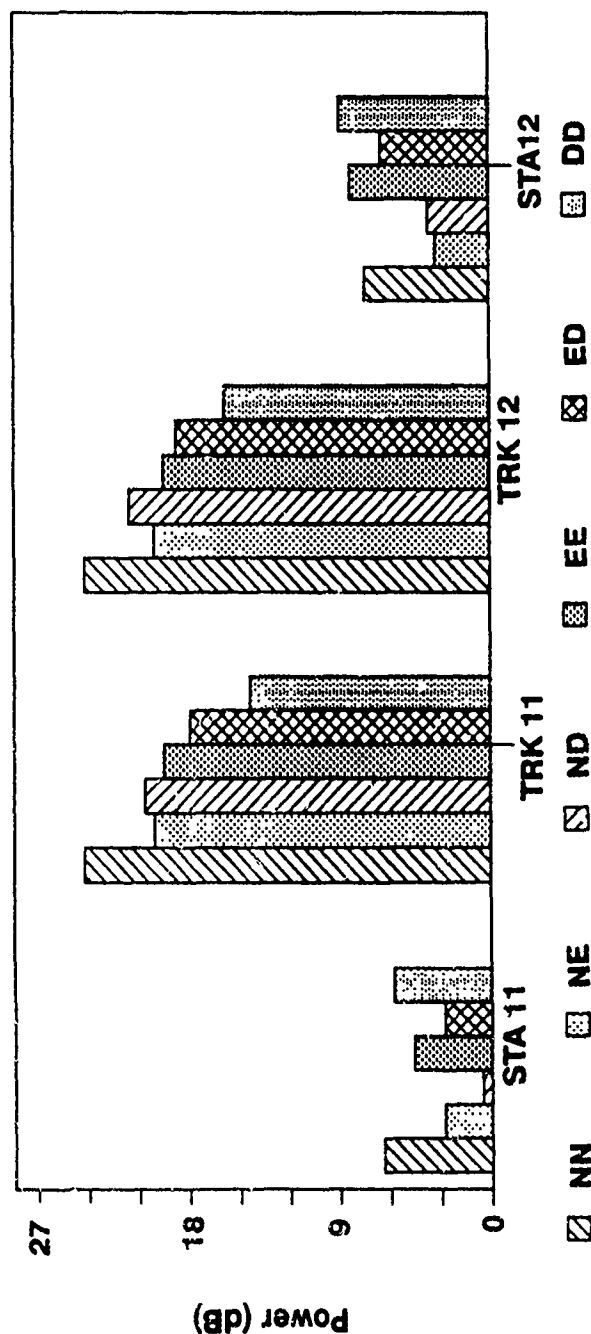
POWER SPECTRA FOR STATIONARY AND MOVING GGSS (Cont.)



- Increased spectrum level in TRK 12 at low frequencies supports hypothesis that self-noise increased during track 12 traverse

ENVIRONMENTALLY INDUCED NOISE

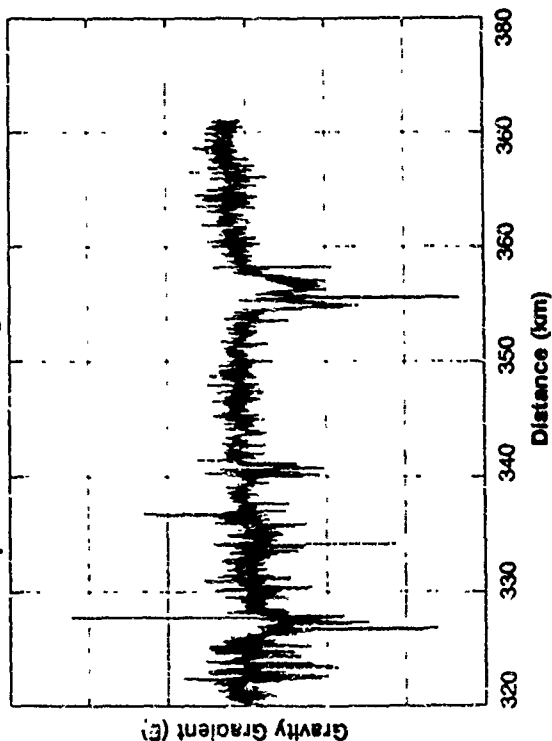
HIGH-FREQUENCY POWER LEVELS, DODGE CITY



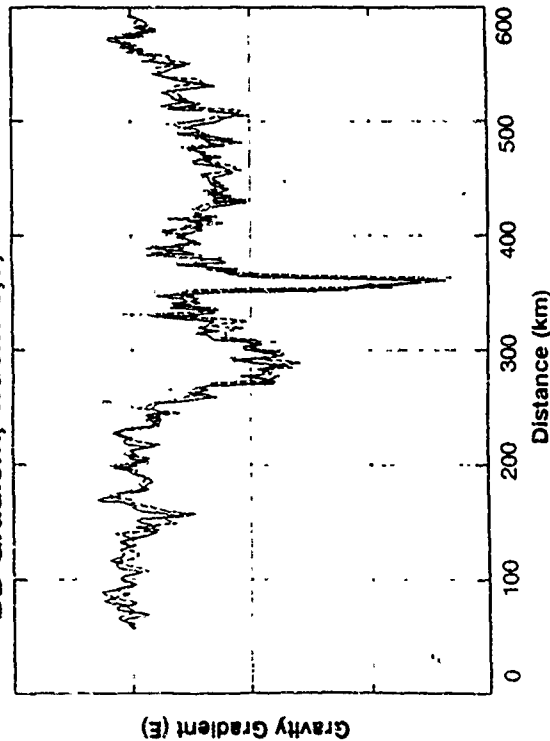
- Figure shows PSD levels in decibels at 0.01 Hz for stationary and moving GGSS
- Low spectral coherence (between tracks 11 and 12) for ND, EE, and ED support hypothesis that high-frequency power in these channels is predominantly caused by induced noise (not gravity gradients)
- Conclusion: Induced noise level is about 12 dB higher than self-noise of stationary GGSS

REPEATABILITY OF GRADIENT MEASUREMENTS, ALBUQUERQUE

Closeup View Showing Data Consistency



DD Gradient, Tracks 8,9, and 10

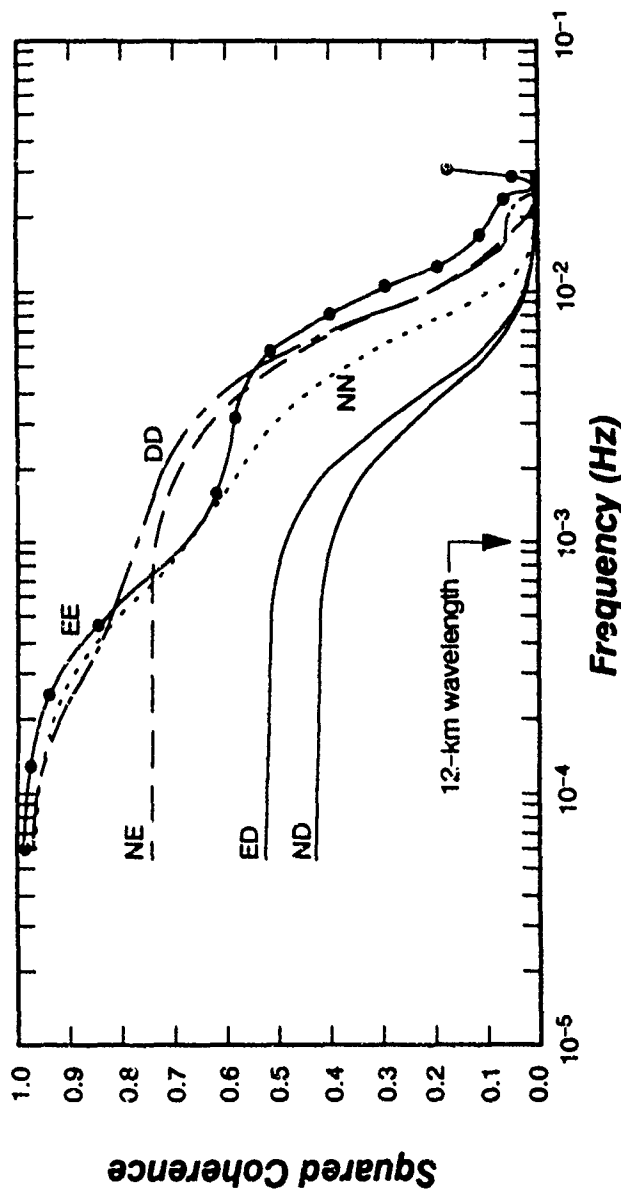


- Upper plot shows closeup of large DD gravity feature
- Tracks 8,9, and 10 are slightly displaced for visualization
- A few isolated spikes are visible in lower plot
- These data show obvious repeatability in data

OBJECTIVE MEASURE OF REPEATABILITY BETWEEN TRACKS 8 AND 10

G-17143
10-11-89

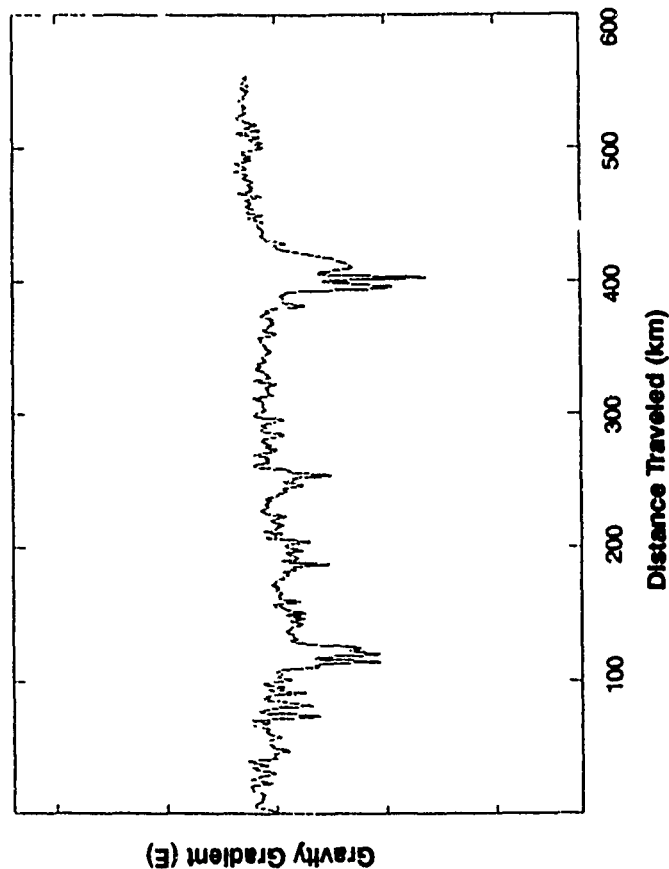
Squared Coherences, Tracks 8 and 10



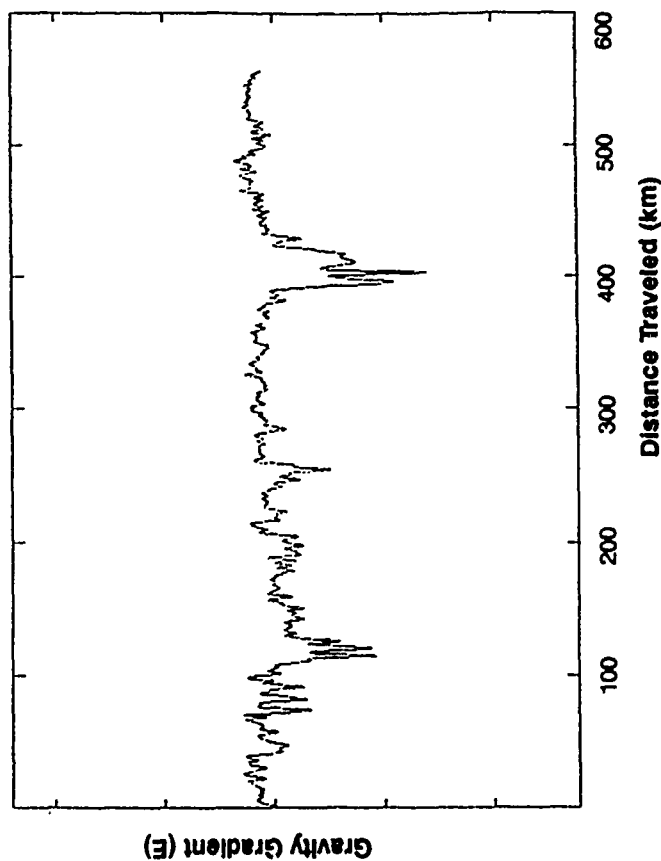
- Squared coherence measures fraction of variance in one time series explained by a linear time-invariant transformation of another time series
- Squared coherence is estimated using a canonical-variates state-space modeling technique
- NN, EE, and DD have largest coherences (C), because their signal-to-noise ratios (SNR) are largest ($SNR = \frac{C}{1-C}$)

EXAMPLES OF TIME SERIES HAVING HIGH COHERENCES

Lowpass DD gradient ($C > 0.95$)
Track 8



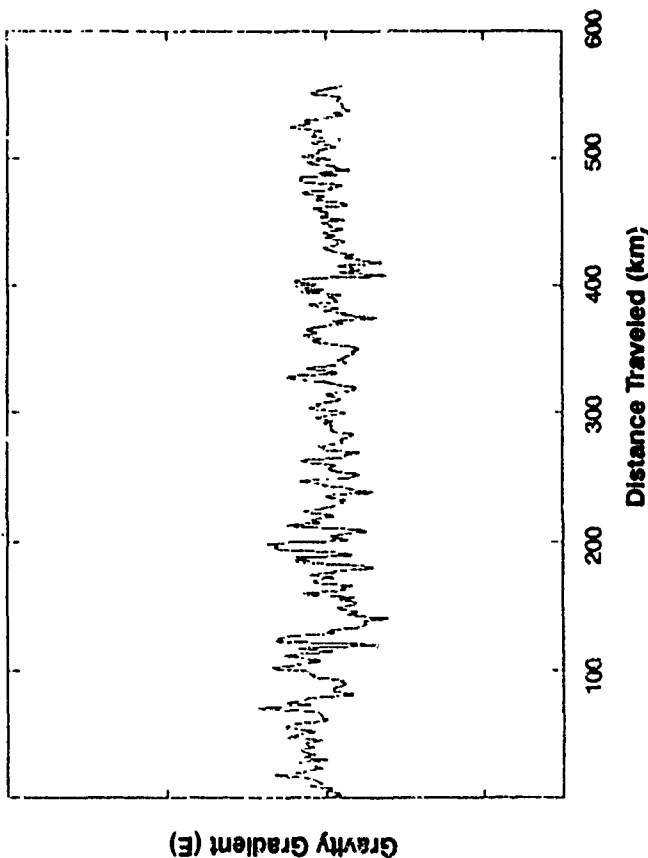
Lowpass DD gradient ($C > 0.95$)
Track 10



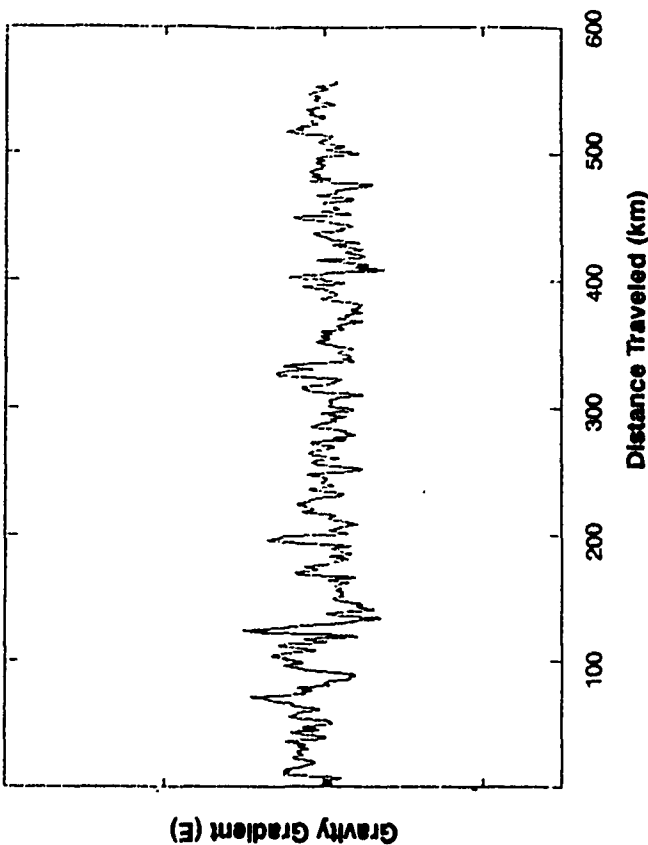
Lowpass filter has half-power frequency
corresponding to 60-km wavelength

EXAMPLES OF TIME SERIES HAVING LOW COHERENCES

Lowpass ED gradient ($C = 0.5$)
Track 8

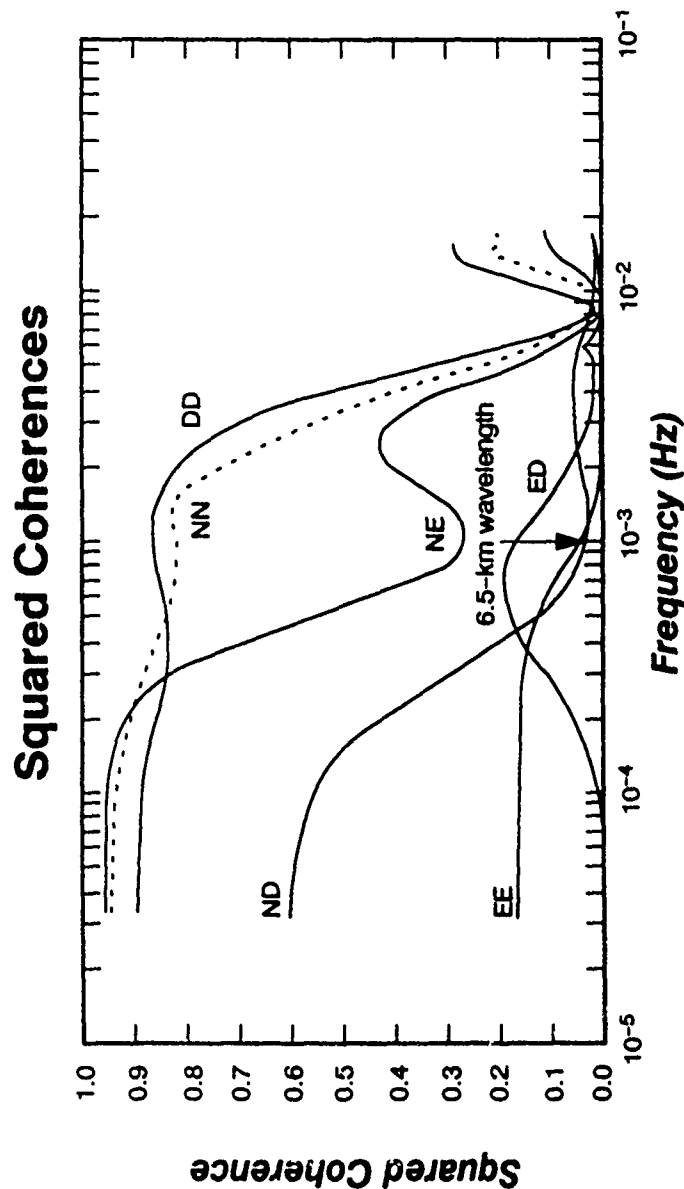


Lowpass ED gradient ($C = 0.5$)
Track 10



Lowpass filter has half-power frequency
corresponding to 60-km wavelength

REPEATABILITY BETWEEN TRACKS 11 AND 12

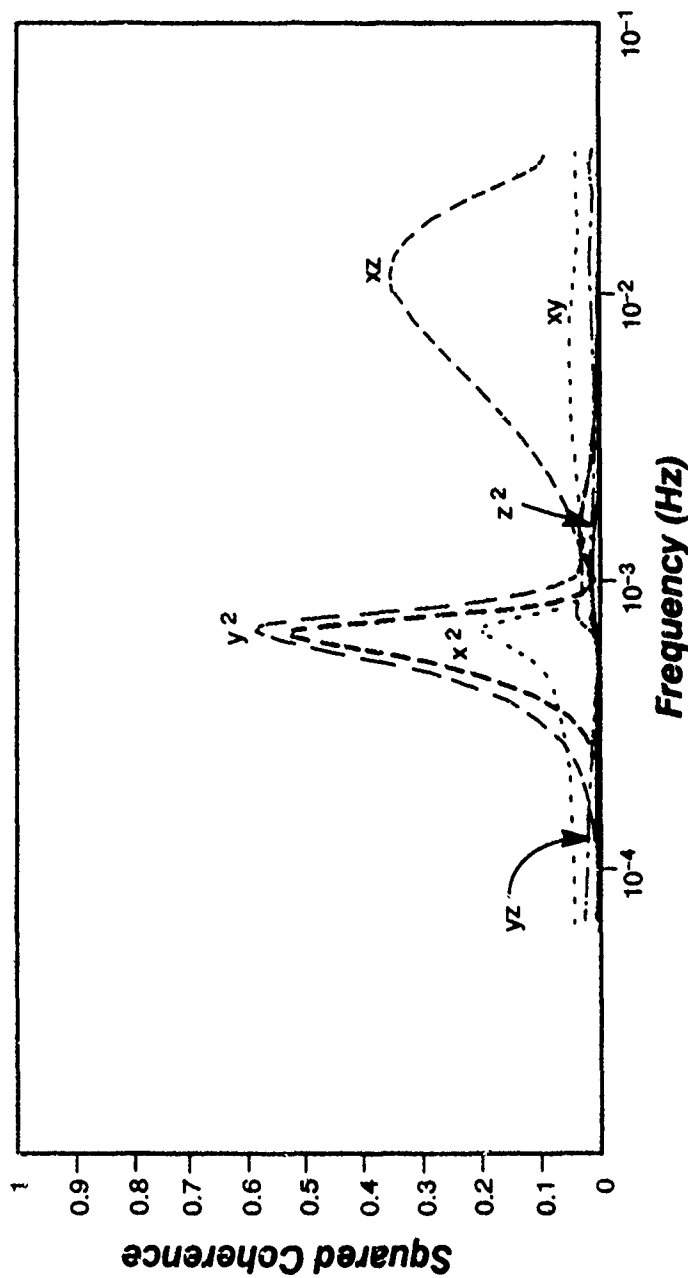


- NN and DD gradients are most repeatable because they have highest signal levels
- Gradients involving gravity changes in east direction (*predominantly along-track direction*) have small signal levels and are incoherent (except for NE at wavelengths longer than 25 km)

ACCELERATION-INDUCED GGSS MEASUREMENT ERROR

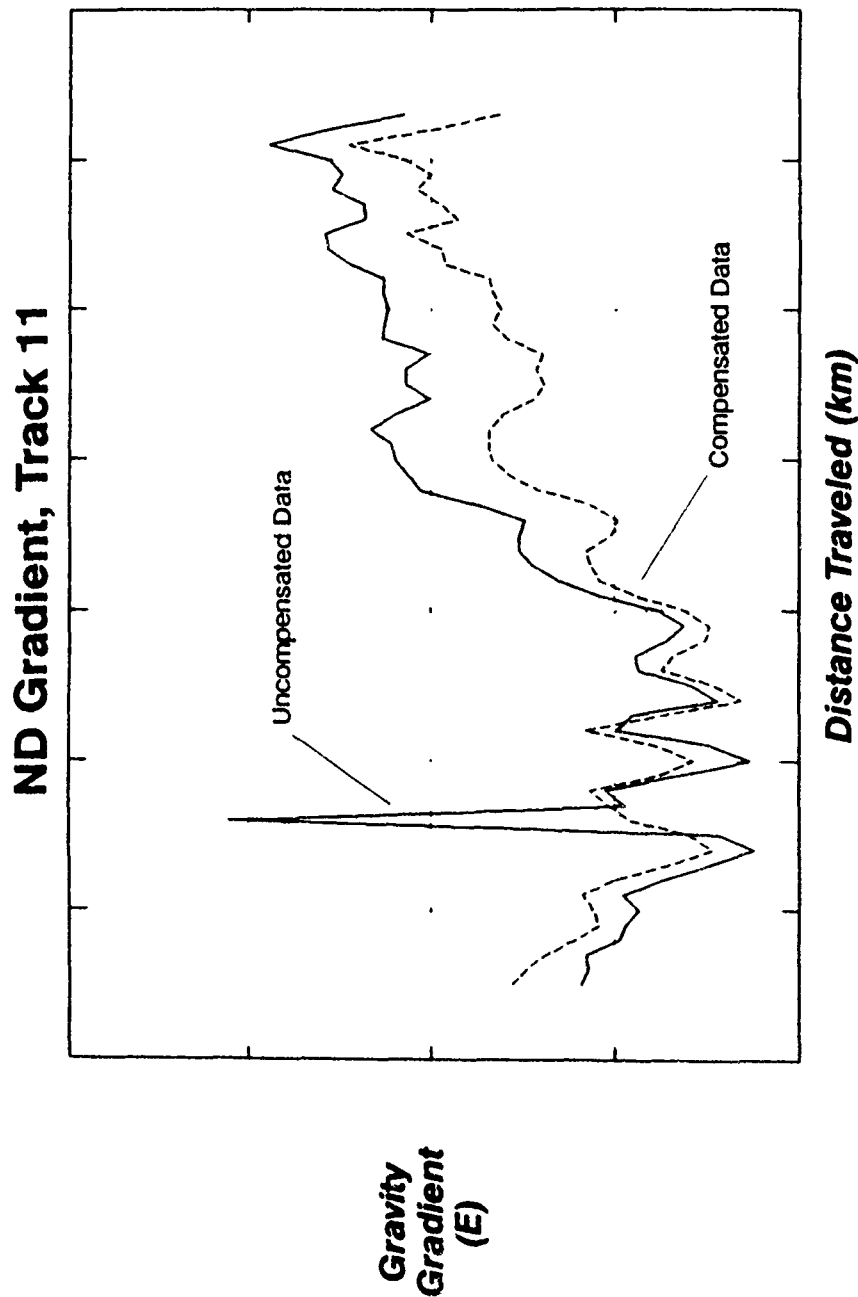
G-17146
10-11-89

Squared Coherence Between GGI1, Inline, and Acceleration Power, Track 11



- Peak at 7×10^{-4} Hz shows that acceleration powers (lowpass squared acceleration components x^2 , y^2 , z^2 , xy , xz , yz) are correlated with GGI output signal near carouselling frequency (and at higher frequencies for xz)
- State-space model (developed to estimate coherence) provides basis for compensation of GGI data using acceleration measurements
- Note: Inline signals near 7×10^{-4} Hz are heterodyned to low frequencies when the carouselled GGI outputs are transformed to local-level coordinates

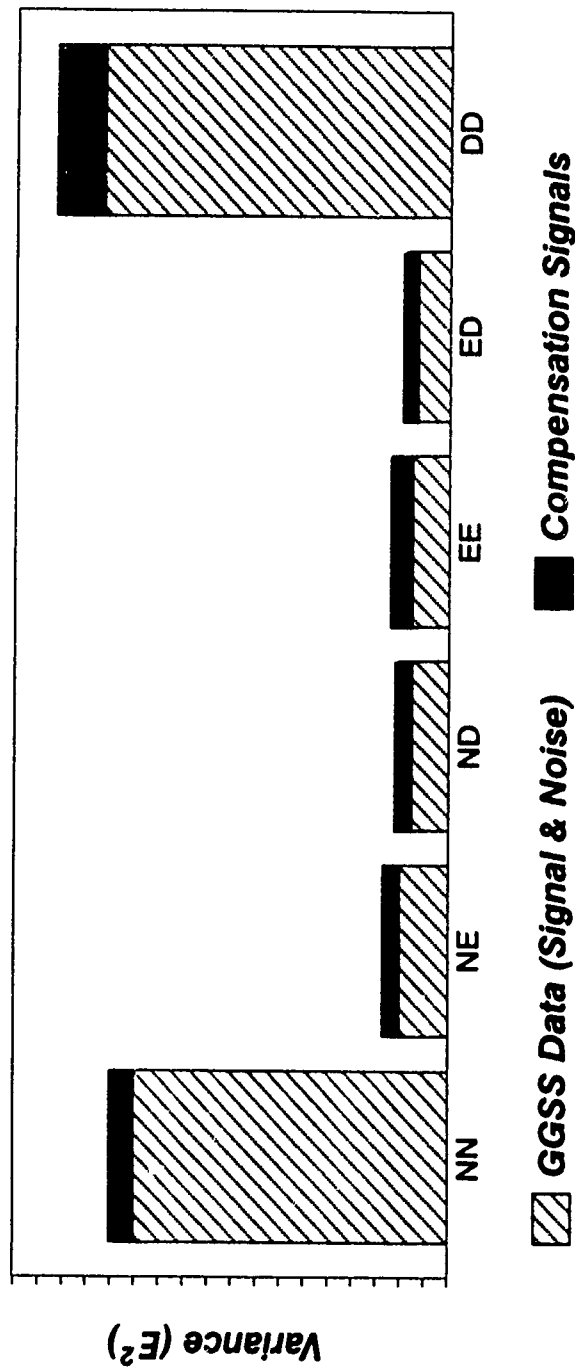
EXAMPLE OF ACCELERATION COMPENSATION



Example shows that compensation is broadband

COMPENSATION VARIANCES

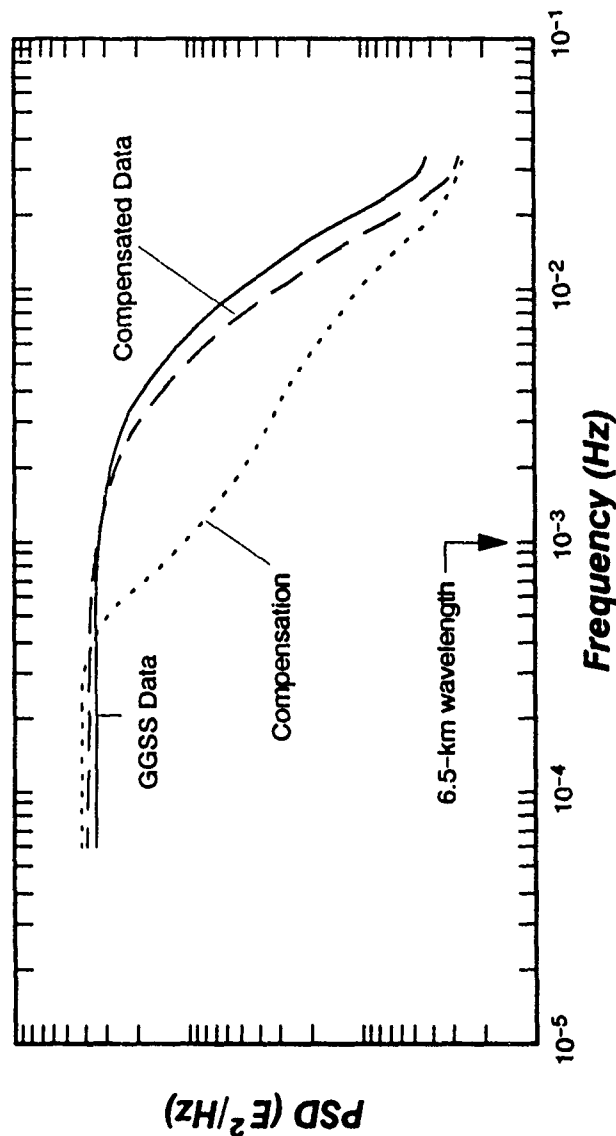
Variances: GGSS Data and Compensation Signals, Track 11



- Acceleration compensation variances are significant for all gradient elements
- Largest fractional improvement occurs for NE, ND, EE, and ED gradients

COMPENSATION POWER SPECTRA

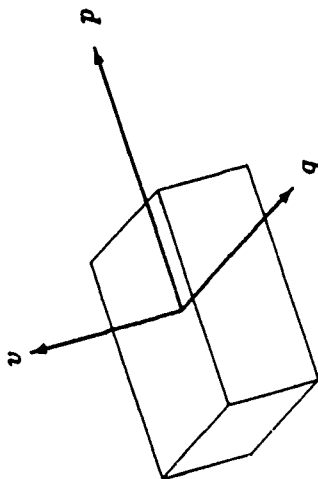
Spectra for ED, Track 11



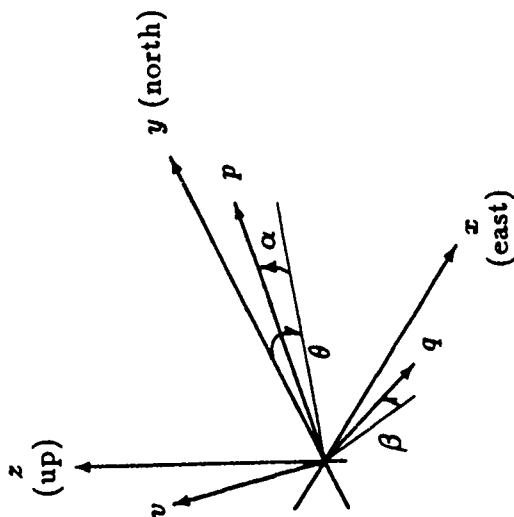
- Compensation reduces high-frequency noise level 2.2 dB
- Apparent over compensation at low frequencies may be spectrum estimation limitation with finite time series
- *Conclusion:* Additional vibration compensation technique should be considered

ENROUTE SELF-GRADIENT CALIBRATION

Body Frame



Coordinate Systems



- Original motivation: rail car gradiometer calibration
- Self-gradients are biases in body frame
- Directional changes of survey vehicle modulate self-gradients in local-level frame
- Transform measurements into body frame and subtract a mean

VEHICLE SELF GRADIENTS

Gravity gradiometer measures linear combinations of gradients in the instrument (I) frame

These measurements are transformed to a local-level (l) frame and expressed in terms of the individual gradients

$$Z_l = \begin{bmatrix} T_{NN} & T_{NE} & T_{ND} \\ T_{EN} & T_{EE} & T_{ED} \\ T_{DN} & T_{DE} & T_{DD} \end{bmatrix} = C_i^l Z_i C_i^l$$

The measured gradients consist of earth's field (e), self-gradients (s) and noise (N)

$$Z_l = \Gamma_{el} + \Gamma_{sl} + N_l$$

If the gradiometer platform were constrained not to rotate with respect to host vehicle, then Γ_{sl} would be time invariant (a bias)

Thus we are motivated to transform the measurements into a frame in which the gradiometer platform does not rotate

VEHICLE SELF GRADIENTS IN THE BODY FRAME

Varying attitude and heading define a time varying transformation between body coordinates (b) and the local level frame (l)

$$Z_b = C_b^l(t) Z_l C_l^b(t) = C_b^l \Gamma_{el} C_l^b + \Gamma_{sb} + C_b^l N_l C_l^b$$

Since Γ_{sb} is constant, it is easily estimated and removed if enough measurements are taken along a traverse to reduce the path average of the earth gradients, i.e.,

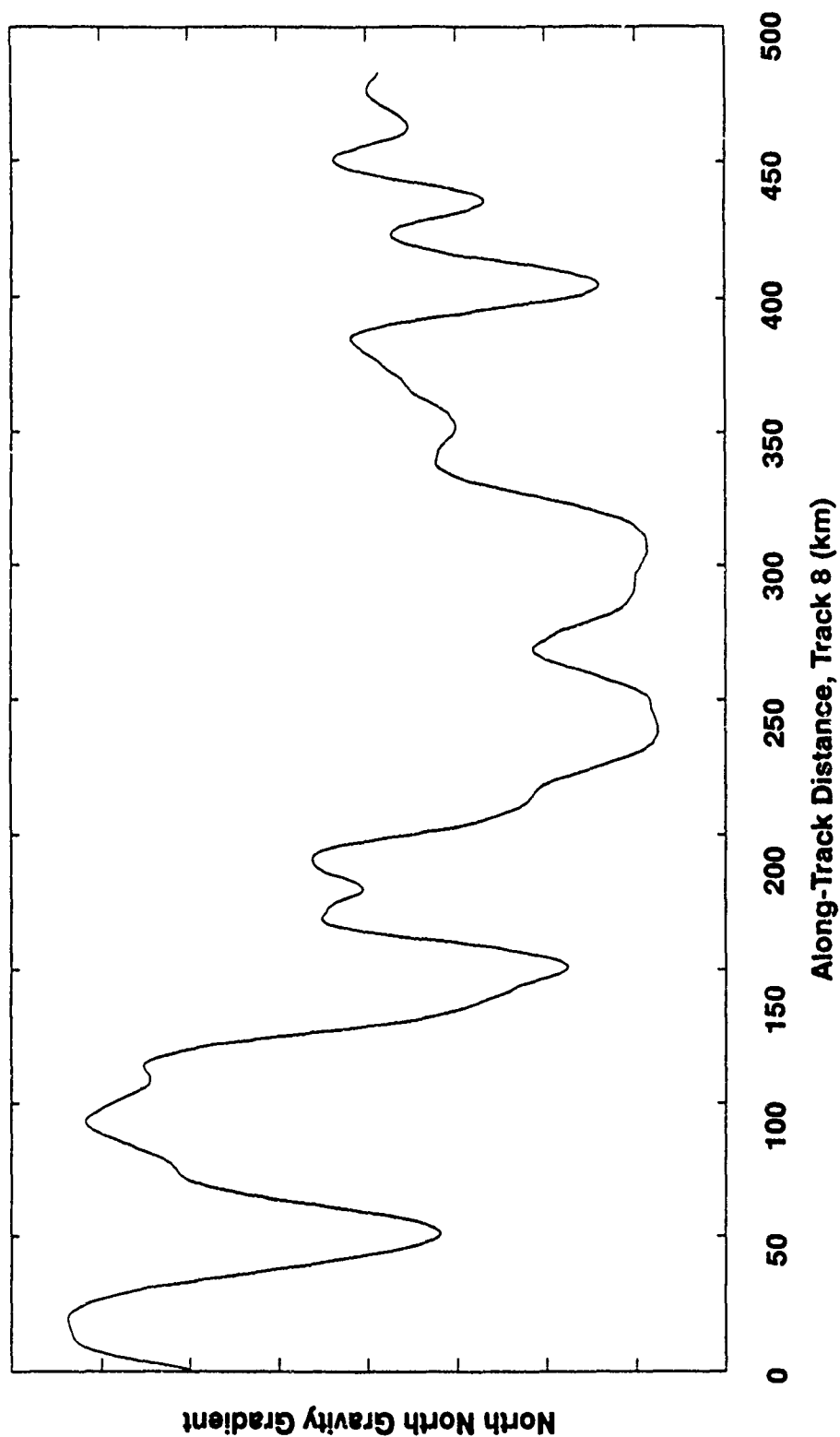
Average of Z_b is equal to Γ_{sb} if averaging interval $\Delta t \gg$ correlation distance of $(C_b^l \Gamma_{el} C_l^b)$ and that of the noise

Once the self gradients have been estimated, rotate the measurements back to the local level frame

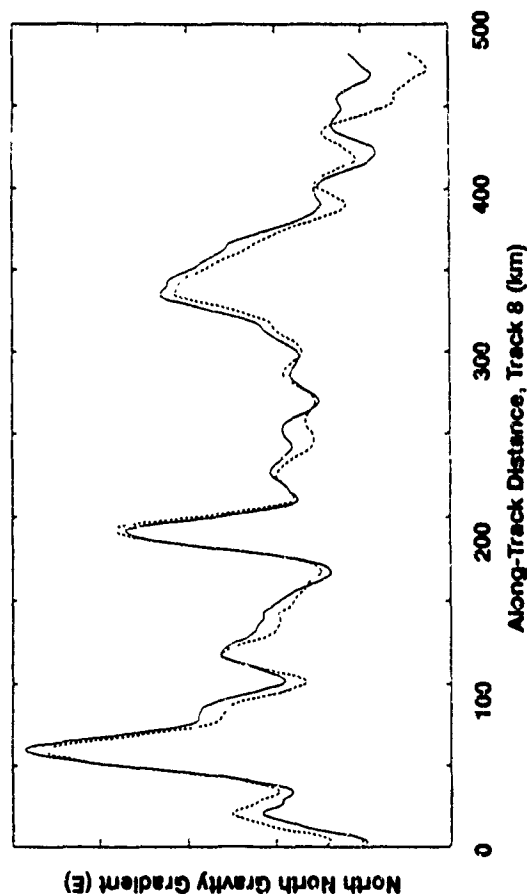
$$Z_l' = C_l^b [(Z_b - Z_b(\text{average}))] C_b^l$$

Foregoing formulation considers only second-order gradients which transform as above — higher-order self-gradients have smaller effect

TYPICAL ALBUQUERQUE TRACK SELF-GRADIENT COMPENSATION



TYPICAL ALBUQUERQUE TRACK SELF-GRADIENT COMPENSATION



RMS Difference*

	nn	ne	nd	ee	ed	dd
Before Compensation	0.291	0.300	0.763	0.170	0.672	0.203
After Compensation	0.282	0.307	1.720	0.170	0.772	0.194

* Normalized by the standard deviation of the corresponding gradient on the outbound track

IMPLICATIONS OF SELF-GRADIENT ANALYSIS ON RAIL TEST DATA

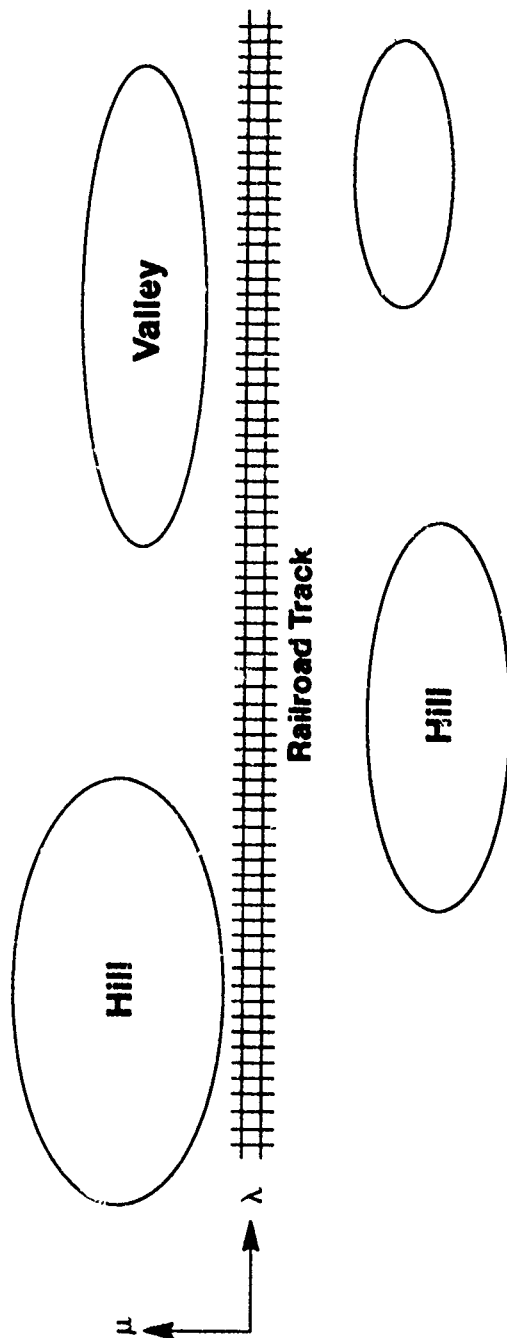
- **Compensation is significant**
- **However it does not contribute to a major share of the residual gradient signal**
- **Result is typical of all gradient elements, all three Albuquerque tracks**
- **Similar, but smaller effect on the Dodge City tracks**

PRIMARY CONCLUSIONS FROM DATA ANALYSIS

- **Self-noise levels of stationary GGSS data are 12 dB to 18 dB lower than high-frequency noise levels on tracks 11 and 12**
- **Repeatability varies with frequency and gradient signal strength**
 - Stronger signals, e.g., NN, EE, and DD on tracks 8 and 10, had coherences > 0.75 for wavelengths longer than 15 km
 - Weaker signals, e.g., EE and ED on tracks 11 and 12, had coherences < 0.20 for all wavelengths
- **Our computations for acceleration and self-gradients are significant, but they account for only a fraction of the total measurement noise**

SPECIAL GRAVITY GRADIENT SIGNATURE ALONG RAILROAD TRACKS

RATIONALE FOR OBSERVED DIRECTIONAL BEHAVIOR OF GRADIENTS



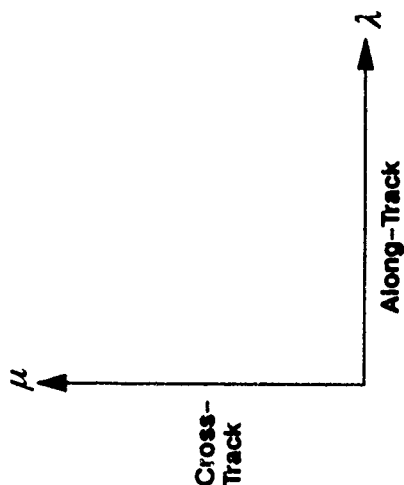
- rms λ - gradient is small due to gentleness of railbed slopes and elevation of grade above density contrasts
- rms λ - gradient is smaller for same reasons as above and reduced rms of value cross gradients vs. inline gradients
- rms μ - gradient is large due to mass contrast on opposite sides of railroad grade
- rms μ - gradient is moderate for same reasons as above but offset by reduced rms of cross gradients vs inline gradients
- rms μ - gradient is small due to cross-track uniformity of roadbed
- rms z - gradient behaves like μ μ -gradient (by Laplace's Equation)

SUMMARY OF DIRECTIONAL DEPENDENCE OF HORIZONTAL-INLINE GRADIENTS

DATA TRACK	TRAVERSE ROUTE	rms GRADIENTS NORTH (N) AND EAST (E) $\frac{\sigma_{NN}}{\sigma_{EE}}$	rms GRADIENTS ALONG-TRACK (λ) AND CROSS-TRACK (μ) $\frac{\sigma_{\mu\mu}}{\sigma_{\lambda\lambda}}$
8	Albuquerque ➡ La Junta	0.82	3.68
9	La Junta ➡ Albuquerque	0.81	3.85
10	Albuquerque ➡ La Junta	0.81	3.71
11	La Junta ➡ Dodge City	2.60	3.00
12	Dodge City ➡ La Junta	2.70	2.15

Also note higher rms on Albuquerque route $\frac{\sigma_{\lambda}(8, 9, 10)}{\sigma_{\lambda}(11, 12)} \sim 1.7$

IDEALIZED MODEL OF GRADIENT ANISOTROPY ALONG-TRACK VS CROSS-TRACK



Consider Case When

- 1) Vertical deflection variance is independent of track direction
- 2) RMS along-track gradient is a fraction, a of the RMS cross-track gradient

$$\sigma_{\mu}^2 = \sigma_{\lambda}^2$$

$$\sigma_{\lambda\lambda} = a\sigma_{\mu\mu}$$

For attenuated white noise disturbance potential model,* foregoing implies that along-track deflection correlation distance, D_{λ} stretches in accordance with

$$D_{\lambda} = D_{\mu}/a$$

where D_{μ} is the cross-track correlation distance

* Similarly scaled relations apply to other gravity models

QUICK LOOK AT EFFECT OF GRADIENT ANISOTROPY ON RAILBED DEFLECTION SURVEY DENSIFICATION



For Δ small compared to the correlation distance, D_λ , rms deflection estimation error, is given by

$$\xi_{\text{rms}} = \sigma_\xi f\left(\frac{\Delta}{D_\lambda}\right)$$

Where $f\left(\frac{\Delta}{D_\lambda}\right)$ depends upon the estimator's statistical gravity model and additional gravity sensors used to aid in the interpolation.

Case I: Isotropic field assumed ($D_\lambda = D_\mu = D$) and survey error specification is:

$$\xi_{\text{rms}} \leq \xi_{\text{max}}$$

Implies maximum transfer distance is

$$\Delta \leq D f^{-1}(\xi_{\text{max}}/\sigma_\xi)$$

Case II: Deflection correlation distance along-track, D_λ is multiple of D ,

$$D_\lambda = D/a$$

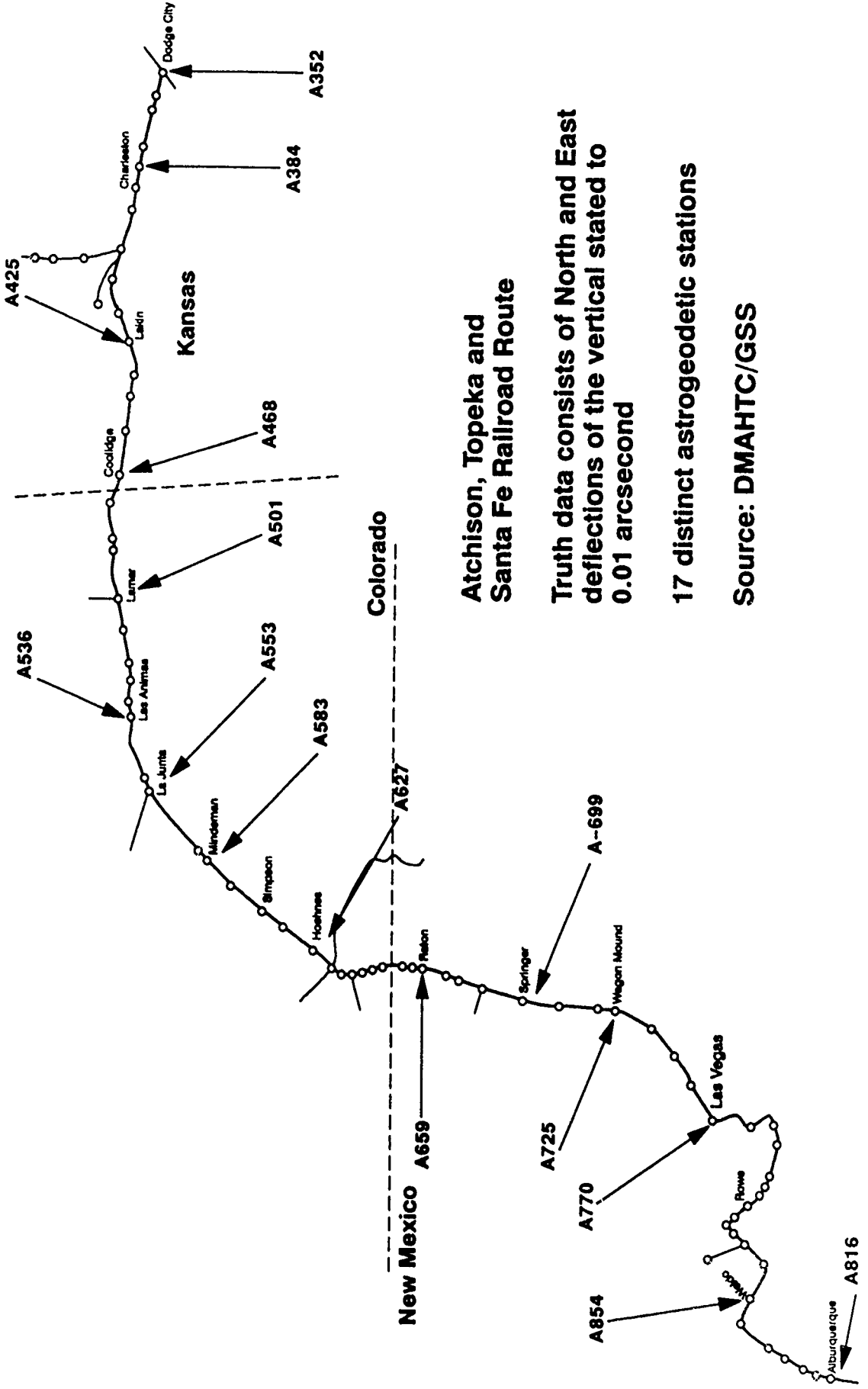
Implies maximum transfer distance increases to

$$\Delta' \leq D_\lambda f^{-1}(\xi_{\text{max}}/\sigma_\xi) = \Delta/a$$

COMPARISONS WITH TRUTH DATA

ASTRO SITE LOCATIONS

TRUTH DATA



Atchison, Topeka and
Santa Fe Railroad Route

Truth data consists of North and East
deflections of the vertical stated to
0.01 arcsecond

17 distinct astrogeodetic stations

Source: DMAHTC/GSS

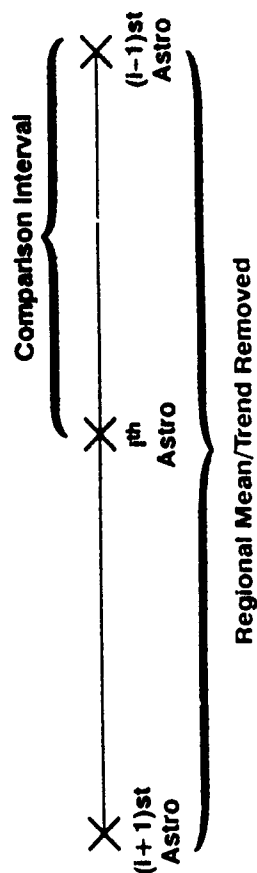
COMPARISONS WITH TRUTH DATA

- Insufficient signal strengths of along-track, vertical gradients precluded comparisons with δg_z
- Similar situation for along-track deflection of the vertical estimates
- Cross-track deflection data spaced at excessive astro station "tie-point" distances to be conclusive
- Comparisons formulated to provide qualitative performance indicator as follows

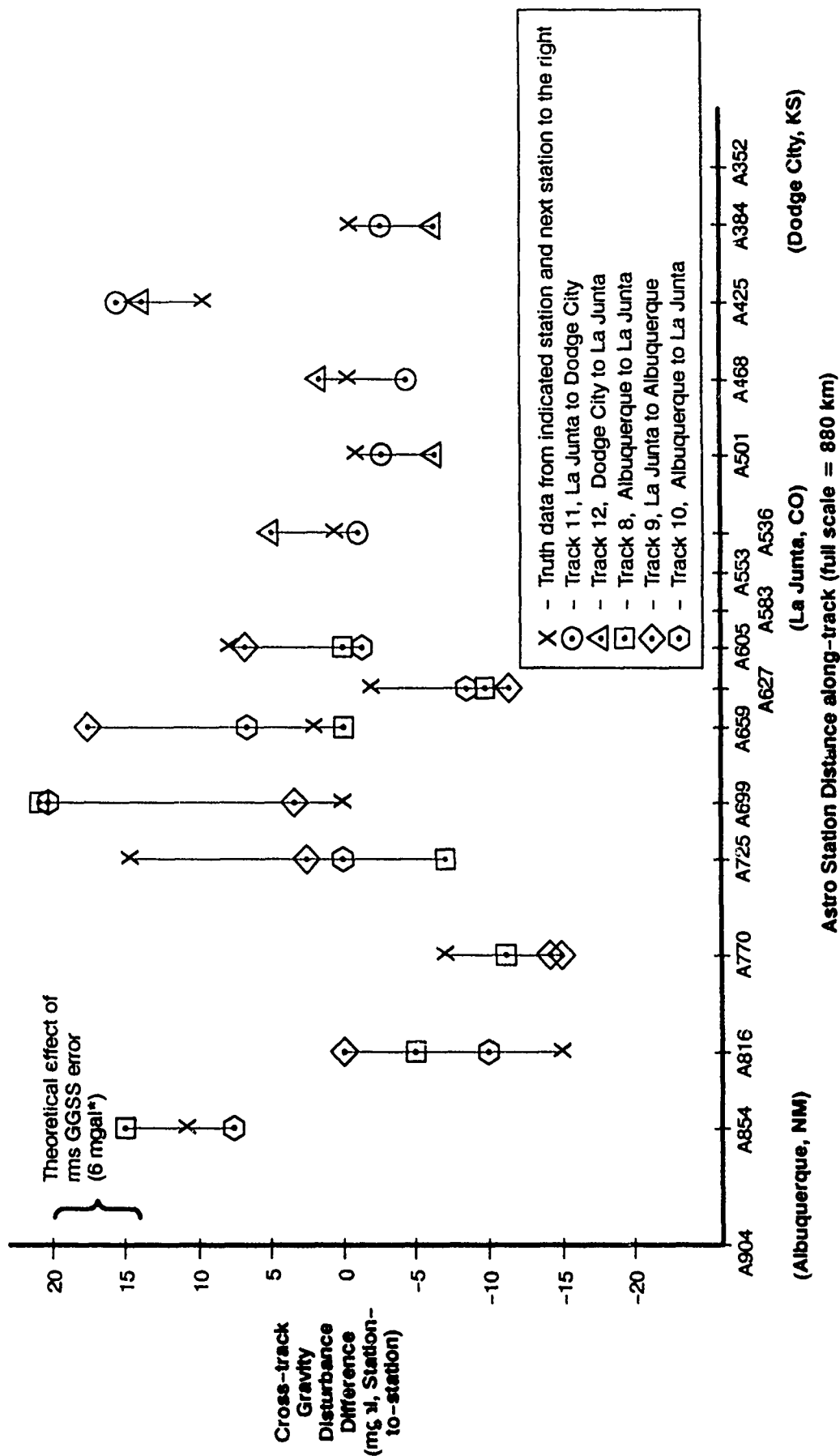
Truth data = station-to-station deflection difference less "regional trend"

GGSS data = integrated $\lambda\mu$ - cross gradients less "regional mean"

Regional mean and trend computed over range defined by three astro stations



TRUTH DATA VS GGSS ESTIMATES



* Varies with station spacing

SUMMARY FINDINGS FROM RAIL TESTS

- **Severe vibration environment dominated the data and its reduction**
- **GGSS demonstrated operational robustness despite abuse not typically applied to inertial instruments**
- **System measured strong gravity gradient signals with excellent repeatability**
- **Weak gradient signals were submerged beneath acceleration-induced noise**
- **Data quantified hitherto unknown gravity gradient structure of railroad beds**
- **Along-track smoothness will reduce railroad astro survey densification costs significantly**

Obtaining Earth Surface and Spatial Deflections of the Vertical from
Free-Air Gravity Anomaly and Elevation Data Without Density Assumptions.

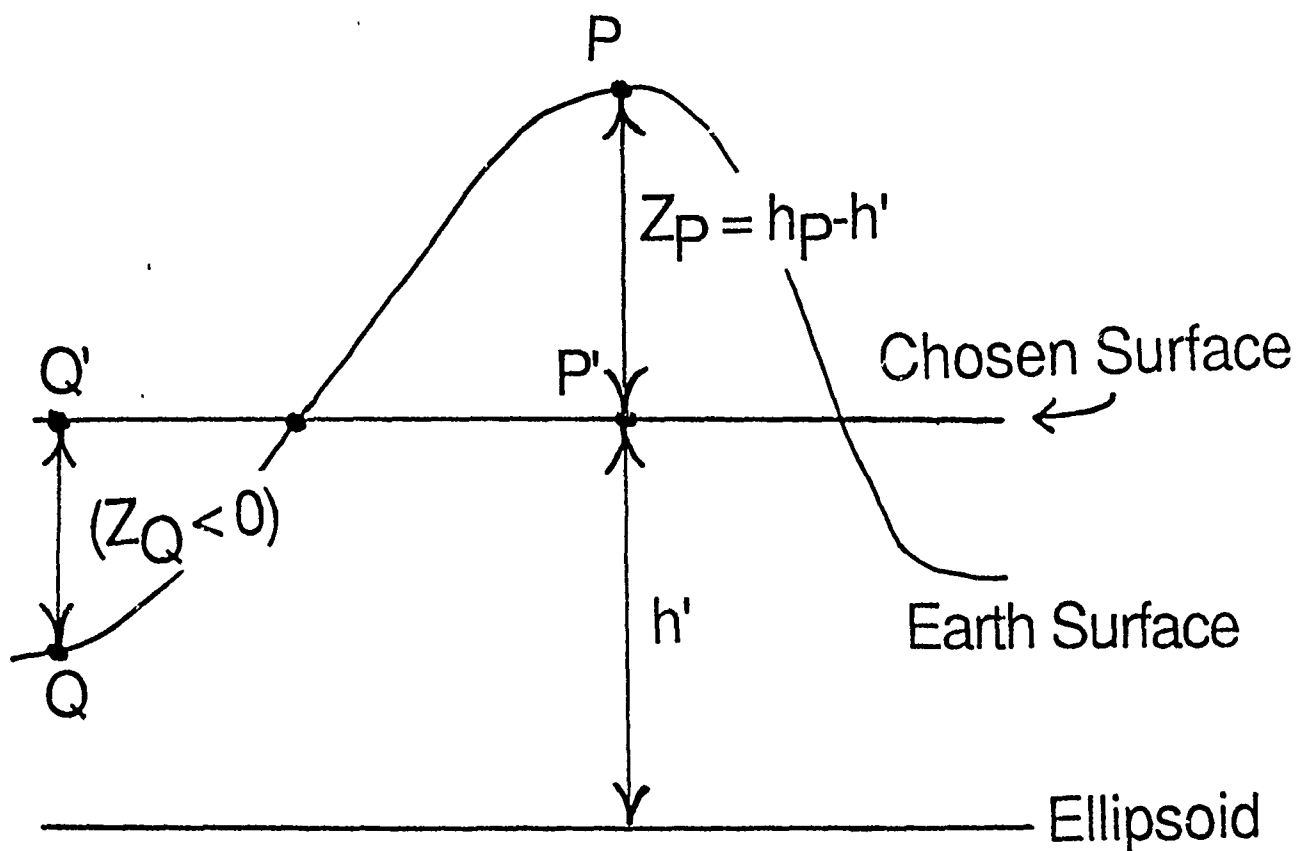
DAVID M. GLEASON

GEOPHYSICS LABORATORY
HANSCOM AFB, BEDFORD, MA. 01731

ABSTRACT: Moritz (1980) presents a density-free scheme allowing for the analytical continuation of a given set of free-air gravity anomalies to any desired level surface if a corresponding set of elevations (e.g., above MSL) is available. An efficient spectral implementation of this scheme is discussed by Sideris (1987). A subsequent spectral execution of the planar Vening-Meinez equation on the continued anomalies yields deflections of the vertical on the chosen level surface. The deflections are brought back to the Earth's surface via a spectrally implemented Taylor series. The series' convergence rate depends on a) the ruggedness of the local topography and b) the resolution of the input gravity and elevation gridded data. Deflections at a constant altitude above the level surface are obtained through a routine spectral execution of the planar upward continuation integral. Two sites, having diverse topographies, were surveyed for 1' by 1' mean free-air anomaly and elevation values and for smaller sets of astronomically-determined deflections to serve as control or "truth" values. In a topographically-tranquil, but gravimetrically turbulent Oklahoma site the overall RMS of the differences between true and predicted deflections was 0.3 arc secs and in a rugged New Mexico site, using less reliable truth data, the RMS was 0.6 arc secs. Potential pitfalls of the 2 dimensional Fast Fourier Transform pair are discussed with an emphasis on unwanted circular convolution effects which, if unaccounted for, can increase the error in predicted deflections by as much as 100%.

OBTAINING EARTH SURFACE AND
SPATIAL DEFLECTIONS OF THE
VERTICAL FROM MEAN FREE-AIR
GRAVITY ANOMALY AND ELEVATION
DATA WITHOUT DENSITY
ASSUMPTIONS.

DAVID M. GLEASON
GEOPHYSICS LABORATORY
HANSCOM AFB, MA. 01731



Runge's Thm. states one can always find a harmonic function T^* , arbitrarily close to T_{EXTERNAL} , that can be regularly continued (be it upward or downward) from the ground to a chosen level surface.

So

$$\Delta g_P = \Delta g'_P + z_P \cdot \frac{\partial \Delta g'_P}{\partial z} + \frac{z_P^2}{2!} \cdot \frac{\partial^2 \Delta g'_P}{\partial z^2} + \dots$$

$$\xi_P = \xi'_P + z_P \cdot \frac{\partial \xi'_P}{\partial z} + \frac{z_P^2}{2!} \frac{\partial^2 \xi'_P}{\partial z^2} + \dots$$

$$\eta_P = \eta'_P + z_P \cdot \frac{\partial \eta'_P}{\partial z} + \frac{z_P^2}{2!} \frac{\partial^2 \eta'_P}{\partial z^2} + \dots$$

- The $\Delta g'$ set reflects the earth's exterior (not, interior) gravity field. Used in Stokes' formula, it yields a T' which is harmonic above the chosen surface and which agrees with the actual T on and above the Earth's surface.

- So, under such a continuation of T_{EXT} , masses outside the chosen surface are, in effect, shifted to its interior.

Again

$$\Delta g_P = \Delta g'_{P'} + z_P \cdot \frac{\partial \Delta g'_{P'}}{\partial z} + \frac{z_P^2}{2!} \cdot \frac{\partial^2 \Delta g'_{P'}}{\partial z^2} + \dots$$

Moritz' density-free inverse solution is given by

$$\Delta g'_{P'} = g^0_P + g^1_{P'} + g^2_{P'} + g^3_{P'} + \dots$$

where

$$g^0_P = \text{the observed } \Delta g_P$$

$$g^1_{P'} = -z_P \cdot \frac{\partial g^0_P}{\partial z}$$

$$g^2_{P'} = -z_P \cdot \frac{\partial g^1_{P'}}{\partial z} - \frac{z_P^2}{2!} \frac{\partial^2 g^0_P}{\partial z^2}$$

Etc., Etc.

- In $g^1_{P'} = -z_P \cdot (\partial \Delta g / \partial z)$, the partial will be treated as a planar surface operator.

i.e.

$$\begin{aligned}
 g^1_{P'} &= -z_P \cdot \frac{\partial g^0_P}{\partial z} \\
 &\cong -z_P \iint_{-\infty}^{\infty} \frac{g^0(x,y) - g^0(x_P, y_P)}{[(x-x_P)^2 + (y-y_P)^2]^{3/2}} dx dy
 \end{aligned}$$

which is a convolution.

NOTES:

1). Due to only a finite grid of Δg input values, the spectrum of

$$\Delta g_{\text{REDUCED}} = \Delta g_{\text{GIVEN}} - \Delta g_{\text{S.H. EXPAND}}$$

is computed .

2). As in all applications of the 2D FFT pair, be aware of

- Aliasing
- Spectral Leakage
- Circular (non-linear) Convolution Effects

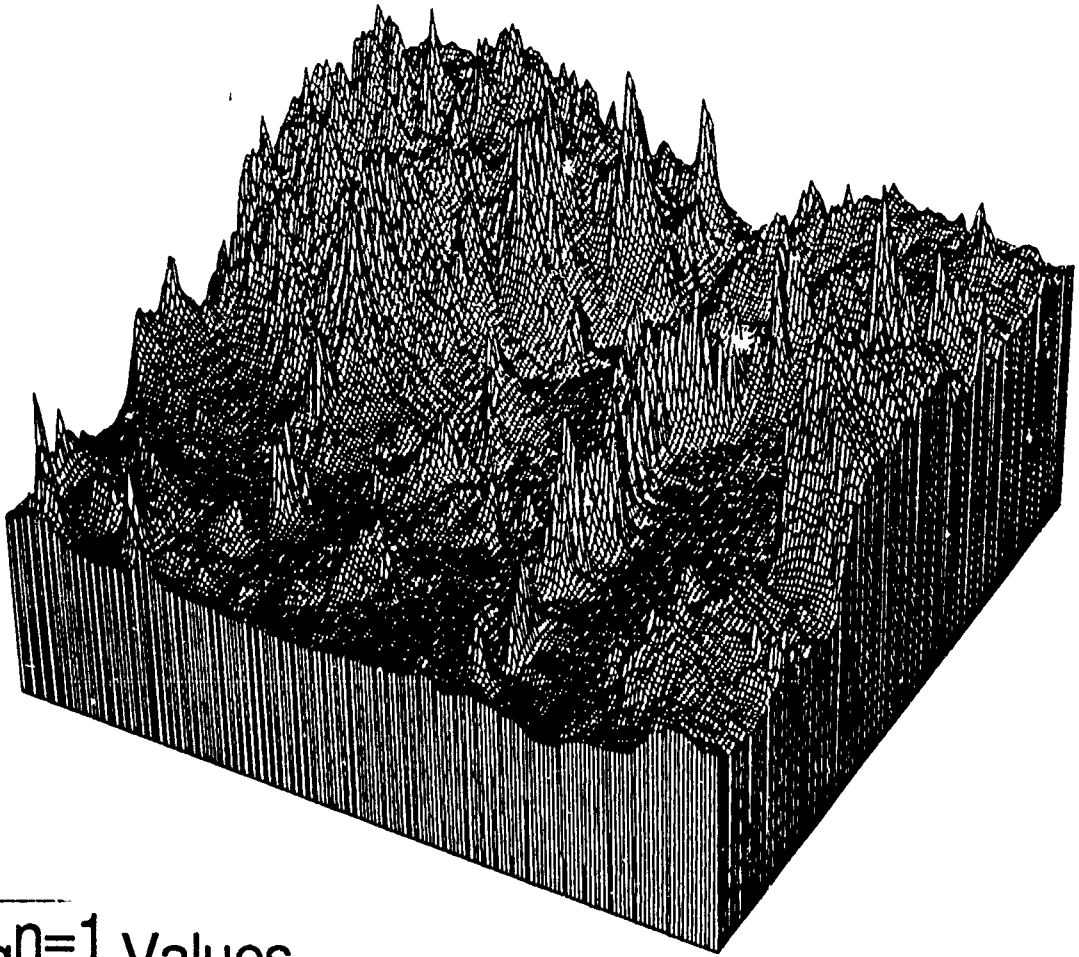
NOTES:

1. After obtaining the gridded set of $\Delta g'$ values on the chosen surface, one can immediately obtain gridded sets of ξ' and η' deflections on the chosen surface via a routine spectral execution of the planar Vening Meinez eqn using the applicable transfer functions.

2. One can then obtain gridded sets of spatial deflections at a constant altitude h above the chosen level surface through a routine spectral execution of the planar upward continuation integral (using the u.c. transfer function $e^{-\omega h}$).

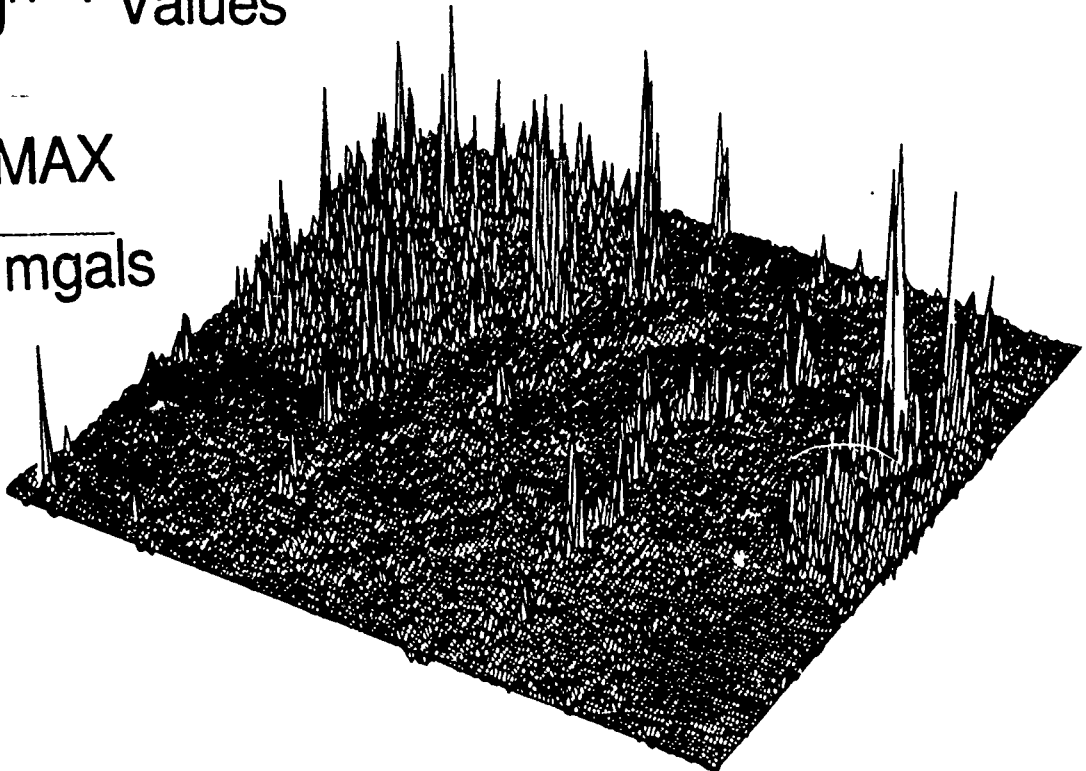
3. One can efficiently obtain gridded deflections on the irregular Earth surface via a spectral execution of the Taylor Series linking ξ'_P and η'_P to ξ_P and η_P .

Topography of Central 3° by 3° New Mexico Area.



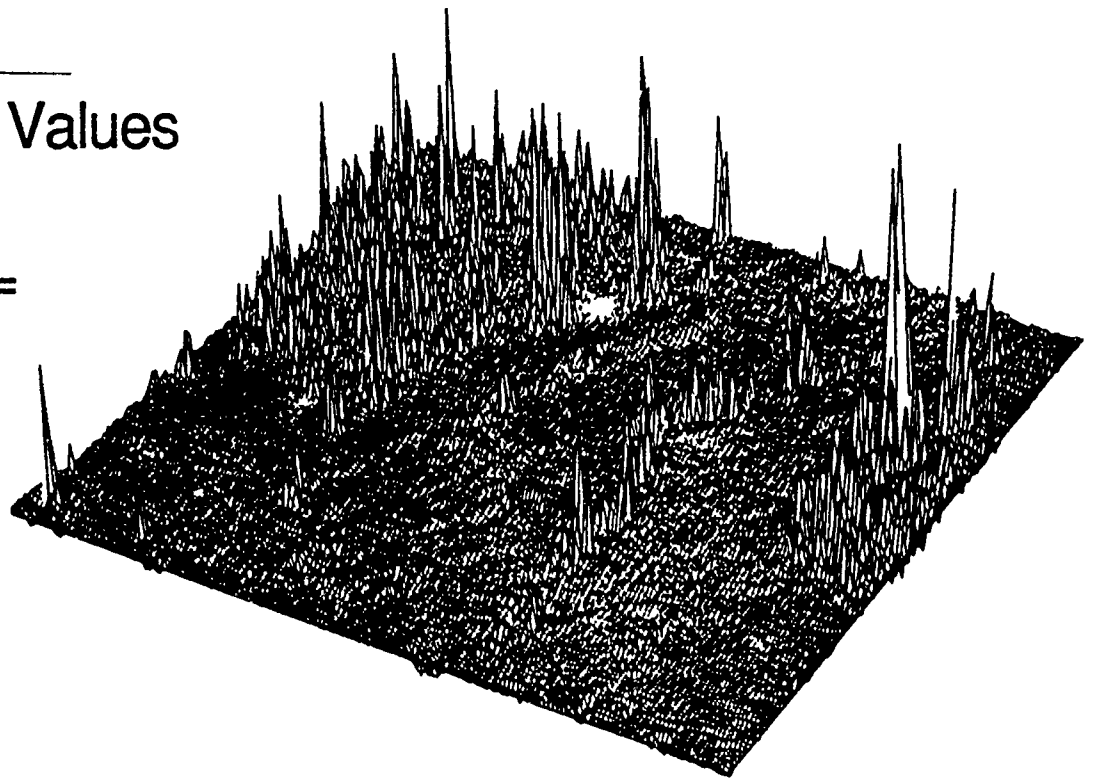
$\overline{g^{n=1}}$ Values

$\overline{g^1_{MAX}}$
= 86 mgals



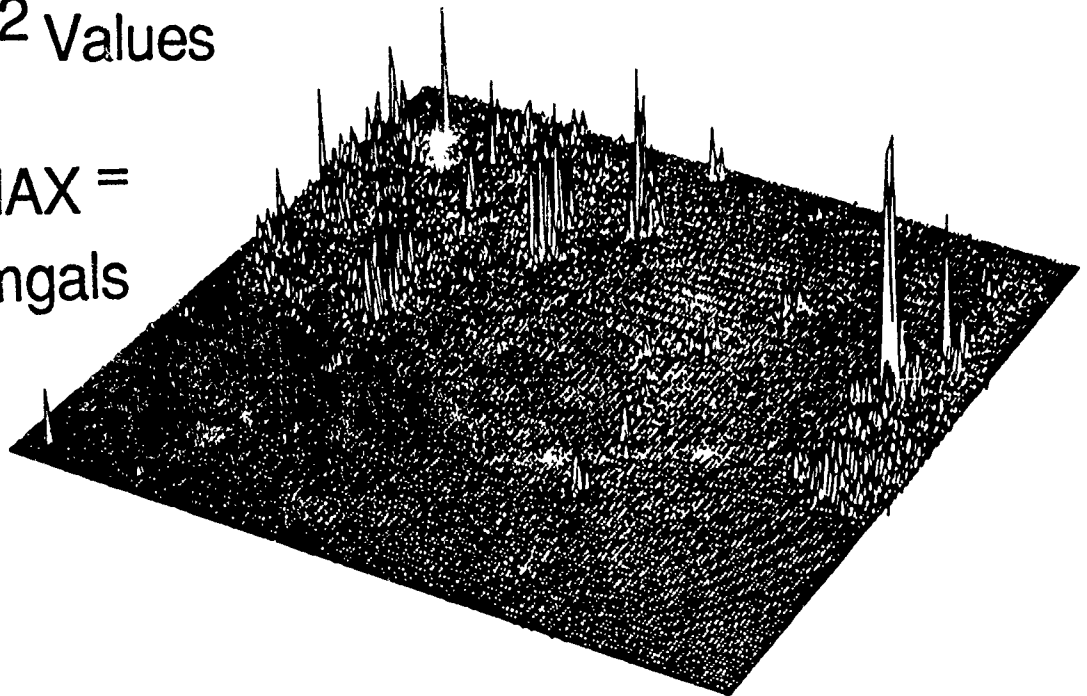
$g^{n=1}$ Values

$g^1_{MAX} =$
86 mgals



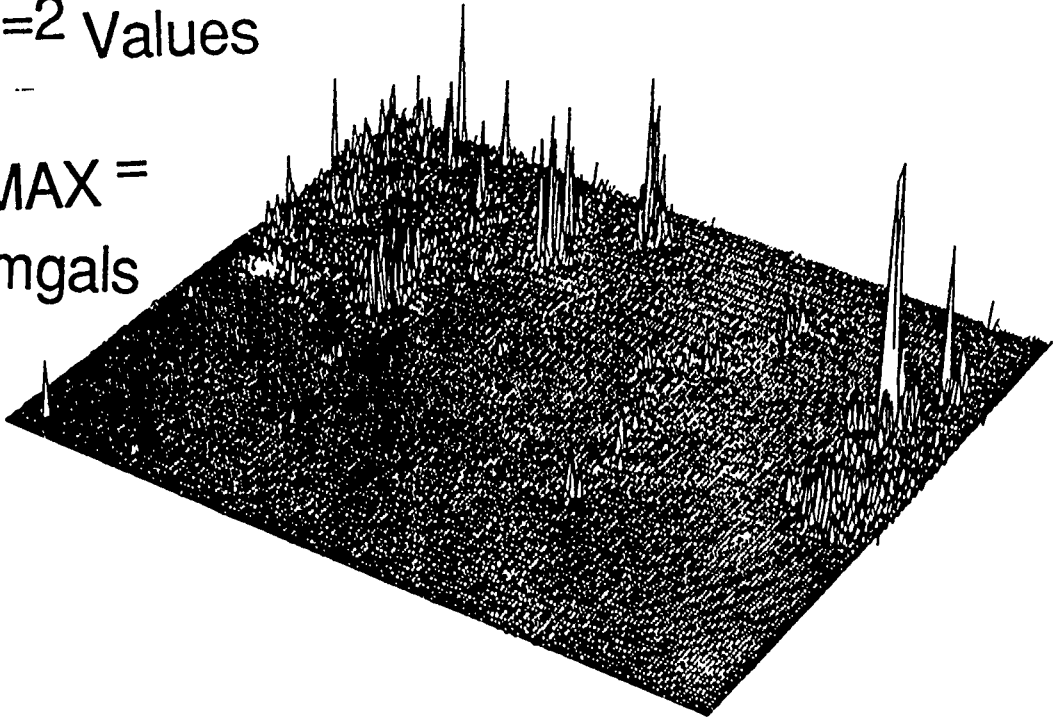
$g^{n=2}$ Values

$g^2_{MAX} =$
72 mgals



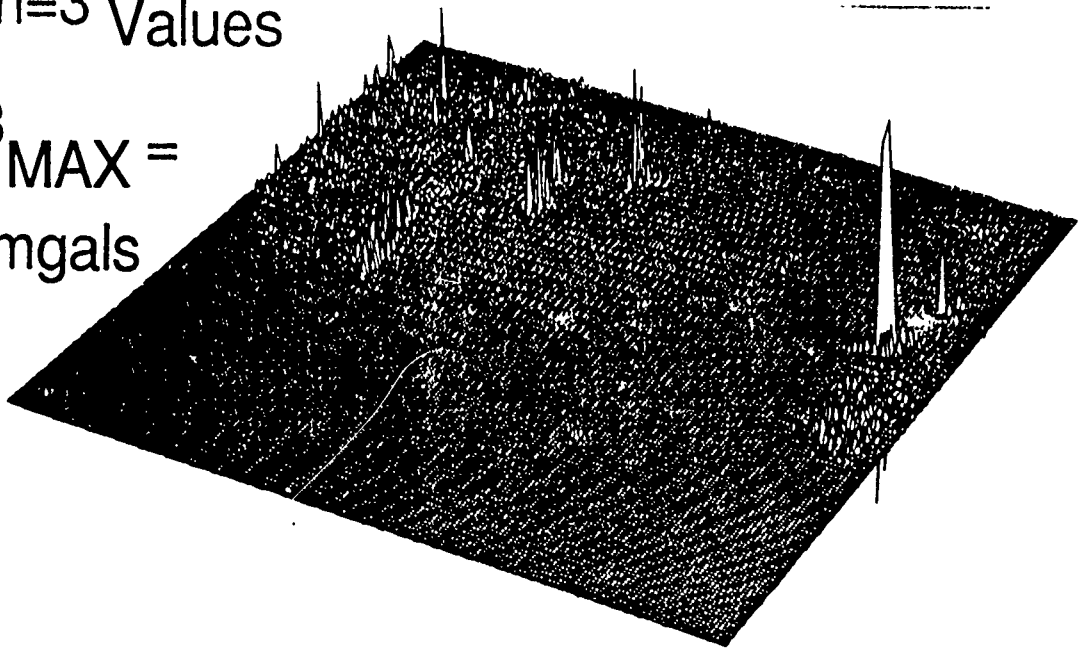
$\overline{g^{n=2}}$ Values

$g^2_{MAX} =$
72 mgals



$\overline{g^{n=3}}$ Values

$g^3_{MAX} =$
60 mgals



Overall RMS values of 378 (Astro-Predicted) ξ and η differences, in arc secs, from 1' New Mexico data and the Newer Astro set.

n Truncation Level	ξ	η
0	0.61"	0.75"
1	0.59"	0.74"
2	0.59"	0.74"
3	0.59"	0.74"

NOTE:

$$\xi_{\text{Predicted}} = \Phi - \phi^* \quad \text{while}$$

$$\xi_{\text{Astro}} = \Phi - \phi$$

where $\phi^* - \phi = (f^* h/R) \sin 2\phi$, is the well-known reduction for the normal curvature of the plumb line.

- The predicted (gridded) deflections were interpolated to the astro locations.

From Data Types and Their Spectral Properties, by K.P. Schwarz:

Percentage of Total Value, by Harmonic Degree n , for T_z and T_{zz} (i.e., Δg and $\partial\Delta g/\partial z$).

low $n \in (2,36)$ (5° grid)	medium (37,360) (30' grid)	high (361,3600) (3' grid)	very high (3601,36000) (18" grid)
T_z 22.5	41.9	32.7	2.8
T_{zz} 0.0	0.8	39.0	60.2

• NOTES:

A 1' grid $\Leftrightarrow n_{\max}=10800$

A 30" grid $\Leftrightarrow n_{\max}=21600$

SUMMARY:

1. The spectral approach allows for efficient predictions of deflections and height anomalies at a resolution matching the input data.
2. The $n=1$ topographic corrections were beneficial in near-mountain splashes where the input Δg and h data was reliable but were detrimental in such areas where the data was suspect.
3. The extraction of ultra-high frequency information from lower order 1' or 30" mean gradients is questionable.
4. Noise in such input data might render higher order (e.g. $g^{3,4,5,6,\dots}$) corrections meaningless.
5. Interpolated grids of anomalies and heights fail to account for higher frequency terrain effects.

Distinguishing Nuclear- from Conventionally- Armed Cruise Missiles with a Gravity Gradiometer

**Dr. John A. Parmentola
Center for Science and International Affairs
John F. Kennedy School of Government
79 John F. Kennedy Street
Harvard University
Cambridge, MA 02129**

Abstract

I will discuss an analysis of an application of the gravity gradiometer, that has been designed at Draper Laboratories, which might be useful during missile production for distinguishing conventional from nuclear armed cruise missiles in a nonintrusive way. The motivations for exploring this potentially important application of this device will also be discussed.

Distinguishing Nuclear From Conventionally Armed Cruise Missiles

I. Brief Introduction

Arms control and START :

**Long-range nuclear sea-launched
cruise missiles or SLCMs.**

**For the U.S. these are the various
versions of the Tomahawk.**

**For the Soviets these are the SS-N-
21s.**

Cruise Missiles :

Pilotless aircraft

Sophisticated autonomous guidance

Fly low to avoid radar

Nuclear or conventional payloads

Variety of launch platforms

Cruise missiles along with their protective cannisters are loaded into launchers.

Upon firing the cruise missile breaks through the cannister while being propelled by a rocket motor.

Rocket motor burns until cruising speed is reached, then a turbofan engine takes over.

Guided to its target by local terrain maps and for the conventional version an additional digital image of target.

The issues I want to address in this talk are :

(1) Why are long-range nuclear SLCMs an important issue ?

(2) What problems do SLCMs pose for verification ?

(3) How could a gravity gradiometer contribute to a SLCM verification scheme ?

The quick answers to these questions are :

(1) Because long-range nuclear SLCMs are a contentious issue within START. There are important political, military, and economic factors which contribute to this situation.

(2) Several design characteristics of long-range SLCMs make verification of limits on SLCMs relatively hard, but far from impossible in my opinion.

(3) Because long-range nuclear- and conventionally-armed SLCMs have significantly different internal mass distributions a gravity gradiometer could effectively distinguish between them. This would ensure that nuclear cruise missiles are not being falsely counted as conventional under an arms control treaty.

II. Why worry about Sea-Launched Cruise Missiles or SLCMs ?

There are military, economic, and political dimensions to this question.

Military:

Sneak attack of bomber bases and command and control system with a small number of stealthy SLCMs. No early warning !

Economic:

The costs of deploying an effective early warning system are high.

Political:

SLCMs contributed to the stopping of START. The most contentious aspect has been verification.

Simplest situation is a ban on both conventional and nuclear. U.S. Navy opposes a total ban, because it likes the conventional anti-ship version.

Domestically the public has demanded reductions and it is unlikely that SLCMs will be excluded.

Arms control might provide the means for controlling the threat, save the country some money for an early warning system, and solve some political problems.

III. What are long-range SLCMs ?

I will restrict my discussion to U.S. cruise missiles.

U.S. Tomahawk:

Land-attack nuclear has a range of 2800 km.

Land-attack conventional has a range of 1500 km. Has shorter range due to much longer and heavier warhead, less fuel, and more guidance equipment for targeting.

Anti-ship conventional has a range of 500 km. Even more guidance equipment, because it goes after moving targets and has less efficient engines.

Verification problems:

Nuclear and conventional versions all have the same airframe.

Minor visual external differences are not useful for distinguishing between them.

Launchers are dual-purpose.

This implies that NTM is useless. More intrusive forms of monitoring are required such as on-site inspections of :

Storage facilities

Service facilities

Testing

Deployment modes

Production - Gravity Gradiometer

IV. Some difficulties with SLCM verification

Simplest situation:

Total ban on all long-range SLCMs - Requires the dismantling of infrastructure needed to produce, store, service, test, and train with these weapons.

Much harder situation :

Problems occur when a category is allowed. Infrastructure for conventional anti-ship version of Tomahawk useful for producing long-range nuclear SLCMs.

Difficulties with verifying a ban on nuclear with a limit on conventional :

Possibility that nuclear warhead is mated to a cruise missile in the factory and designated as conventional. This could be detected nonintrusively with nuclear radiation detectors or intrusively with x-rays or a beam of neutrons.

It is not necessary that a nuclear warhead be mated in the factory to cheat. What is needed is a tested production line. Place a dummy warhead with the same mass distribution as nuclear warhead. This could be detected nonintrusively with a gravity gradiometer.

If an effective nonintrusive method of distinguishing nuclear and conventional can be found then tags can be used to identify legal cruise missiles throughout their life-cycle.

V. Using the Gravity Gradiometer for Production Monitoring

Mass density distributions of a nuclear and conventional Tomahawk :

Nuclear warhead is more than twice as dense, half as long, and more forward in location than the conventional warhead.

More than half the volume of fuel in the nuclear version is in roughly the same location as the warhead in the conventional version; however the density of the fuel is roughly 20 % less than the warhead.

Draper three gradiometer device:

A properly packaged and field tested device would cost about 2 million dollars, i.e. the price of a Tomahawk.

This version would minimize errors due to jitter.

Accurate to the 1 Eotvos unit level.

Response time is relatively short.

Place on a tripod in a room.

A Tomahawk would pass by the device at a certain rate while the gradiometer responded and provided a complete scan of the missile.

It would be desirable to allow for several different scans along the missile length at different distances from the missile axis.

Since the response time of the device is relatively short the time required to scan a cruise missile is not a significant factor in the monitoring process.

The resolution of the device, i.e. its capability of discerning details about the individual components of a cruise missile, is easy to control by limiting how close to the missile the gradiometer can approach.

Estimating the distance for a hypothetical measurement:

Specify the desired level of accuracy. Assume for the moment that cruise missile is a very long cylinder of uniform density.

An inaccuracy in a measurement of the radial gradient of the gravitational field translates into an uncertainty in the determination of the mass density or

$$\delta F'/F' = \delta \rho/\rho$$

$$\delta \rho/\rho = r^2 \delta F' / [2\pi a^2 \rho G]$$

$$\delta F' = 1 \text{ Eotvos unit}$$

$$\delta \rho/\rho = 0.02$$

$$a = 0.265\text{m}$$

$$\rho = 2 \times 10^3 \text{ kg/m}^3$$

$$r \approx 1\text{m}$$

Model of mass density used in the calculations :

The aluminum skin of the hemispherical nose and its volume mass density are approximated by points located at their respective centers of mass.

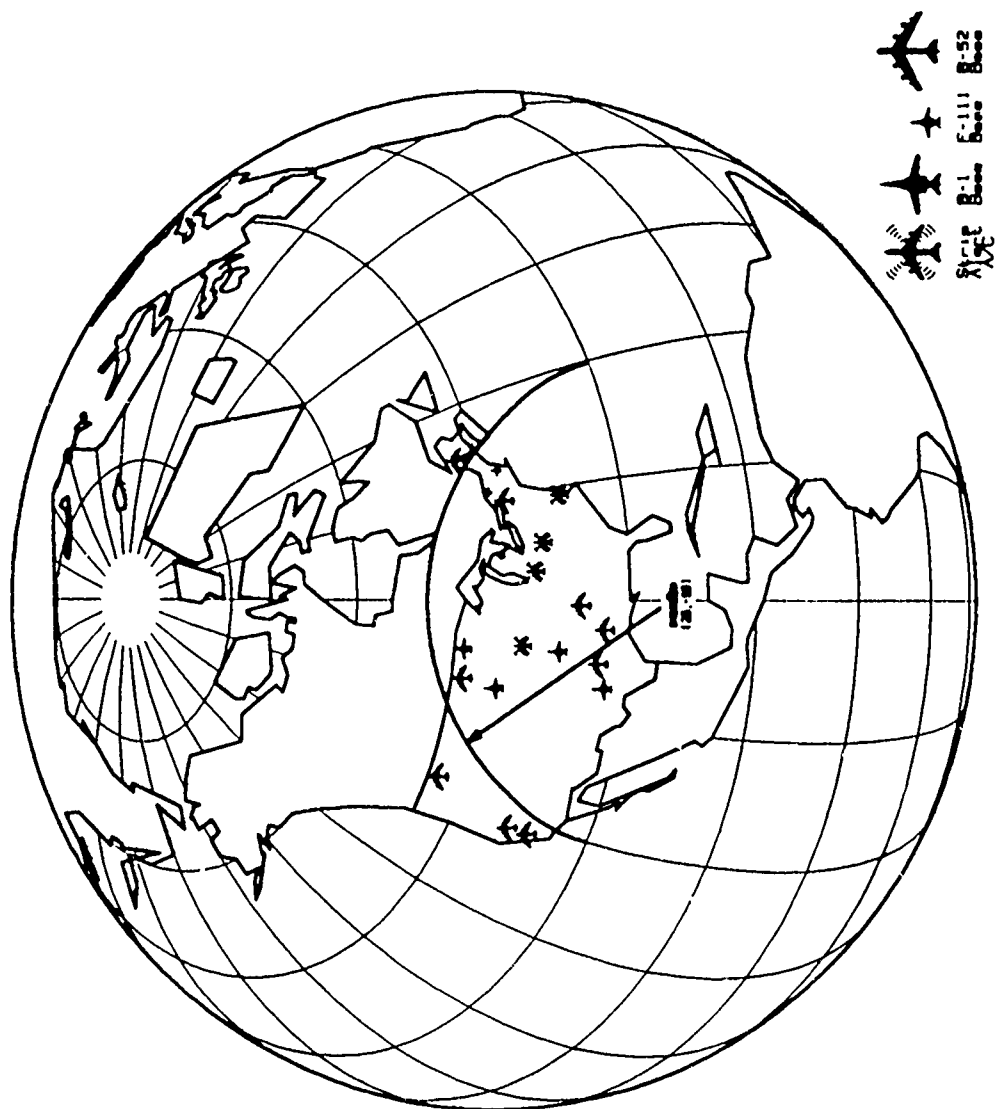
The remaining components including the airframe are treated as lines of mass along the axis of the missile.

For this model the gradiometer will be sensitive to the mass per unit length.

Results :

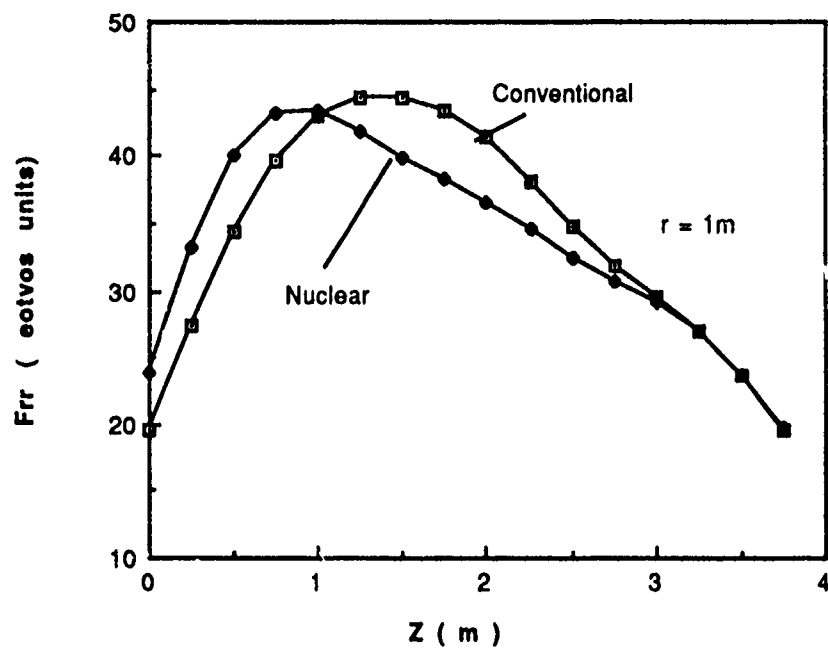
Simulation of the radial gradient of the radial component of the gravitational field, F_{rr} , produced by a conventional and nuclear cruise missile along their length.

If measurements are not made continuously along the missile axis, then the stepsize, i.e. the distance between measurements, must be less than the size of an object in order to resolve it.

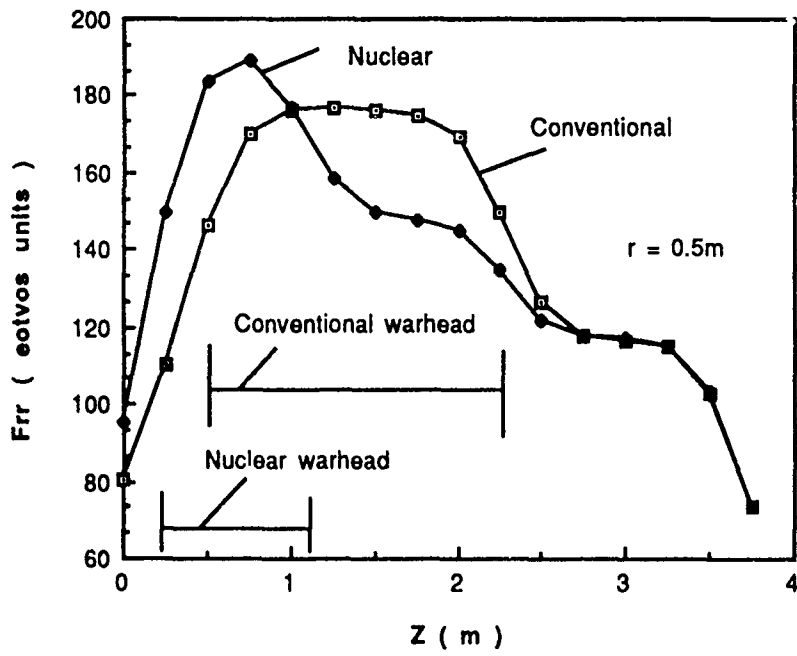




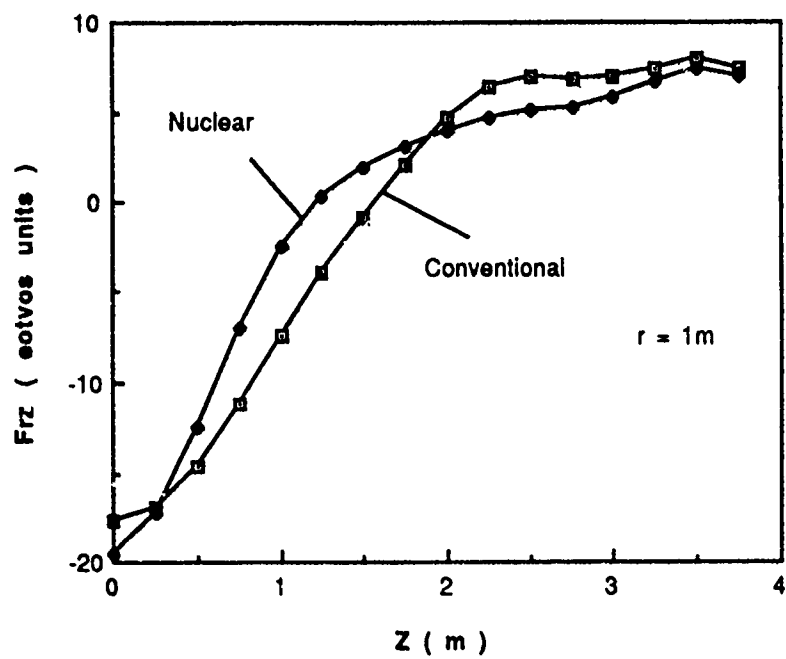
Radial Gradient Comparison at $r = 1\text{m}$



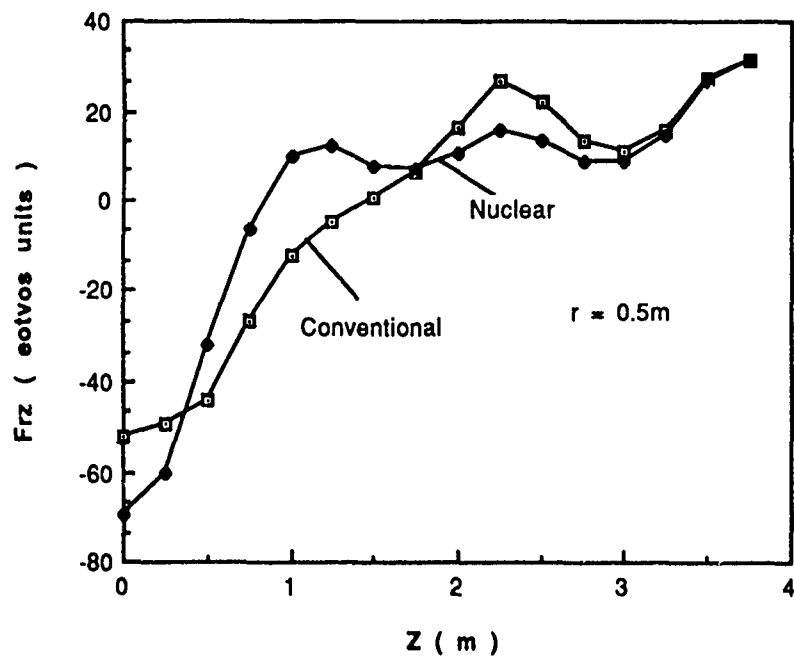
Radial Gradient Comparison at $r = 0.5\text{m}$



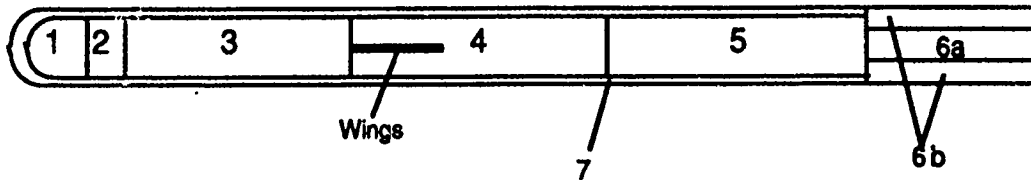
Radial Gradient Comparison at $r = 1\text{m}$



Radial Gradient Comparison at $r = 0.5\text{m}$



Model of Conventional SLCM

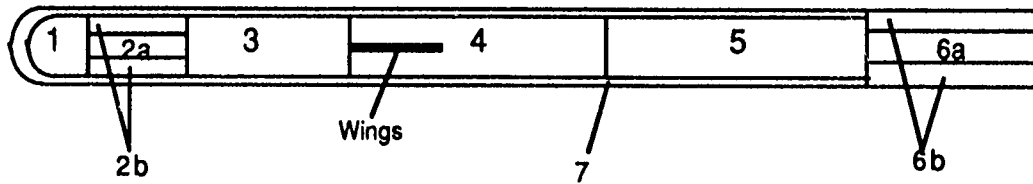


Section	Component	Mass	Length	Radius	Skin Thickness	Average Density
1 *	Guidance System	68 kg.	.646m	.252m	.013m	.61gm/cc
2	Fuel	27	.128	.252	.013	1.07
3	Warhead	456	1.770	.252	.013	1.30
4**	Fuel	176	1.400	.244	.021	.67
5	Engine	59	1.640	.252	.013	.18
6a	Fuel	178	.652	.220	.000	1.80
6b	Rocket	121	.652	.265	.000	2.70
7	Skin or Airframe	365	5.590			2.70

1* - Nose is assumed to be a hemisphere of radius .252m.

4** - Wings are included in airframe which accounts for smaller inner radius. Top surface of wings is assumed to have an area of 1.02 m² and the mass of the wings is assumed to be 52.5 kg.

Model of Nuclear SLCM



Section	Component	Mass	Length	Radius	Skin Thickness	Average Density
1 *	Guidance System	46 kg.	.458m	.252m	.013m	.61 gm/cc
2a	Warhead	123	.866	.130	.000	2.70
2b	Fuel	123	.866	.252	.013	.97
3	Fuel	260	1.220	.252	.013	1.07
4 **	Fuel	176	1.400	.244	.021	.67
5	Engine	59	1.640	.252	.013	.18
6a	Fuel	178	.652	.220	.000	1.80
6b	Rocket	121	.652	.265	.000	2.70
7	Skin or Airframe	365	5.590			2.70

1* - Nose is assumed to be a hemisphere of radius .252m.

4** - Wings are included in airframe which accounts for smaller inner radius. Top surface of wings is assumed to have an area of 1.02 m² and the mass of the wings is assumed to be 52.5 kg.

17th Gravity Gradiometry Conference

12 - 13 October, 1989

Air Force Geophysics Laboratory
Hanscom AFB

Advances in Dynamic Estimation

Dave Son nabend
Jet Propulsion Laboratory
California Institute of Technology

Abstract

In prior years I have talked about magnetic isolation of instruments, with only short allusions to our work in dynamic estimation to deal with rotation correction in floated gradiometers. This year's talk will be almost entirely devoted to estimation. As the theory has been exposed at other conferences and seminars, and is a central topic in my book on gradiometry, it will only be sketched here. However, there are several new developments, including improvements to our models and filters, application to a Lunar Observer mission, and computational techniques for dealing with self gravity. Also, if no one from NASA Hq. shows up, I'll discuss NASA's latest plans in gravity measurements.

17th Gravity Gradiometry Conference

ADVANCES IN DYNAMIC ESTIMATION

Dave Sonnabend

JET PROPULSION LABORATORY
CALIFORNIA INSTITUTE OF TECHNOLOGY

DYNAMIC ESTIMATION

INTRINSIC TENSOR

$$\mathbf{T} = \mathbf{\Gamma} + \omega^2 \mathbf{I} - \boldsymbol{\omega} \boldsymbol{\omega}^T - \varepsilon \dot{\boldsymbol{\omega}}$$

$$Tr(\mathbf{T}) = 2\omega^2$$

FLOATED INSTRUMENT DYNAMICS

$$m\ddot{\mathbf{x}} = \mathbf{f}$$

$$\mathbf{J}\dot{\boldsymbol{\omega}} + (\varepsilon \boldsymbol{\omega})\mathbf{J}\boldsymbol{\omega} = \mathbf{f} \times \mathbf{r}$$

Kinematic Equations

Measurement Equations

Constraints

ESTIMATION STATE

$$\mathbf{x} = [\mathbf{f}, \boldsymbol{\omega}, \boldsymbol{\theta}, \boldsymbol{\gamma}] \quad (14 \text{ Elements})$$

$$\boldsymbol{\gamma} = [\Gamma_{11}, \Gamma_{12}, \Gamma_{13}, \Gamma_{22}, \Gamma_{23}]$$

MEASUREMENTS

$$\left. \begin{array}{l} \text{Linear Accelerometer} \\ \text{Angular Accelerometer} \\ \text{Rate Gyro} \\ \text{Star Tracker} \\ \text{Gradiometer} \end{array} \right\} \begin{array}{l} \text{Up to 21} \\ \text{Components} \end{array}$$

GRADIENT SIGNAL STATISTICS

- Random Geology Model: Surface is an infinite plane littered randomly with mass points.

$$\mu \equiv \mathbf{E}\{\gamma\} = \mathbf{0}$$

- Static gradient covariance:

$$\Lambda \equiv \mathbf{E}\left\{(\gamma - \mu)(\gamma - \mu)^T\right\} = \frac{3\pi G^2 \rho}{32h^4} \left(\mu_m + \frac{\sigma_m^2}{\mu_m} \right) \begin{bmatrix} 8 & 0 & 0 & 0 & -4 & 0 \\ 0 & 4 & 0 & 0 & 0 & 0 \\ 0 & 0 & 4 & 0 & 0 & 0 \\ -4 & 0 & 0 & 0 & 3 & 0 \\ 0 & 0 & 0 & 0 & 0 & 1 \end{bmatrix}$$

FILTERS

- 3 Filters Used
 - Kalman (not stabilized)
 - U-D
 - SRIF
- U-D and SRIF based on Bierman Algorithms.
- For high initial covariance ($M_0 \times 10^{12}$), Kalman filter experienced catastrophic failure.
- For high drag process noise, Kalman filter experienced numerical divergence.
- U-D and SRIF agree to parts in 10^{13} in covariance trace after 8000 steps.

Time

10^4

10^3

10^2

10

.1

0

ω

Γ_{13}

ω_1

.01

163

10^{-3}

σ_T

10^{-4}

Γ_{11}

10^{-8}

10^{-4}

ω
RAD/SEC

10^{-10}

10^{-11}

PROPELLANT

100 kg SPHERICAL BLOB

A PRIORI LOCATION COVARIANCE

$$M_{\text{loc}} = \sigma^2 I_3$$

$$\sigma = 0.3 \text{ m}$$

TANK 0.5, 1 m FROM GRADIOMETER IN VARIOUS DIRECTIONS

$$\Gamma_o = \frac{Gm}{r^3} = 6.67 \text{ E}$$

ACCELEROMETER ENSEMBLES

CONFIGURATION (0.5 m EDGE)	PROOF MASS
TRIANGLE	F
SQUARE	FC
TETRAHEDRON	FC
OCTAHEDRON	F
CUBE FACES	F
CUBE CORNERS	FC

NOISE LEVEL

SENSITIVE	$1.3 \times 10^{-12} \text{ m/sec}^2 - \text{Hz}^{1/2}$
INSENSITIVE	$2.5 \times 10^{-10} \text{ m/sec}^2 - \text{Hz}^{1/2}$

GRADIENT

ASSUMED SYMMETRIC

NOT ASSUMED TRACELESS

$$M_g = \sigma^2 I_6$$

$$\sigma = .01 \text{ E}$$

MEASURES OF FINAL COVARIANCE P_g

$(\text{Tr} P_g)^{1/2} = \text{ROOT SUM OF VARIANCES OF } \Gamma$

$|P_g|^{1/12} = 12\text{th ROOT OF VOLUME OF } 1\sigma \text{ HYPERELLIPSOID}$

Results

Gradiometer		Propellant			$T_r P_{loc})^{1/2}$ mm	Results		Notes
Shape	Proof Mass	Location				$(T_r P_g)^{1/2}$ mE	$ P_g ^{1/12}$ mE	
–	–	–	–	–	520.000	24.500	10.000	A Priori
Sq	F	1.0	0	0	4.030	17.366	2.927	Baseline
Sq	F	1.0	0	0	39.945	17.366	2.927	10 kg
Tet	F	1.0	0	0	0.476	14.294	2.362	
Sq	C	1.0	0	0	.037	10.191	1.306	
Tet	C	1.0	0	0	.039	2.780	1.093	
Cube F	F	1.0	0	0	0.581	14.262	2.340	
Cube C	F	1.0	0	0	.042	9.872	0.564	
Cube C	C	1.0	0	0	.031	0.725	0.270	
Sq	F	1.0	0	0	2.961	17.266	2.047	double size
Sq	F	1.0	0	0	5.225	17.527	3.930	half size

BUT THE PROPELLANT STICKS TO THE WALL

- 1. CAN DEVELOP 2 PARAMETER SHAPE AND
FIELD MODEL**
- 2. CAN DEVELOP SLOSH MODEL AND DO
DYNAMIC ESTIMATION**

CONCLUSIONS

- MORE IS MERRIER
- TETRAHEDRON ALWAYS BEATS SQUARE
- CUBIC PROOF MASS MUCH BETTER THAN FLAT
- BIGGER IS BETTER
- TANK DIRECTION MATTERS FOR SQUARE - FLAT, NOT OTHERS TRIED
- CLOSER ONLY SLIGHTLY WORSE
- IT WORKS!

G ADJUSTMENT

From CODATA 1986 Adjustment of the

Fundamental Physical Constants:

$$\begin{aligned} G &= 6.67259 \times 10^{-11} \text{ m}^3/\text{kg}\cdot\text{sec}^2 \\ \sigma &= 8.5 \times 10^{-15} \text{ m}^3/\text{kg}\cdot\text{sec}^2 \end{aligned}$$

SOURCE: Physics Today, 8-89, Part II

RESULTS ON THE ESTIMATION OF GEOPOTENTIAL COEFFICIENTS FROM A SIMULATION OF A SATELLITE GRAVITY GRADIOMETER MISSION

Srinivas V. Bettadpur, Bob E. Schutz, John B. Lundberg

Center for Space Research, University of Texas at Austin, Austin, Tx 78712

The NASA Satellite Gravity Gradiometer Mission, designed to measure the tensor of gradients of accelerations due to gravity, promises a substantial increase in the knowledge of the fine scale features of the gravity field of the earth. One possible mission scenario consists of the gradiometer mounted in a satellite traveling in a polar, frozen perigee, drag free orbit and measuring the six components of the tensor of gravity gradients in a suitable reference frame.

Some results are reported from an initial simulation of the estimation of the geopotential coefficients from measurements made on such a satellite gradiometer mission. Using a small reference gravity field (18 by 18 subset of a GEMT1 error model), the gradiometer observations along a true orbit were simulated in a geocentric equatorial coordinate frame. Zero mean Gaussian random noise with different standard deviations were added to the simulated observations. During the estimation process, the observations were modeled along a nominal orbit using Pines' fully normalized, nonsingular formulation. To simulate a range of orbit accuracies, the differences between the nominal and true orbits were varied from 16, 69 and 19 meters to 16, 69 and 19 cm in the radial, transverse and normal directions, respectively. The geopotential coefficients were estimated from a least squares fit of the simulated gradiometer data in the presence of different levels of observation noise and orbit errors. The estimated coefficients were then compared to the coefficients of the reference gravity field, in the sense of degree averaged errors and the errors produced in a global geoid.

The results obtained from the initial simulations indicate that to recover the global geoid to about a centimeter root mean square error, the instrument must have a sensitivity of 10^{-4} E.U. and the radial orbit accuracy must be within 20 cm. For example, with errors of 16, 69 and 19 cm in the radial, transverse and normal directions, and with 10^{-4} E.U. noise, the global geoid error was 0.6 cm (RMS). On the other hand, with the same orbit error, but with 10^{-2} E.U. noise, the global geoid error increased to 45 cm (RMS).

Significant errors in the estimated coefficients are seen to be caused by the adjustments required to model the systematic gradient residual due to the point mass term μ/r . The permissible radial orbit error is governed by the ratio of this systematic residual gradient to the noise level.

These results, while demonstrating the role of some error sources in the process of estimation, provide a baseline against which the results of approximate methods can be compared.

RESULTS FROM THE ESTIMATION OF GEOPOTENTIAL COEFFICIENTS
FROM A SIMULATION OF A
SATELLITE GRAVITY GRADIOMETER MISSION

Srinivas Bettadpur

Bob E. Schutz

John B. Lundberg

Oct. 12, 1989

Center for Space Research

The University of Texas at Austin

SATELLITE GRAVITY GRADIOMETER MISSION

Measurement of spatial variation of acceleration due to gravity

Global, High resolution study

Goals :

Determine high degree and order (≈ 180) geopotential field

Applications :

- * Precision Orbit Determination
- * Navigation
- * Oceanography

ANALYSIS OF DATA

Measurements : Gradients of gravity in an instrument frame

Data :

- * Orientation of the instrument frame
- * Angular velocity of the instrument frame
- * Orbit of the satellite carrying the gradiometer

Unknown :

Coefficients of the spherical harmonic expansion
of the geopotential

ASSUMPTIONS FOR THE SIMULATIONS

- * 4 second data sampling with 10^{-4} or 10^{-2} E.U.
noise
- * Signal consists only of the static geopotential
- * Gradients are available in Geocentric, Earth fixed frame
- * Orbit of the satellite is separately available
- * Error Sources :
 - Orbit errors
 - Observation noise

OBSERVATION MODEL

$$\vec{G}(t_k) = \nabla [\nabla U(\vec{r}(t_k))]$$

$$G_{ij}(\vec{r}(t_k)) = \sum_{n,m} [\alpha_{nmij}(\vec{r}(t_k)) C_{nm} + \beta_{nmij}(\vec{r}(t_k)) S_{nm}]$$

$$y_k(\vec{r}_T) = y_k(\vec{r}_N) + \nabla [y_k(\vec{r}_N)] \delta \vec{r}_N + \epsilon_k$$

$$= H_k(\vec{r}_N) \bar{x} + B_k \delta \vec{r}_N + \epsilon_k \quad ; \quad k=1, \dots, j$$

THE ESTIMATOR

$$y = H(\vec{r}_N) \bar{x} + \bar{\varepsilon}$$

$$E[\varepsilon] = 0$$

$$E[\varepsilon \varepsilon^T] = \sigma^2 I$$

$$\hat{x} = (H^T H)^{-1} H^T y$$

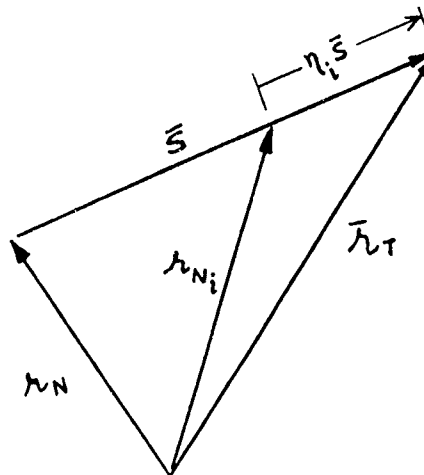
DESCRIPTION OF SIMULATIONS

Orbits :

- * TRUE : 32 day ground track repeat period,
frozen perigee, circular, polar orbit
- * BASIC NOMINAL : Fits true orbit with errors
(worst case)
16, 69, 19 m Radial, Transverse, Normal
- * OTHER NOMINAL : Obtained geometrically
from TRUE and BASIC NOMINAL orbits

$$\vec{r}_{N_i} = \vec{r}_T - \eta_i \cdot \vec{s} \quad , \quad 0 < \eta_i < 1$$

Best case fit : 16, 69, 19 cms



DESCRIPTION OF SIMULATIONS (contd.)

True Field

- * 18 by 18 GEMT1 error model

Simulated Observations :

- * Along TRUE orbit,
- * from TRUE field,
- * at 4 sec. intervals, for 5 days

Noise :

- * additive $N(0, \sigma^2)$ noise
- * for $\sigma = 10^{-4}$ and $\sigma = 10^{-2}$ E.U.

DESCRIPTION OF SIMULATION (contd.)

Estimated Field :

$$y = \nabla [\nabla U (\vec{r}_T)] - \nabla [\nabla (\frac{\mu}{r_N})]$$

- * Compute partials on the NOMINAL orbit
- * Estimate same coefficients as in the TRUE field

Normal Equations :

- * Square Root Free Givens' Rotations
- * CRAY X-MP/24 at UTCHPC

DESCRIPTION OF SIMULATIONS (contd.)

Description of errors :

* Fractional error

$$\begin{aligned}\delta_n &= \frac{1}{2n+1} \sum_{m=0}^n \delta_{nm} \\ &= \frac{1}{2n+1} \sum_{m=0}^n \left[\frac{\text{true} - \text{estimated}}{\text{true}} \right]_{nm}\end{aligned}$$

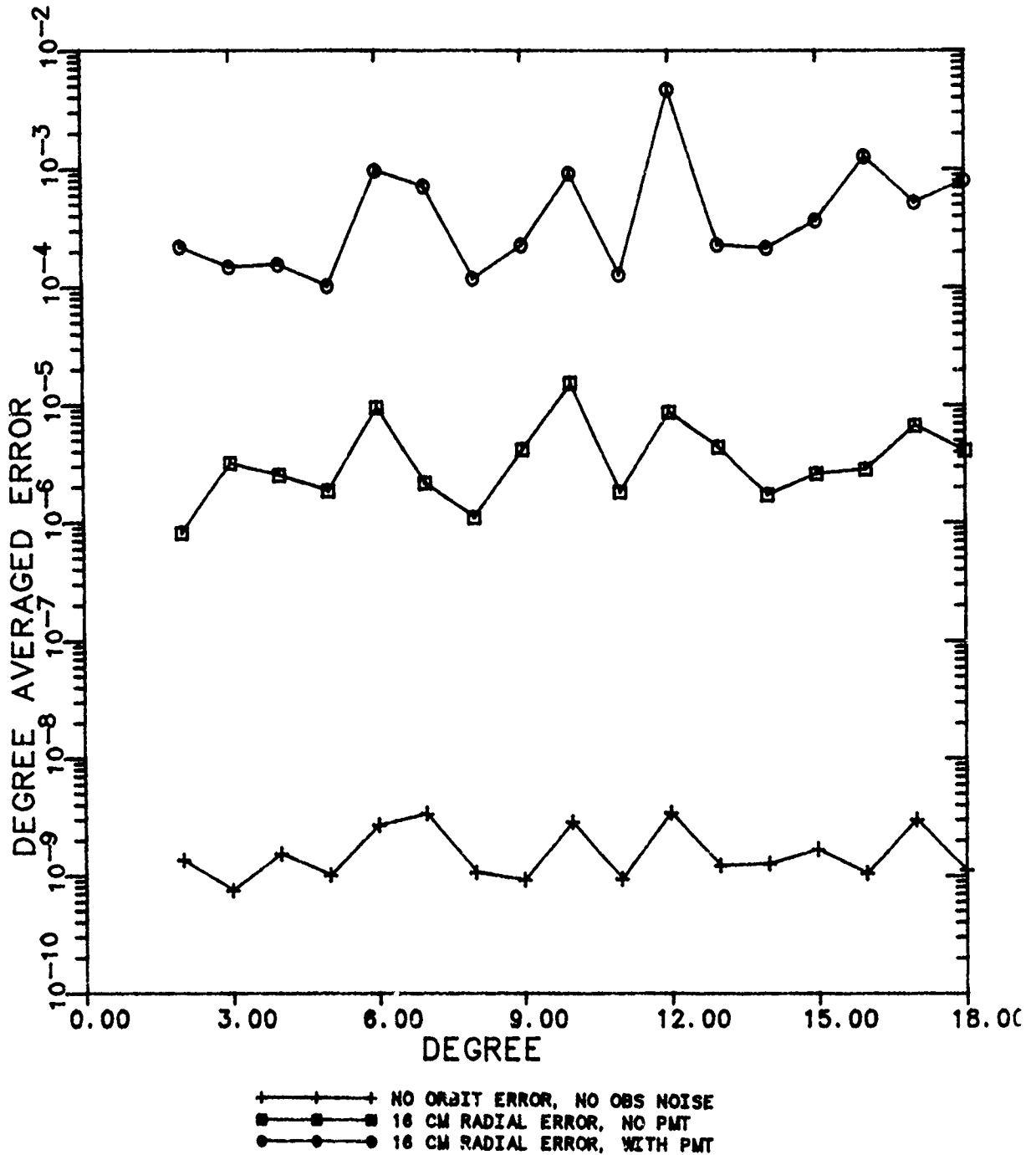
* Root mean square global "geoid" errors

THE POINT MASS TERM $\frac{\mu}{r}$

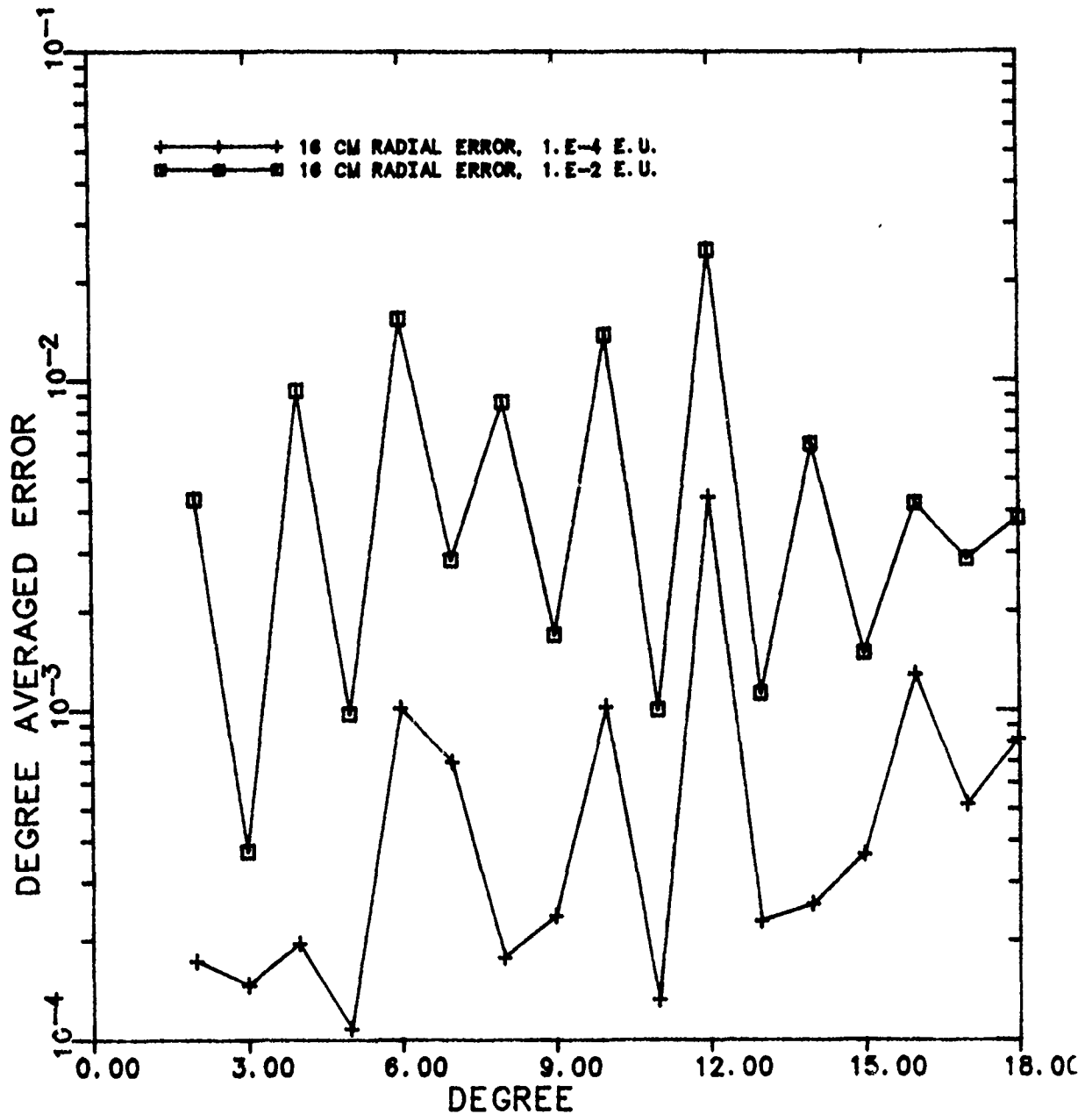
Maximum change of gradient for PMT					
Radial distance (in meters)	100	50	5	1	0.3
$[\Delta G_{ij}]_{\max}$ ($\times 10^{-4}$ E.U.)	1325	663	66	13	4

Maximum change of gradient for perturbation field 360 by 360 field OSU86F ($\times 10^{-4}$ E.U.)			
Displacement (in meters)	Radial	Transverse	Normal
100	5	2	3
50	3	1	2
5	0.3	0.1	0.2
1	0.05	0.02	0.03
0.3	0.016	0.006	0.01

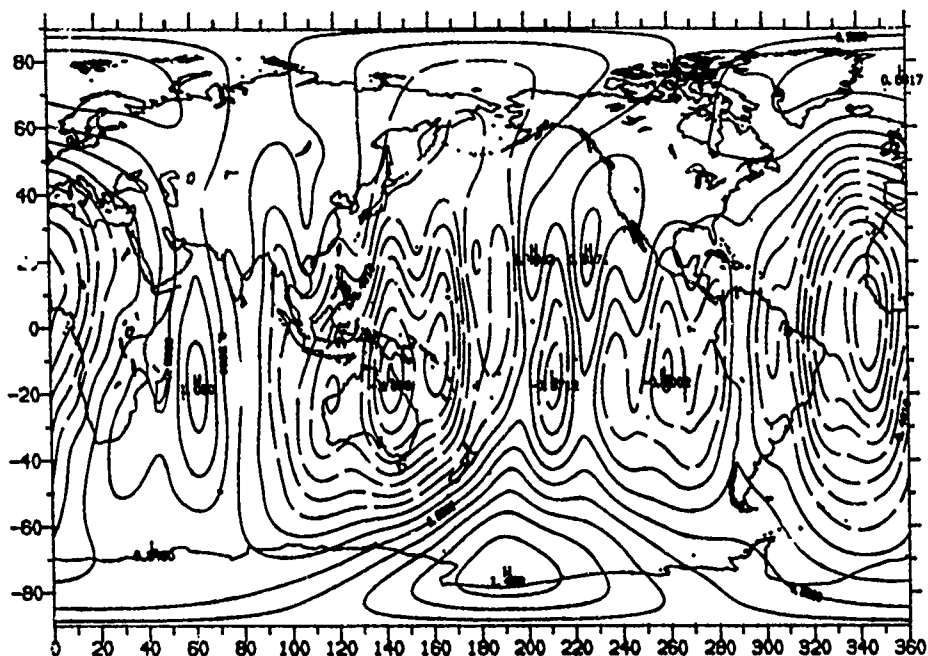
DEGREE AVERAGED FRACTIONAL ERROR AT END OF 5 DAYS
GRAVITY FIELD 18 BY 18 SUBSET OF GEMT1
EFFECTS OF ORBIT ERRORS



DEGREE AVERAGED FRACTIONAL ERROR AT END OF 5 DAYS
GRAVITY FIELD 18 BY 18 SUBSET OF GEMT1
EFFECTS OF ORBIT ERRORS AND OBSERVATION NOISE

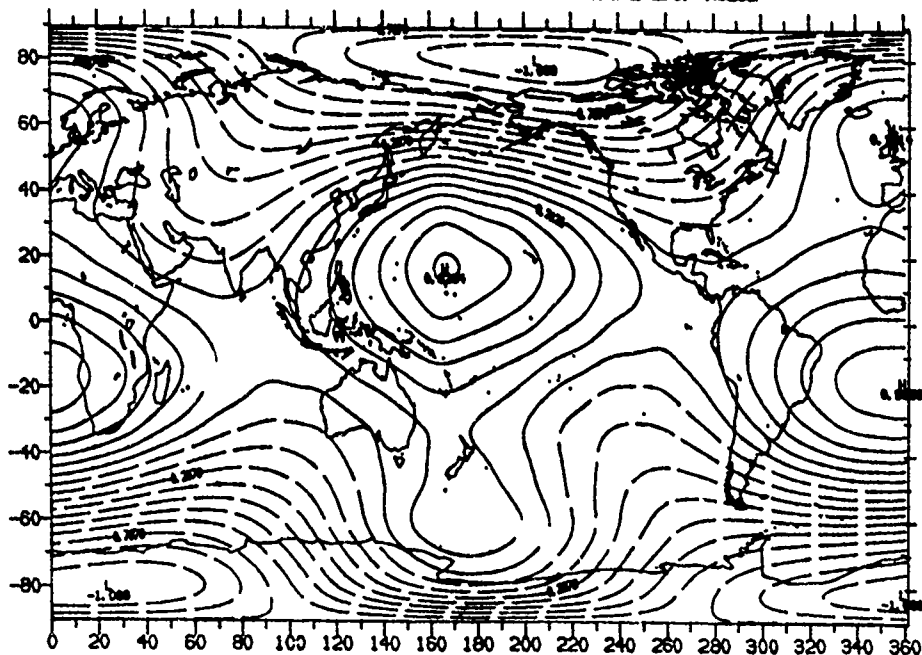


GEOID DIFFERENCE BETWEEN TRUE AND ESTIMATED FIELD
ORBIT ERROR (R.T.N) = (16.69, 19) CM. 1.E-4 E.U. NOISE



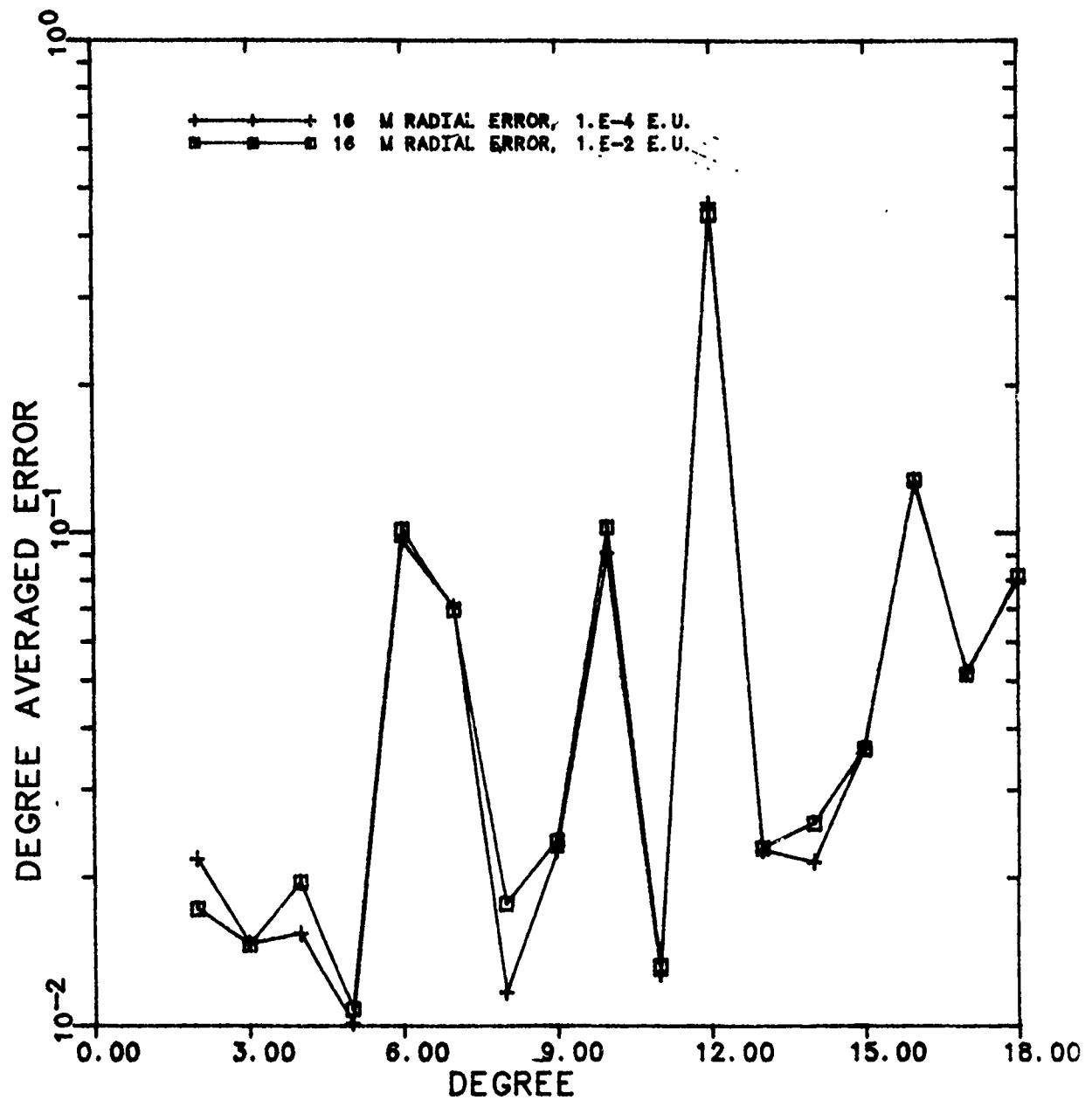
CONTOUR INTERVAL = 0.200 CM
MINIMUM = -1.86 MAXIMUM = 1.46
MEAN = 0.16 RMS = 0.60

GEOID DIFFERENCE BETWEEN TRUE AND ESTIMATED FIELD
ORBIT ERROR (R.T.N) = (16.69, 19) CM. 1.E-2 E.U. NOISE



CONTOUR INTERVAL = 0.100 M
MINIMUM = -1.09 MAXIMUM = 0.63
MEAN = -0.17 RMS = 0.45

DEGREE AVERAGED FRACTIONAL ERROR AT END OF 5 DAYS
GRAVITY FIELD 18 BY 18 SUBSET OF GEMT1
EFFECTS OF ORBIT ERRORS AND OBSERVATION NOISE



RESIDUAL GRADIENTS FROM ERROR IN PMT

Radial orbit error = 16 meters						
Component	G_{xx}	G_{xy}	G_{xz}	G_{yy}	G_{yz}	G_{zz}
Avg resid (10^{-4} E.U.)	187	114	196	156	170	273

- * Systematic residual gradient is compensated by estimated coefficients
- * Low degree and order coefficients absorb the residual

CONCLUSIONS

- * Residual gradient due to PMT affects errors in all coefficients.**
- * Allowable radial orbit error determined by ratio of residual gradient to the noise level.**

Explicitly model the PMT residual

Radial position from GPS tracking

- * Convergence of the iterative corrections of the gravity field and the orbit ?**
- * Simultaneous estimation of the orbit and the gravity field ?**

The Use of Gradiometers in Space to Monitor Changes in the Earth's Gravity Field.

Oscar L. Colombo, University of Maryland Astronomy Program,
Code 626, NASA Goddard Space Flight Center, Greenbelt, Maryland
20771.

Tides, and a variety of processes of non-tidal nature associated with the oceans, the cryosphere, and the atmosphere, exert variable loads on the solid earth, resulting in fluctuations of the external gravitational field. A gravity gradiometer in orbit can, in principle, monitor those changes to study both the loading phenomena and the mechanical properties of the earth's interior governing the response to the loading. Current space techniques, involving laser ranging to spacecraft, can reveal only broad zonal features. An orbiting gradiometer may provide a more complete picture. Given sufficient accuracy, and enough observing time, such an instrument could reveal the geographical distribution, in both latitude and longitude, of changes that occur at frequencies ranging from daily to secular. The gradients of such gravitational changes have most of their power in the band from once per orbital revolution (100 minutes) to once per tenth of revolution. Because of their long wavelengths, they can be sensed at much higher altitudes than the sharper signals of crustal origin that are the main concern of missions such as GRM or Aristoteles. Surface forces like drag are much weaker and less of a problem, and a mission may last for several years, instead of several months. Typically, the signals are of the order of 10^{-7} E, and Paik's cryogenic instrument could allow their resolution at the 1 percent level after one year of continuous observation. The bandwidth of the GRM device (1 Hz) is much larger than needed for this application. However, useful life can be seriously limited by the gradual boiling off of the liquid He coolant. Perhaps instruments of a different kind, able to operate in space for many years, may be constructed specially for sensing the long-wave changes in gravity.

THE USE OF GRADIOMETERS IN SPACE FOR MONITORING CHANGES IN THE GRAVITY FIELD OF THE EARTH

OSCAR L. COLOMBO

**UNIVERSITY OF MARYLAND ASTRONOMY PROGRAM
(NASA GODDARD SFC, CODE 626,
GREENBELT, MD. 20771.)**

Vertical Motion from Glacial Rebound (cm a^{-1})

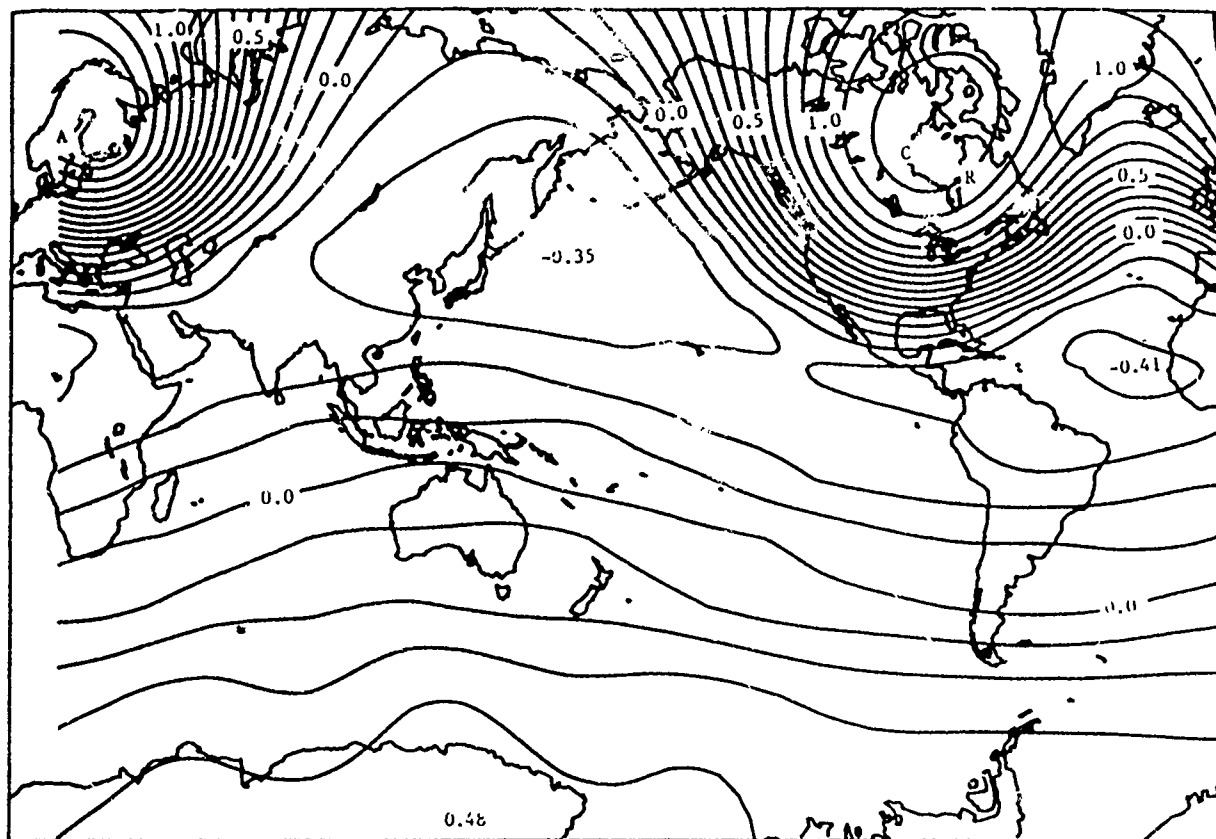


Fig. 5. Present-day rate of change in the radial position of the surface of the solid earth calculated from simplified model of postglacial rebound. Units are centimeters per year. Measured uplift with respect to sea level [Wu and Peltier, 1983] at A, Angermann River (0.9 cm/yr.); R, Richmond Gulf (1.25 cm/yr); C, Churchill (1.0 cm/yr).

CHANGES IN GRAVITY FIELD OF GEOPHYSICAL INTEREST:

TYPICAL AMPLITUDES: $10^{-10} G - 10^{-11} G$ ($G = \text{NORMAL GRAVITY}$)

" SPACE WAVELENGTHS: $10^3 \text{ km} - 10^4 \text{ km}$

" PERIODS: $12 \text{ hs} - 1 \text{ year} - 10^4 \text{ years}$

Table 1. Some Recent Estimates of Temporal Variations in Zonal Harmonics of the Earth's Gravitational Field

<i>Source</i>	<i>Reference</i>	<i>Variation</i>	ΔC_{20}	ΔC_{30}
• earthquakes	Chao & Gross (1987)	nonperiodic w/long period trend	$\pm 5 \times 10^{-13}/\text{yr}$	$\pm 2 \times 10^{-13}/\text{yr}$
• deglaciation rebound of crust	Yoder et al. (1983)	secular (observed)	$-3.0 \times 10^{-11}/\text{yr}$	n.a.
	Rubincam (1984)	on LAGEOS	$-2.6 \times 10^{-11}/\text{yr}$	n.a.
• snow cover	Chao et al. (1987)	periodic: annual semiannual	1×10^{-10} amp 3×10^{-11} amp	6×10^{-11} amp 1×10^{-11} amp
• continental drift Greenland moving at 10 cm/yr in latitude with a depth of immersion of 50 km	Sconzo (1980)	secular	$\pm 2 \times 10^{-14}/\text{yr}$	n.a.
• tidal breaking	Paddack (1967)	secular	$< -5 \times 10^{-13}$	n.a.
• earth, ocean tides	Christodoulidis et al. (1988) and others	periodic (observed)	-- variable -- nontidal contributions lumped in tidal recoveries at forcing frequencies	-- variable --
• air pressure & groundwater	Gutierrez & Wilson (1988)	periodic: annual	1×10^{-9} amp (shows atmosphere/oceans to be ~10 times water storage at annual and ~3 times at semiannual periods)	n.a.
		semiannual	1.5×10^{-10} amp	n.a.
• changes in sea due to ice cap/ glacial melting	Peltier (1988) Yuen et al. (1987)	secular	$2 \times 10^{-11}/\text{yr}$ $2 \text{ to } 8 \times 10^{-12}/\text{yr}$	n.a. $2 \text{ to } 7 \times 10^{-12}/\text{yr}$
• growth of the Antarctic ice sheet equivalent to drop in sea level of 0.3 mm/year	Yuen et al. (1987)	secular	$5 \text{ to } 10 \times 10^{-12}/\text{yr}$	$6 \text{ to } 11 \times 10^{-12}/\text{yr}$
• continental water storage, aquifers, lakes	Chao (1988)	periodic: annual semiannual secular	1.5×10^{-10} amp 5×10^{-11} amp $1 \times 10^{-12}/\text{yr}$	1.4×10^{-10} amp 4×10^{-11} amp n.a.

POSSIBLE TECHNIQUES FOR MEASURING GRAVITY CHANGES FROM SPACE:

SATELLITE LASER TRACKING

PRINCIPLE: MAPS LONG-WAVE ZONAL SIGNALS BY DETECTING LARGE RESONANT ORBITAL PERTURBATIONS

REQUIREMENTS: ONE LAGEOS/STARLETTE-TYPE SATELLITE FOR EACH TWO ZONALS (APPROX. 4 SATELLITES ROUGHLY EQUISPACED IN INCLINATION TO RESOLVE ZONAL CHANGES TO DEGREE 8, OR 25 DEGREES RESOLUTION)

LIMITATIONS: DRAG CORRUPTS SIGNALS, ONLY ZONALS RESOLVABLE, SEVERAL SPACECRAFT NEEDED.

GPS TRACKING

PRINCIPLE: MEASURES WHOLE FIELD (ZONAL AND NON-ZONAL) BY TRACKING OF A LOW SPACECRAFT CARRYING A GPS RECEIVER, BY SIGNALS FROM THE GPS SATELLITES.

REQUIREMENTS: ADDITIONAL RECEIVERS ROUND THE WORLD TO CORRECT CLOCK ERRORS IN TRANSMITTERS AND ORBITING RECEIVER

LIMITATIONS: HIGH PHYSICAL STABILITY OF VARIOUS COMPONENTS NEEDED, BUT NO GOOD CONTROL ON CONDITIONS ON GPS SATELLITES, OR ON GROUND RECEIVERS; DRAG.

GRM-TYPE SATELLITE SATELLITE TRACKING

PRINCIPLE: MEASURES WHOLE FIELD WITH TWO DRAG-FREE SPACECRAFT A FEW HUNDREDS OF KM APPART ON SAME ORBIT, TRACKING EACH OTHER BY TWO WAY DOPPLER/LASER.

REQUIREMENTS: DRAG FREE SPACECRAFT, HIGH PHYSICAL STABILITY OF COMPONENTS.

LIMITATIONS: REQUIRES VERY GOOD NON-GRAVITATIONAL FORCE COMPENSATION (DRAG, RADIATION PRESSURE, ETC.).

CRYOGENIC GRAVITY GRADIOMETER

PRINCIPLE: MEASURES WHOLE FIELD BY SENSING DIFFERENCE MODE BETWEEN ALIGNED ACCELEROMETERS BY SENSING WITH S.Q.U.I.D.S. THE MAGNETIC FLUX DISPLACED BY SUPERCONDUCTING PROOF MASSES.

REQUIREMENTS: SIMILAR TO GRM-TYPE SAT.-SAT. TRACKING.
HIGH PHYSICAL/MECHANICAL STABILITY, REJECTION OF COMMON MODE.

LIMITATIONS: SELF-GRAVITATION, VIBRATIONS, RESIDUAL COMMON MODE ACCELERATIONS, SCALE FACTOR CALIBRATION.

CHARACTERISTICS OF A GRADIOMETER MISSION FOR MAPPING TEMPORAL CHANGES IN GRAVITY

ACCURACY: 10^{-5} TO 10^{-6} E FOR A BANDWIDTH OF 0.01. Hz

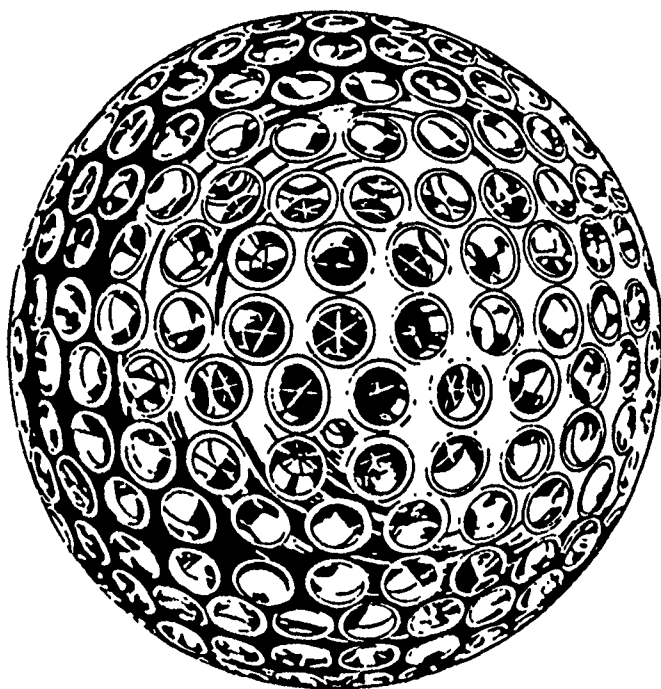
BECAUSE CHANGES CANNOT BE MEASURED DIRECTLY ON EARTH, A GOOD DEAL OF NEW SCIENCE CAN BE OBTAINED.

SIGNALS HAVE LONG SPATIAL WAVE LENGTHS, SO THERE IS SLOW ATTENUATION WITH ALTITUDE: A HIGH ORBIT (600-1000 KM) CAN BE CHOSEN.

WITH ORBIT 600-1000 KM HIGH: MUCH LESS DRAG THAN FOR GRM MISSION. DRAG FREE SYSTEM CAN USE HELIUM BOILOFF OF CRYOGENIC GRADIOMETER FOR PROPULSION, SO MUCH LESS WEIGHT THAN USING HYDRAZINE AT 200 KM (MORE THAN ONE ORDER OF MAGNITUDE LESS FOR PROPELLANT ALONE)

A SPACECRAFT ALREADY IN DEVELOPMENT (GP-B) COULD BE USED (DRAG FREE USING HELIUM BOILOFF, CRYOGENIC PAYLOAD, ONE AXIS SPIN STABILIZED, PRECISE ATTITUDE IN INERTIAL SPACE DETERMINED BY TELESCOPES, SPIN MAY HELP SEPARATE SELF-GRAVITATION AND OTHER SPURIOUS SIGNALS FROM THE DESIRED GRAVITATIONAL INFORMATION.

BECAUSE OF GREAT SENSITIVITY REQUIRED, PROBLEMS LIKE SELF-GRAVITATION CAN BE DIFFICULT TO SOLVE.



△ J2 (CM OF WATER)

1 CM



△ GRAVITY

10^{-10} G



△ ORBIT (RESONANT, IN METERS)

1.5 M

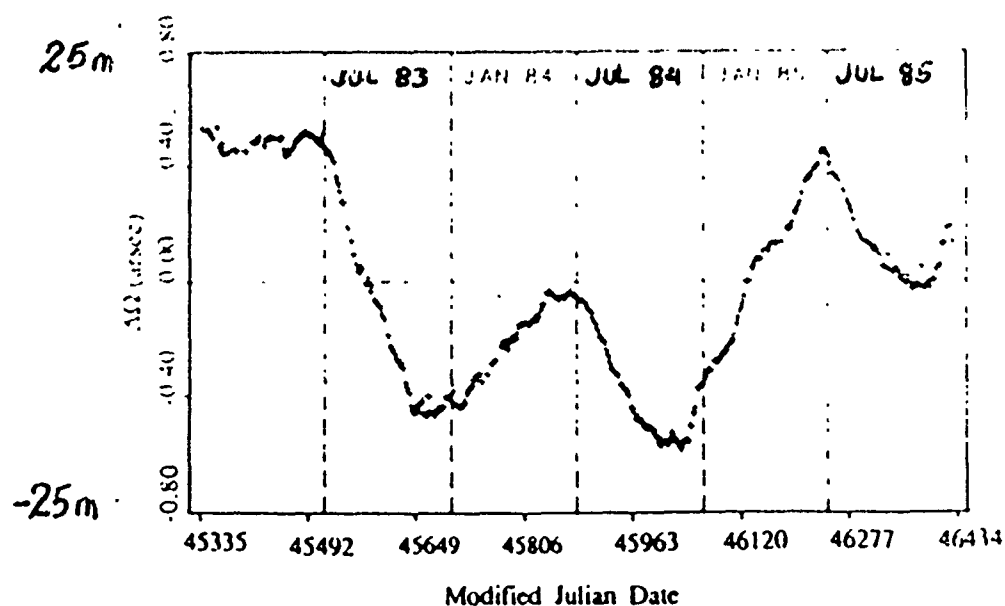


Fig. 1. History of Starlette node residual obtained from the three-year continuous orbit using the nominal force and measurement models.

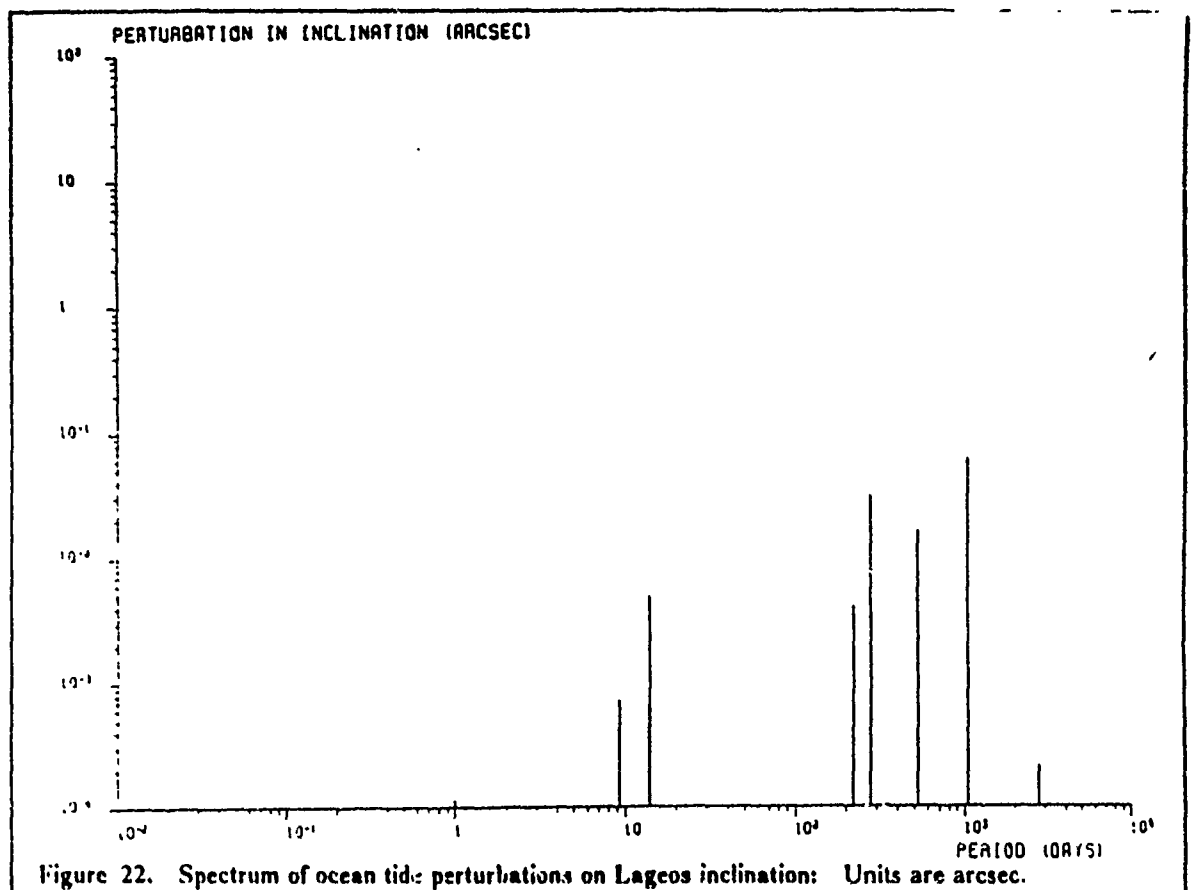


Figure 22. Spectrum of ocean tide perturbations on Lageos inclination: Units are arcsec.

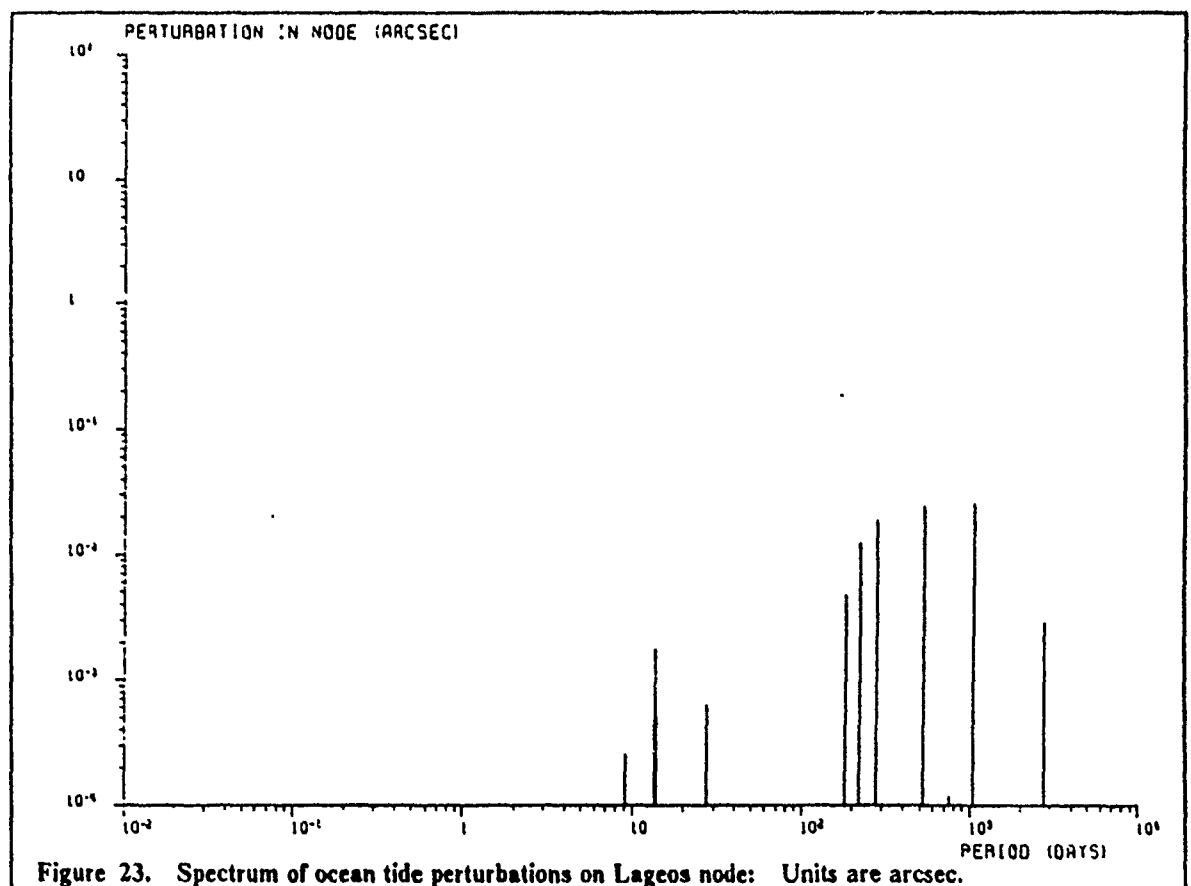
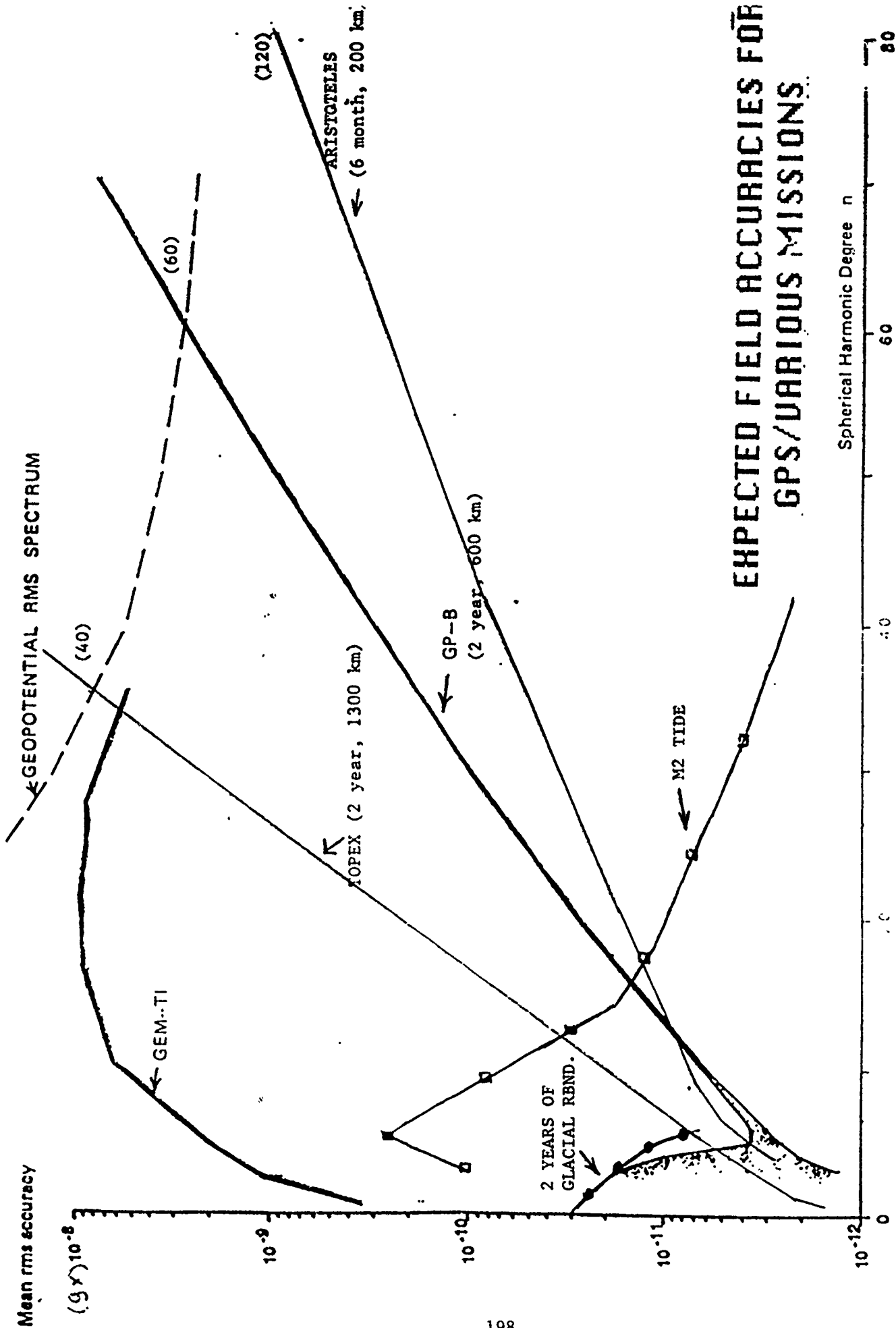
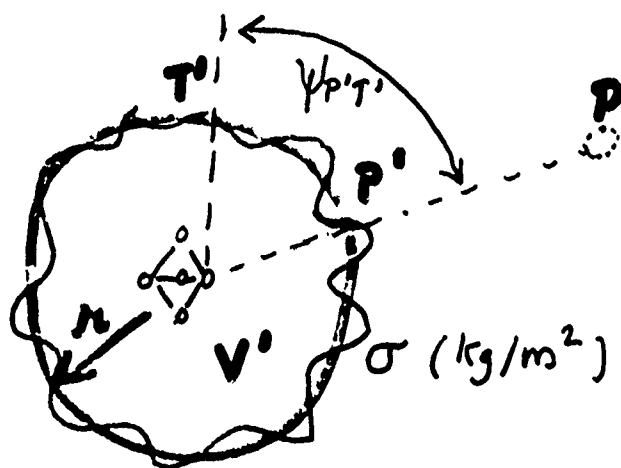
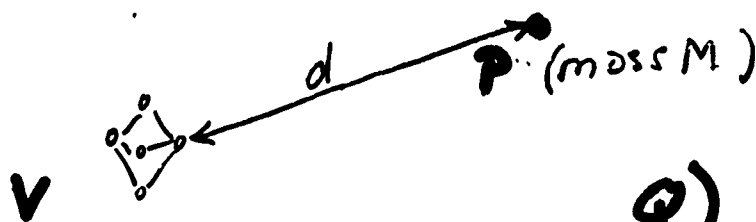


Figure 23. Spectrum of ocean tide perturbations on Lageos node: Units are arcsec.



SELF-GRAVITATION . (FOOLING A 2ND AND 3RD GRADIENT DETECTOR)



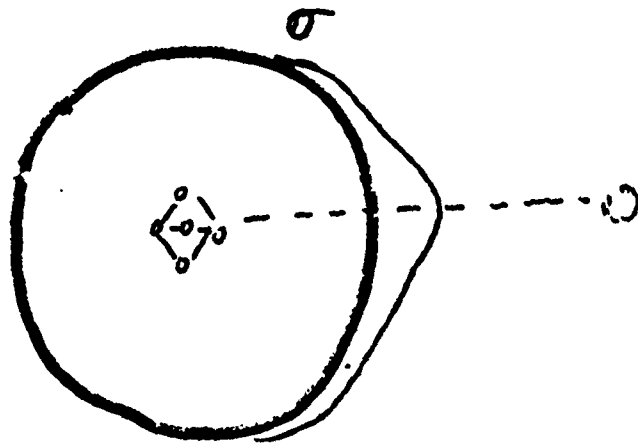
Q) Is there a density distribution σ on a sphere of radius R about the gradiometer such that the potential $V' = V$ inside the sphere?

A) YES

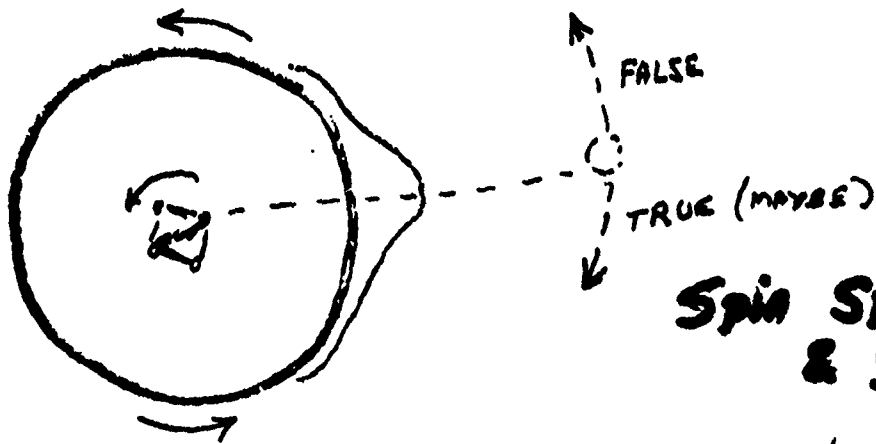
$$\sigma(T') = \frac{M}{4\pi R} (d^2 - R^2) [d^2 + R^2 - 2dR \cos(\psi_{T'P'})]^{-3/2}$$

Q) Is σ realistic?

σ looks like this:



One possible solution:

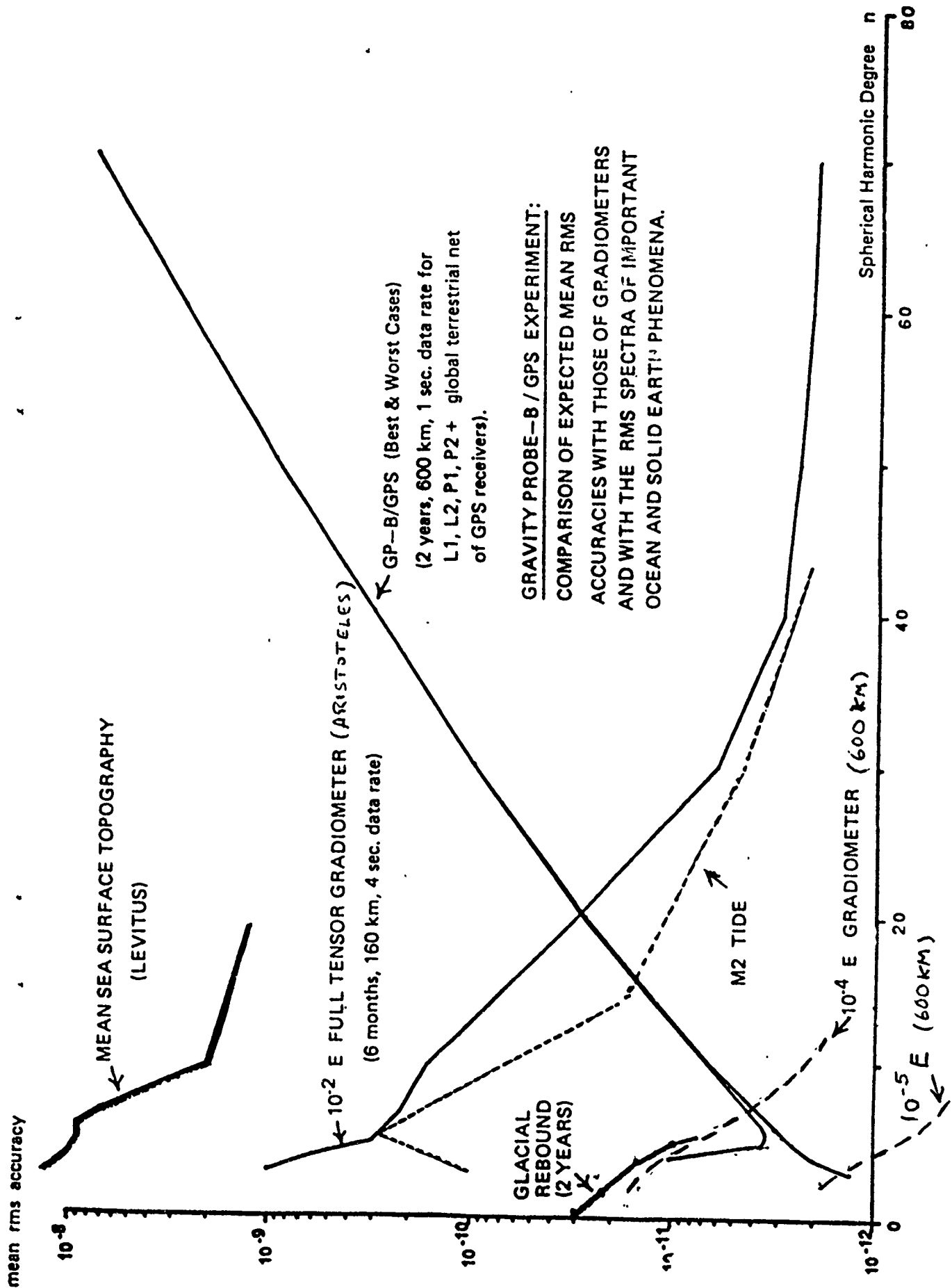


**Spin Spacecraft
& gradiometer**

(while trying to prevent
counter-rotating waves!)

Advantages:

- One axis is inertially stable
- Telescope can point along axis to a star (attitude sensor)
- Separation in frequency of gravity from instrumental & spacecraft "noise" sources —



GRAVITY PROBE-B / GPS EXPERIMENT:

COMPARISON OF EXPECTED MEAN RMS

ACCURACIES WITH THOSE OF GRADIOMETERS
AND WITH THE RMS SPECTRA OF IMPORTANT
OCEAN AND SOLID EARTH PHENOMENA.

Q) IS σ REALISTIC?

A) IF ONE IS CONCERNED WITH 2ND AND HIGHER GRADIENTS, YES.

BECAUSE:

(1) ONLY SPHERICAL HARMONICS WITH DEGREE $n > 2$ CONTRIBUTE, AND THEIR INTEGRALS ON THE SPHERE — THEIR MASSES — ARE 0
(REDISTRIBUTIONS WITHOUT NET CHANGE IN MASS)

(2) THE EXPANSION CONVERGES VERY FAST, SO 2ND GRADIENT COMES FROM 2ND HARMONIC TO ORDER $(\frac{R}{a}) \approx 10^{-7}$
3RD GRAD. " 3RD " " " " "

$$\sigma(T') = \frac{M}{4\pi a^2} \sum \left(\frac{R}{a}\right)^{n+1} (2n+1) P_n(\psi_{p,T'})$$

Max(P_n) = 1, so IF $a = 1m$, $M = 6 \times 10^{24} \text{ Kg}$ (Earth)

$$\sigma_2 < 3 \times 10^3 \text{ Kg/m}^2 \text{ (WHOLE EARTH)}$$

$3 \times 10^3 \times 10^{-10} \text{ Kg/m}^2$ (TIME VARIATION SOURCE IS $< 3 \times 10^{-7} \text{ Kg/m}^2$)

AND $\sigma_3 < 10^{-7} \sigma_2$

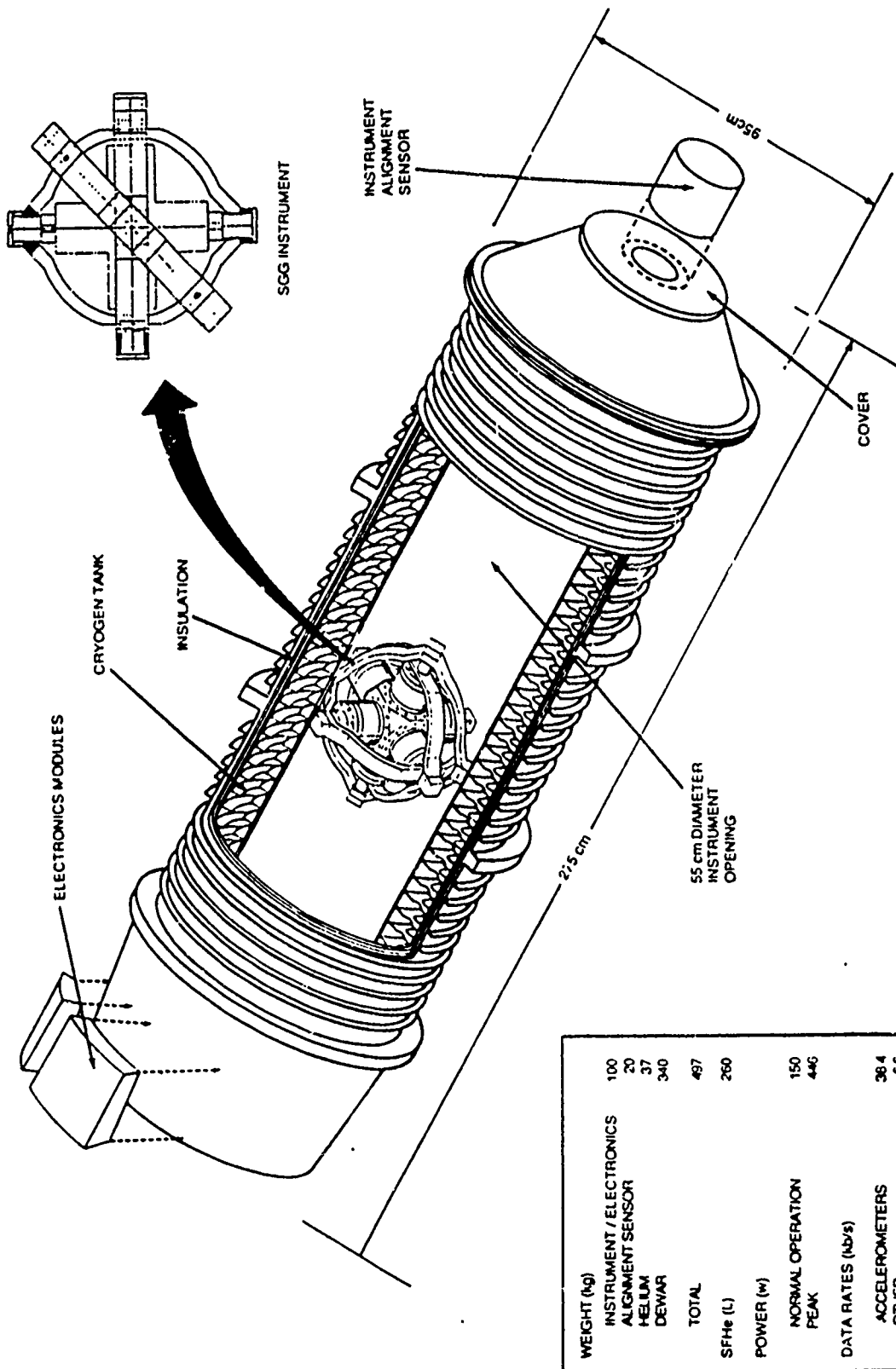


Figure 4-9. SGG Experiment Module concept - modified GRM.

Inversion of Airborne Gravity Gradient Data,
South-western Oklahoma

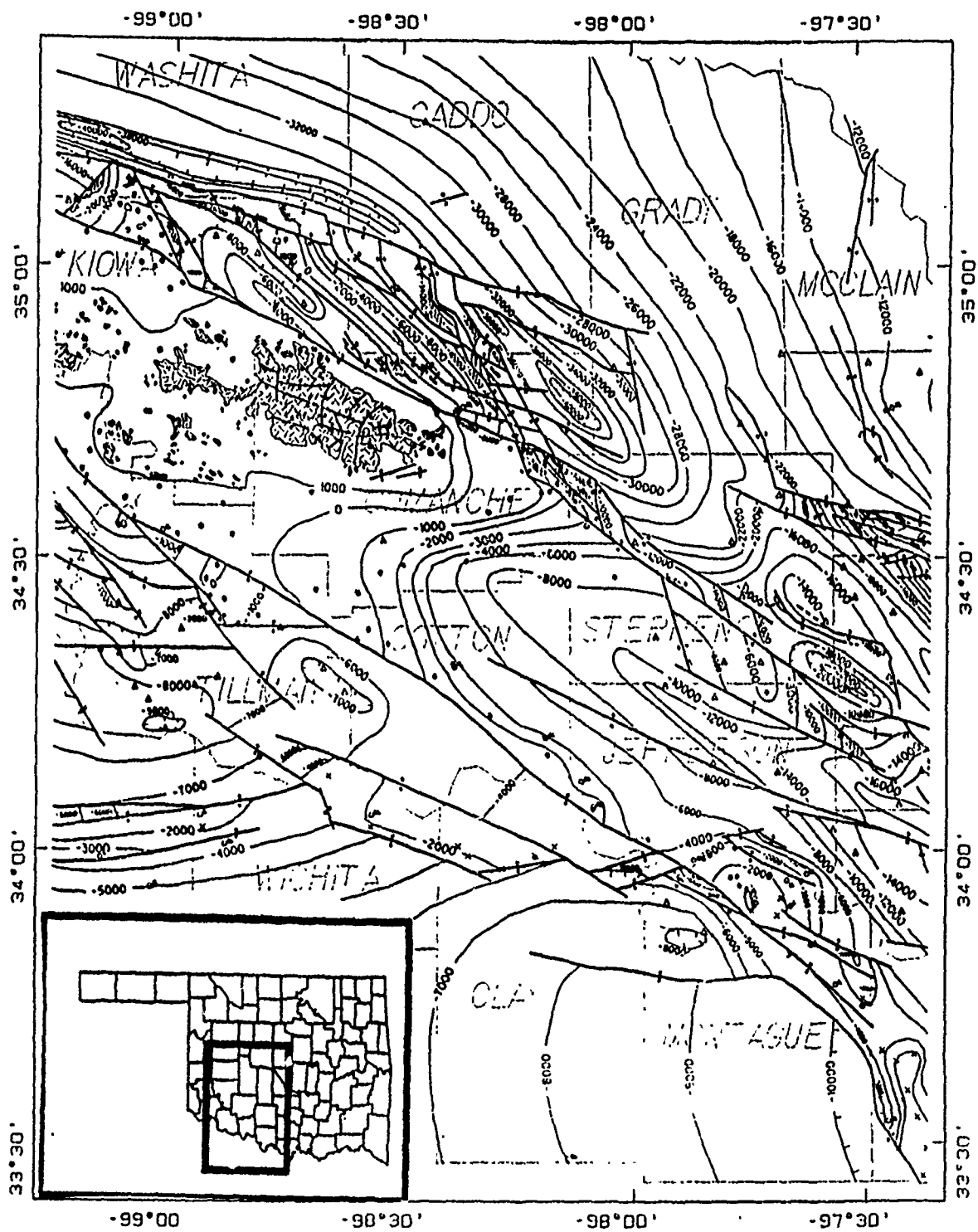
D. W. Vasco (Center for Computational Seismology Lawrence
Berkeley Laboratory, Department of Geology and
Geophysics, University of California, Berkeley, CA
94720; 415 486-7312)

C. L. Taylor (Geophysics Laboratory, Hanscom AFB, MA,
01731; 617 377-3078)

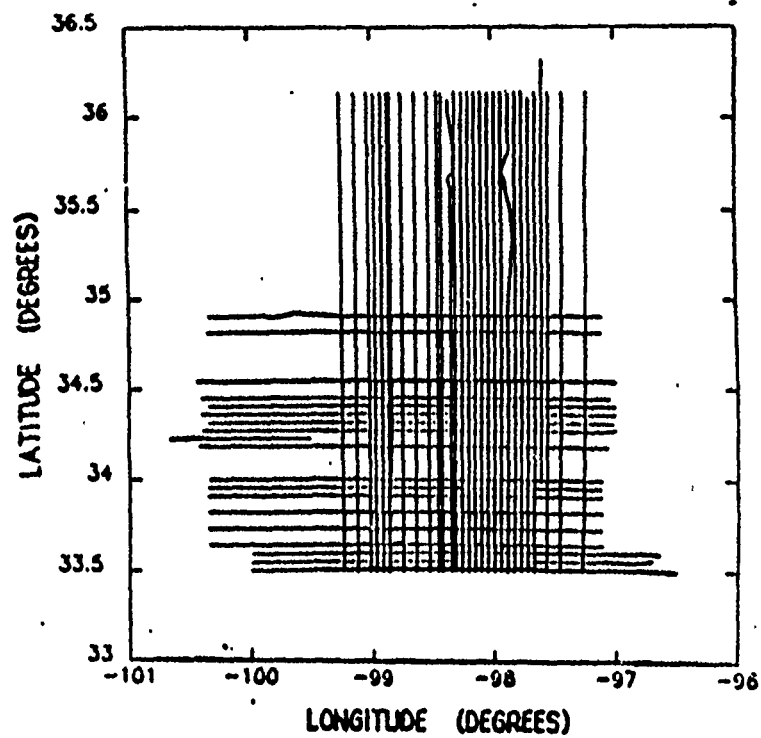
We present a preliminary interpretation of gravity gradient anomalies. The diagonal elements of the gradient tensor, as recorded by the Bell airborne Gravity Gradient Survey System (GGSS), are used to compute the basement topography in south-western Oklahoma. This is accomplished through a non-linear inverse procedure based on the conjugate gradient algorithm. In general the resulting model contains a ridge of shallow basement material (<3.0 km) trending east south-east. This ridge is bounded on the north and the south by troughs in the basement which extend as deep as 10.0 km. The gradient field which results from this model fits most of the GGSS observations within their estimated errors of 12.0 E. The depths also agree with a set of available oil well depths to the basement and with inferred faults in these igneous rocks. In order to assess the derived solution, the problem was linearized about the final solution and linear parameter resolution and parameter covariances were computed. For the most part these basement depths are well resolved and the resolution matrix is diagonally dominant. Furthermore, the parameter standard errors are small, the majority are less than 1.0 km. Only 26 parameters out of 98 have errors larger than this.

**INVERSION OF AIRBORNE GRAVITY
GRADIENT DATA, SOUTH-WESTERN
OKLAHOMA.**

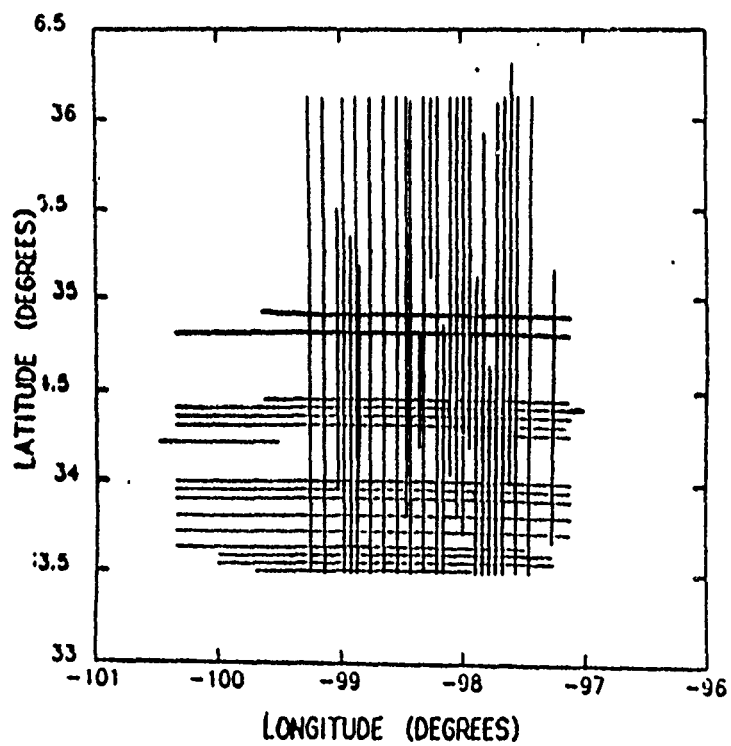
**D. W. VASCO & C. L. TAYLOR
GEOPHYSICS LABORATORY (AFSC)
HANSCOM AFB, MA 01731-5000**



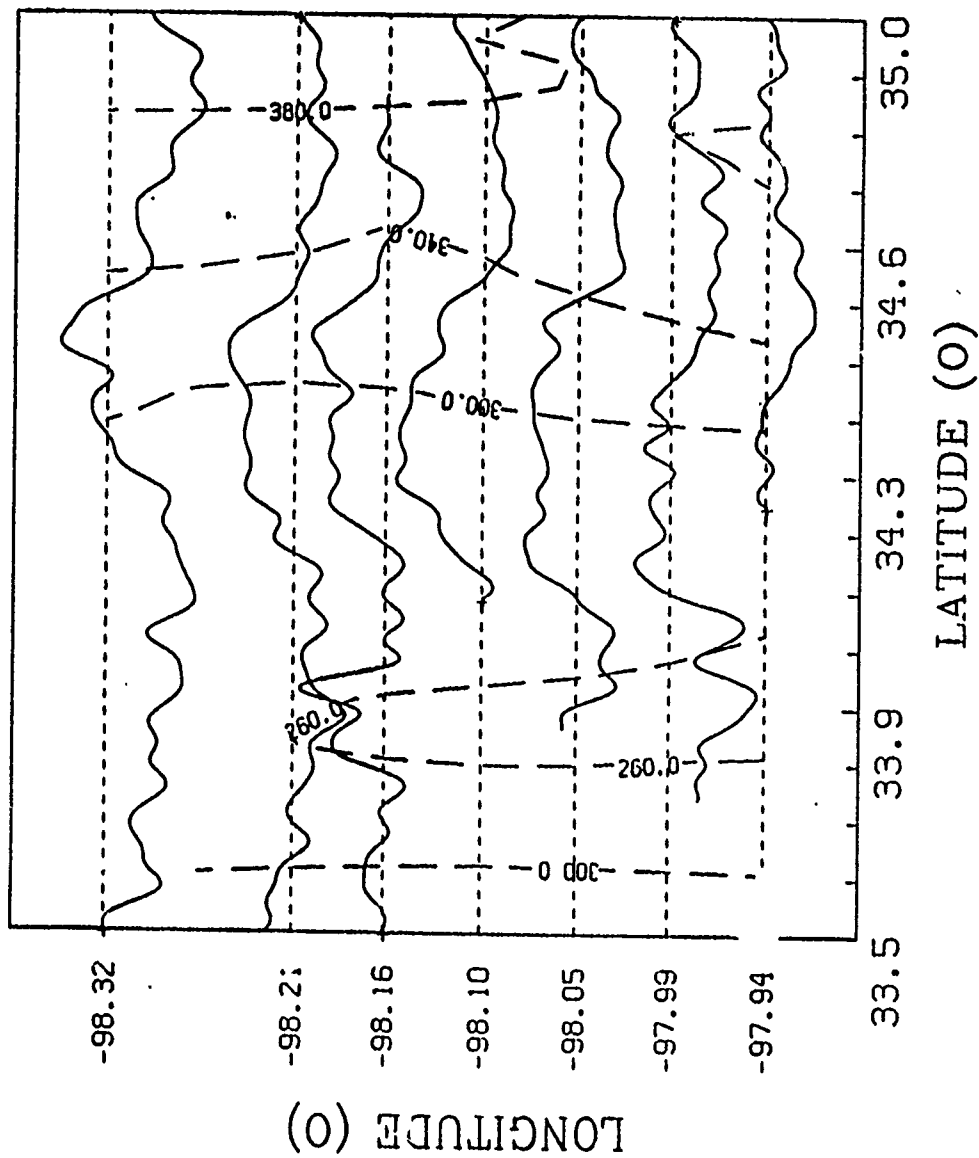
AERIAL VIEW OF ORIGINAL SET OF TRACKS.

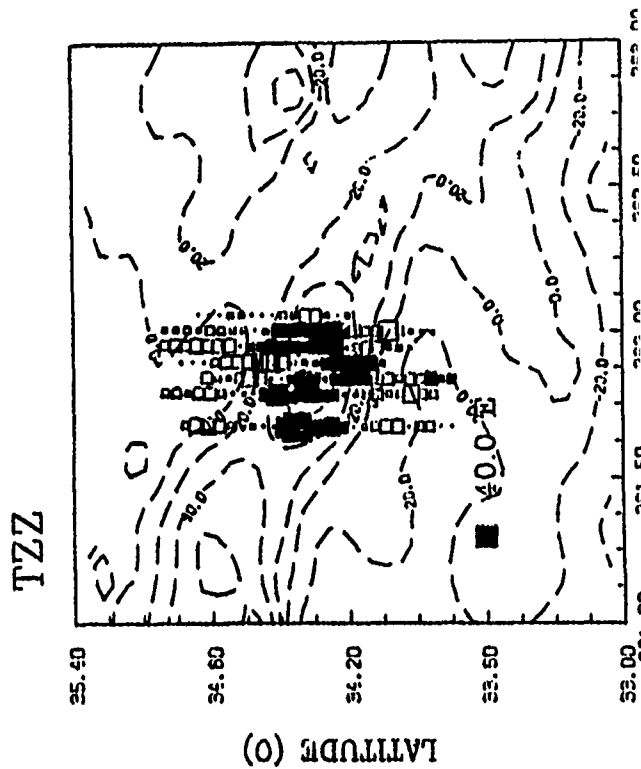
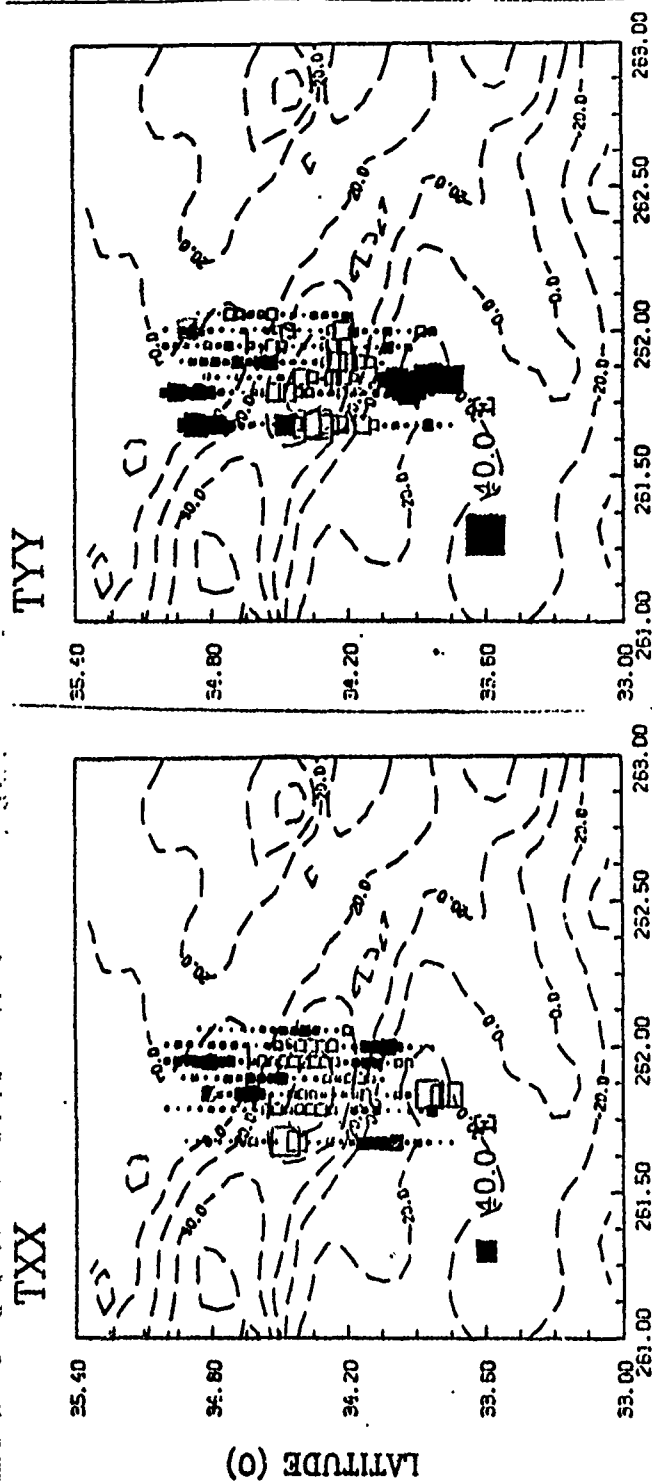


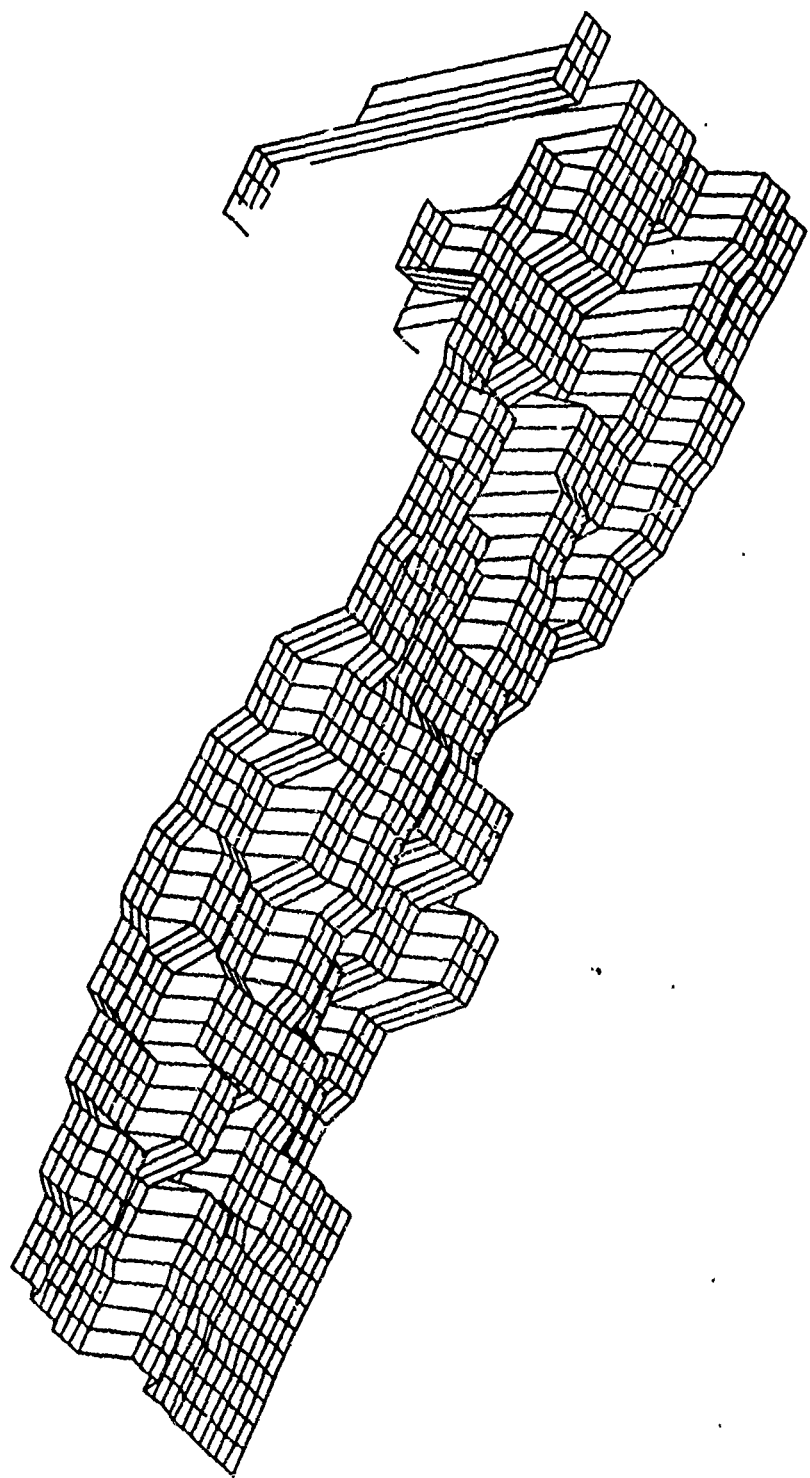
AERIAL VIEW OF TRACKS AFTER PLATFORM
ACCELERATION EDITING.



TZZ COMPONENTS TRACKS 41-48







For a prism defined by:

$$\alpha_1 \leq \xi_1 \leq \alpha_2, \beta_1 \leq \xi_2 \leq \beta_2, \gamma_1 \leq \xi_3 \leq \gamma_2$$

where ξ are the source coordinates, then the diagonal elements of the gradient tensor are:

$$T_{xx} = \rho G \arctan(\xi_2 \xi_3 / \xi_1 r) \Big|_{\alpha} \Big|_{\beta} \Big|_{\gamma}$$

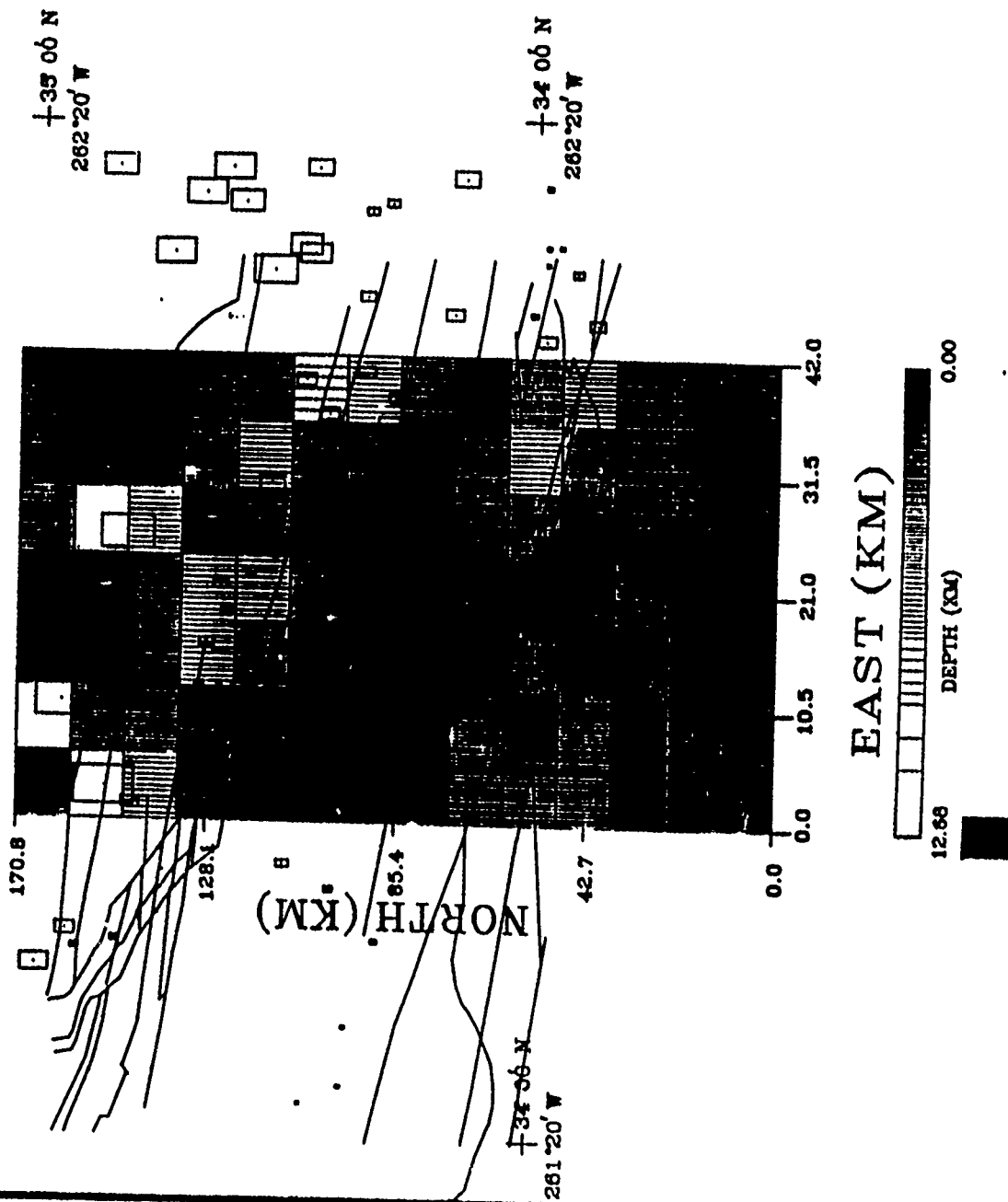
$$T_{yy} = \rho G \arctan(\xi_1 \xi_3 / \xi_2 r) \Big|_{\alpha} \Big|_{\beta} \Big|_{\gamma}$$

$$T_{zz} = \rho G \arctan(\xi_1 \xi_2 / \xi_3 r) \Big|_{\alpha} \Big|_{\beta} \Big|_{\gamma}$$

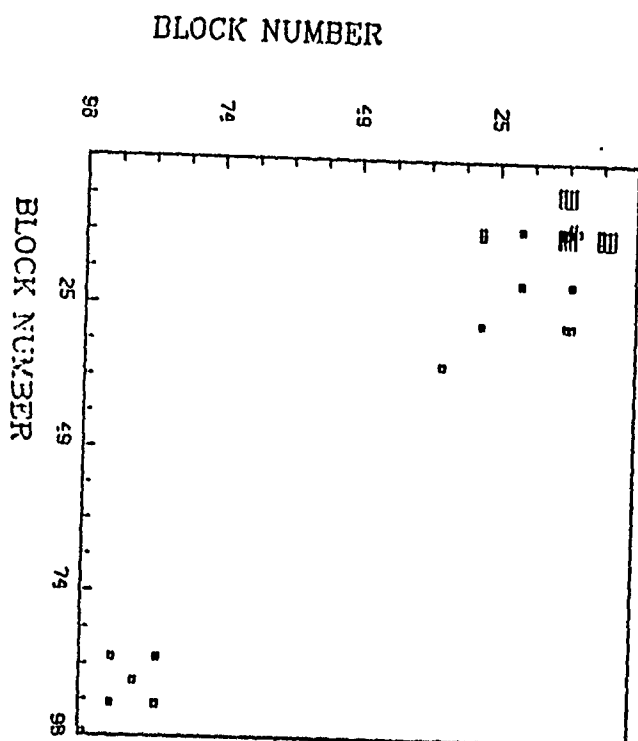
where : G = gravitational constant
 ρ = density contrast
 r = source-receiver distance

The objective functional is:

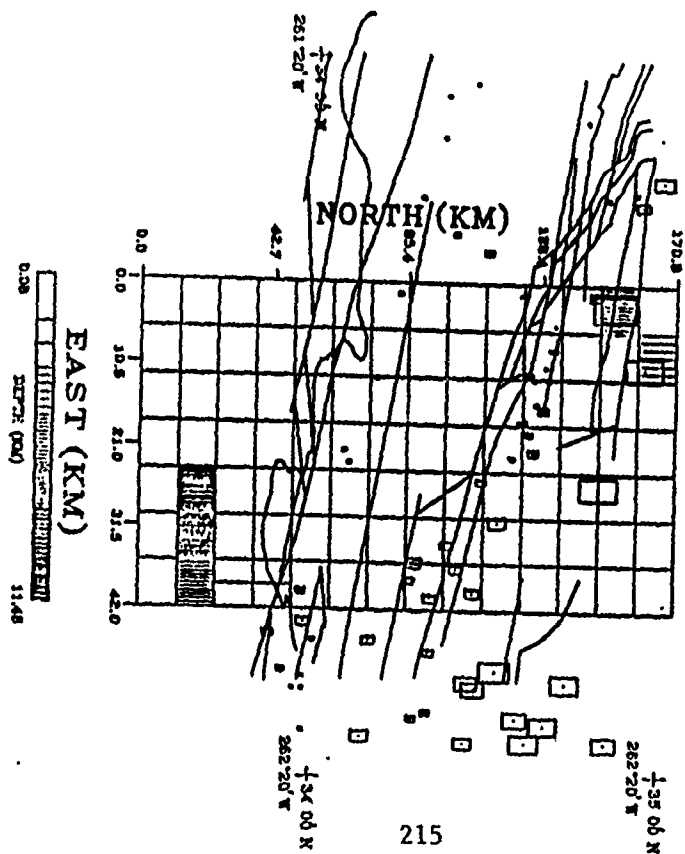
$$\rho G^2 \sum_{i=1}^M \left[(T_{xx}^{oi} - \sum_{l=1}^N \arctan(\xi_2 \xi_3 / \xi_1 r) |_{\alpha' | \beta' | \gamma'})^2 + \right. \\ (T_{yy}^{oi} - \sum_{l=1}^N \arctan(\xi_1 \xi_3 / \xi_2 r) |_{\alpha' | \beta' | \gamma'})^2 + \\ \left. (T_{zz}^{oi} - \sum_{l=1}^N \arctan(\xi_1 \xi_2 / \xi_3 r) |_{\alpha' | \beta' | \gamma'})^2 \right]$$

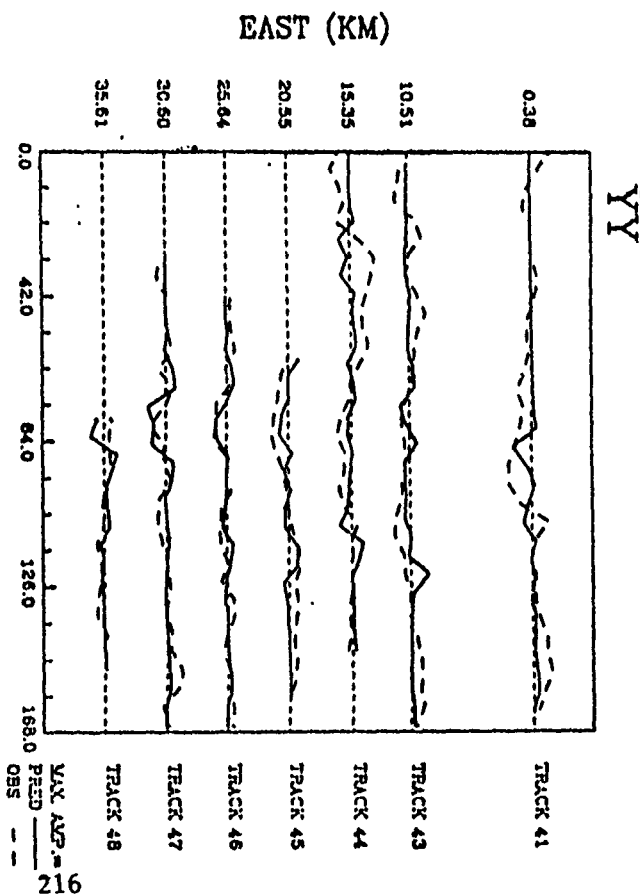
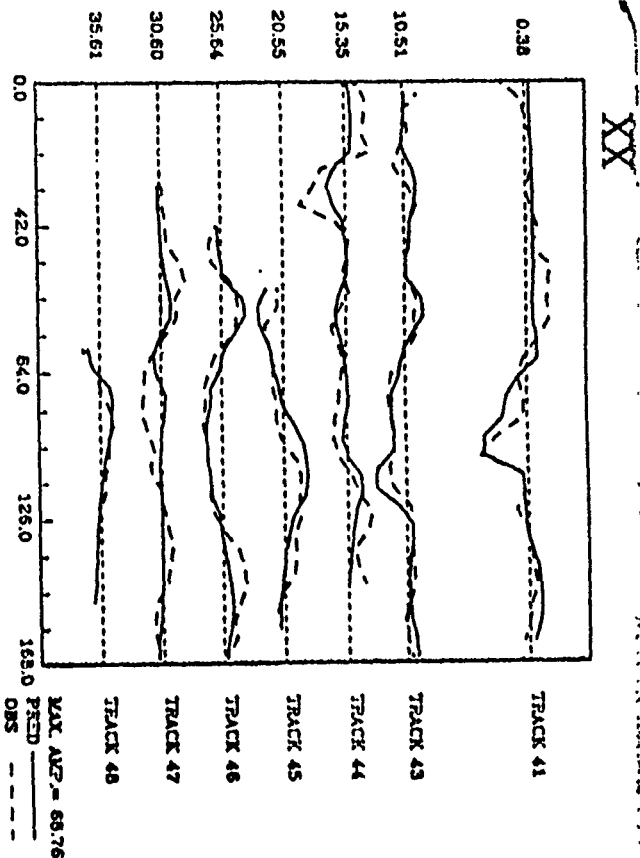


MODEL VARIANCE MATRIX

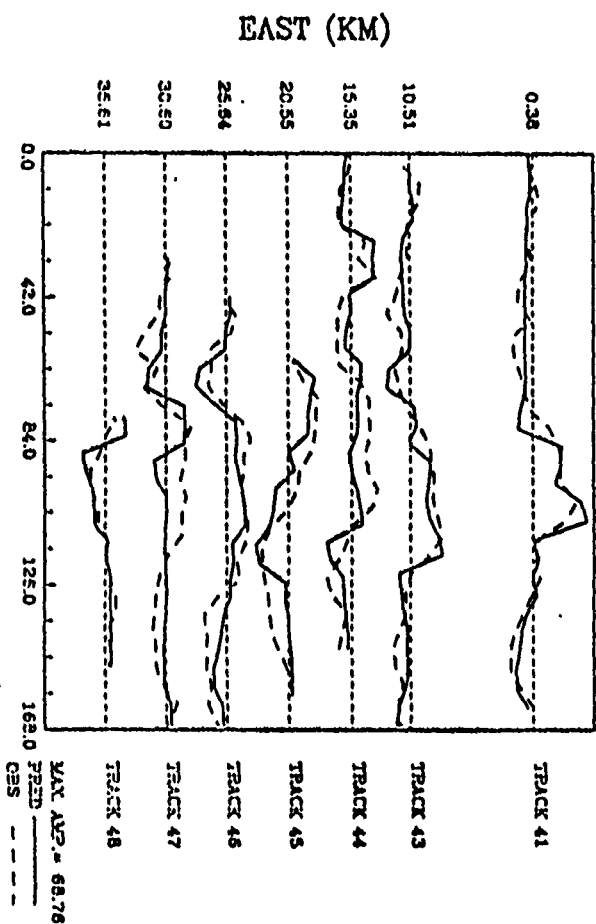


MODEL ERROR



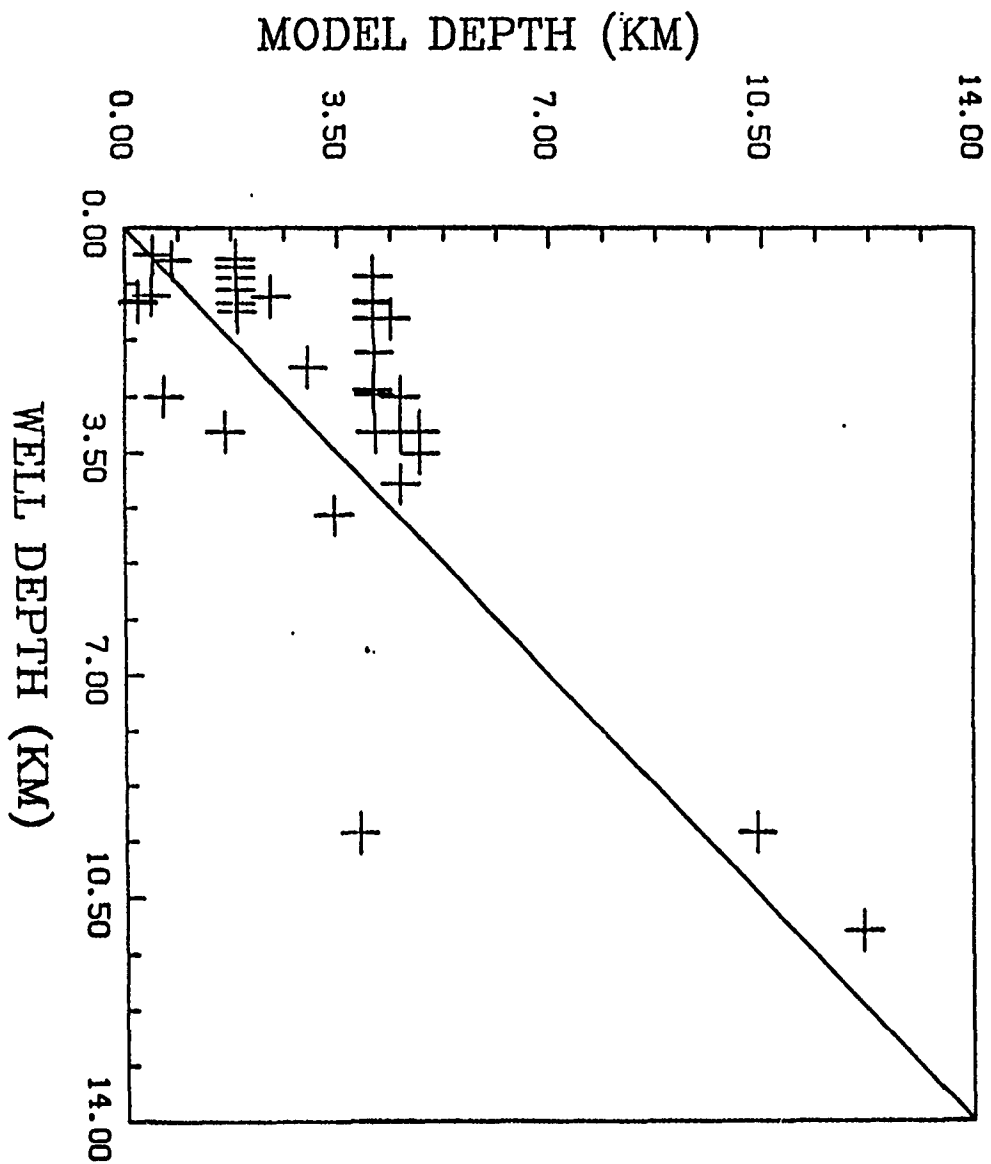


ZZ



NORTH (KM)

BASEMENT DEPTHS



Conclusions:

- *The signal, with a maximum of 57.5 E is above the estimated noise level of 12.0 E and coherent between the seven tracks.
- *The basement model presents a coherent structural feature trending west-northwest to east-southeast. This ridge of higher density material agrees with known basement faults.
- *The model resolution of a majority of the prisms is adequate and the standard errors are quite low, most less than 1.0 Km.
- *The derived solution agrees with known basement structure and available oil well data.

DEVELOPMENT OF A MOBILE GRAVITY GRADIOMETER FOR GEOPHYSICAL EXPLORATION

FJ van Kann, MJ Buckingham, MH Dransfield, AG Mann,
PJ Turner, R Matthews, RD Penny and C. Edwards.

Physics Department,
The University of Western Australia,
Nedlands, Western Australia 6009.

We present a description of a superconducting gravity gradiometer designed for geophysical use. The initial target sensitivity is $1 \text{ Eo}/\sqrt{\text{Hz}}$ in a frequency band below 1Hz.

The OQR instrument, which measures an off-diagonal component [xy] of the gradient tensor, consists of two perpendicular sensors with parallel pivot axes aligned along the vertical z-axis. This configuration of dual Orthogonal Quadrupole Responders enables rejection of angular accelerations about the pivot axis. Rotation about each of the other two axes is controlled independently.

Each of the quadrupole sensors is carefully balanced mechanically at room temperature and, since the pivot is integral to the sensor, this balance is preserved at low temperature. Residual off-balance compensation and matching between each sensor in the pair is achieved magnetically using superconducting trim coils.

Motions are sensed by pairs of superconducting pancake coils arranged in current differencing configurations with SQUID readouts. Apart from that desired, the signal from the primary pair of coils contains small residual terms resulting from the common mode accelerations perpendicular to the pivot axis. Signals from a set of secondary coils are combined passively to eliminate the effects of the common mode acceleration vector. Residual sensitivity to z-axis angular acceleration is treated in a similar way.

Rotation about each of the other two axes is measured optically and controlled by a servo referenced to a room temperature inertial system. The latter is a gimballed platform stabilised by a pair of phase modulated fibre optic gyros to about $2 \cdot 10^{-5} \text{ (rad/sec)}/\sqrt{\text{Hz}}$. The cold gradiometer package is also mounted on gimbals, in this case driven by diamagnetic actuators. The thermal environment in which the package is mounted is carefully controlled and maintains an operating temperature constant to within a few tens of μK at about 5K.

Many of the gradiometer's features have been proved under laboratory conditions and we are presently engaged in testing the complete package prior to transferring it and its support systems into a mobile laboratory in readiness for field trials. Moving base tests are scheduled to begin before the end of the year at the Dongara natural gas fields 300 km north of Perth in Western Australia.

Frank van Kann

Michael Buckingham

Mark Dransfield

Tony Mann

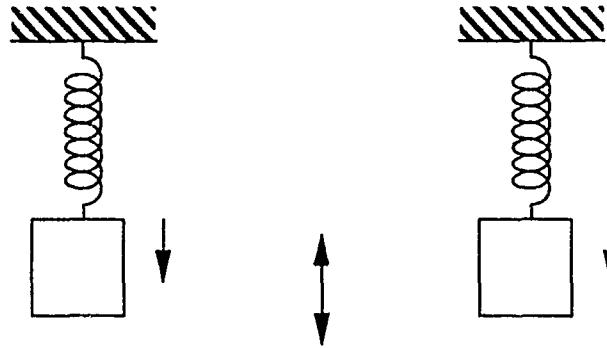
Peter Turner

Rob Penny

Rob(R2D2) Matthews

Cyril Edwards

Spring balance sensors (in line or shear gradients)



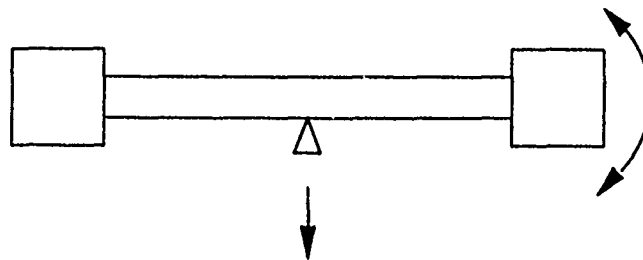
same mechanism for common force and differential force stiffness

⇒ trade off:

low stiffness for high sensitivity

high stiffness for high CMRR (dynamic range problem)

Beam balance sensors (shear gradients)



different mechanisms for common force and differential force stiffness

- low differential force stiffness ≈ 1 Hz \Rightarrow high sensitivity
- high common force stiffness ≈ 1 kHz \Rightarrow high CMRR possible
- tune CMRR during assembly to > 125 dB

$$\tau = \epsilon_{ijk} (g_k(0) M_j + \Gamma_{kl}(0) M_{jl} + \dots)$$

$$g_i \Rightarrow g_i + a_i$$

$$\Gamma_{ij} \Rightarrow \Gamma_{ij} + R_{ij} = G_{ij} \quad \text{i.e. symmetric + antisymmetric}$$

$$\tau = \begin{pmatrix} M_{yy} - M_{zz} & 0 & 0 \\ 0 & M_{zz} - M_{xx} & 0 \\ 0 & 0 & M_{xx} - M_{yy} \end{pmatrix} \cdot \begin{pmatrix} \Gamma_{yz} - \omega_y \omega_z \\ \Gamma_{zx} - \omega_z \omega_x \\ \Gamma_{xy} - \omega_x \omega_y \end{pmatrix} \\ - \begin{pmatrix} M_{yy} + M_{zz} & 0 & 0 \\ 0 & M_{zz} + M_{xx} & 0 \\ 0 & 0 & M_{xx} + M_{yy} \end{pmatrix} \cdot \begin{pmatrix} \alpha_x \\ \alpha_y \\ \alpha_z \end{pmatrix}$$

$$\tau_z = \frac{m}{12} (l^2 - b^2) G_{xy} \quad m = \text{mass}, l = \text{length}, a = b = \text{width}$$

Two bars:-

$$\sigma \propto (\tau_A - \tau_B) + \Delta(\tau_A + \tau_B) + \Delta A_x \ddot{x} + \Delta A_y \ddot{y} + (\Delta S_{xx} - \Delta S_{yy}) \ddot{x} \ddot{y}$$

signal	common mode	residual dipole	induced dipole

$$\tau_A - \tau_B = 2 \frac{m}{12} (l^2 - b^2) (\Gamma_{xy} - \omega_x \omega_y)$$

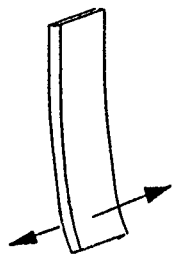
$$\tau_A + \tau_B = 2 \frac{m}{12} (l^2 + b^2) (\alpha_z)$$

$$\Omega = \text{earth rotation rate} = 7.3 \cdot 10^{-5} \text{ rad/sec} = 15^\circ/\text{hr}$$

$\delta\omega_y, \delta\omega_x = \text{platform angular velocities}$

$$\omega_x \omega_y \Rightarrow \Omega (\sin\theta \cos\phi \cdot \delta\omega_y - \cos\theta \cdot \delta\omega_x)$$

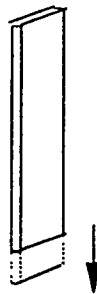
PIVOT DEFORMATION UNDER LOAD



TORSION

$$\frac{a b^3}{L}$$

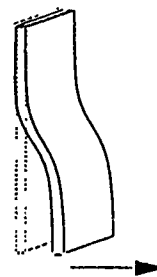
3 Hz



STRETCH

$$\frac{a b}{L}$$

5 kHz

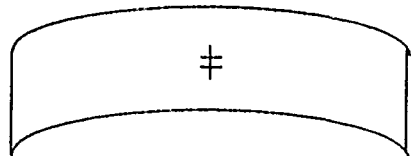
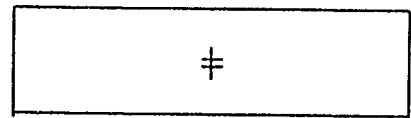
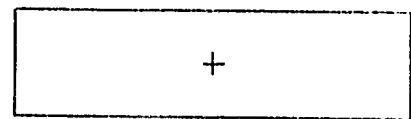
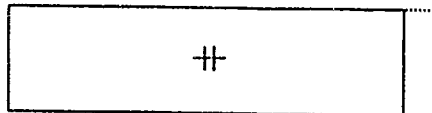
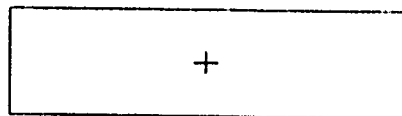


s-BEND

$$\frac{a b^3}{L^3}$$

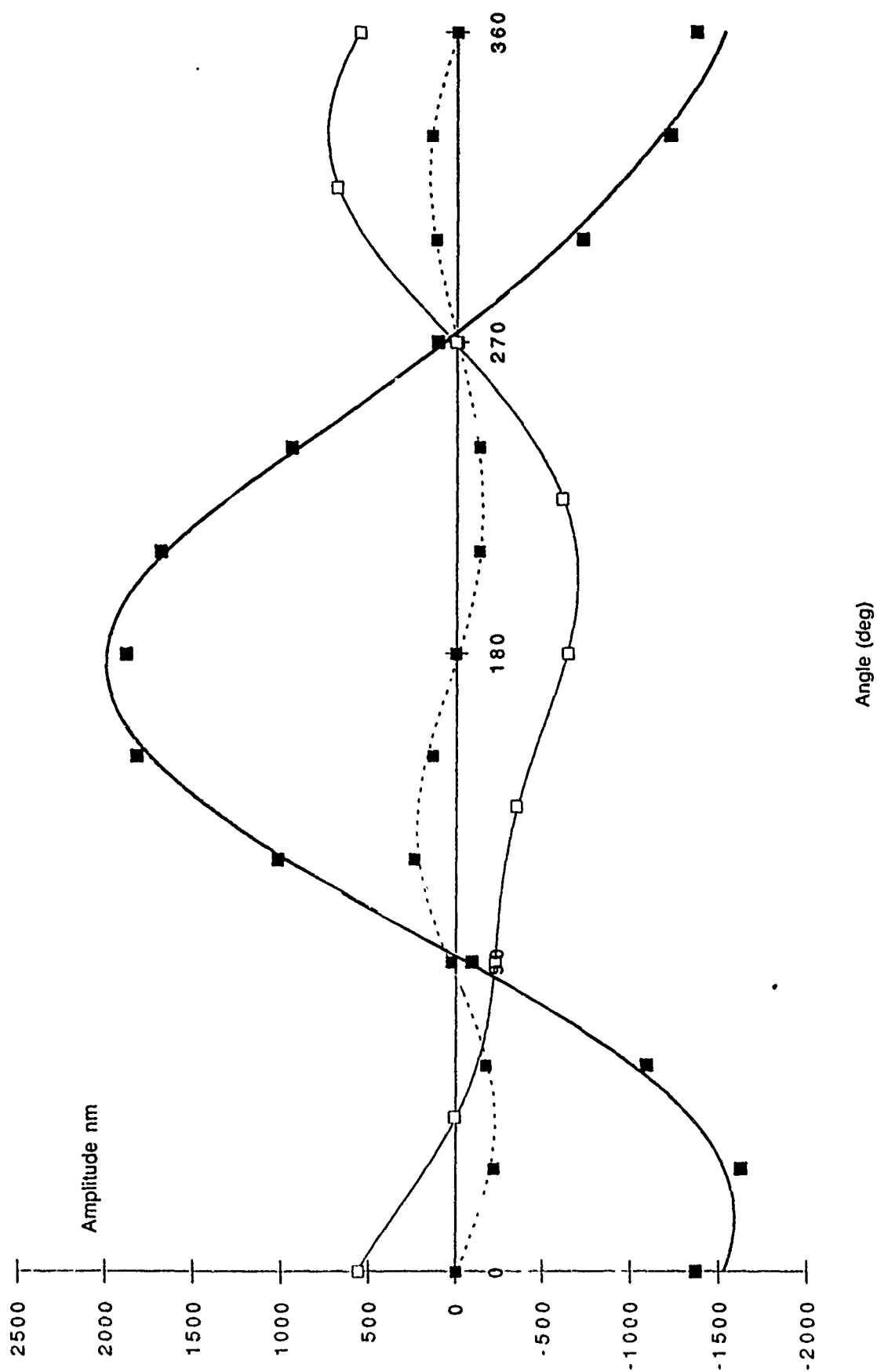
1 kHz

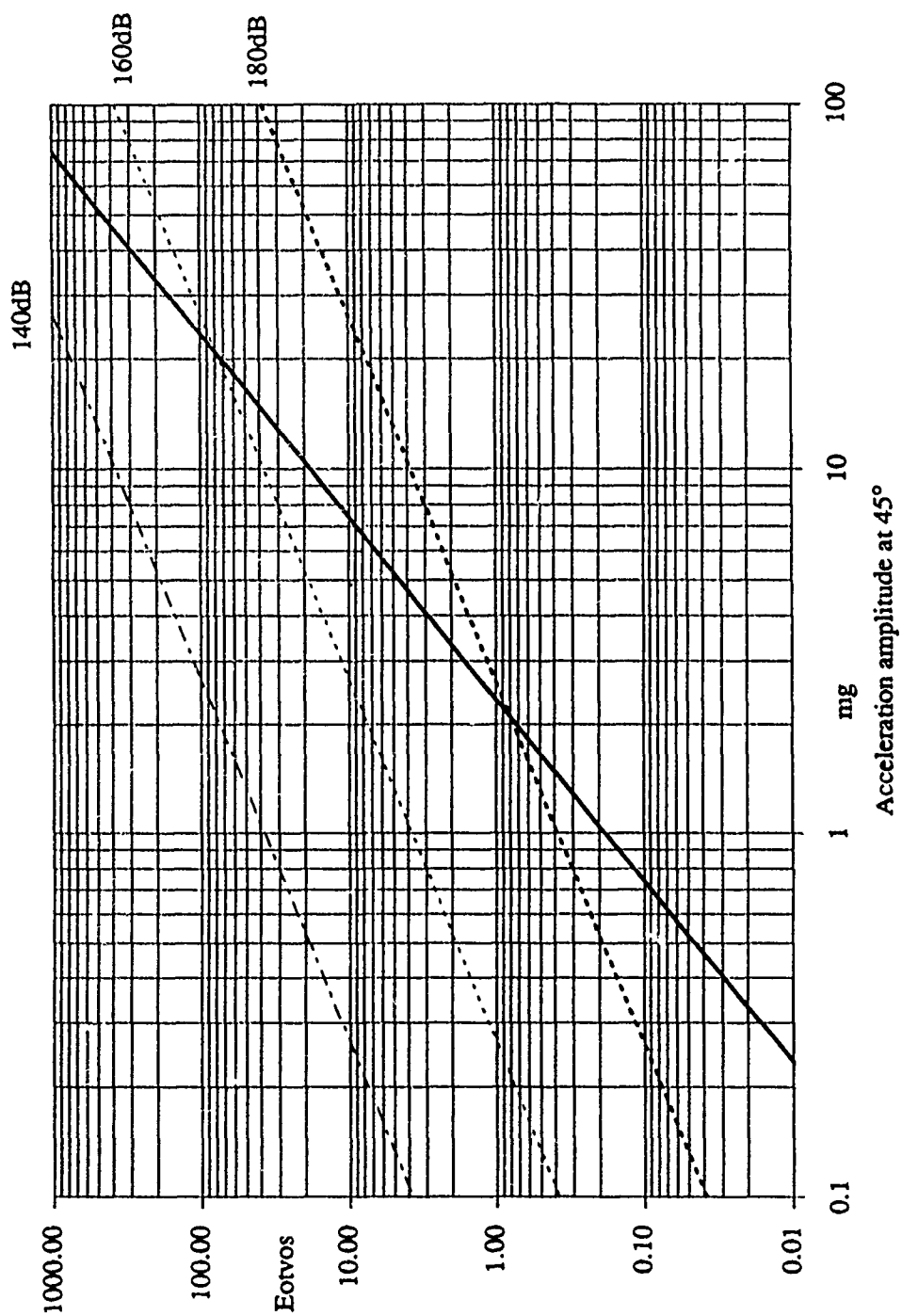
BAR DEFORMATIONS IN A FORCE FIELD (IDEAL PIVOT)

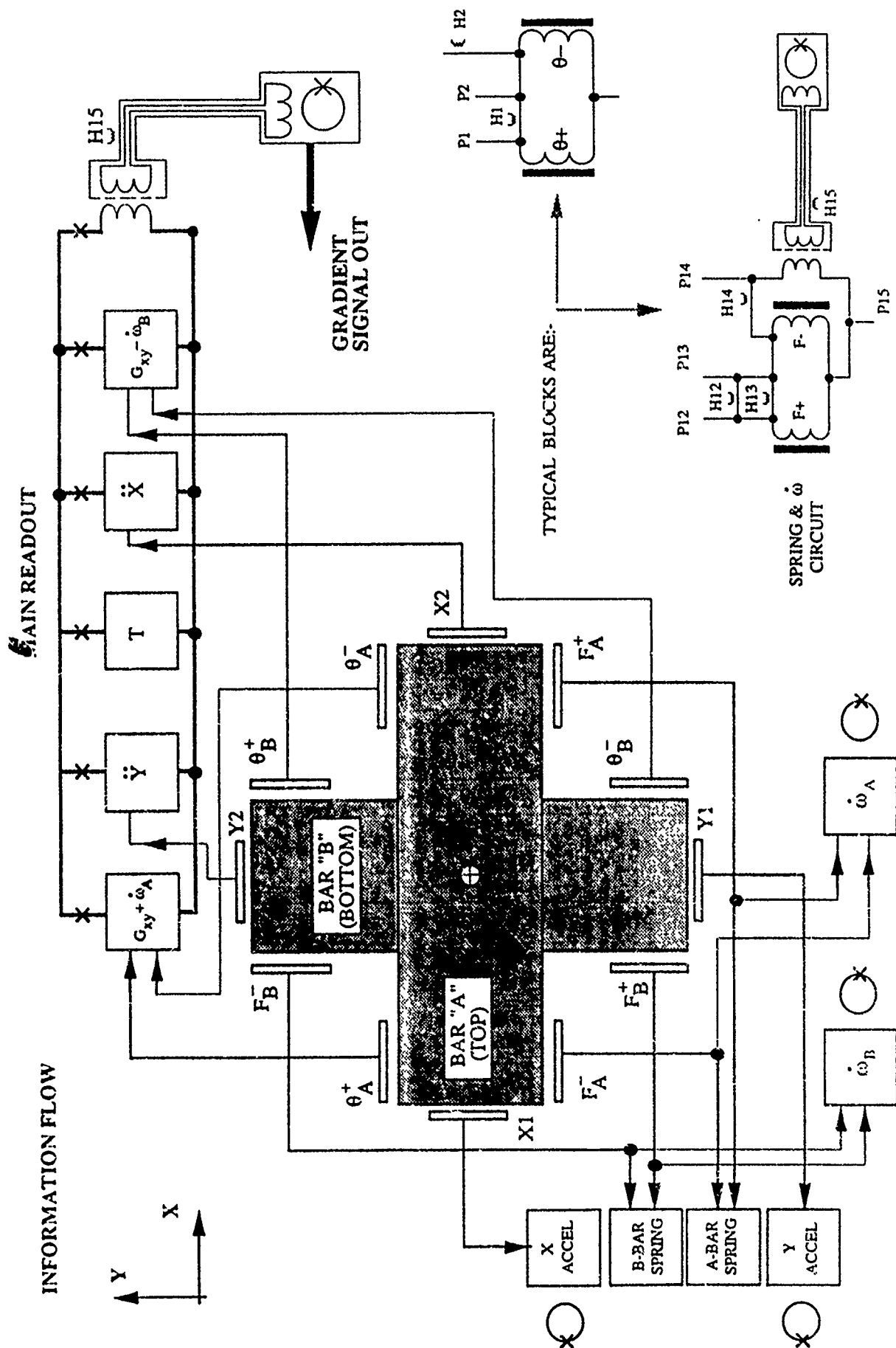


STRETCH

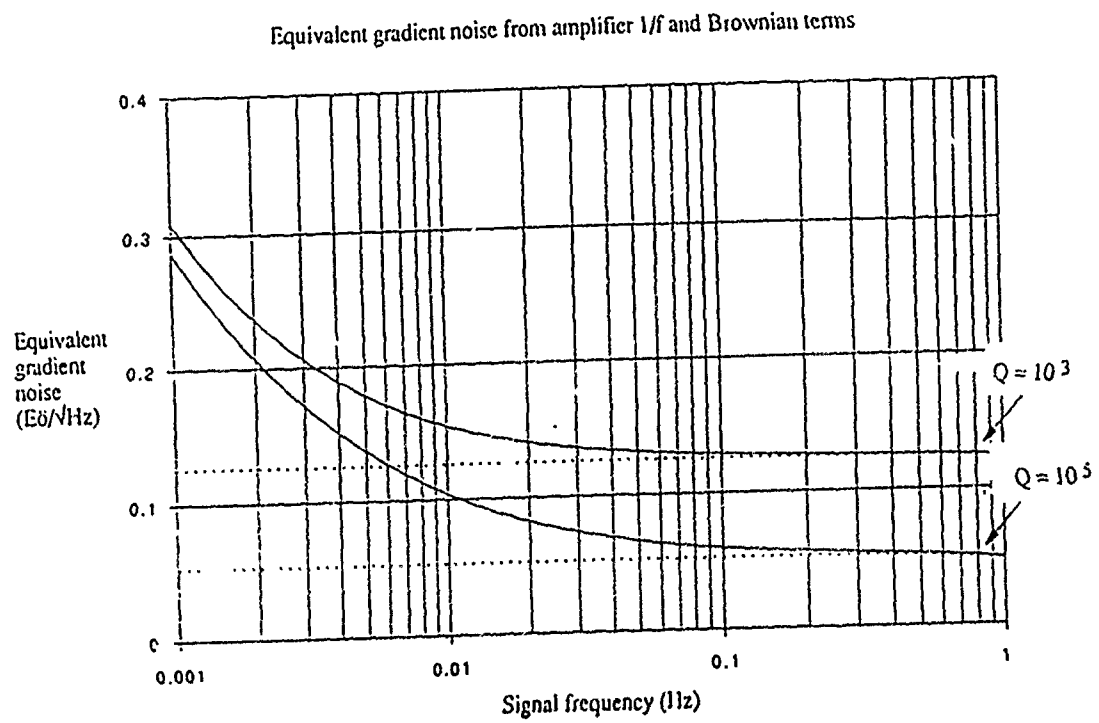
FLOP







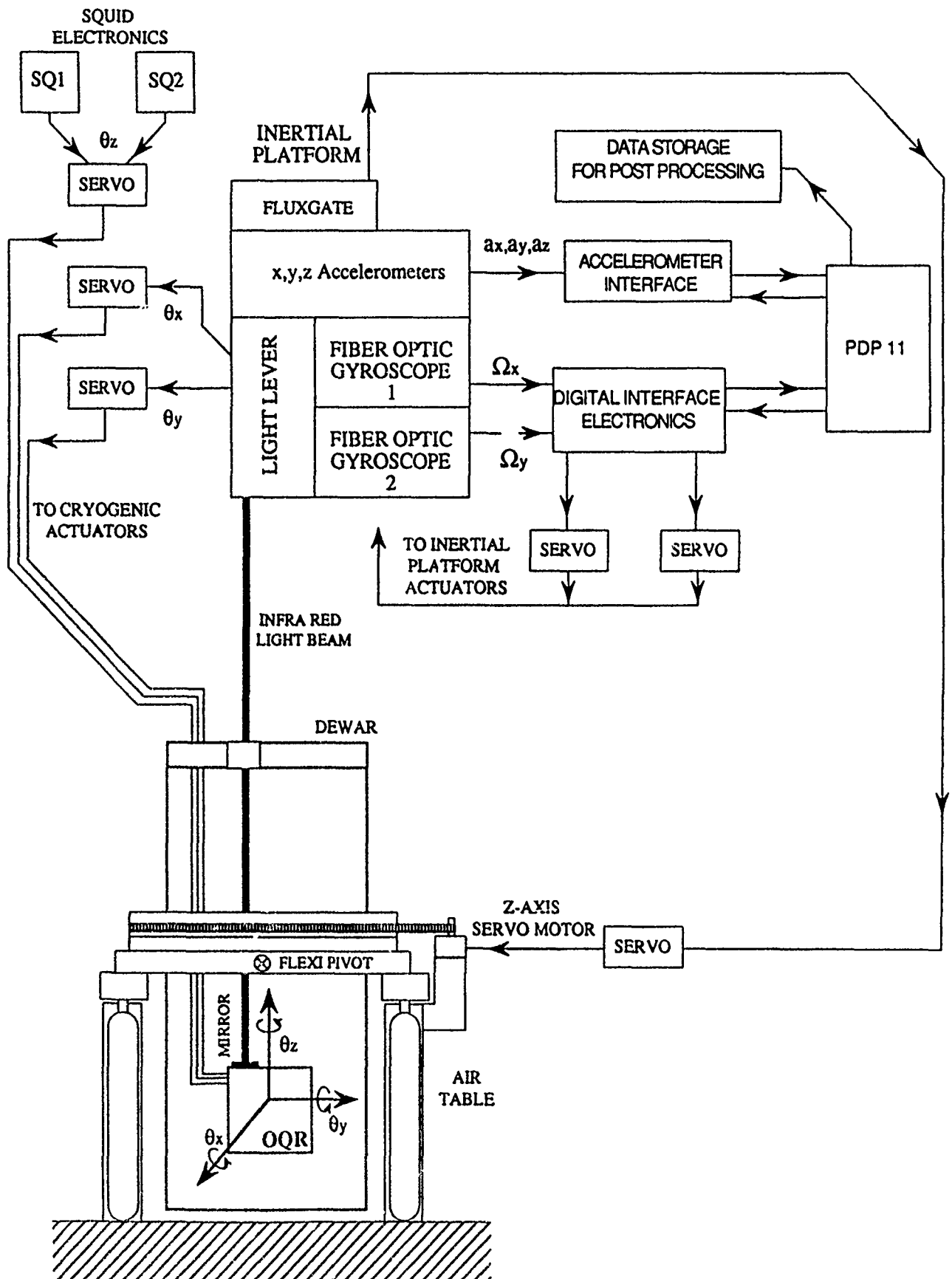
Basic detector noise

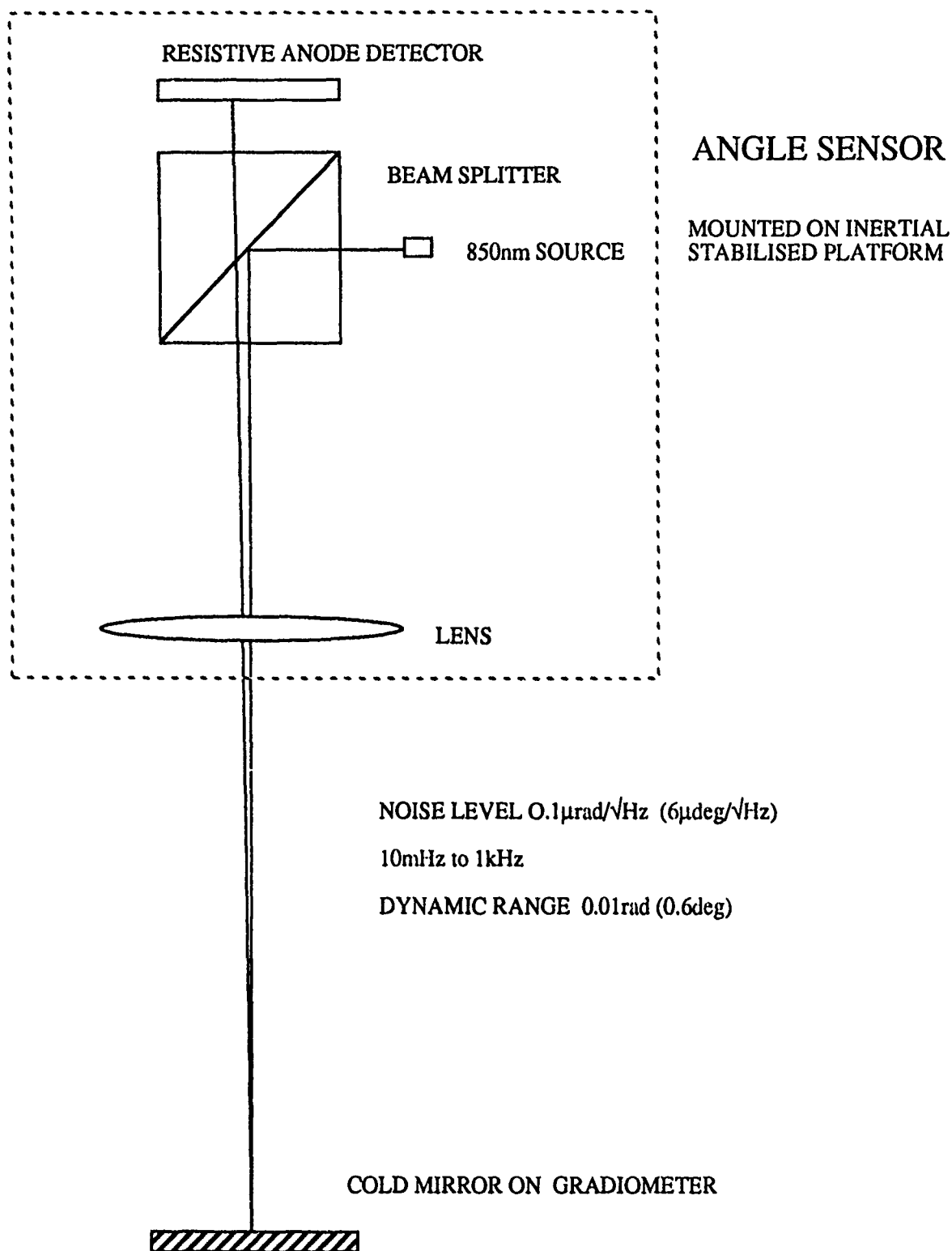


Coloured noise

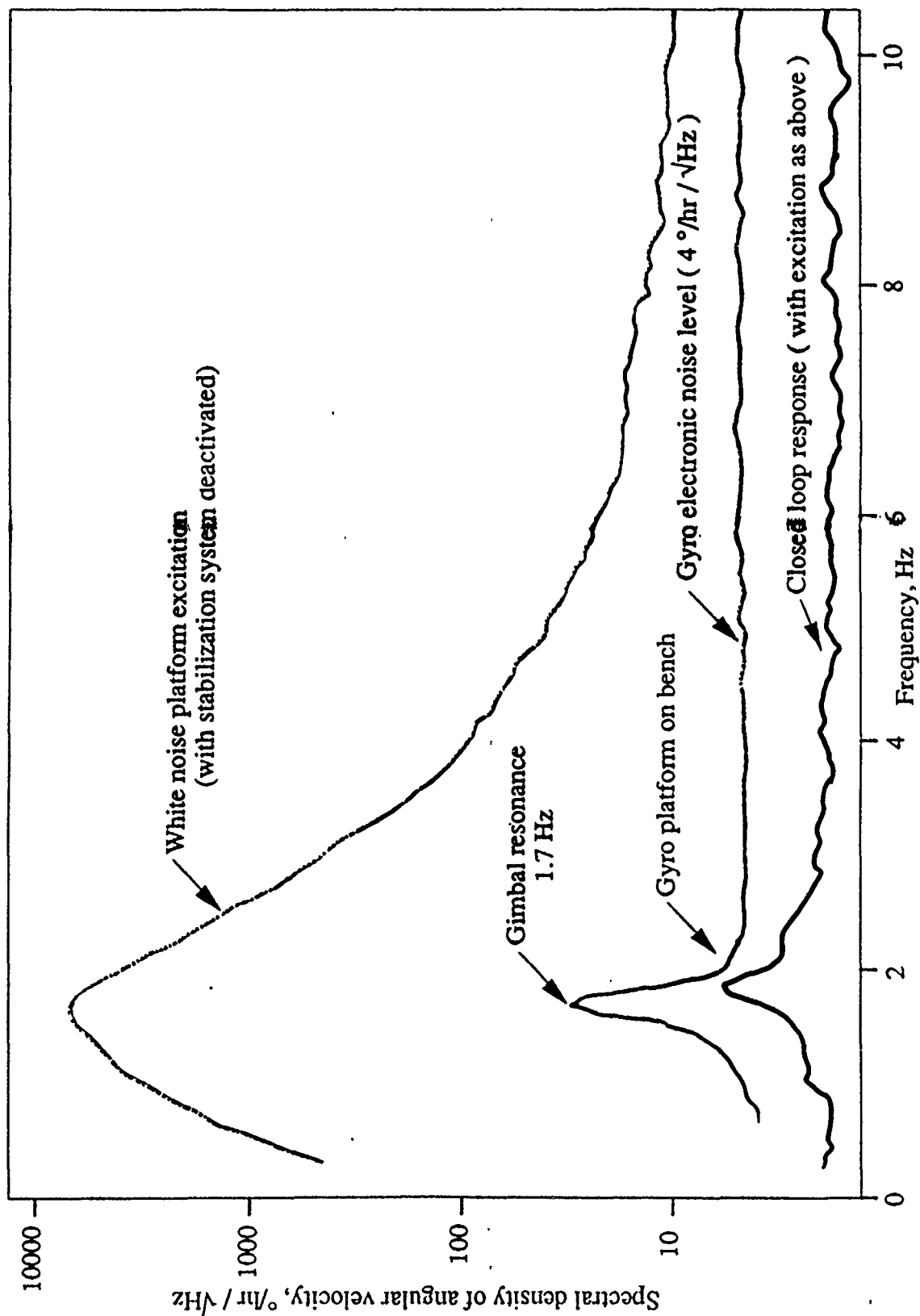
- down conversion
- thermal
- flux creep

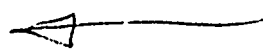
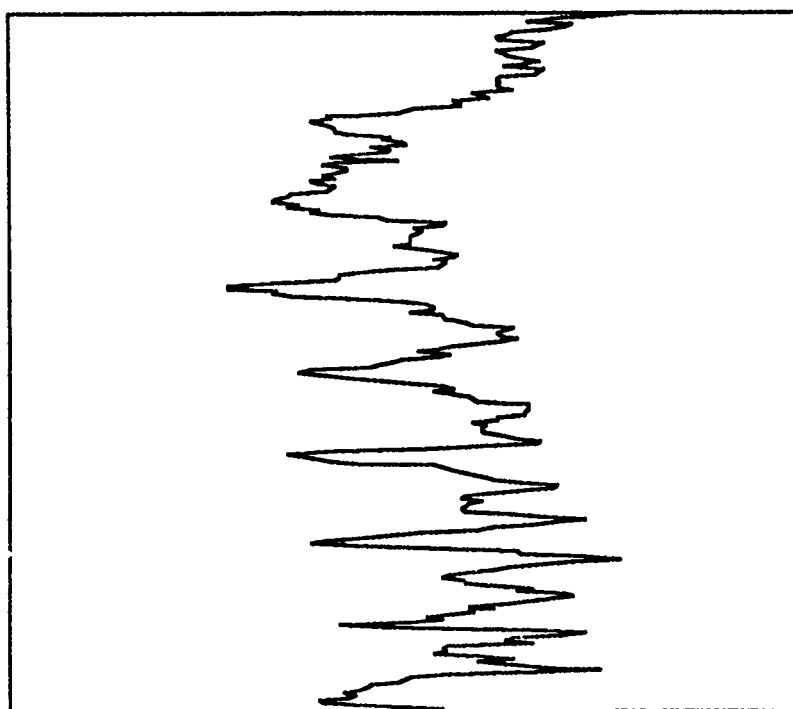
ROTATIONAL STABILISATION



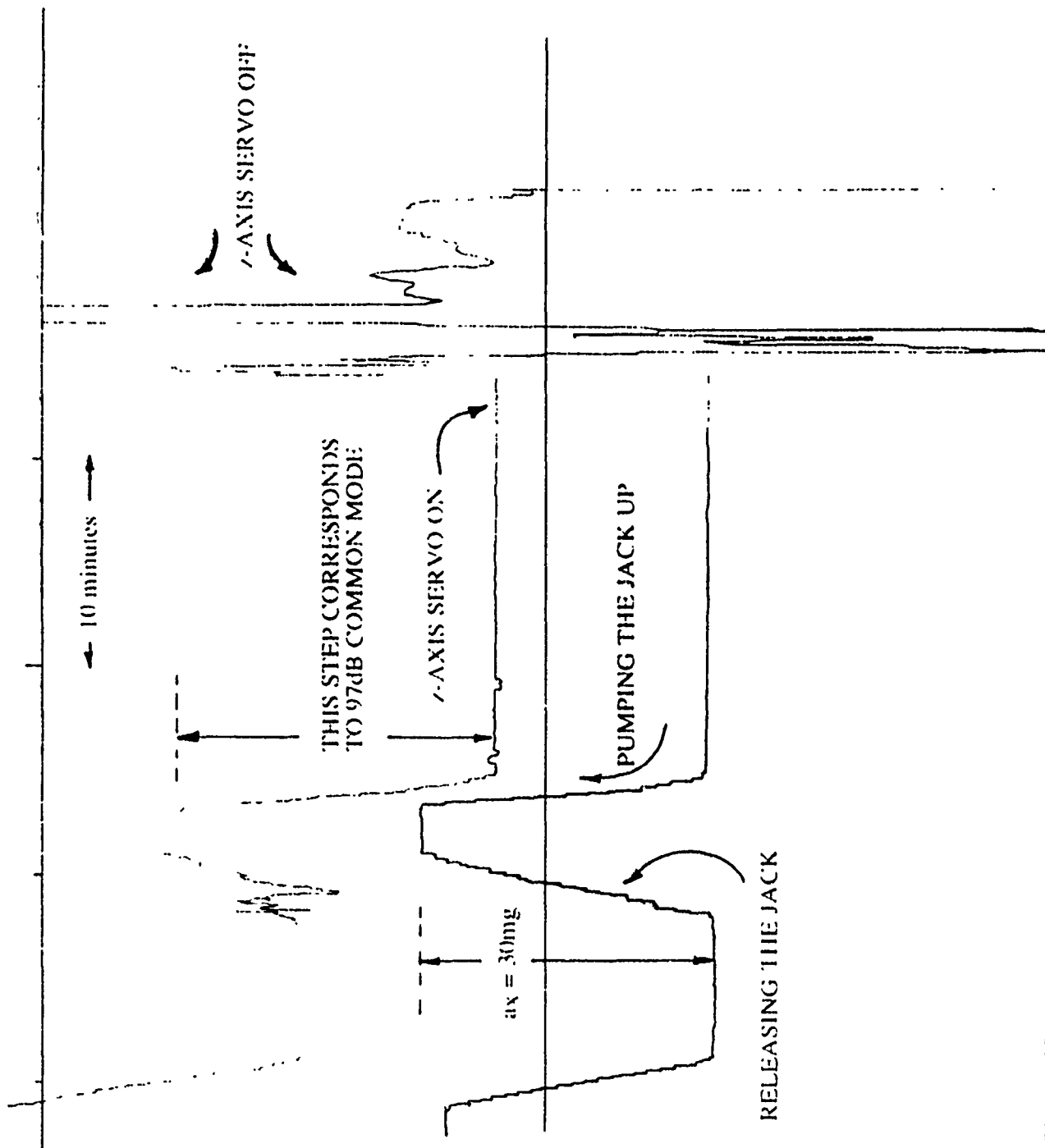


Fibre Optic Gyro - Stabilized Platform Performance Data

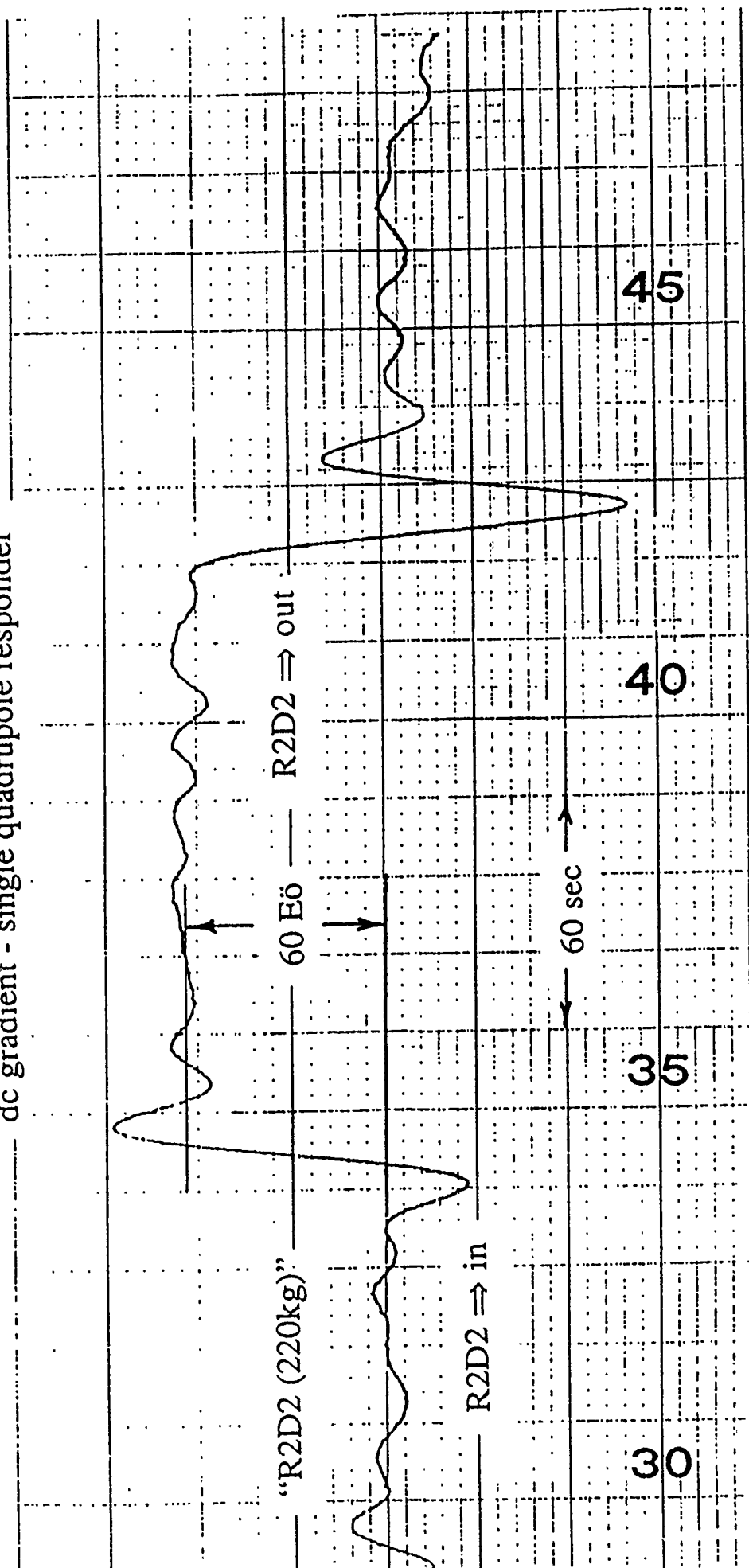




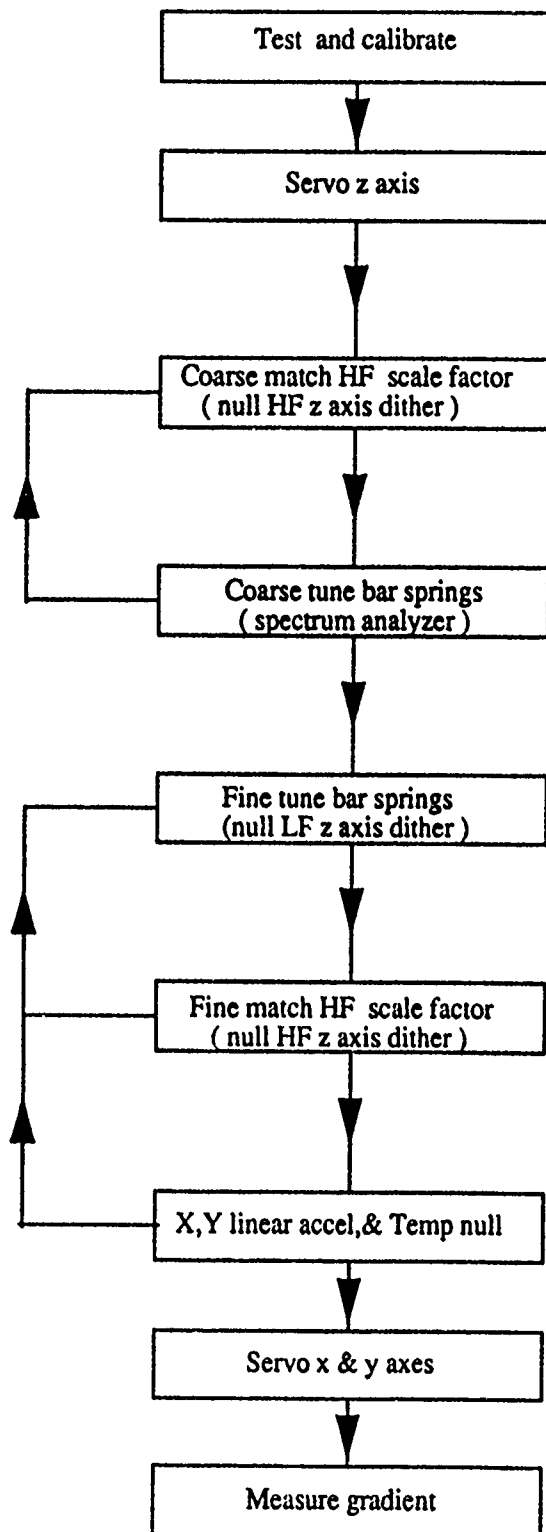
das ist die



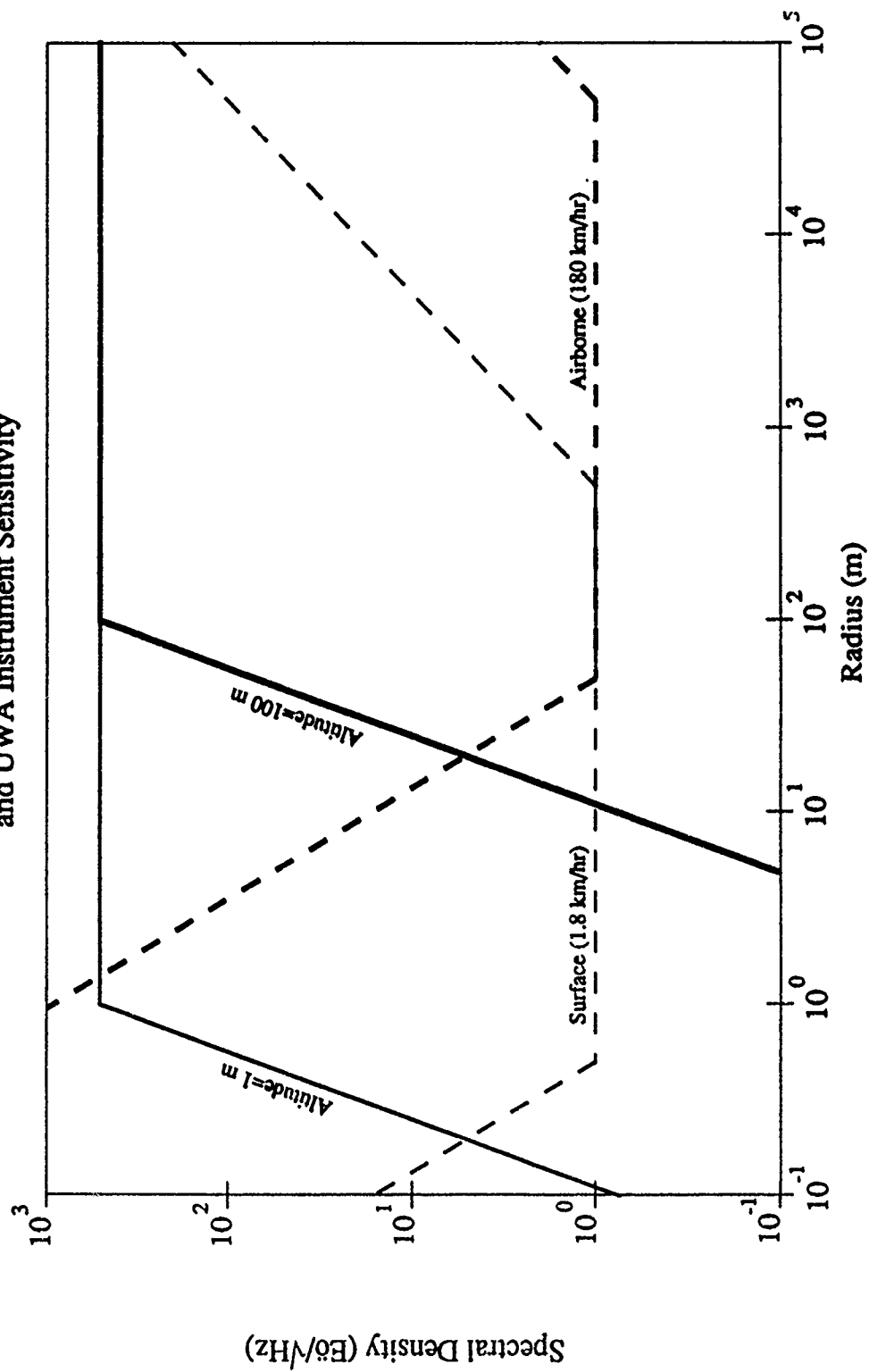
dc gradient - single quadrupole responder



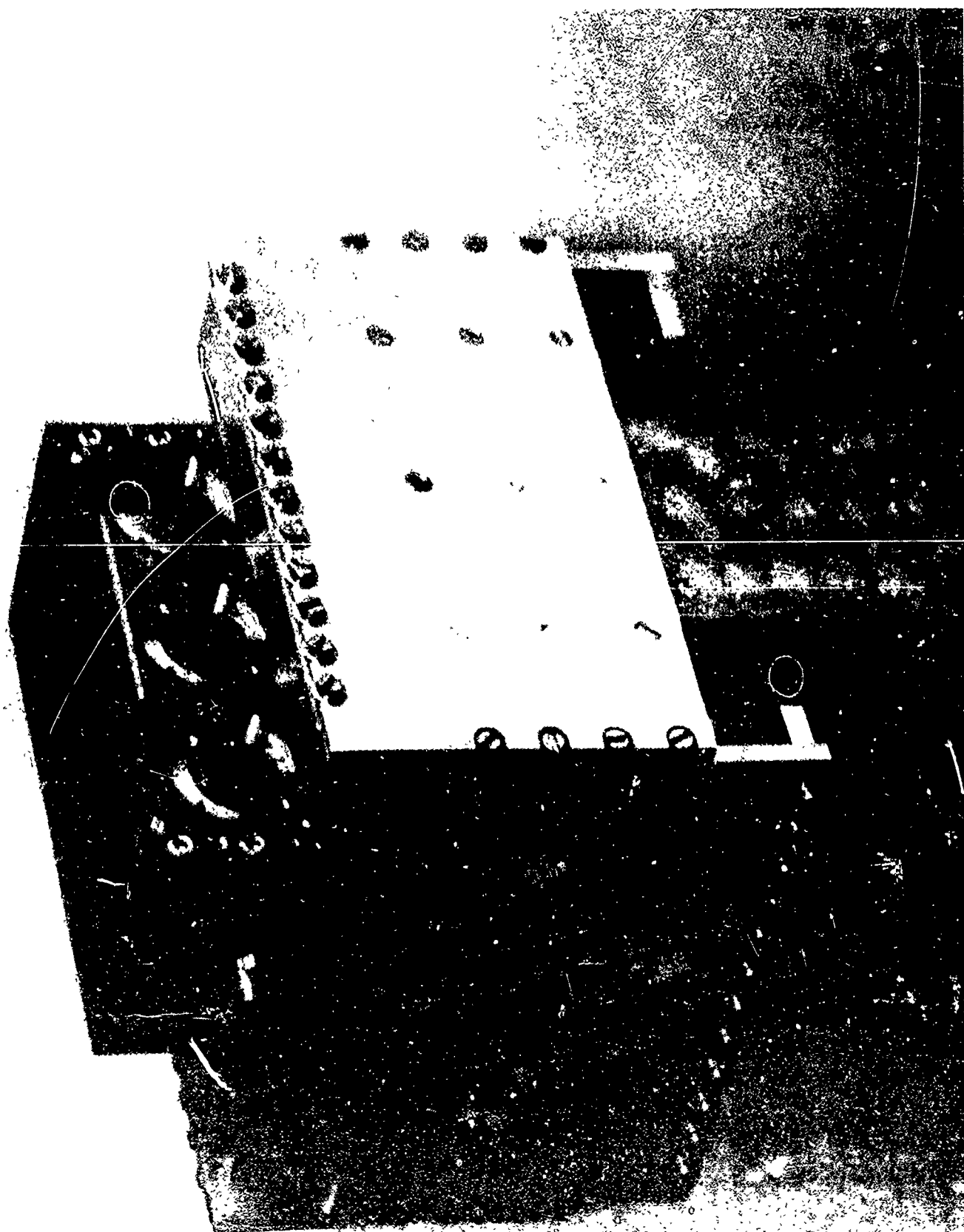
Set up Procedure

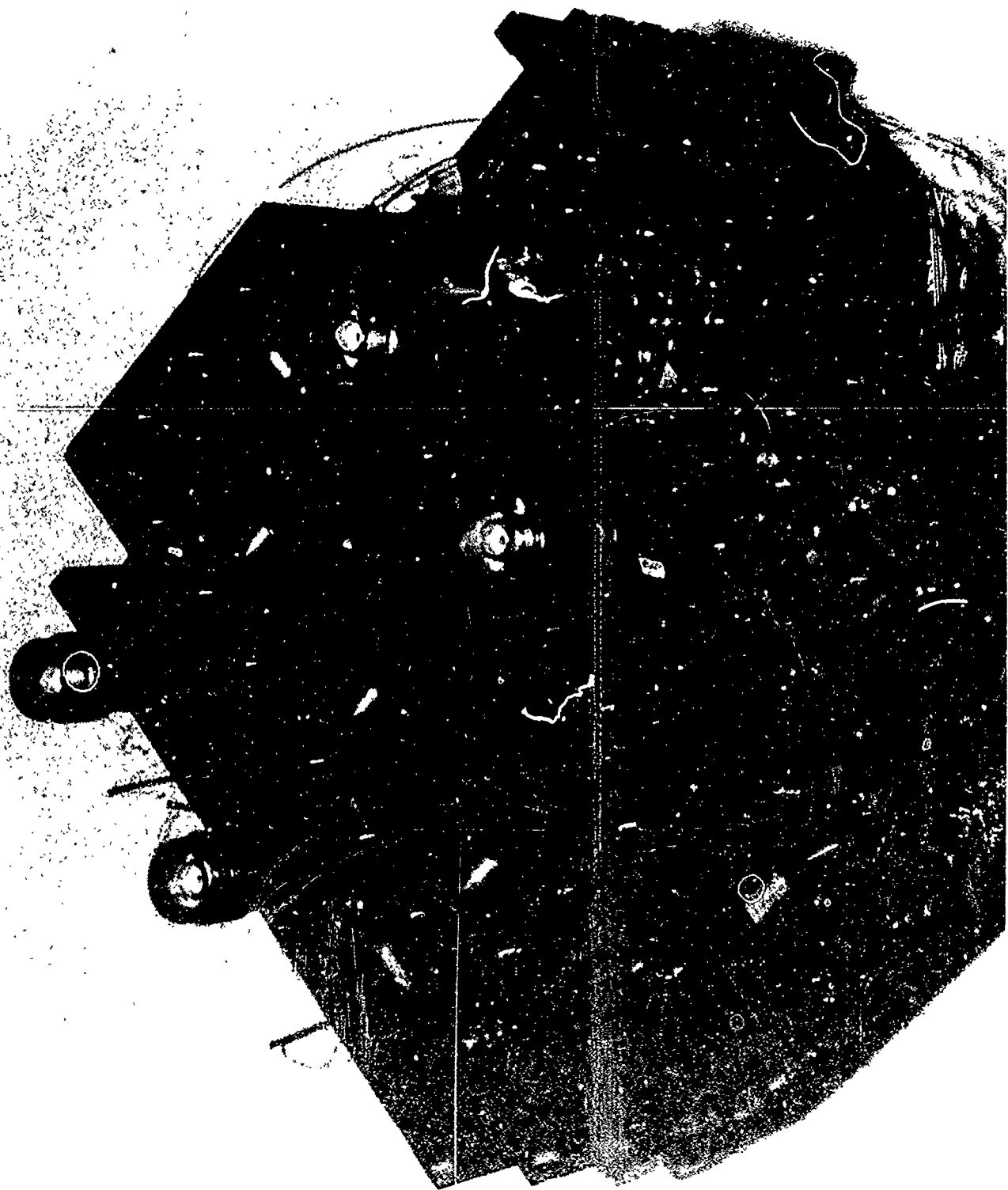


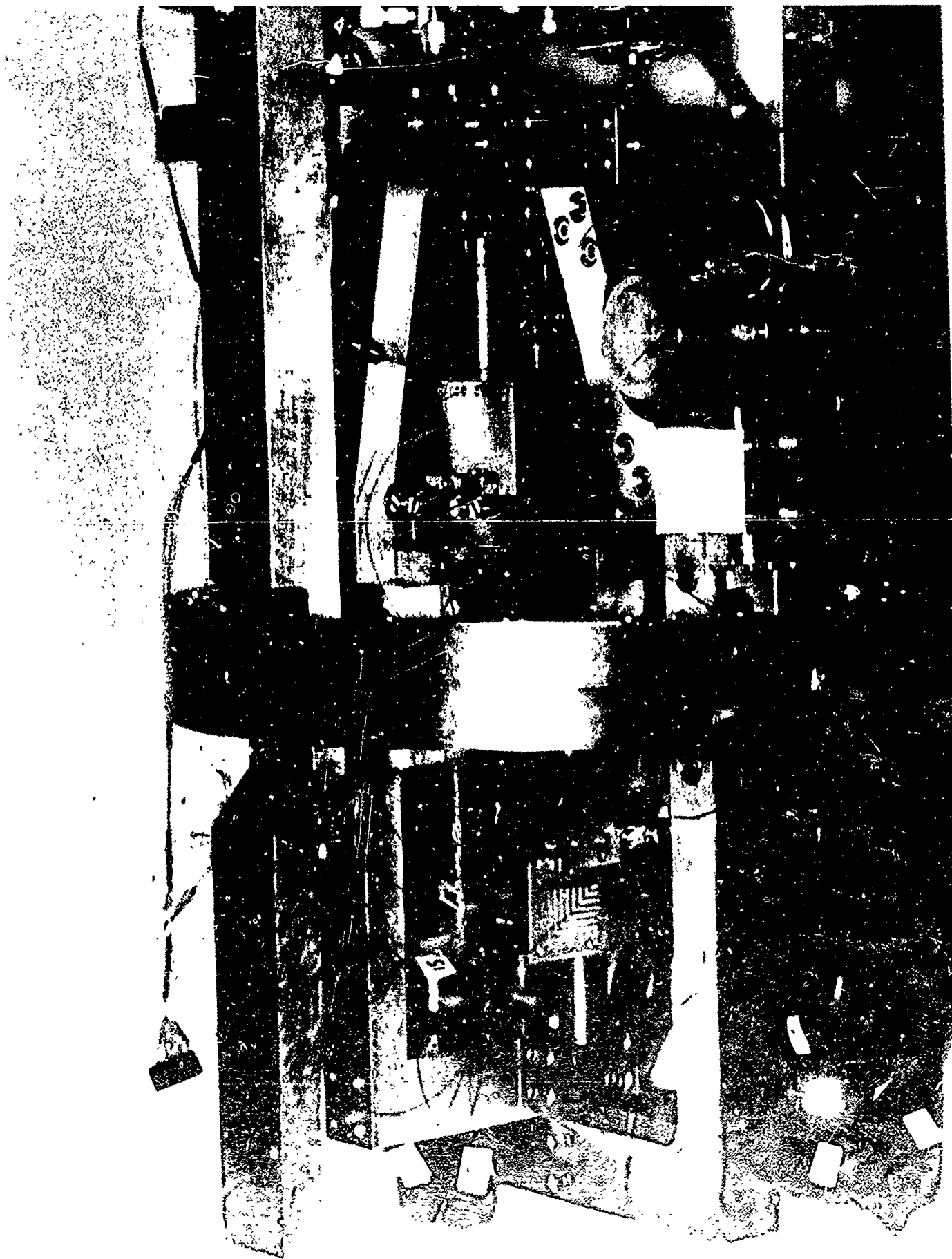
XY Gravity Gradient:
Spectral Density for 1 gm cm^{-3} Density Contrast
and UWA Instrument Sensitivity

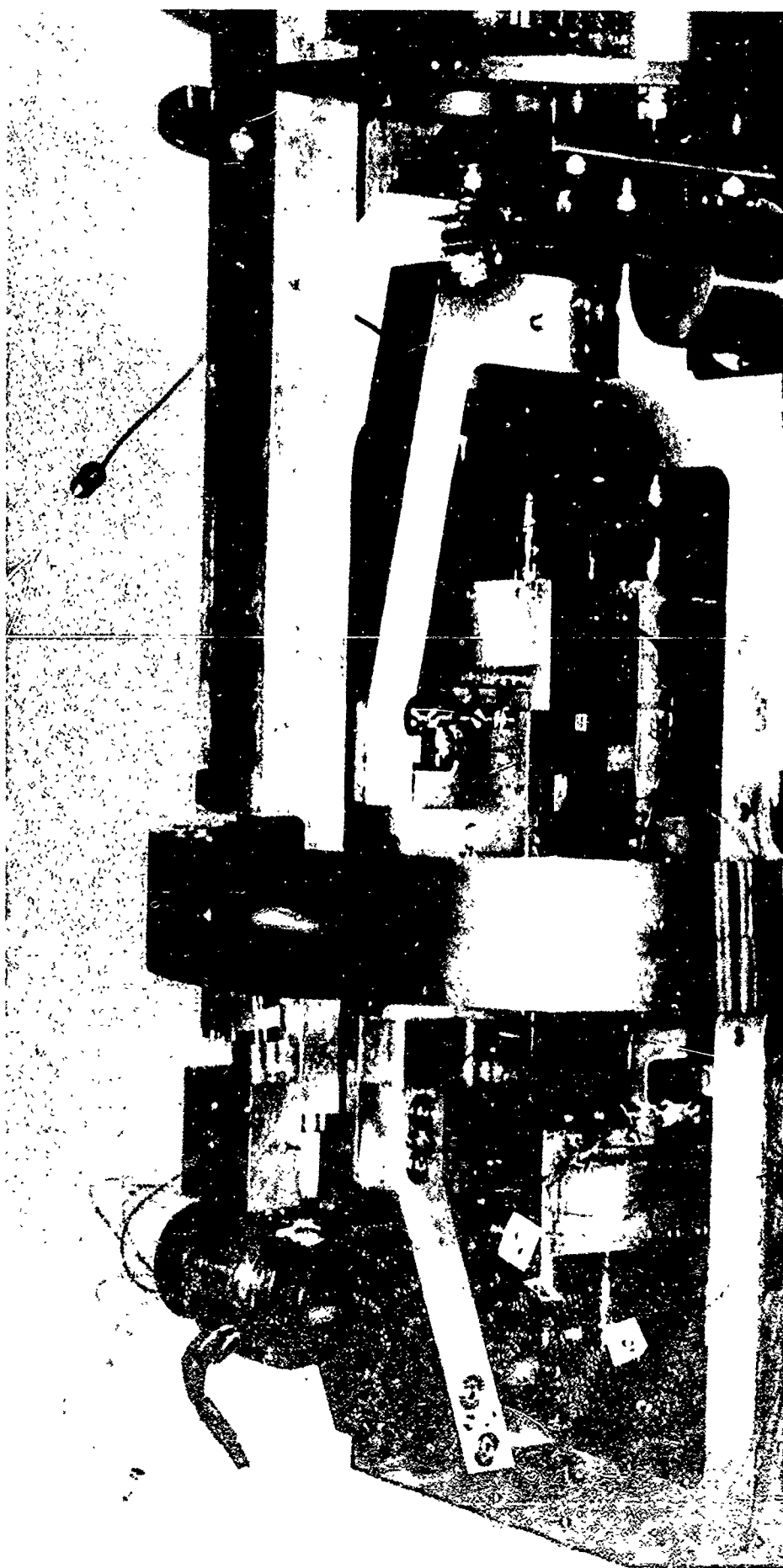


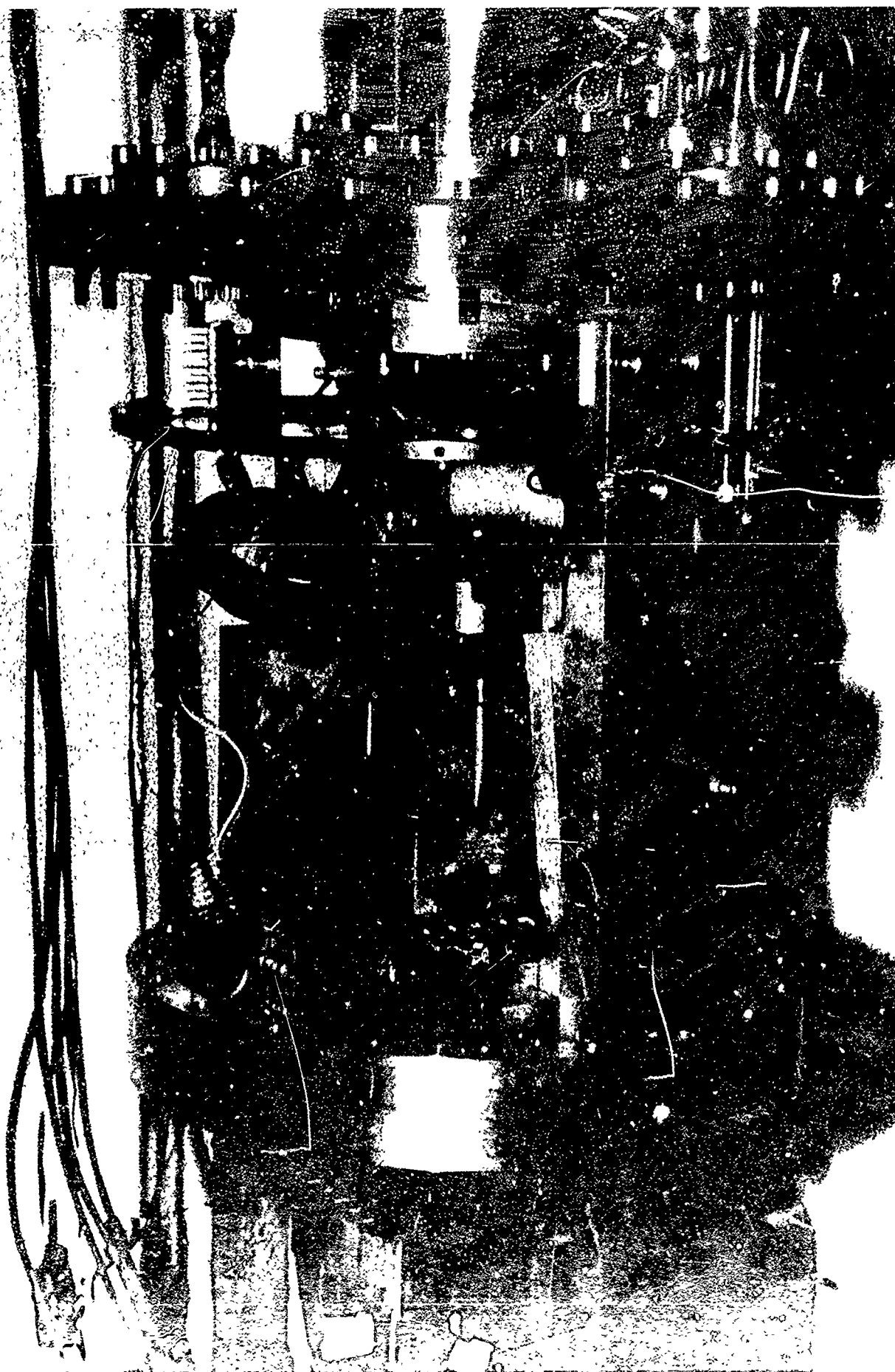


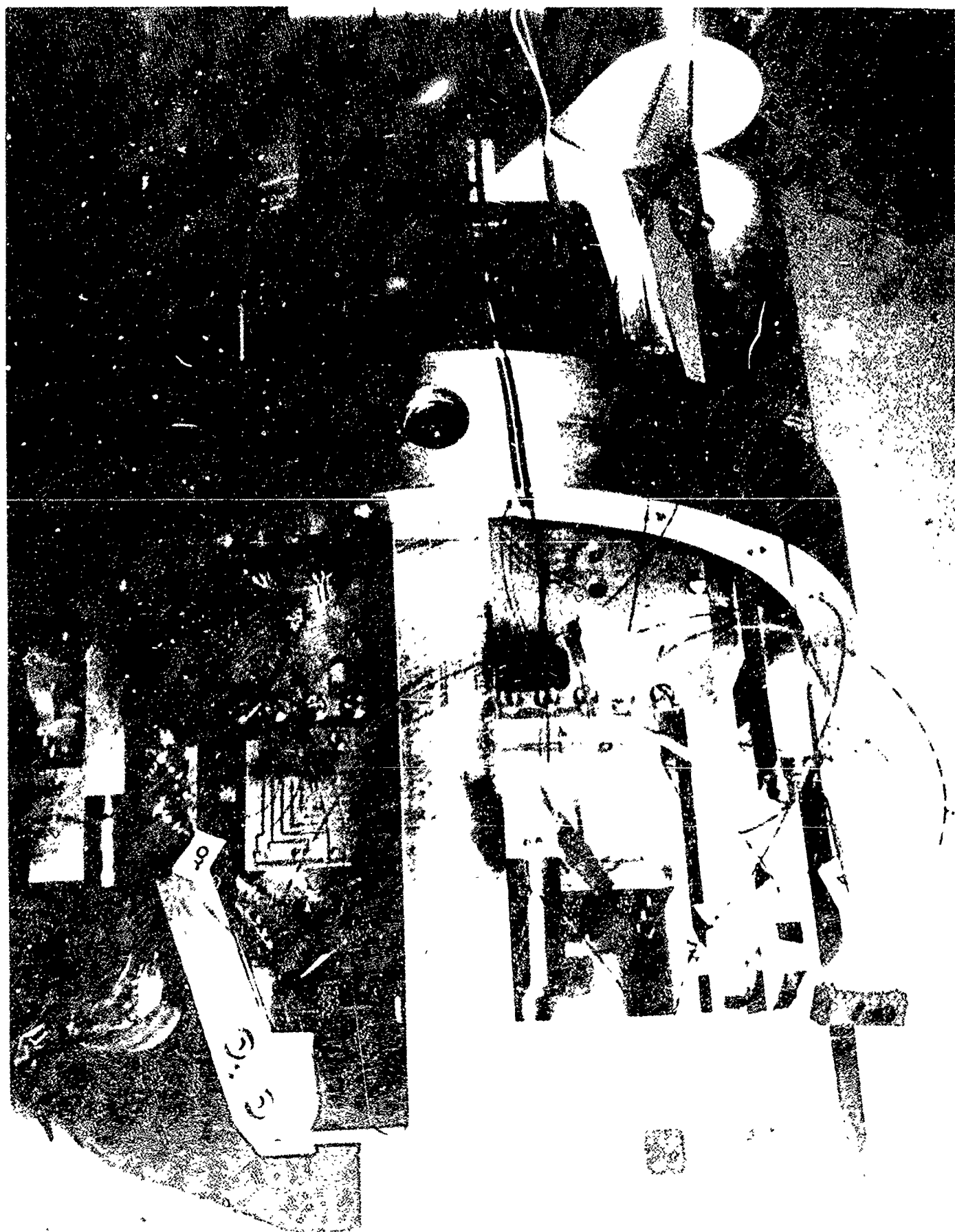


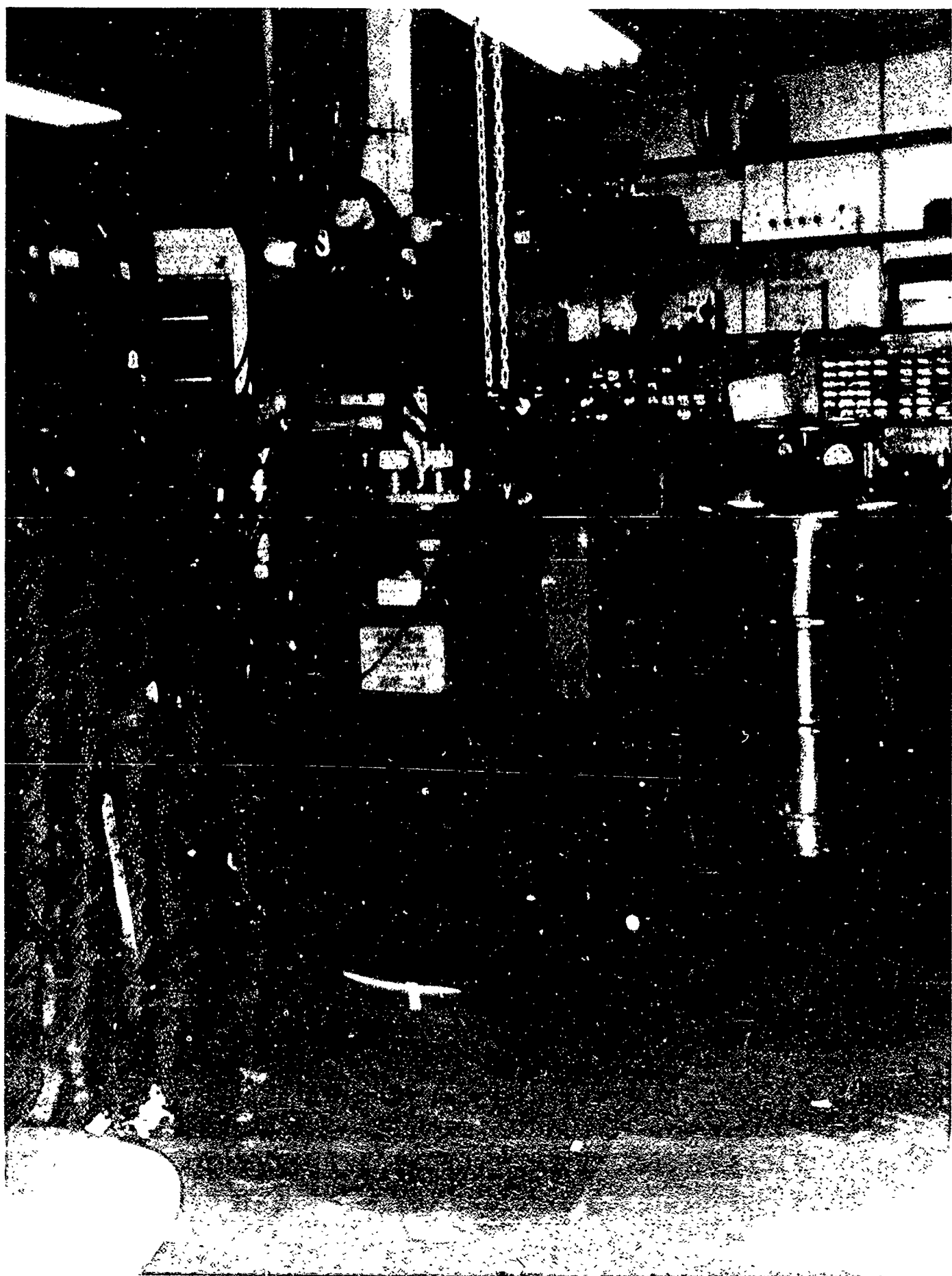


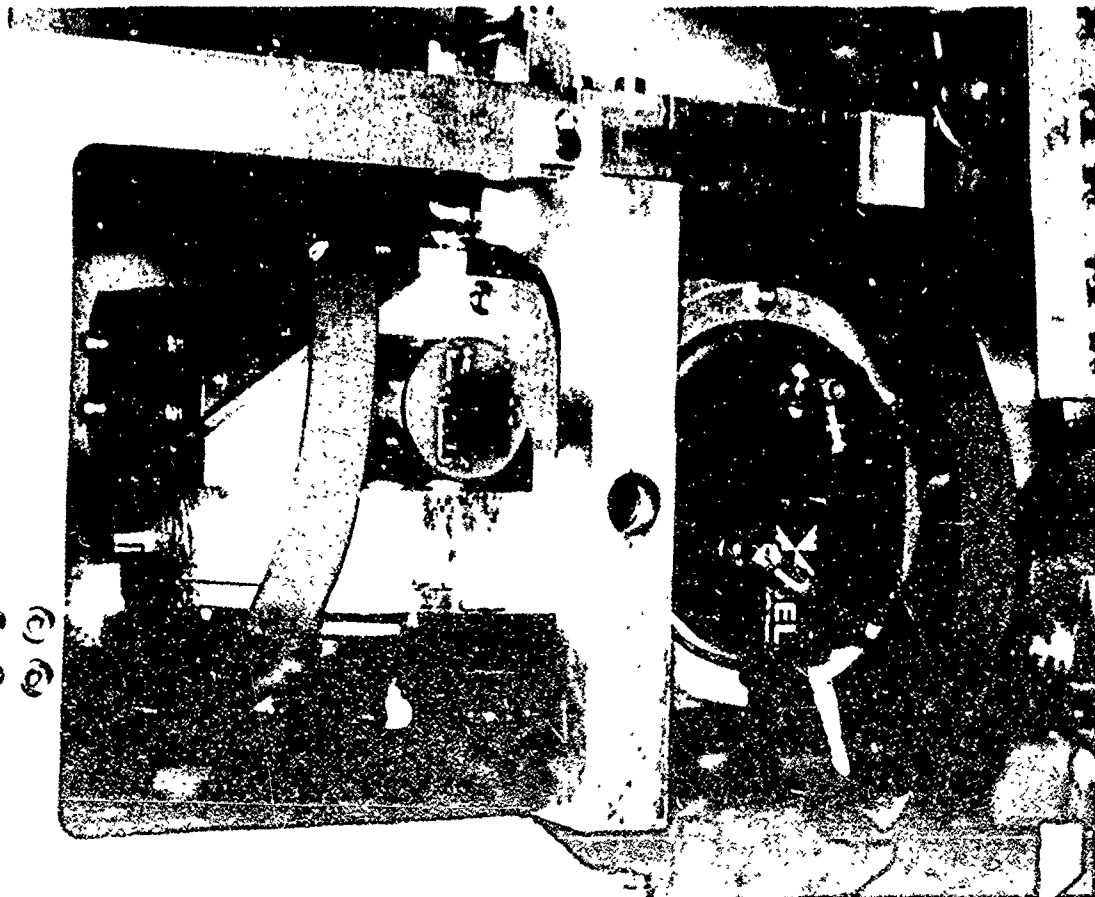
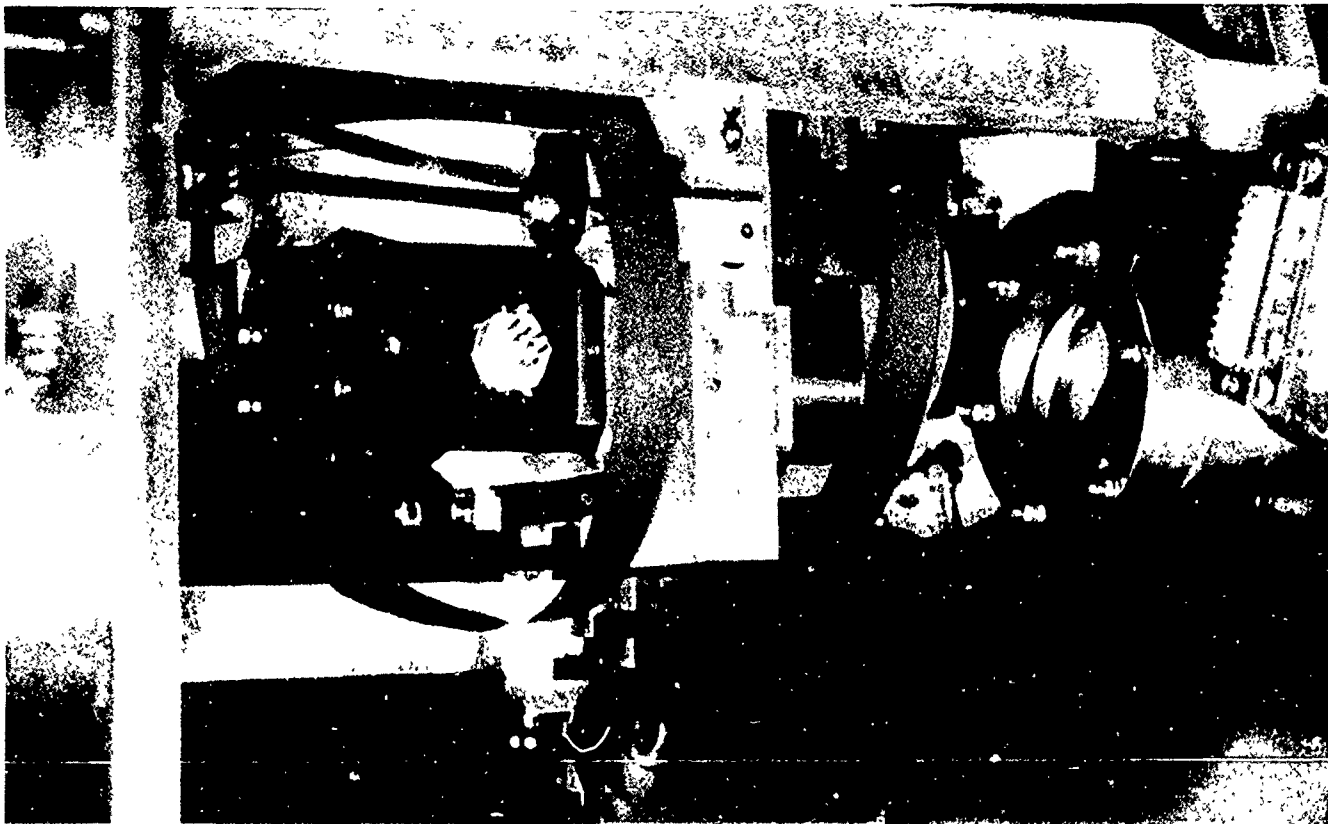












DEVELOPMENT OF THE MODEL III SUPERCONDUCTING GRAVITY GRADIOMETER

M. V. Moody, Q. Kong and H. J. Paik

Department of Physics and Astronomy
University of Maryland, College Park, MD 20742

The development of a three-axis superconducting gravity gradiometer, SGG, is continuing at the University of Maryland. The instrument is being developed under a NASA contract for the purpose of precision gravity experiments and gravity field mapping from an orbiting platform. Testing of the Model III SGG has recently begun. This device was designed to meet the sensitivity requirements of NASA for a global gravity mapping mission ($3 \times 10^{-4} \text{ E Hz}^{-1/2}$).

The SGG utilizes three pairs of spring mass systems in which proof mass motion, induced by a gravitational force or an acceleration, modulates supercurrents. The superconducting circuits are configured such that these supercurrents are passively summed and differenced before being measured by SQUID amplifiers. Also, in order to operate in both terrestrial and space environments, the proof masses in the SGG use a superconducting levitation scheme which has minimal effect on the differential mode spring constant.

The primary enhancement of the Model III over previous designs is the incorporation of a passive superconducting negative spring. Using the negative spring to cancel the spring constant of the mechanical spring, the noise contribution of the SQUID amplifier can be suppressed. The results of the Model III SGG tests will be presented.

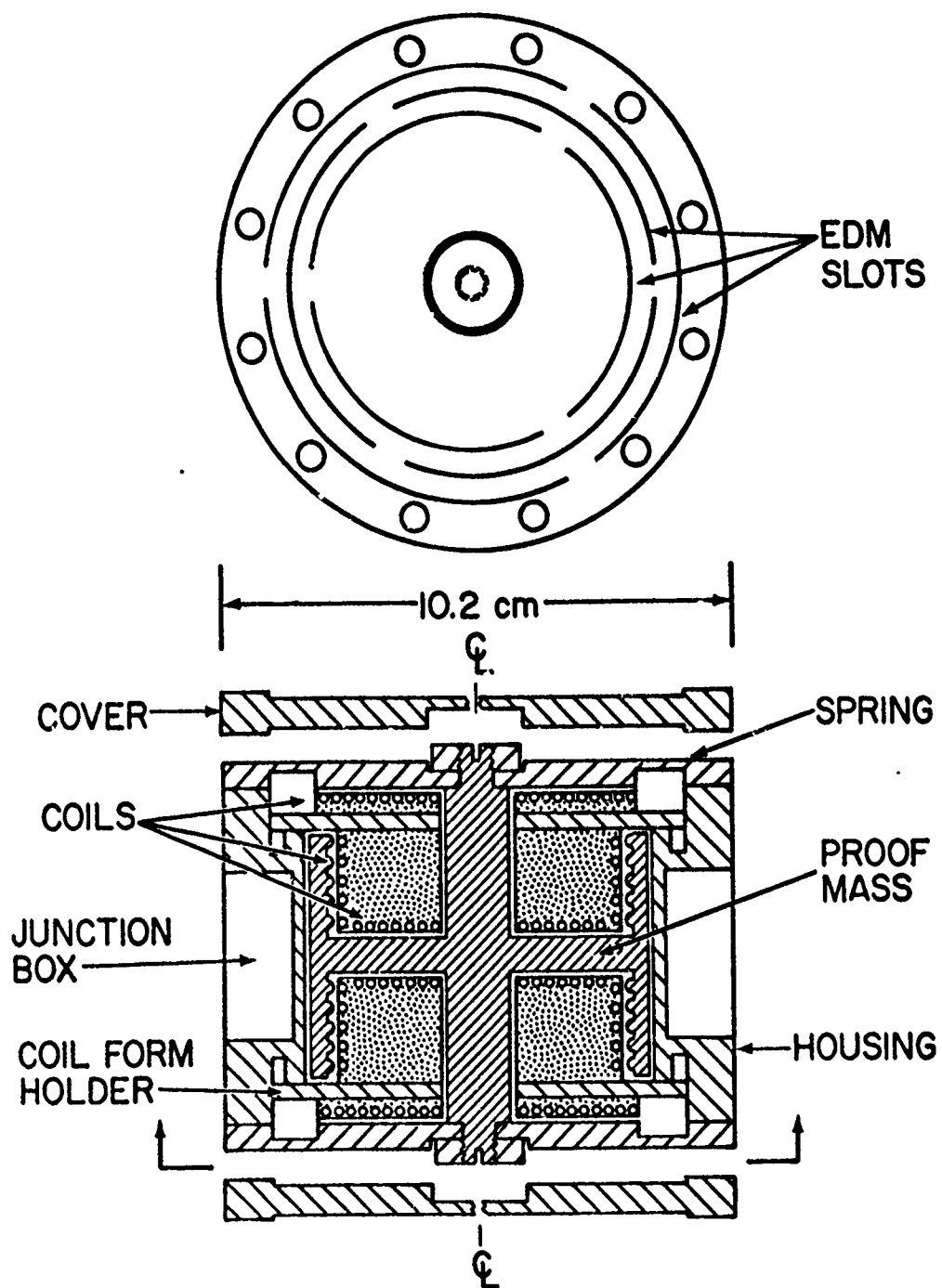
Using the SGG to measure the Laplacian of the gravitational potential, a composition independent, null test of the inverse square law of gravity can be performed. Sensing tilt of the SGG platform with a laser and photodiode, we have demonstrated that tilt is the primary error source in this experiment when using a 1600 kg pendulum as the source. Methods for reducing this and other errors using a three-axis SGG will be discussed.

DEVELOPMENT OF THE MODEL III SUPERCONDUCTING GRAVITY GRADIOMETER

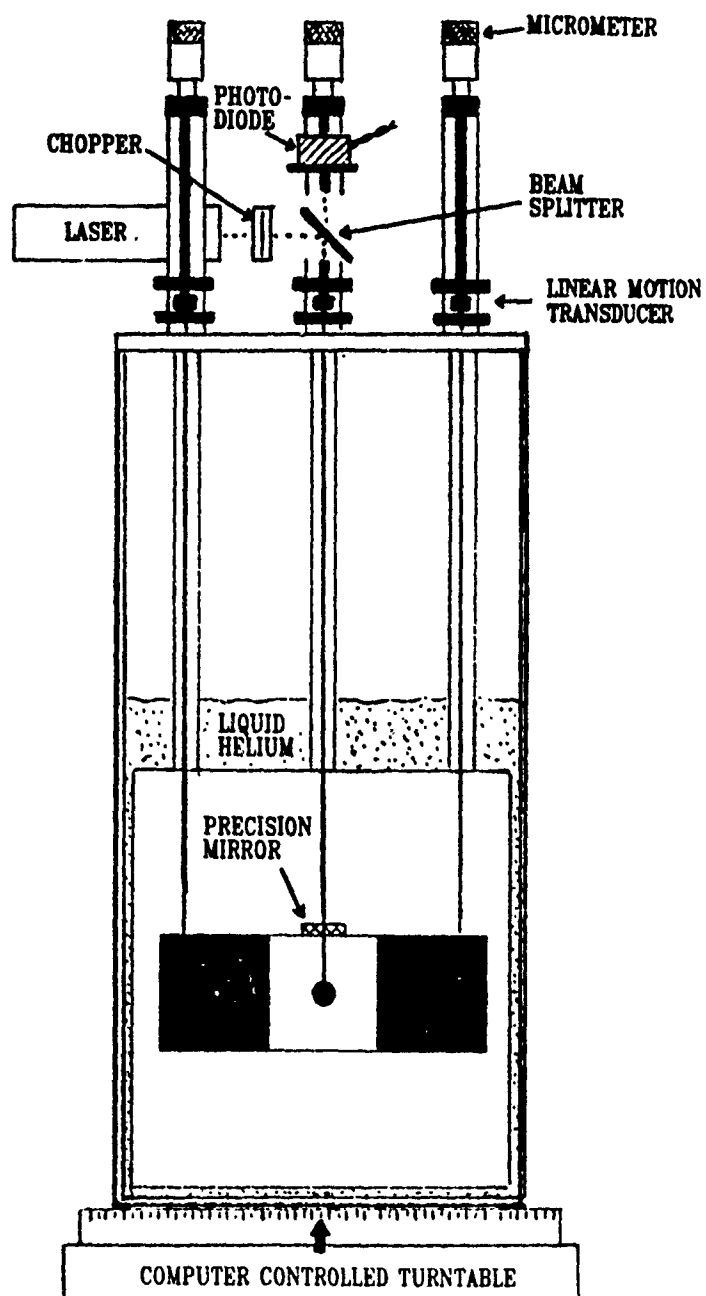
M. V. Moody, Q. Kong and H. J. Paik

**Department of Physics and Astronomy
University of Maryland, College Park, MD 20742**

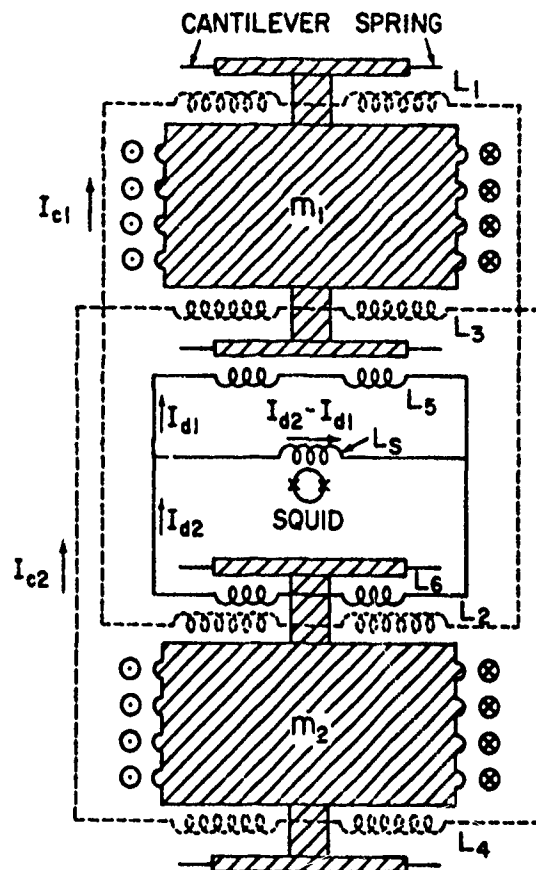
ACCELEROMETER CROSS SECTION



EXPERIMENTAL CONFIGURATION



SCHEMATIC OF MODEL III SGG



SENSING CIRCUIT:

Adjust ratio of I_{d1} to I_{d2} to balance out sensitivity to common-mode accelerations.

LEVITATION CIRCUIT:

Energy ($\phi^2/2L$) is constant for differential motion.
 \therefore increases only common mode ω_0 .

INTRINSIC SPECTRAL NOISE

$$S_r(f) = \frac{8}{m\ell^2} \left[k_B T \frac{2\pi f}{Q(f)} + \frac{(2\pi f_0)^2}{2\beta\eta} E_A(f) \right]$$

= BROWNIAN MOTION + AMPLIFIER

FOR BEST COMMERCIALY AVAILABLE SQUID:

$$E_A(f) = 3 \times 10^{-30} \text{ J Hz}^{-1}$$

TO REDUCE AMPLIFIER NOISE CONTRIBUTION LOWER f_0

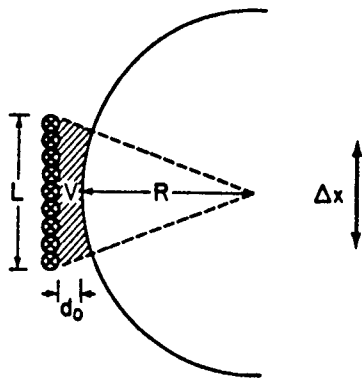
1. In g_E use "push-pull" levitation.

$$f_0 = 8 \text{ Hz}, \quad S(f) = 2 \times 10^{-3} \text{ E Hz}^{-2}$$

2. Superconducting negative spring.

$$f_0 = 1 \text{ Hz}, \quad S(f) = 2 \times 10^{-4} \text{ E Hz}^{-2}$$

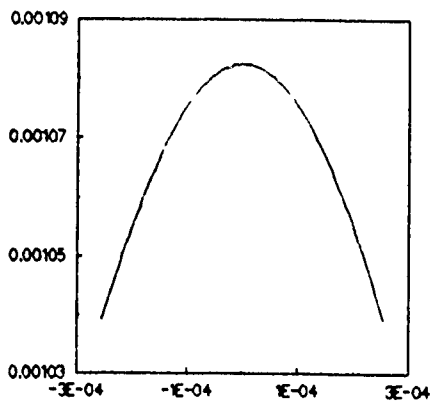
SUPERCONDUCTING NEGATIVE SPRING



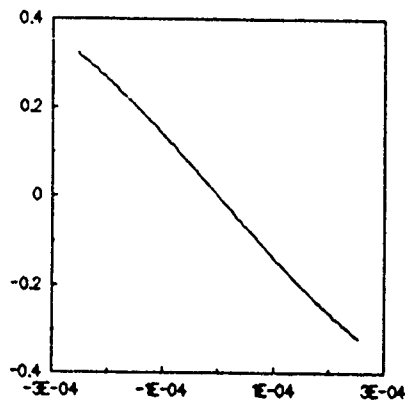
$$\text{ENERGY} = \mu_0 n^2 |^2 V(0) / 2V(x)$$

NEGATIVE SPRING

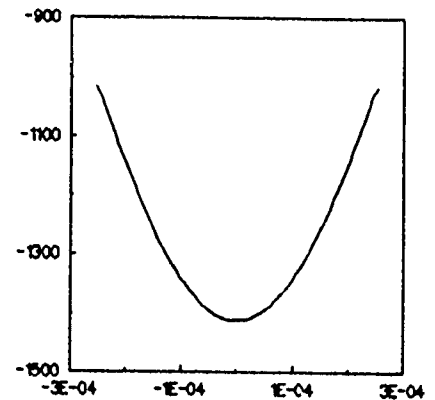
ENERGY vs. POSITION



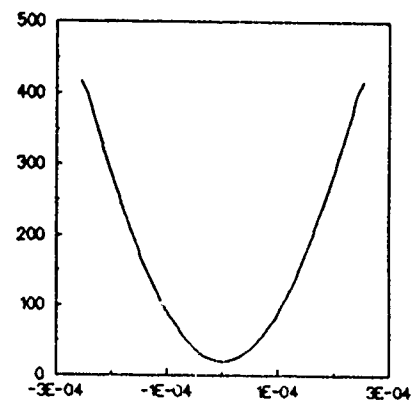
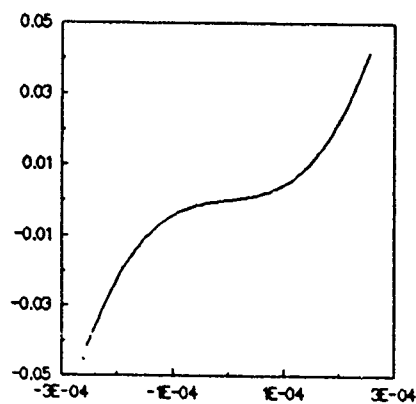
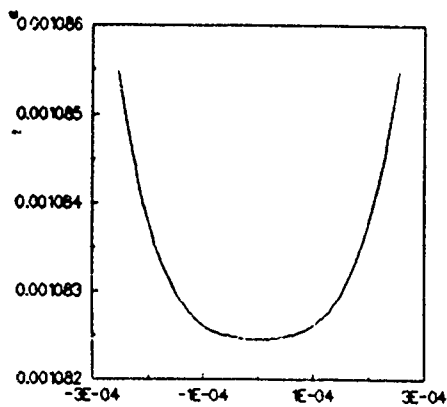
FORCE vs. POSITION



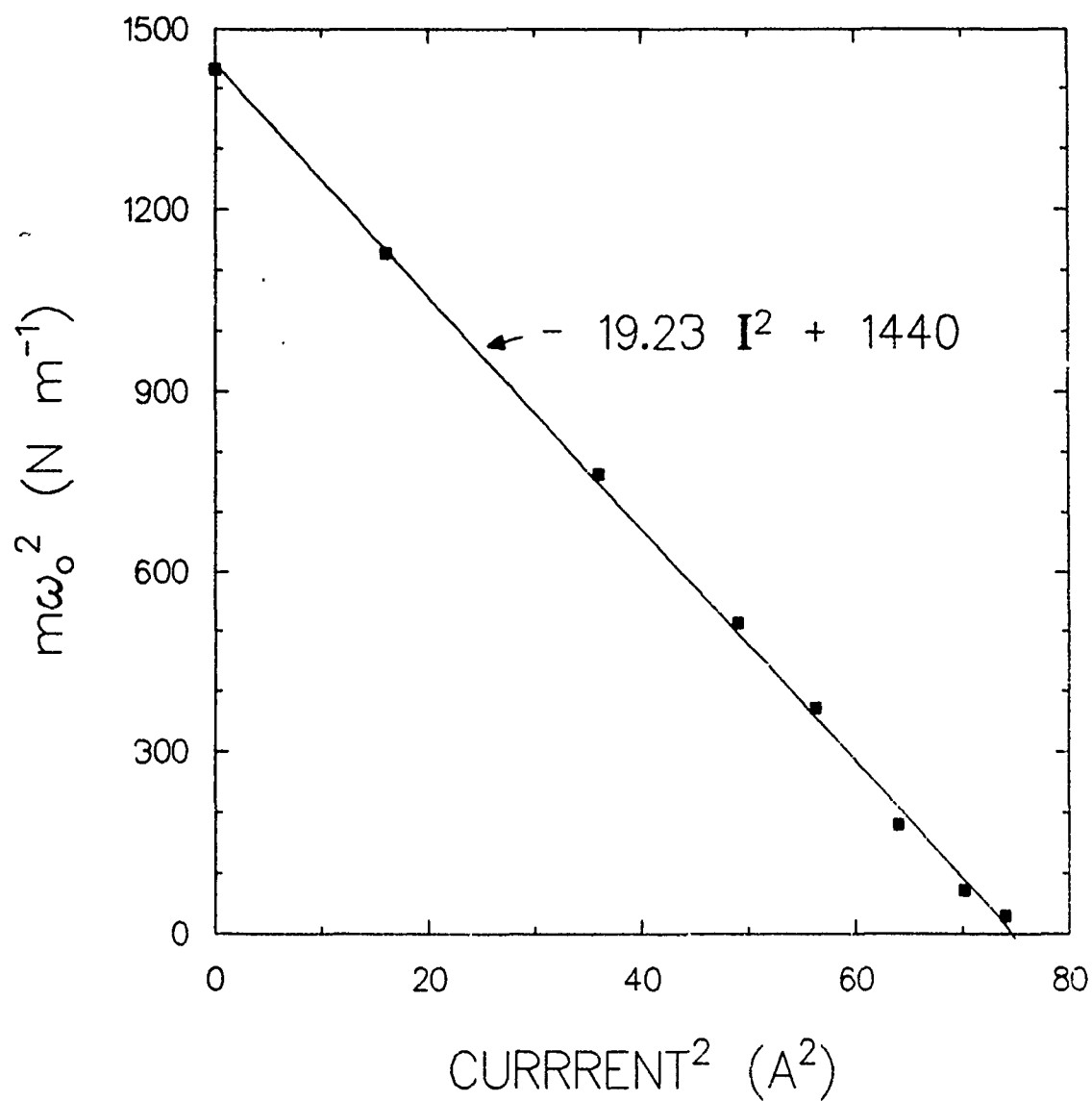
SPRING CONSTANT vs. POSITION



NEGATIVE + LINEAR SPRING



SGGM NEGATIVE SPRING TEST



PRIMARY ERROR SOURCES

$$\Gamma' = \Gamma$$

+ CENTRIFUGAL ACCELERATION

$$[1 - (\mathbf{A} \cdot \mathbf{\Omega})^2] \mathbf{\Omega}^2(t)$$

+ COMMON-MODE ACCELERATION (TILT)

$$(1/l)(\delta n_{-l} + h_s \mathbf{A}) \cdot \vec{\theta}(t) \times \mathbf{g}_E$$

+ ANGULAR ACCELERATION

$$\delta n_{+l} \times \mathbf{A} \cdot \vec{\alpha}(t)$$

CALIBRATION AND ERROR COEFFICIENTS

ADJUST DRIVE CURRENT IN TRANSDUCERS TO OBTAIN
X TILT, Y TILT OR VERTICAL SHAKING.

COMMON-MODE CALIBRATION

$$g = \hat{n} \cdot \vec{\theta} \times \vec{g}_E$$

GRADIOMETER CALIBRATION

$$\Gamma(2f) = [1 - (\hat{n} \cdot \hat{\Omega})^2] \Omega^2(f)$$

MEASURE MISALIGNMENT

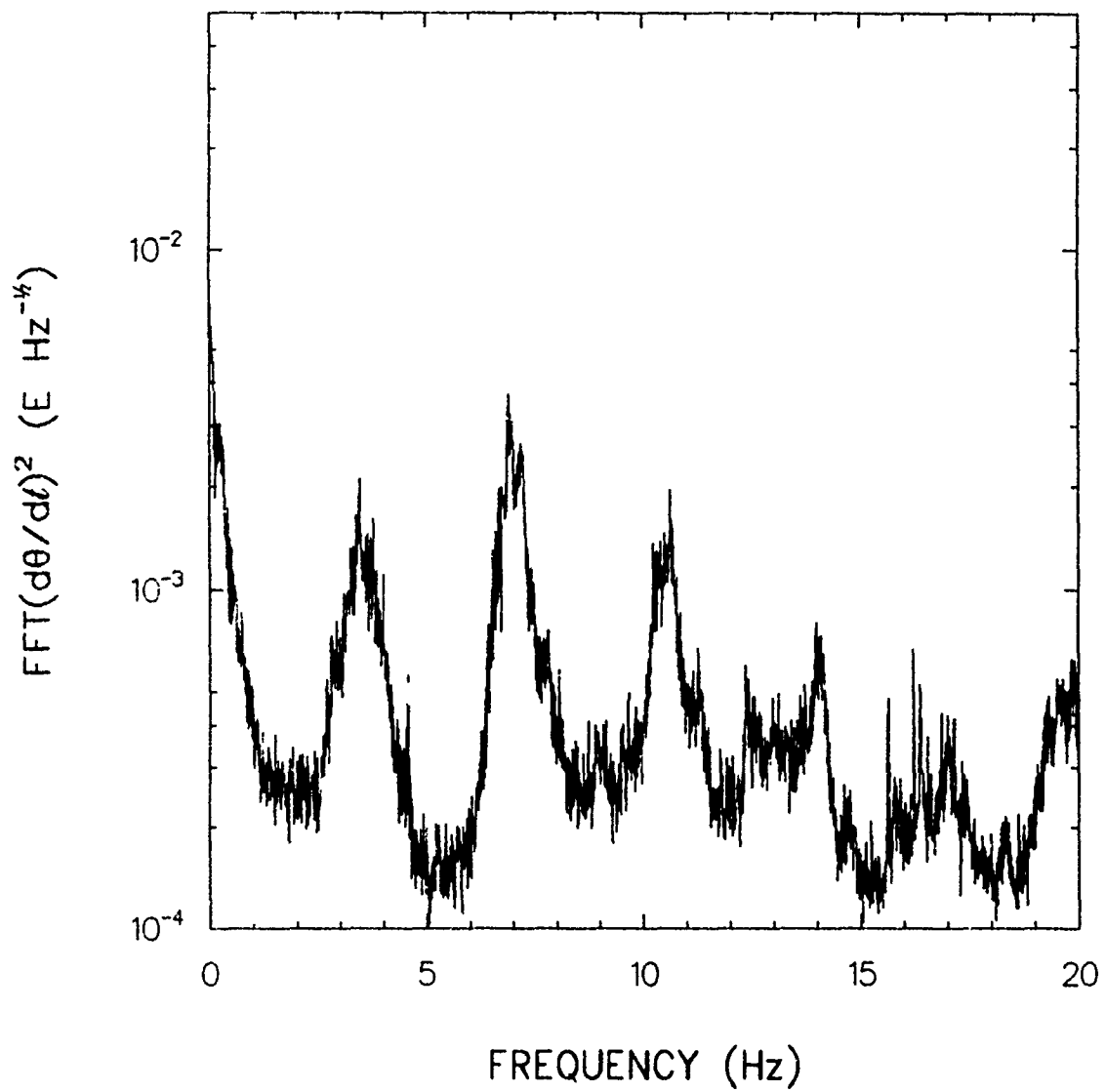
$$\delta\Gamma(f) = -(1/l) \delta\vec{n}_{-l} \cdot \vec{\theta} \times \vec{g}_E + \delta\vec{n}_{+l} \times \hat{n} \cdot 2\pi f \vec{\theta}$$

$$\delta n_{-l} = 3.4 \times 10^{-4} \quad (\text{adjusted at room temperature})$$

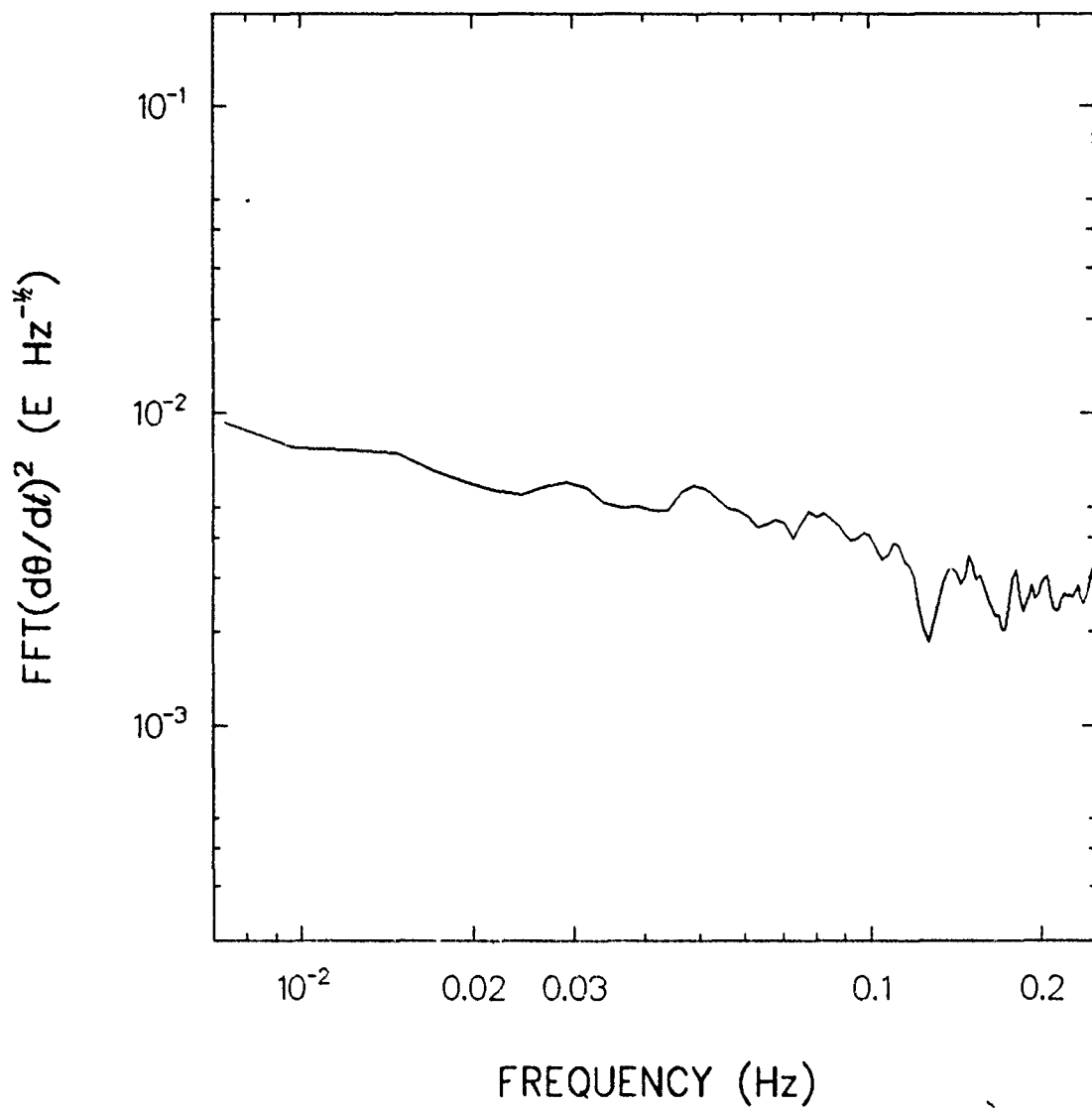
$$\delta n_{+l} = 5.0 \times 10^{-3} \quad (\text{not adjusted})$$

DETERMINE CENTRIFUGAL ACCELERATION IN TWO DIMENSIONS

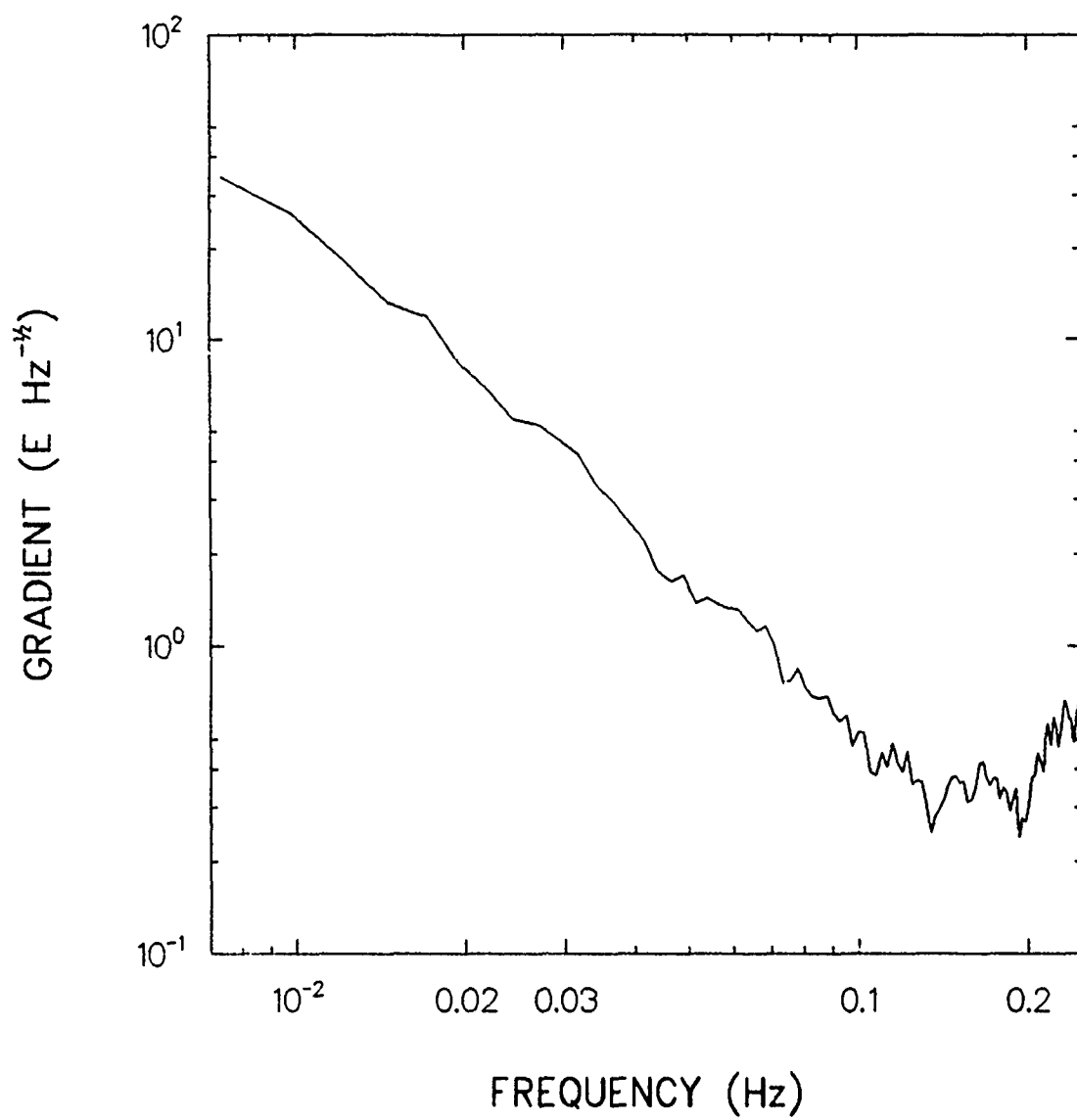
CENTRIFUGAL ACCELERATION PERPENDICULAR TO AXIS



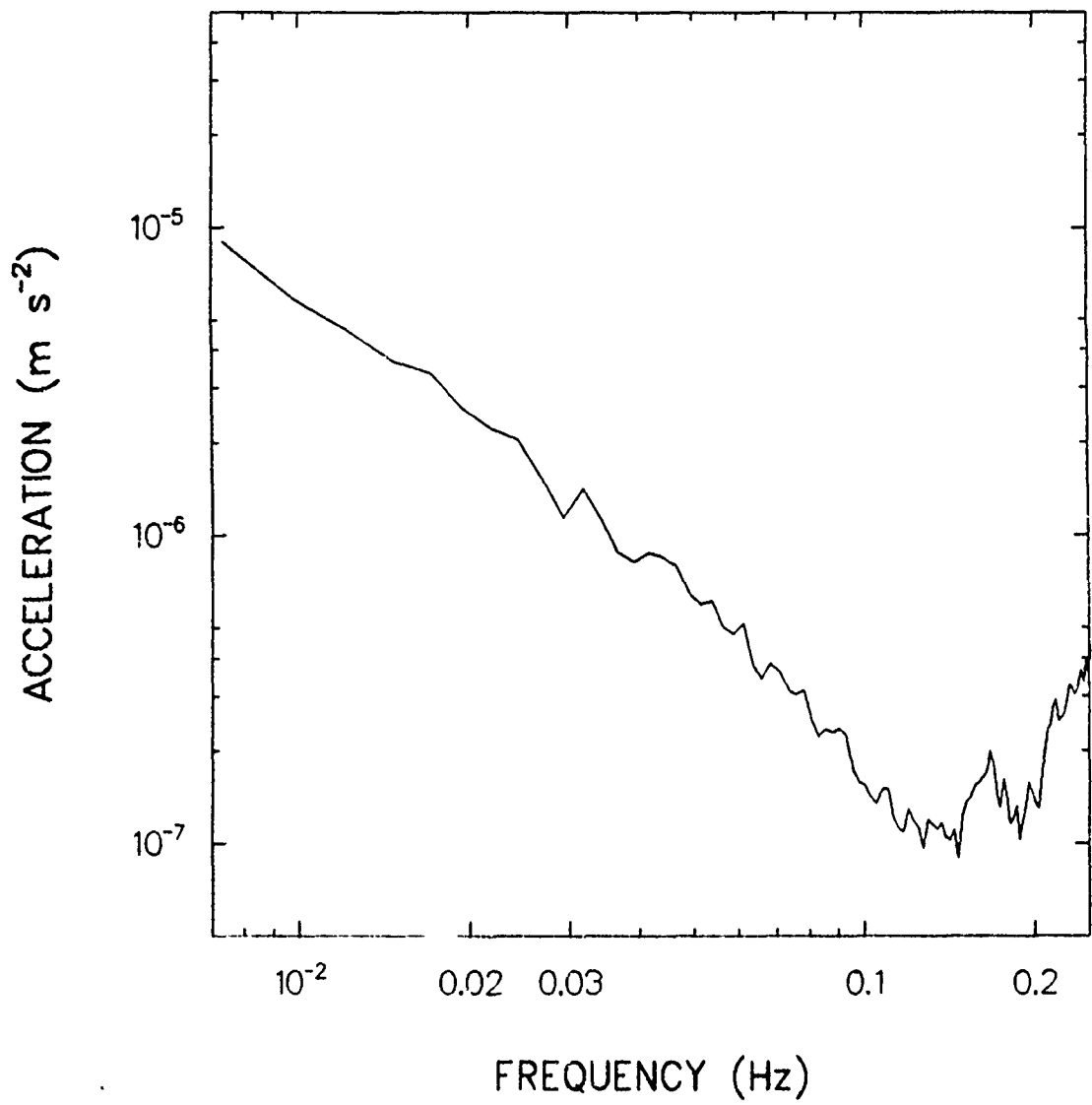
CENTRIFUGAL ACCELERATION PERPENDICULAR TO AXIS



DIFFERENTIAL-MODE SENSE



COMMON-MODE SENSE



NOISE IN THE SENSING CIRCUIT

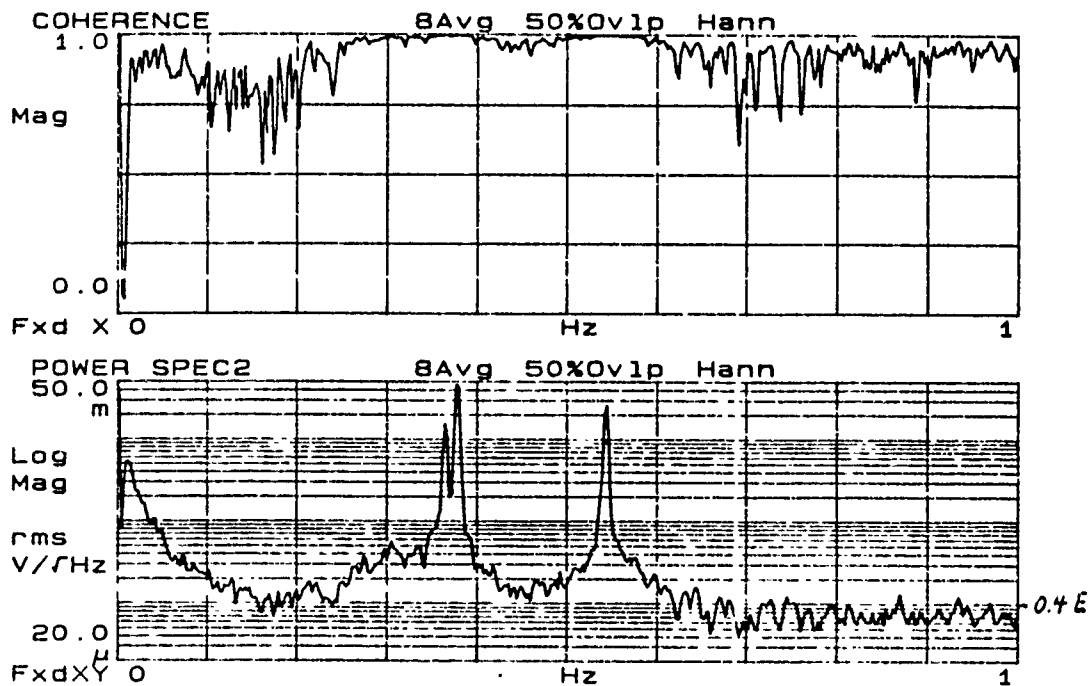
FLUX LEAKAGE

$$\text{out: } \phi(t) = \phi[1 - \alpha(1 - e^{-t/\tau})]$$

$$\text{in: } \phi(t) = \alpha\phi(1 - e^{-t/\tau})$$

$$\tau = 50 \text{ s}, \quad \alpha = 2 \times 10^{-9}, \quad \text{with } B = 0.5 \text{ tesla}$$

BALANCE BOTH SENSING CIRCUITS

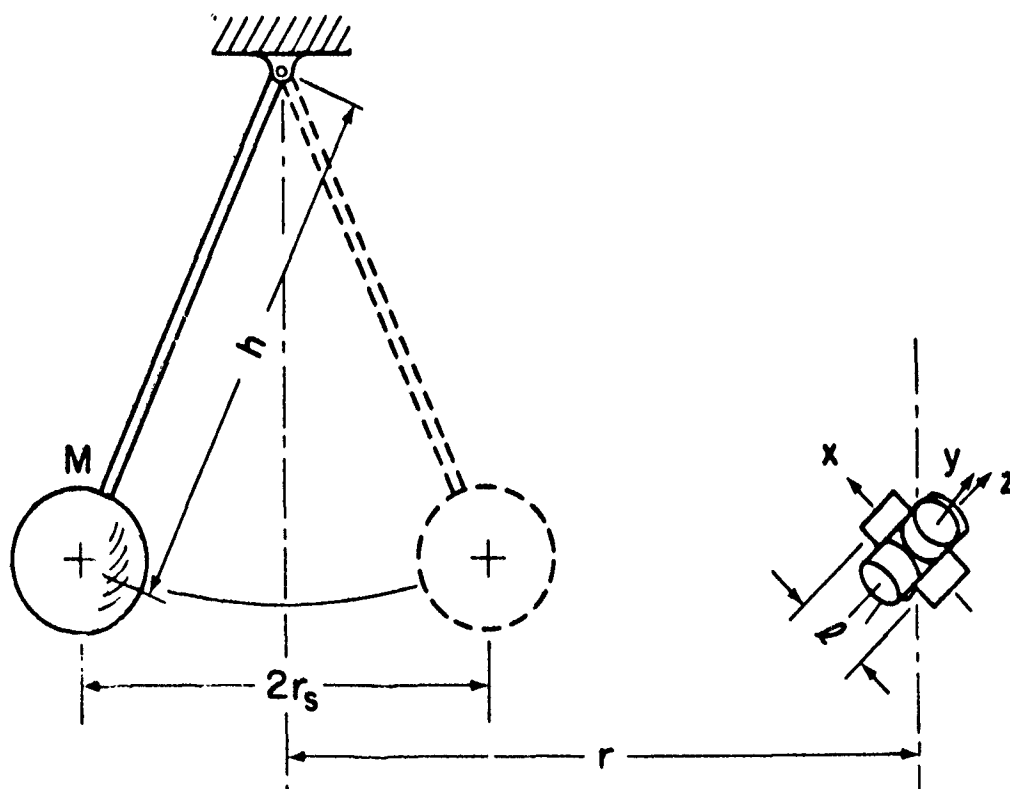


Composition Independent Null Test of the Inverse Square Law of Gravitation

Test for non-Newtonian potential of the form

$$\phi(r) = -G \frac{m}{r} (1 + \alpha e^{-r/\lambda})$$

$$\nabla^2 \phi(r) = 0 - G \frac{m \alpha}{r \lambda^2} e^{-r/\lambda}$$



TILT IS THE PRIMARY ERROR SOURCE

REDUCING SENSITIVITY TO TILT IN A SINGLE-AXIS GRADIOMETER

$$\begin{aligned}\delta\Gamma(\omega) &= \delta\vec{n}_L \cdot \vec{\theta}(\omega) \times \vec{g}_E \\ &= \vec{\theta}(\omega) \cdot \vec{g}_E \times \delta\vec{n}_L\end{aligned}$$

$$\delta\vec{n}_L \equiv \hat{n}_1 - \hat{n}_2 \perp \hat{n}$$

1. ALIGN \hat{n} HORIZONTAL
2. ROTATE ABOUT \hat{n} TILL $\delta\vec{n}_L \parallel \vec{g}_E$

Removal of tilt and scale factor mismatch errors with a three axis gradiometer.

$$\Gamma'_{11} = \alpha \Gamma_{11} + h_1 \hat{n}_1 \cdot \vec{\vartheta} \times \vec{g}_E$$

$$\Gamma'_{22} = \beta \Gamma_{22} + h_2 \hat{n}_2 \cdot \vec{\vartheta} \times \vec{g}_E$$

$$\Gamma'_{33} = \gamma \Gamma_{33} + h_3 \hat{n}_3 \cdot \vec{\vartheta} \times \vec{g}_E$$

$$\begin{aligned} \sum \Gamma'_o &= \Gamma'_{11} + \frac{h_1}{h_2} \Gamma'_{22} + \frac{h_1}{h_3} \Gamma'_{33} \\ &= \alpha \Gamma_{11} + \beta \frac{h_1}{h_2} \Gamma_{22} + \gamma \frac{h_1}{h_3} \Gamma_{33} + h_1 (\hat{n}_1 + \hat{n}_2 + \hat{n}_3) \cdot \vec{\vartheta} \times \vec{g}_E \end{aligned}$$

Rotate gradiometer 120 degrees twice and sum,

$$\begin{aligned} \sum \Gamma'_o + \sum \Gamma'_{120} + \sum \Gamma'_{240} &= \left(\alpha + \beta \frac{h_1}{h_2} + \gamma \frac{h_1}{h_3} \right) (\Gamma_{11} + \Gamma_{22} + \Gamma_{33}) \\ &= \dots \nabla^2 \phi \end{aligned}$$

DEVELOPMENT OF A SUPERCONDUCTING SIX-AXIS ACCELEROMETER

E. R. Canavan, H. J. Paik, and J. W. Parke

Department of Physics and Astronomy
University of Maryland, College Park, MD 20742

The three-axis superconducting gravity gradiometer being developed at Maryland for an orbiting gravity mapper requires very precise platform stabilization, particularly against angular motion noise. The key component of the stabilized platform is a superconducting six-axis accelerometer. The accelerometer can also function as a complete inertial navigation system, and with the gradiometer it forms a gradiometer-aided inertial navigation system.

The device senses the motion of a single levitated niobium proof mass with respect to its housing using superconducting AC inductance bridges and a SQUID amplifier. The proof mass, composed of three intersecting square slabs, fits inside a housing of complementary shape formed by 8 titanium cubes mounted in the corners of a large hollow cube. The face of each titanium cube adjacent to the proof mass holds a levitation and a sensing coil. The 24 levitation and the 24 sensing coils are connected to form circuits that provide levitation and sense displacement in each of the 6 degrees of freedom.

The first prototype of the device has been built and operated successfully. The measured values for resonance frequency, sensitivity, and other parameters match very well to those given by a detailed analytical model. The model predicts that by optimizing electro-mechanical coupling, which at present is small, and using a better SQUID, the accelerometer should be able to achieve a base noise level of 10^{-13} g/ $\sqrt{\text{Hz}}$ and 10^{-10} rad/s²/ $\sqrt{\text{Hz}}$. Larger coupling should be achieved in a prototype under development.

Development of a Superconducting Six Axis Accelerometer

**E.R. Canavan, H.J. Paik, & J.W. Parke,
University of Maryland,
College Park, MD 20742**

Goal:

To develop an accelerometer that is:

- Extremely sensitive
- Compact
- Measures all 6 degrees of freedom
- Compatible with the SGG

Principle of Operation:

- Single magnetically levitated mass
 \Rightarrow responds in all degrees of freedom:

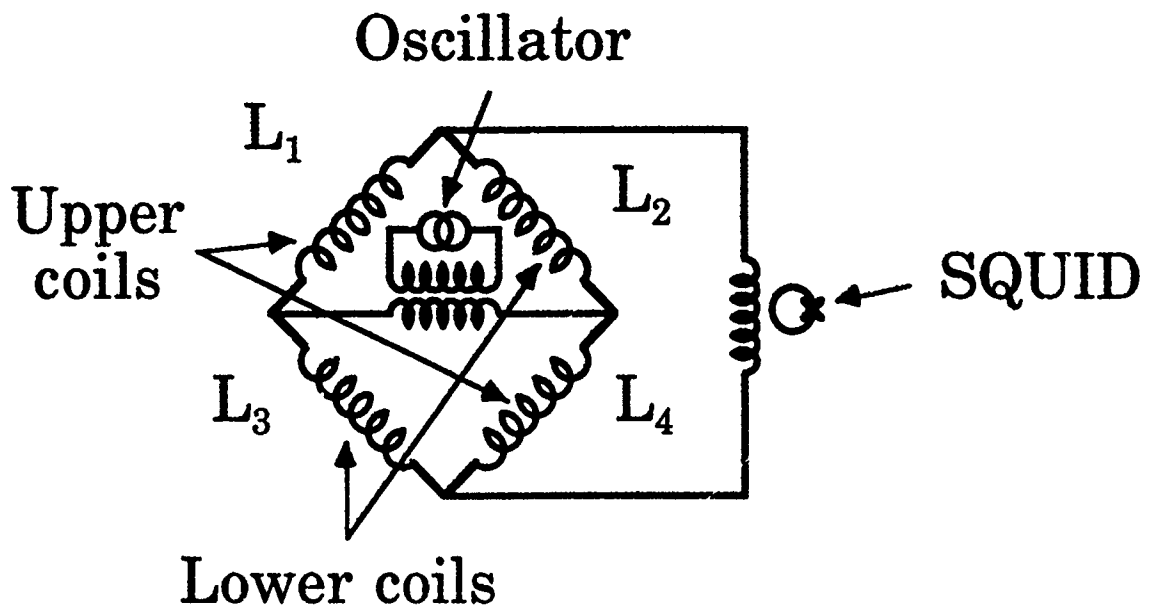
$$\ddot{\mathbf{q}} \rightarrow \mathbf{q}, \quad \mathbf{q} = \{ r_x, r_y, r_z, \theta_x, \theta_y, \theta_z \}$$

- Displacements alter the inductance of 24 coils surrounding the mass:

$$L = L_0 + \Lambda q + O(q^2)$$

- Coils are arranged into 6 AC inductance bridges, each sensitive to motion in a different degree of freedom.

Sensing Circuit



Operation:

- Circuit analysis gives:

$$i_{SQ} = \frac{(L_2 L_3 - L_1 L_4) i_{osc}}{(L_1 + L_2)(L_3 + L_4) + L_{SQ} \sum L_i}$$

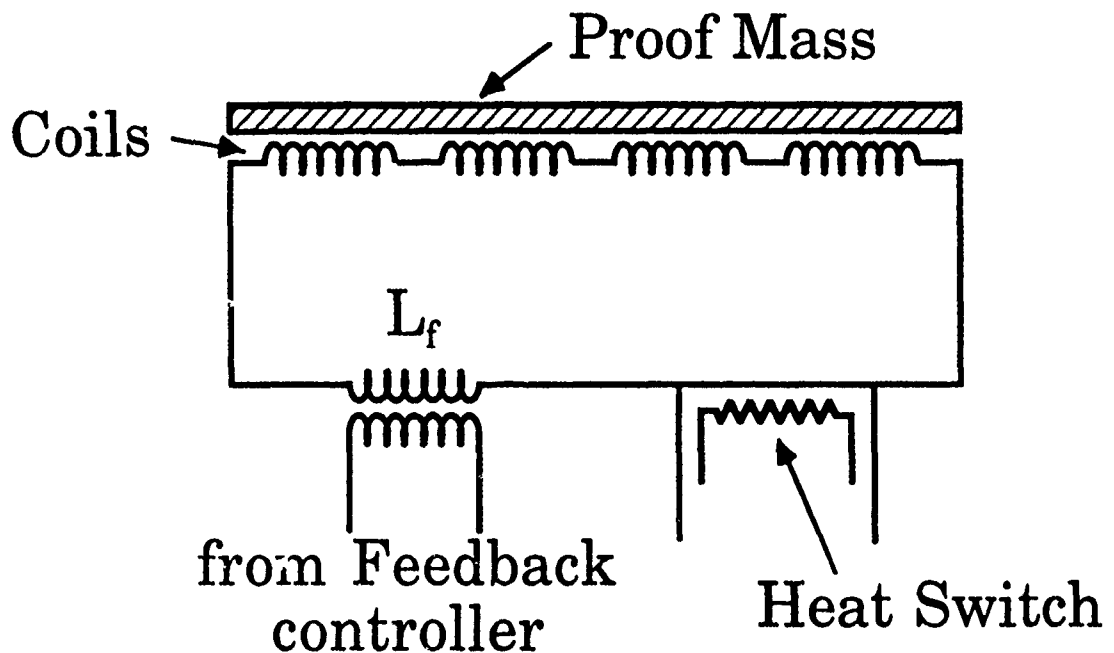
- By geometry,

$$L_1, L_4 = L_0 - \Lambda_S r_x ; L_2, L_3 = L_0 + \Lambda_S r_x$$

$$\Rightarrow i_{SQ} = \left(\frac{\Lambda_S i_{osc}}{L_0 + L_{SQ}} \right) r_x$$

\Rightarrow SQUID output, after demodulation, is proportional to r_x .

Levitation Circuit



- Pulsing heat switch while applying current I_L traps I_L in the loop.
Choose I_L to minimize q .

$$V = \frac{\phi^2}{2(L_f + \sum L_i)}$$

$$= \frac{(4L_0 + L_f)I_L^2}{2} - 2\Lambda_L I_L^2 r_x + \frac{8\Lambda_L^2 I_L^2 r_x^2}{4L_0 + L_f}$$

$$\Rightarrow f_{DC} = 2\Lambda_L I_L^2, \quad k = \frac{16\Lambda_L^2 I_L^2}{4L_0 + L_f}$$

- Feedback current adds to I_L .

Multiplexed Operation

All 6 sensing circuits are connected in series with a single SQUID. Each bridge is driven at a different frequency ω_i and the output of the SQUID is fed to 6 lock-in amplifiers where the signals from the 6 bridges are demodulated.

Materials Considerations

- Coil Forms

Material: Ti6Al4V

Problem: T_c sensitive to heat treatment; in our case, $T_c > 4.2\text{K}$.

\Rightarrow Need temperature controller to maintain SSA above T_c .

- Superconducting wire

Material: NbTi

Problem: Alloy superconductors are Type-II \Rightarrow drift in I_L due to flux creep \Rightarrow low frequency noise.

Originally used Type-I Nb, but had significant occurrence of thermal stress breakage. (Improper drawing process.)

ANALYTICAL MODEL

1) GENERAL EQUATIONS OF MOTION:

PROOF MASS MOTION W.R.T.

HOUSING DESCRIBED BY $R^P(\theta), r^P$

HOUSING MOTION W.R.T. INERTIAL

FRAME DESCRIBED BY R^H, r^H .

$$\Rightarrow v'' = \omega'' \times (R'' r^P) + R'' \dot{r}^P + r^H$$

$$\omega'' = \omega^H + R'' \omega^P$$

CONSTRUCTING THE LAGRANGIAN AND

DERIVING THE EQUATIONS OF MOTION.

$$\ddot{r}_k^P + \frac{1}{M} \frac{\partial V(\theta, r^P)}{\partial r_k^P} = a_k^E$$

$$a^E = -\ddot{r}^H - \nabla \phi_E - 2\omega^H \times \dot{r}^P - \omega^H \times (\omega^H \times r^P) - \dot{\omega}^H \times r^P$$

THE ANGULAR EQUATIONS OF
MOTION ARE NONLINEAR.

TO FIRST ORDER:

$$\ddot{\theta}_x + \frac{1}{I} \frac{\partial V(\theta, r^p)}{\partial \theta_x}$$

$$= -\dot{\omega}_1^H + \theta_1 \dot{\omega}_3^H - \omega_3^H \dot{\theta}_1 + \omega_2^H \dot{\theta}_2 + \frac{\theta_1}{I} \frac{\partial V}{\partial \theta_1}$$

2. CALCULATION OF POTENTIAL

CALCULATE $V(\theta, r)$ AS IN

INTRODUCTION, BUT INCLUDE 2ND ORDER

TERMS: $L = L_0 + \Lambda x - \frac{\gamma}{2} x^2 - \frac{\beta}{2} \theta^2$

CALCULATING V FOR THE LEVITATION
AND SENSING CIRCUITS FOR EACH
AXIS & SUMMING:

$$V = V_0 - f_{DL} (r_x + r_y + r_z) \\ - f_{DL} (\theta_x(r_z - r_y) + \theta_y(r_x - r_z) + \theta_z(r_y - r_x)) \\ + \frac{1}{2} (k_L + k_S) (r_x^2 + r_y^2 + r_z^2) + \frac{1}{2} (\tau_L + \tau_S) (\theta_x^2 + \theta_y^2 + \theta_z^2)$$

⇒ DOMINANT SPRING CONSTANTS:

$$k_L = 4 \left[I_+^2 \left(\frac{4\Lambda_L^2}{4L_L + L_f} + \frac{\gamma_L}{2} \right) + I_-^2 \frac{\Lambda_L^2}{L_L} \right]$$

$$\tau_L = 4 \left[(I_+^2 + I_-^2) (\Lambda_L d_L + c^2 \gamma_L + \beta_L) + I_-^2 \frac{c^2 \Lambda_L^2}{L_L + L_f} \right]$$

3. CALCULATE TRANSFER FUNCTION

SUBSTITUTING FOR V_i ,

$$\ddot{r}_i + \omega_r^2 r_i = a_i$$

$$\ddot{\theta}_i + \omega_\theta^2 \theta_i = \alpha_i \quad \text{WHERE, FOR EXAMPLE,}$$

$$a_x = a_x^{\text{ext}} + \frac{g_E}{\sqrt{3}} + \frac{g_E}{\sqrt{3}} (\theta_1 - \theta_2)$$

$$\alpha_x = -\dot{\omega}_1^H + \theta_1 \dot{\omega}_3^H - \omega_3^H \dot{\theta}_1 + \omega_2^H \dot{\theta}_2$$

⇒ WANT TO USE CONTROLLER

(SMALL $r_i, \theta_i \Rightarrow$ LESS X-COUPLING)

CALCULATING SENSING CIRCUIT TRANSFER

FUNCTION $\frac{i_x}{r_x}$ (AS IN INTRODUCTION)

& COMBINING WITH ABOVE:

$$H_{axi} \equiv \frac{i_x(\omega)}{a_x(\omega)} = i_{osc} r_x \frac{\omega_s}{L_{sq} + 6L_s} \frac{1}{\omega_r^2 + j\omega_r \frac{\omega}{Q_r} - \omega^2}$$

$$H_{\theta xi} \equiv \frac{i_{\theta x}(\omega)}{\alpha_x(\omega)} = i_{osc} \theta_x \frac{c\omega_s}{L_{sq} + 6L_s} \frac{1}{\omega_\theta^2 + j\omega_\theta \frac{\omega}{Q_\theta} - \omega^2}$$

NOTE: HAVE ADDED VELOCITY-DEPENDENT DAMPING

4. MINIMUM DETECTABLE ACCELERATION

TWO FUNDAMENTAL NOISE SOURCES:

- BROWNIAN MOTION NOISE:

ACCELERATION SPECTRAL DENSITY,

$$S_{a_i}^T = \frac{2 k_B T \omega_r}{m Q}$$

- SQUID AMPLIFIER NOISE:

USING H_{a_i} , CAN RELATE INPUT

CURRENT NOISE SPECTRAL DENSITY, S_I

TO EQUIVALENT ACCELERATION

SPECTRAL DENSITY, $S_{a_x}^{eq}$.

.....

COMBINING, MINIMUM DETECTABLE

$$P_{a_x} = \frac{4 \omega_r}{m} \left(\frac{k_B T}{m Q} + \frac{\omega_r E_s}{\beta_r} \right) \quad (\omega \ll \omega_r)$$

WHERE: ENERGY COUPLING COEFFICIENT

$$\beta_r = \frac{1}{2} \left(\frac{I_c L_q}{L_{sq} + 6 L_s} \right)^2 \frac{L_{sq}}{m \omega_r^2}$$

FOR THE ANGULAR DEGREES OF
FREEDOM, OBTAIN:

$$P_{ax} = \frac{4\omega_0}{I} \left(\frac{k_B T}{Q_0} + \frac{\omega_0 E_s}{\beta_0} \right)$$

WHERE

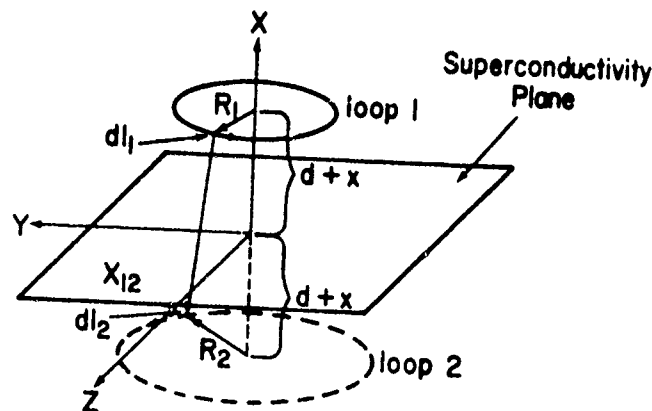
$$\beta_0 = \frac{1}{2} \left(\frac{I_{0s}^2 C \Lambda_s}{L_{sq} + 6L_s} \right)^2 \frac{L_{sq}}{I\omega_0^2}$$

COMPARISON OF MODEL WITH EXPERIMENTAL RESULTS

1) RESONANT FREQUENCIES

TO CALCULATE ω_r, ω_θ NEED $\Lambda_{L,s}, \gamma_{L,s}, \beta$

COMPUTE INDUCTANCE PARAMETERS FROM
FORCE BETWEEN SET OF CONCENTRIC
LOOPS AND THEIR IMAGE CURRENTS



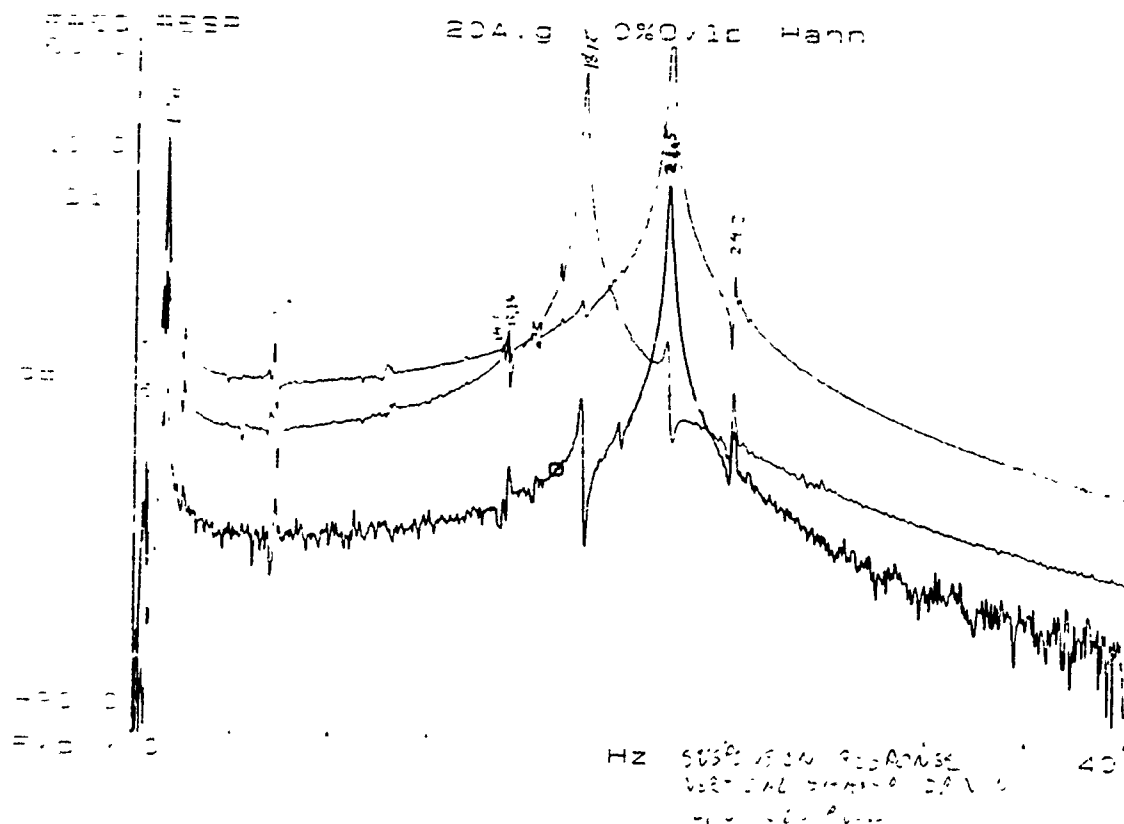
$$F_{12} = \frac{\mu_0}{4\pi} I^2 \sum_{\text{LOOPS}} \sum_{\text{IMAGES}} \oint \oint \frac{x_{12} \partial l_1 \partial l_2}{|x_{12}|^3}$$

EXPAND AND NUMERICALLY INTEGRATE
 $\Rightarrow \Lambda, \gamma$

SIMILARLY TORQUE EQUATION $\Rightarrow \beta$

SUBSTITUTING INTO EQUATION FOR
K.T. GET

$$\omega_f = \sqrt{\frac{K_L + K_s}{m}}, \quad \omega_\theta = \sqrt{\frac{I_L + I_s}{I}}$$



	f_{calc}	f_{exp} [Hz]	
r_x	21.2	21.6	
r_y	20.9	21.5	
r_z	17.8	18.2	
θ_x	13.8	15.0	} MORE DEPENDENT ON β
θ_y	13.9	15.2	
θ_z	14.5	16.2	

2) SENSITIVITY

TO CALCULATE H_{axi} , MUST KNOW I_s

PROBLEM: BRIDGE DRIVEN WITH
TANK CIRCUIT (TO IMPROVE
GAIN, REDUCE RF INTERFERENCE)

SOLUTION: MEASURE $Z(\omega)$

→ CALCULATE CIRCUIT GAIN

→ COMPUTE I_s

RESULTS

	$\langle H_{axi} \rangle_{\text{EXP}}$	$\langle H_{axi} \rangle_{\text{MODEL}}$
X	3.1×10^5	3.5×10^5
Y	9.9×10^3	8.8×10^3
Z	1.6×10^5	2.4×10^5
θ_x	2.1×10^3	2.1×10^3
θ_y	6.0×10^2	6.2×10^2
θ_z	4.7×10^2	4.1×10^2

$\left. \begin{array}{l} \text{ } \\ \text{ } \\ \text{ } \end{array} \right\} [\Phi/g]$
 $\left. \begin{array}{l} \text{ } \\ \text{ } \end{array} \right\} [\Phi/\text{rad}]$
 $\left. \begin{array}{l} \text{ } \\ \text{ } \end{array} \right\} [10/\text{SEC}^2]$

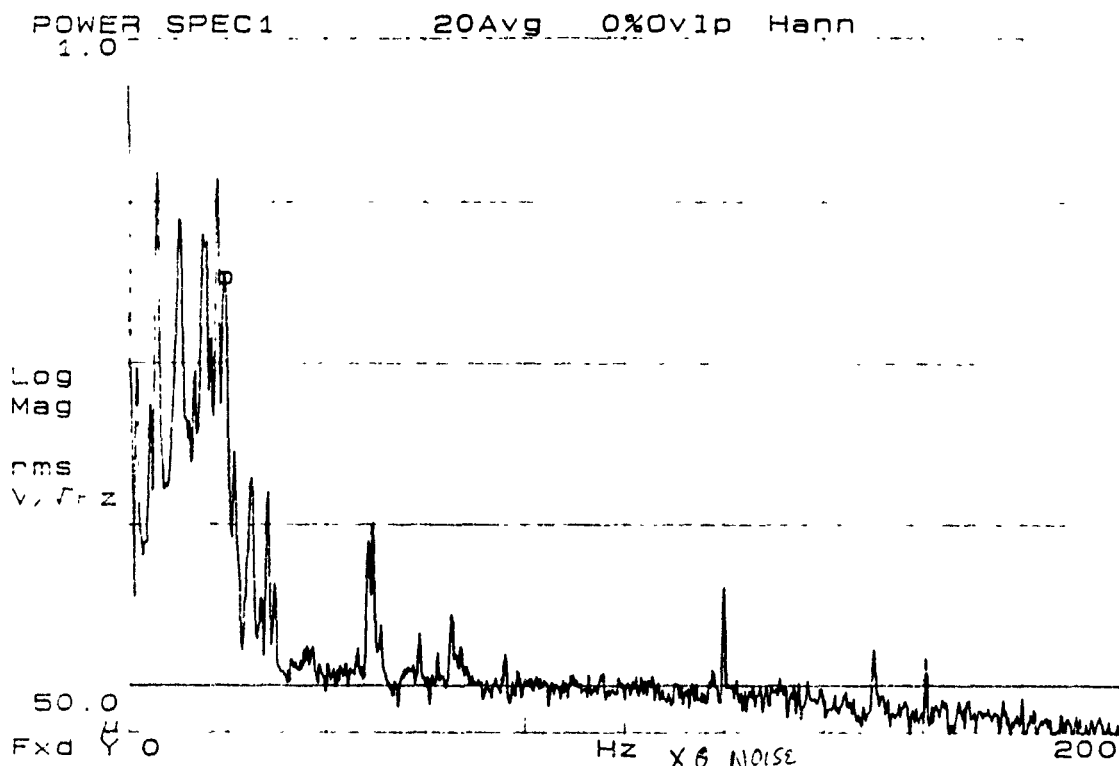
REASONABLY GOOD FIT

3) MINIMUM SIGNAL

FOR QUANTUM DESIGN SQUIDS

$$E_s = 10^{-28} \text{ J/Hz} \Rightarrow S_{\Phi}^{\frac{1}{2}} = 10^{-4} \Phi_0 / \sqrt{\text{Hz}}$$

ACTUALLY SEE THIS LEVEL IN MEASUREMENT



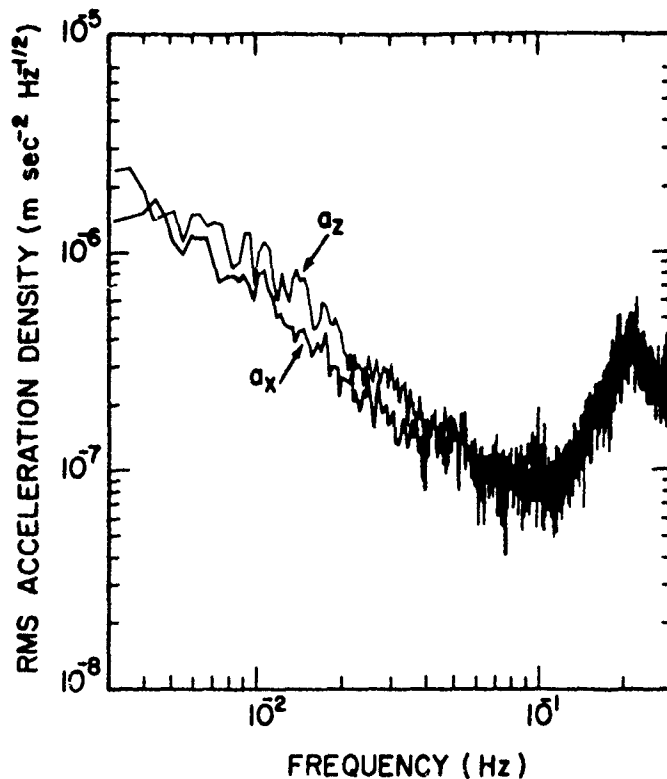
$$\text{EXPERIMENTAL } P_{aK}^{\frac{1}{2}} = S_{\Phi}^{\frac{1}{2}} / \langle H_{aKi} \rangle$$

	$(P_{aK})^{\frac{1}{2}}_{\text{EXP}}$	$(P_{aK})^{\frac{1}{2}}_{\text{MODEL}}$		β
X	3.2×10^{-10}	4.0×10^{-10}	$\frac{1}{\sqrt{\text{Hz}}}$	3.3×10^{-6}
Y	1.0×10^{-8}	1.6×10^{-8}		2.0×10^{-9}
Z	6.4×10^{-10}	5.9×10^{-10}		1.1×10^{-6}
θ_X	4.8×10^{-8}	6.7×10^{-8}	$\frac{\text{rad}}{\sqrt{\text{Hz}}}$	2.0×10^{-5}
θ_Y	1.7×10^{-7}	2.2×10^{-7}		1.8×10^{-6}
θ_Z	2.1×10^{-7}	3.5×10^{-7}		8.7×10^{-7}

279 NOTE $\beta \ll \frac{1}{2} \Rightarrow$ FAR BELLOW POTENTIAL $P_{aK}^{\frac{1}{2}}$

OTHER RESULTS

1) LOW FREQUENCY NOISE



NOTE: "SURF" PEAK CLEARLY VISIBLE
SEISMIC NOISE SHOULD HAVE MINIMUM
AT $\sim (10^{-2} \text{ Hz}, 10^{-10} \frac{\text{m}}{\text{sec}^2})$

\Rightarrow LOW FREQ. NOISE LIMITS SAA
BELOW $\sim 10^{-2} \text{ Hz}$

LOW FREQ. NOISE $\propto \frac{1}{f}$

3) FEED BACK

NEED FOR CONTROLLER:

- LINEARIZE OUTPUT
- REDUCE CROSS COUPLING
- INCREASE DYNAMIC RANGE

USE PID CONTROLLER

FREQ RESP

30Avg 85%Ovlp Hann

CLEAR FIT

87.5

87.5

dB

dB

10.0

12.5

10.0

10.0

dB

dB

-21.0

-24.0

FREQ

Hz

200

OPEN
← LOOP

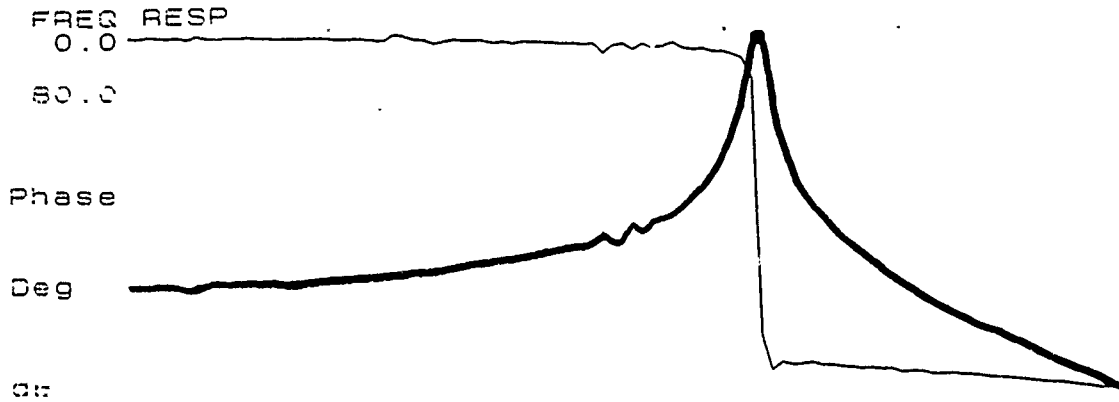
→ CLOSED
LOOP

⇒ FEEDBACK WIDENS BANDWIDTH

CROSS COUPLING

STRONG CROSS COUPLING \Rightarrow MAY NEED MIMO CONTROLLER

MEASURE ON AND OFF DIAGONAL RESPONSE



FIND OFF-DIAGONAL GAIN > 20 dB BELOW
DIAGONAL \Rightarrow SYSTEM DIAGONALLY DOMINANT
 \Rightarrow CAN USE SISO CONTROLLER

OPTIMIZATION

• ULTIMATE PERFORMANCE

$$P_{ax} = \frac{4\omega_r}{M} \left(\frac{k_B T}{Q_r} + \frac{\omega_r E_s}{\beta_r} \right)$$

$$(\beta_r)_{\text{OPT}} = \frac{1}{2}$$

FOR BEST SQUIDS, $E_s = 20\hbar$

$$\Rightarrow P_{ax}^{1/2} \simeq \left[\frac{4\omega_r}{M} \left(\frac{k_B T}{Q_r} \right) \right]^{1/2}$$

$$= 1.4 \times 10^{-13} \frac{\text{g}}{\sqrt{\text{Hz}}}$$

$$(Q_r = 10^5, T = 4.2 \text{ K})$$

SIMILARLY

$$\Rightarrow P_{ax}^{1/2} \simeq \left[\frac{4\omega_\theta}{I} \left(\frac{k_B T}{Q_\theta} \right) \right]^{1/2}$$
$$= 6.6 \times 10^{-11} \frac{\frac{\text{rad}}{\text{sec}^2}}{\text{Hz}}$$

• IMPROVING β

$$\beta_r = \frac{1}{2} \left(\frac{I_r \Lambda_s}{L_{sq} + 6L_s} \right)^2 \frac{L_{sq}}{M \omega_r^2}$$

USING SEPERATE SENSING CIRCUITS:

$$6L_s \rightarrow L_s$$

& IMPEDENCE MATCHING TRANSFORMERS:

$$L_{sq} \rightarrow L_s$$

$$\Rightarrow \beta_r = \frac{1}{8} \frac{I_r^2 \Lambda_s}{M \omega_r^2 d}$$

\Rightarrow DECREASE : M, ω_r, d

\Rightarrow INCREASE : $\Lambda \Rightarrow$ INCREASE TURNS DENSITY, AREA

$I_r \Rightarrow$ IMPROVE COIL MATCHING

\Rightarrow SINGLE LAYER COILS.

MODEL II: LARGE, SINGLE LAYER SENSE/LEV. COIL

FOR $I_r = 1 \text{ AMP}$ $\beta_{II} \approx 10^3 \beta_I$

SUPERCONDUCTING GRAVITY GRADIOMETER MISSION - AN OVERVIEW

Ho Jung Paik

Department of Physics and Astronomy
University of Maryland, College Park, Maryland 20742

Two dedicated space missions proposed for the 1990's hold the promise of providing data for recovering the Earth's gravity anomaly with unprecedented accuracy and resolution: the Aristoteles Mission and the Superconducting Gravity Gradiometer Mission (SGGM). SGGM, the more ambitious of the two, aims at recovering the global gravity field to a precision of two to three mgal with a resolution of 50 km.

The instrument package of SGGM is a three-axis gravity gradiometer which is integrated to a six-axis accelerometer for active platform control. The intrinsic sensitivity of the gradiometer is $10^{-4} \text{ E Hz}^{-1/2}$ and that of the accelerometer is $10^{-13} g_E \text{ Hz}^{-1/2}$ in linear acceleration and $10^{-11} \text{ rad sec}^{-2} \text{ Hz}^{-1/2}$ in angular acceleration. While precise attitude control of the Experiment Module is essential to mission success and is also technically most challenging, pointing accuracy and disturbance isolation requirements of SGGM are less stringent compared to that of other missions, such as Hubble Space Telescope (HST) and Gravity Probe-B (GP-B). Thus, they are within the reach of technologies of the 1990's.

In the recently completed Phase A study, the SGGM study team addressed the problem of scientific requirements and mission feasibility. At the University of Maryland, prototypes of the three-axis gradiometer and the six-axis accelerator are being fabricated, improved and tested. The actual mission hopefully will take place before the year 2000.

SUPERCONDUCTING GRAVITY GRADIOMETER MISSION
- AN OVERVIEW

HO JUNG PAIK

DEPARTMENT OF PHYSICS AND ASTRONOMY

UNIVERSITY OF MARYLAND, COLLEGE PARK, MD 20742

1. SCIENCE OBJECTIVES
2. SUPERCONDUCTING GRAVITY GRADIOMETER
3. SPACECRAFT AND ORBIT
4. DEVELOPMENT SCHEDULE
5. CRYOGENIC REQUIREMENTS

OCTOBER 13, 1989

17TH GRAVITY GRADIOMETER CONFERENCE

HANSCOM AFB, MA 01731

1. Science Objectives

1) Earth's gravity field mapping

- 50 km resolution ($0.5^\circ \times 0.5^\circ$)
- 0.2 mgal gravity anomaly error for $1^\circ \times 1^\circ$

2) Tests of fundamental laws of gravity

- 10^{-10} resolution for inverse square law
- Einstein's field equation for general relativity
- "Magnetic" component of gravity

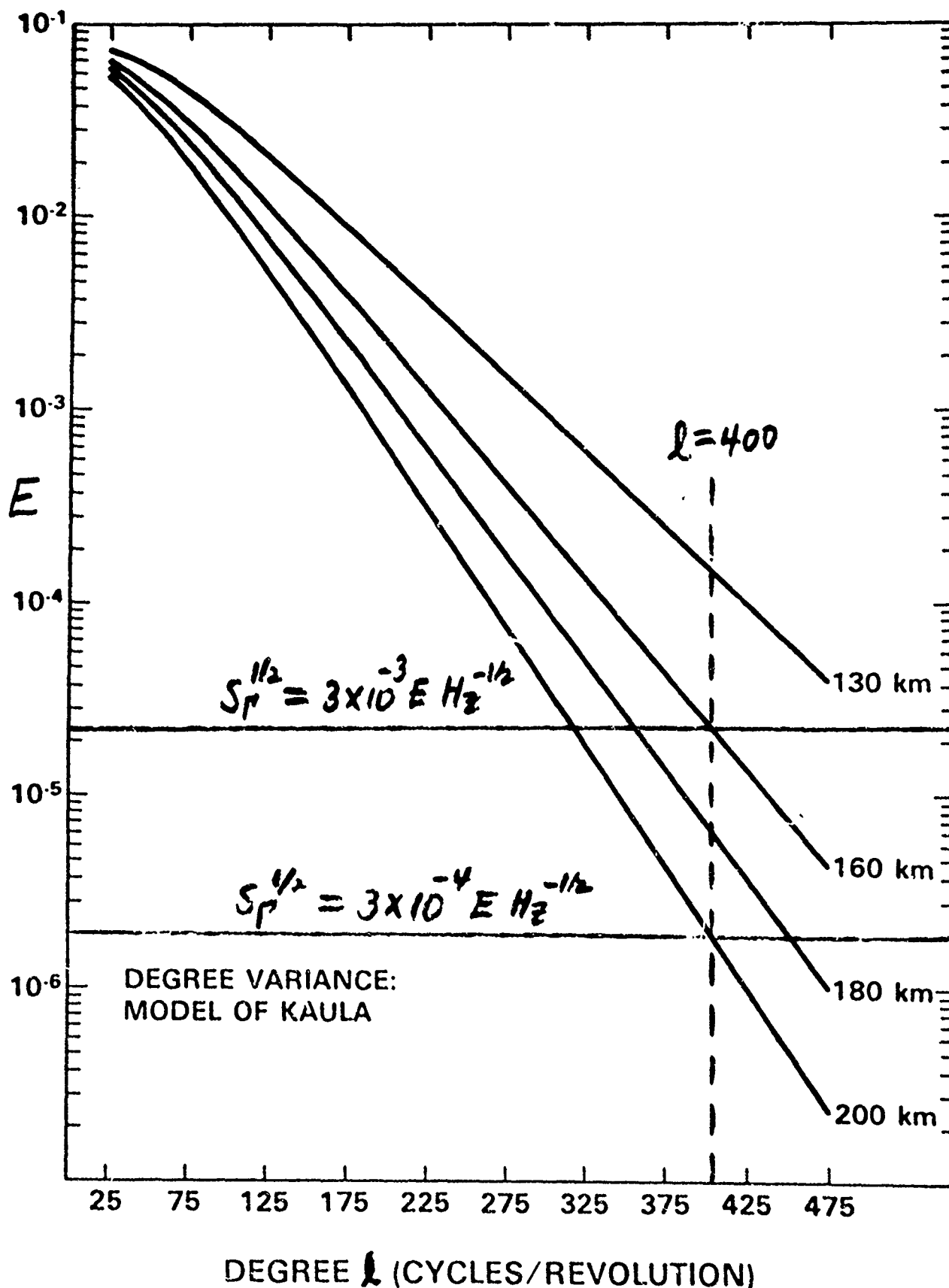
3) Technology development

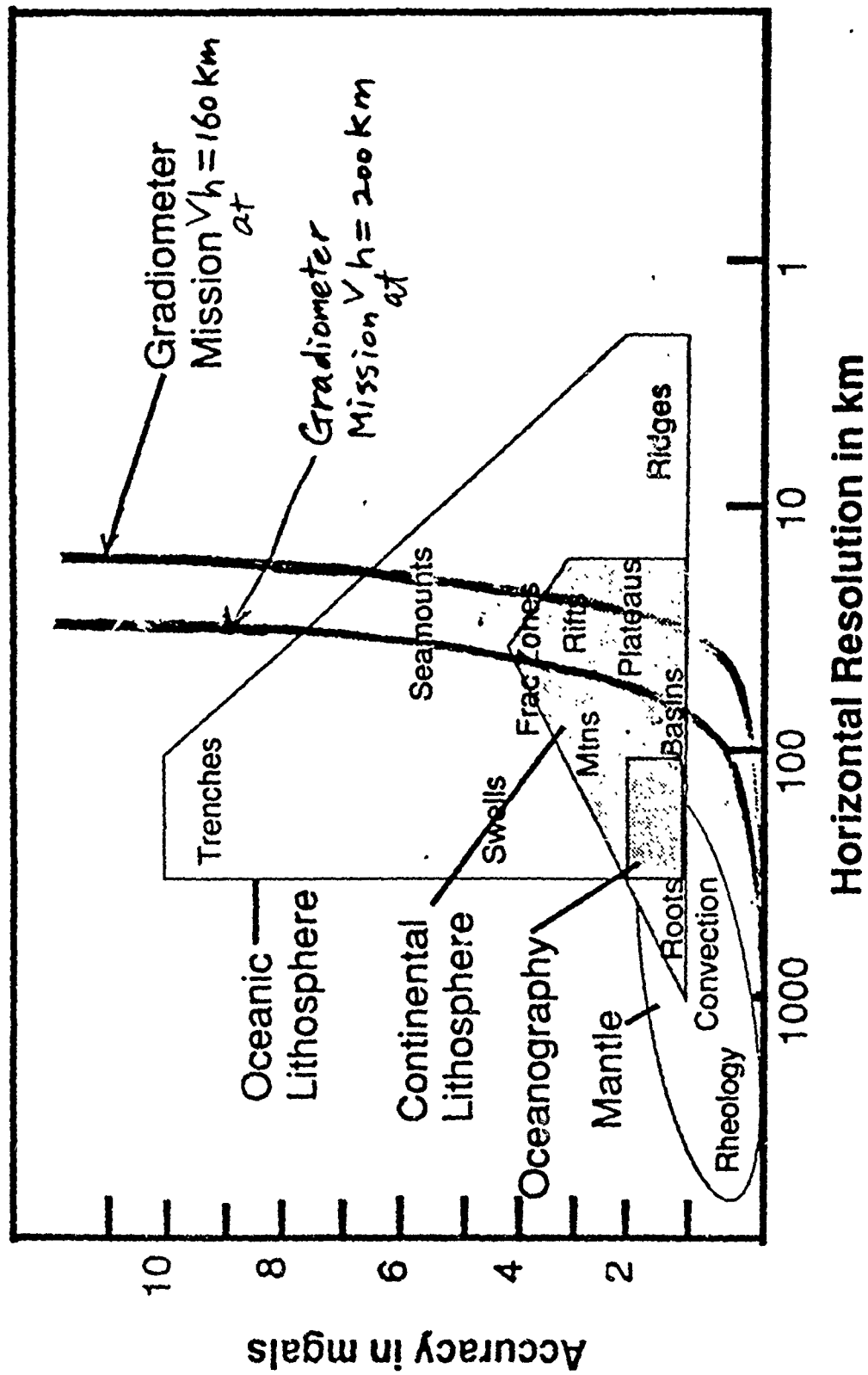
- Moving-base gravity survey
- Precision inertial guidance
- Stable platforms

⇒ Gravity Gradiometer with $10^{-4} \text{ E Hz}^{-1/2}$ sensitivity is required

⇒ Superconducting technology is required.

SPECTRUM OF THE VERTICAL GRAVITY GRADIENT (EU PER COEFFICIENT)





2. Superconducting Gravity Gradiometer

- 1) Operation at LHe temperatures ($T=1.5 \sim 4.2 \text{ K}$)
 - \Rightarrow Low Brownian motion noise
 - \Rightarrow High mechanical stability
- 2) Transduction and differencing by persistent current
 - \Rightarrow Scale factor and null stability
 - \Rightarrow Large dynamic range
- 3) Amplification by SQUID
 - \Rightarrow High sensitivity
 - \Rightarrow Large dynamic range
- 4) Superconducting negative spring
 - \Rightarrow High sensitivity
- 5) Superfluid/normal helium bath
 - \Rightarrow Stable thermal environment
- 6) Superconducting shield
 - \Rightarrow Excellent isolation of EMI

Intrinsic Spectral Noise

$$S_r(f) = \frac{8}{m l^2} \left[K_B T \frac{2\pi f}{Q(f)} + \frac{(2\pi f_0)^2}{2\beta\eta} E_A(f) \right]$$

Design parameters

proof mass	m	1.3 kg
base line	l	0.19 m
resonance frequency	f_0	< 7 Hz
temperature	T	1.5 K
quality factor	Q	$\geq 10^5$
amplifier noise (SHE dc SQUID)	E_A	$3 \times 10^{-30} \text{ J Hz}^{-1}$
energy coupling factor	$\beta\eta$	~ 0.5

Gravity Gradient Noise

Without negative spring

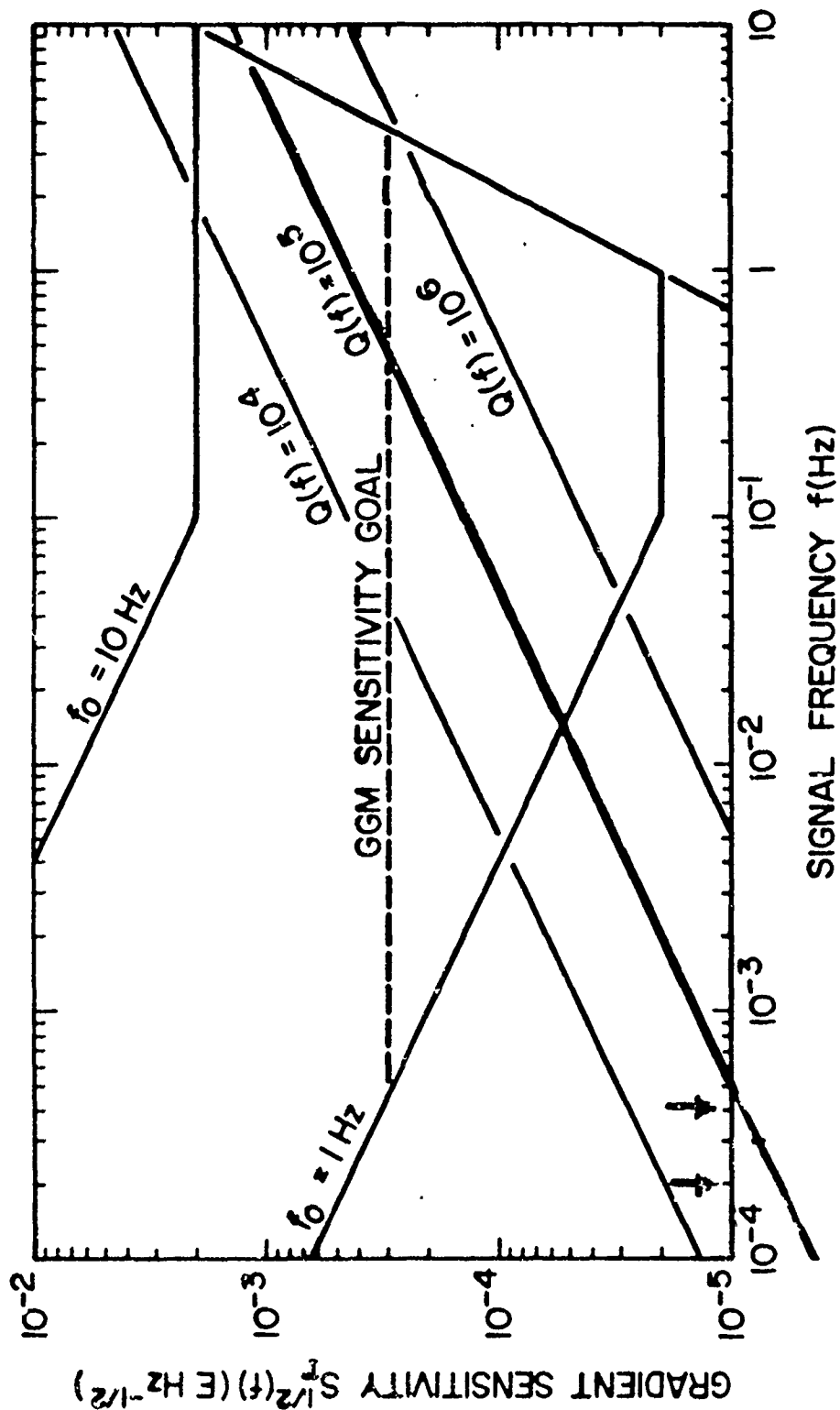
$$S_r^{1/2}(f) = 1 \times 10^{-3} \text{ E Hz}^{-1/2} \text{ at } 0.1 \text{ Hz}$$

With negative spring ($f_0 = 1$)

$$S_r^{1/2}(f) \leq 2 \times 10^{-4} \text{ E Hz}^{-1/2} \text{ at } 0.1 \text{ Hz}$$

Goal set by 1983 workshop $\rightarrow 3 \times 10^{-4} \text{ E Hz}^{-1/2}$

Expected Sensitivity of S/C Gradiometer



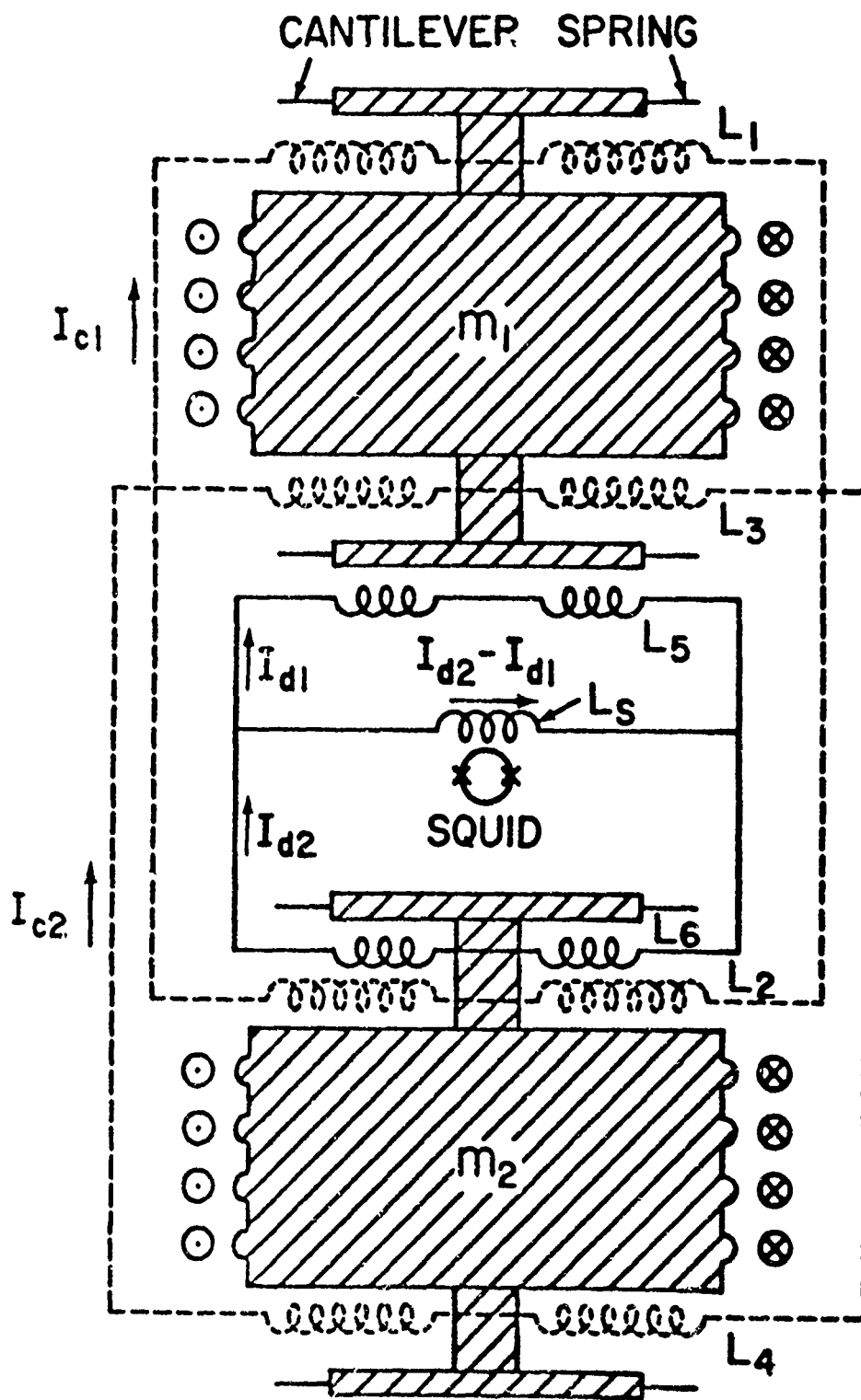
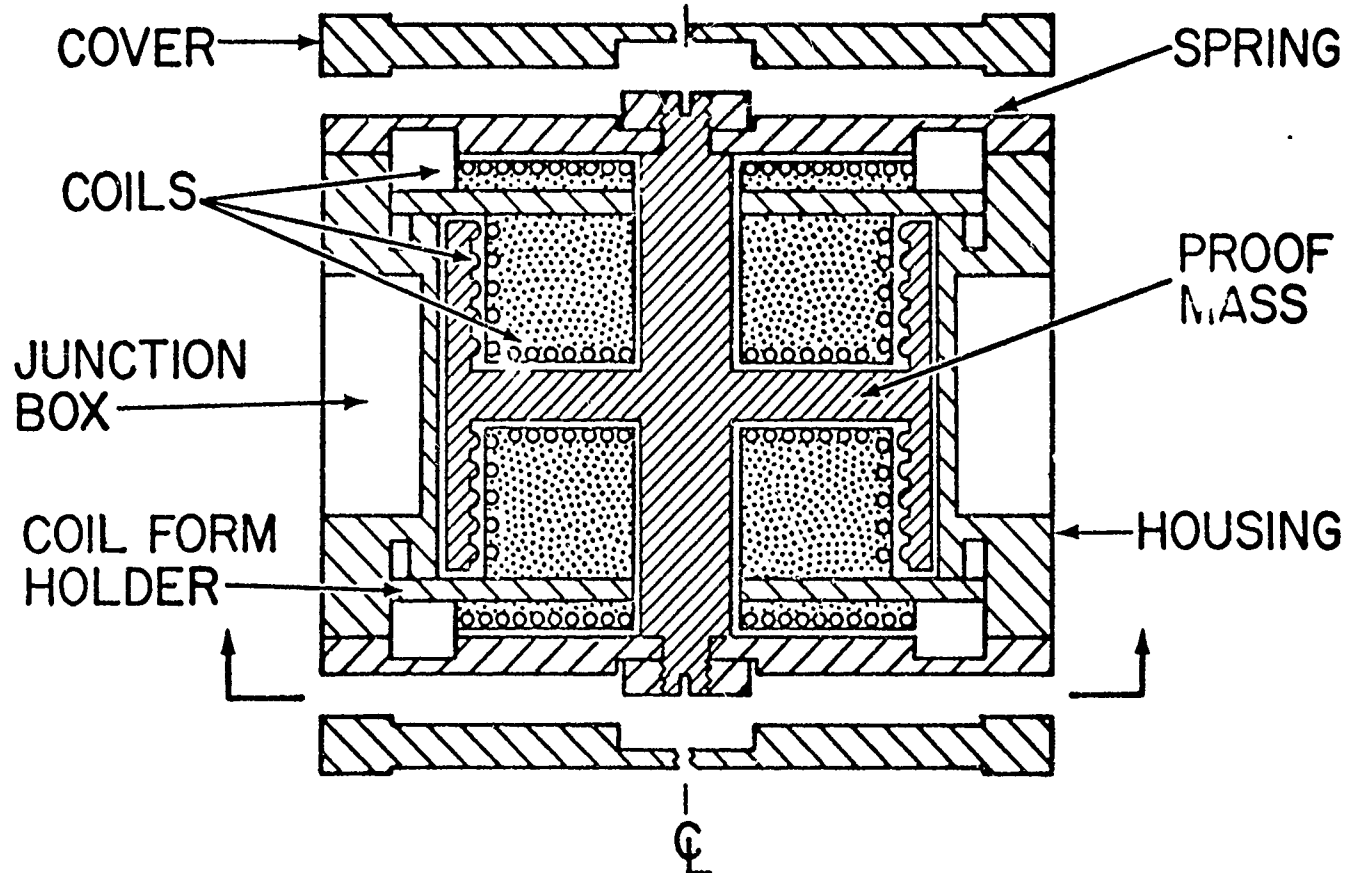
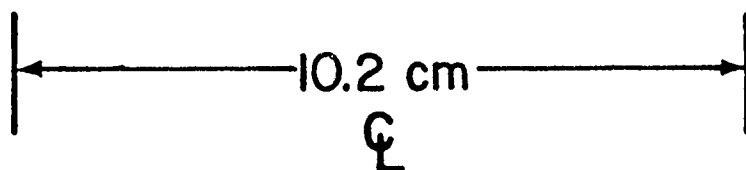
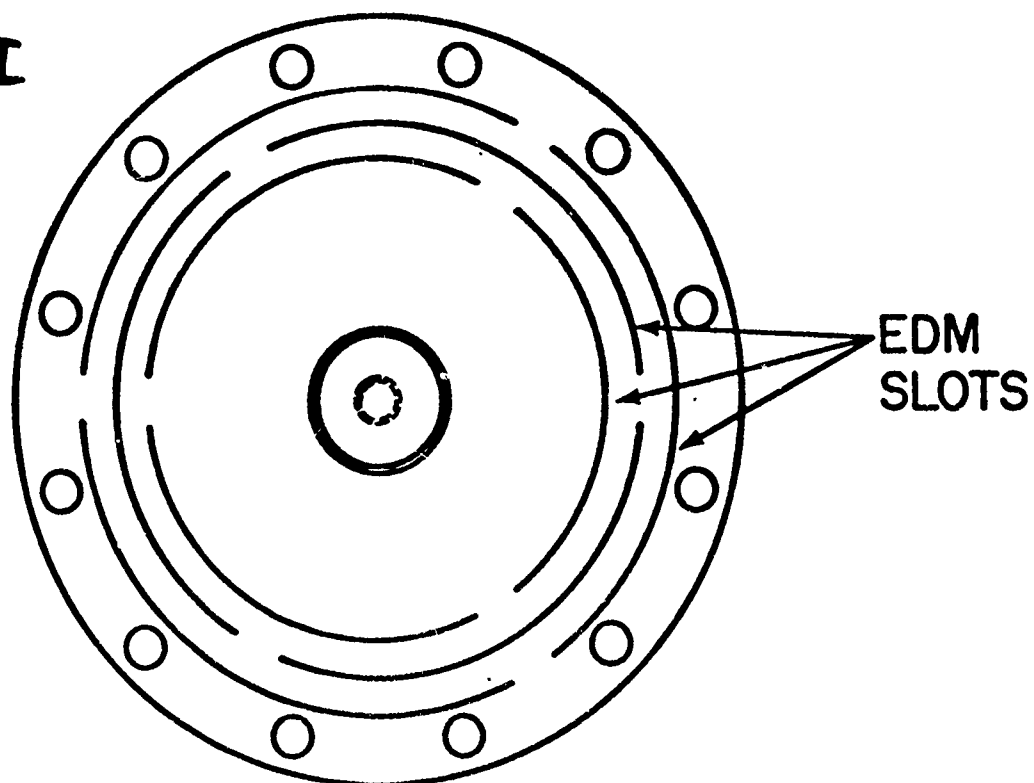


Fig. 2. Circuitry for a superconducting gravity gradiometer.

Model III

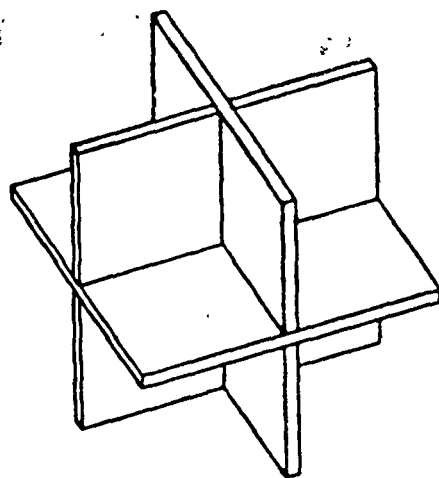


110

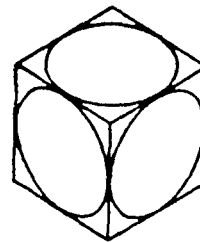
1-3072-7-4D GEOPHYSICS GOAL: $3 \times 10^{-4} \text{ E Hz}^{1/2}$ AT $f = 0.1 \text{ Hz}$

PARAMETER	ERROR MECHANISM	ORIENTATION	REQUIRED CONTROL/KNOWLEDGE	
INSTRUMENT NOISE	$S_f^{1/2} (f)$		$10^{-2} \text{ E Hz}^{-1/2}$	$10^{-4} \text{ E Hz}^{-1/2}$
SCALE FACTOR DRIFT			$2 \times 10^{-6} \text{ hr}^{-1}$	$2 \times 10^{-6} \text{ hr}^{-1}$
DYNAMIC RANGE		INERTIAL EARTH FIXED	$3 \times 10^5 \text{ Hz}^{1/2}$ $10 \times 3 \text{ Hz}^{1/2}$	$3 \times 10^7 \text{ Hz}^{1/2}$ $10^5 \text{ Hz}^{1/2}$
LINEAR ACCELERATION			$2 \times 10^{-6} \text{ E Hz}^{-1/2}$	$2 \times 10^{-8} \text{ E Hz}^{-1/2}$
ALTITUDE STABILITY			$7 \text{ m Hz}^{-1/2}$	$7 \times 10^{-2} \text{ m Hz}^{-1/2}$
POINTING STABILITY		INERTIAL EARTH FIXED	$2 \times 10^{-6} \text{ rad Hz}^{-1/2}$ $3 \times 10^{-4} \text{ rad Hz}^{-1/2}$	$2 \times 10^{-8} \text{ rad Hz}^{-1/2}$ $3 \times 10^{-6} \text{ rad Hz}^{-1/2}$
ATTITUDE RATE			$3 \times 10^{-6} \text{ rad s}^{-1} \text{ Hz}^{-1/4}$	$3 \times 10^{-7} \text{ rad s}^{-1} \text{ Hz}^{1/4}$
ATTITUDE ACCELERATION			$10^{-6} \text{ rad s}^{-2} \text{ Hz}^{-1/2}$	$10^{-8} \text{ rad s}^{-2} \text{ Hz}^{1/2}$
INSTRUMENT TEMPERATURE			$10^{-2} \text{ K Hz}^{-1/2}$	$10^{-4} \text{ K Hz}^{-1/2}$
ELECTRONICS TEMPERATURE			$1 \text{ K Hz}^{-1/2}$	$10^{-2} \text{ K Hz}^{-1/2}$

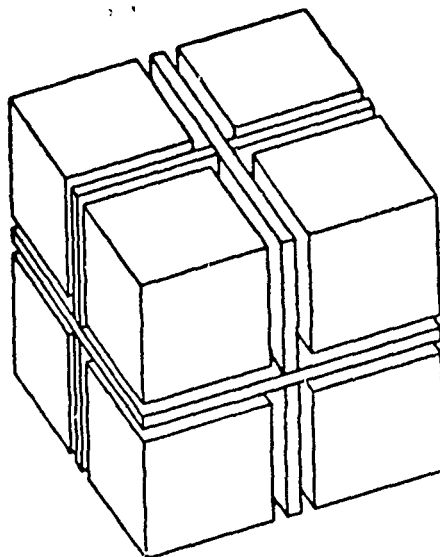
TABLE 3-1 REQUIRED CONTROL/KNOWLEDGE OF INSTRUMENT AND PLATFORM PARAMETERS FOR GEODESY



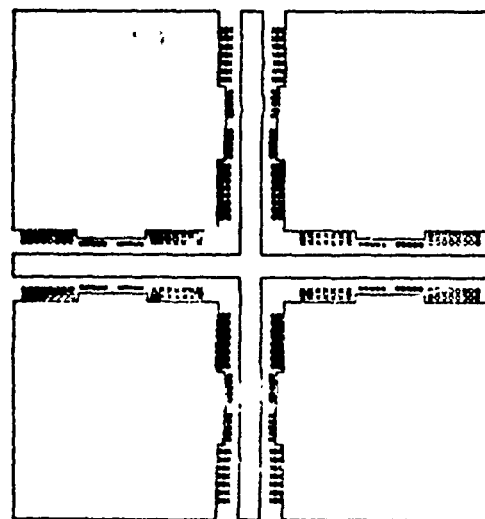
(a) Proof Mass (Niobium)



(b) Coil Form (Titanium)

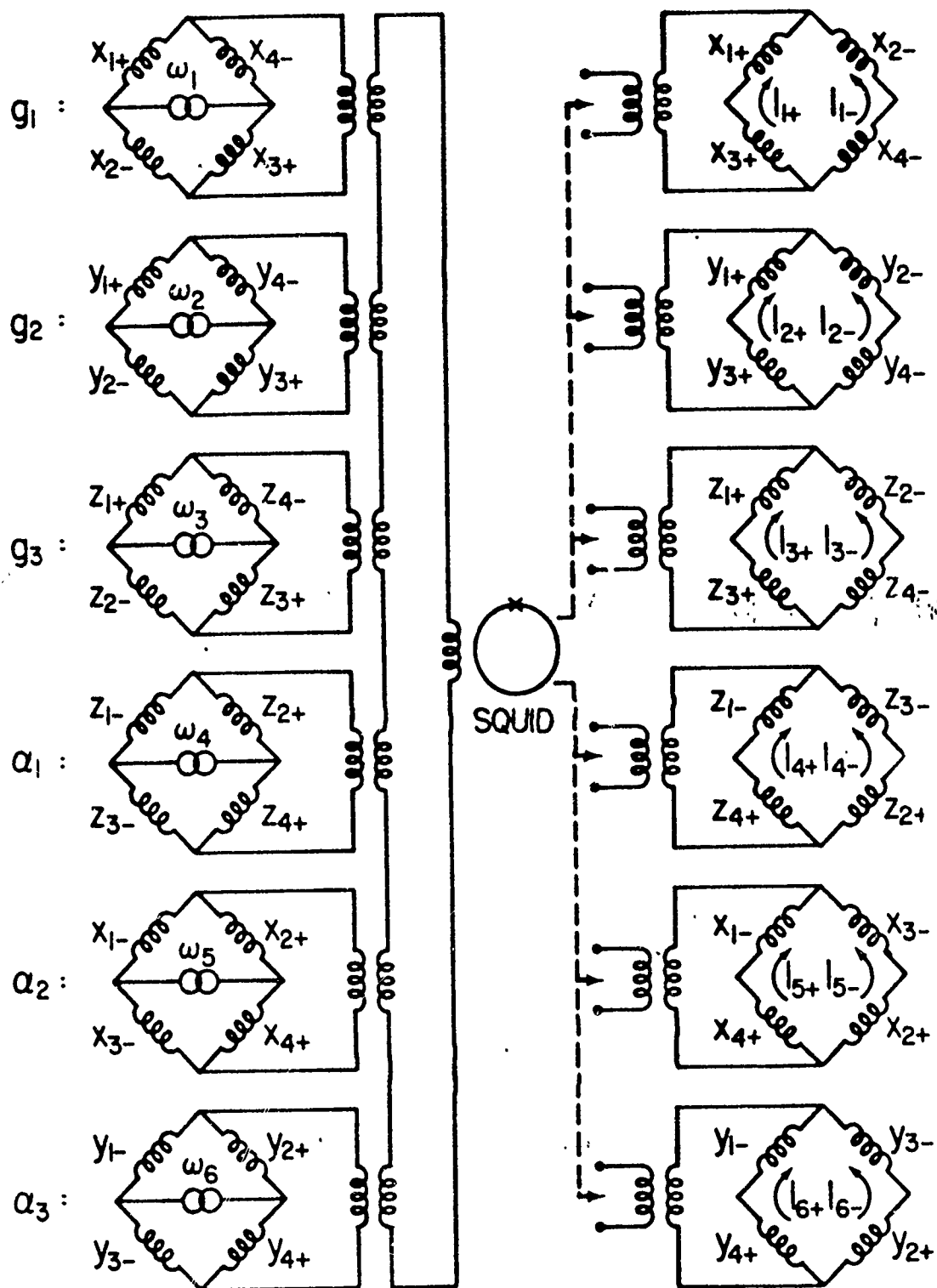


(c) Assembly Drawing

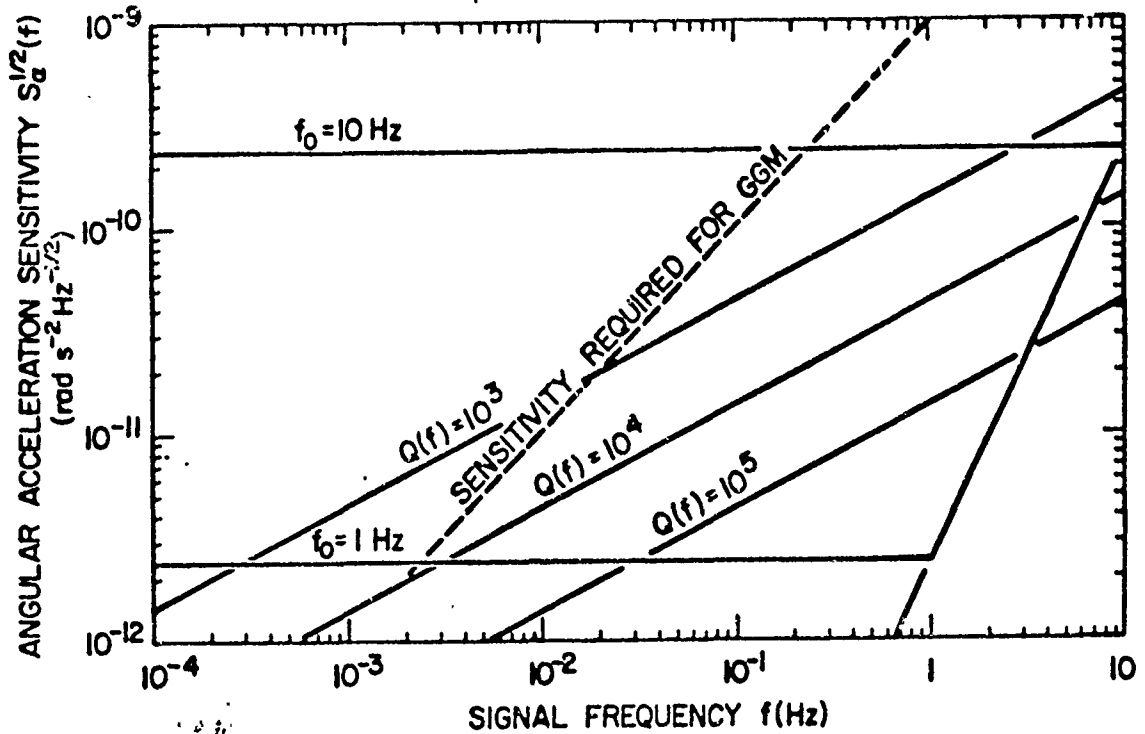
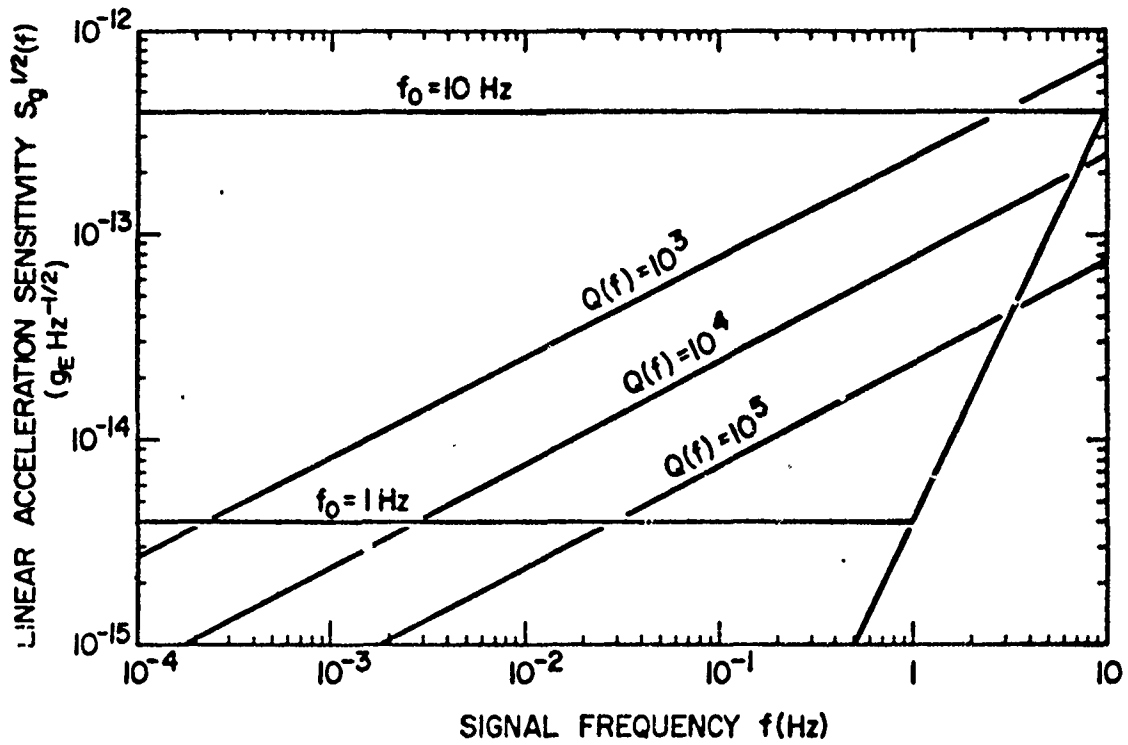


(d) Cross Section View

Fig. 5. Six-Axis Superconducting Accelerometer



Sensing coils \longrightarrow Feedback \longrightarrow Levitation coils



3. Spacecraft and Orbit

- Sun-synchronous ($i = 96.3^\circ$)
- $h = 200 \text{ km}$, $T = 6 \text{ months}$
- Earth-pointing orientation

PS013

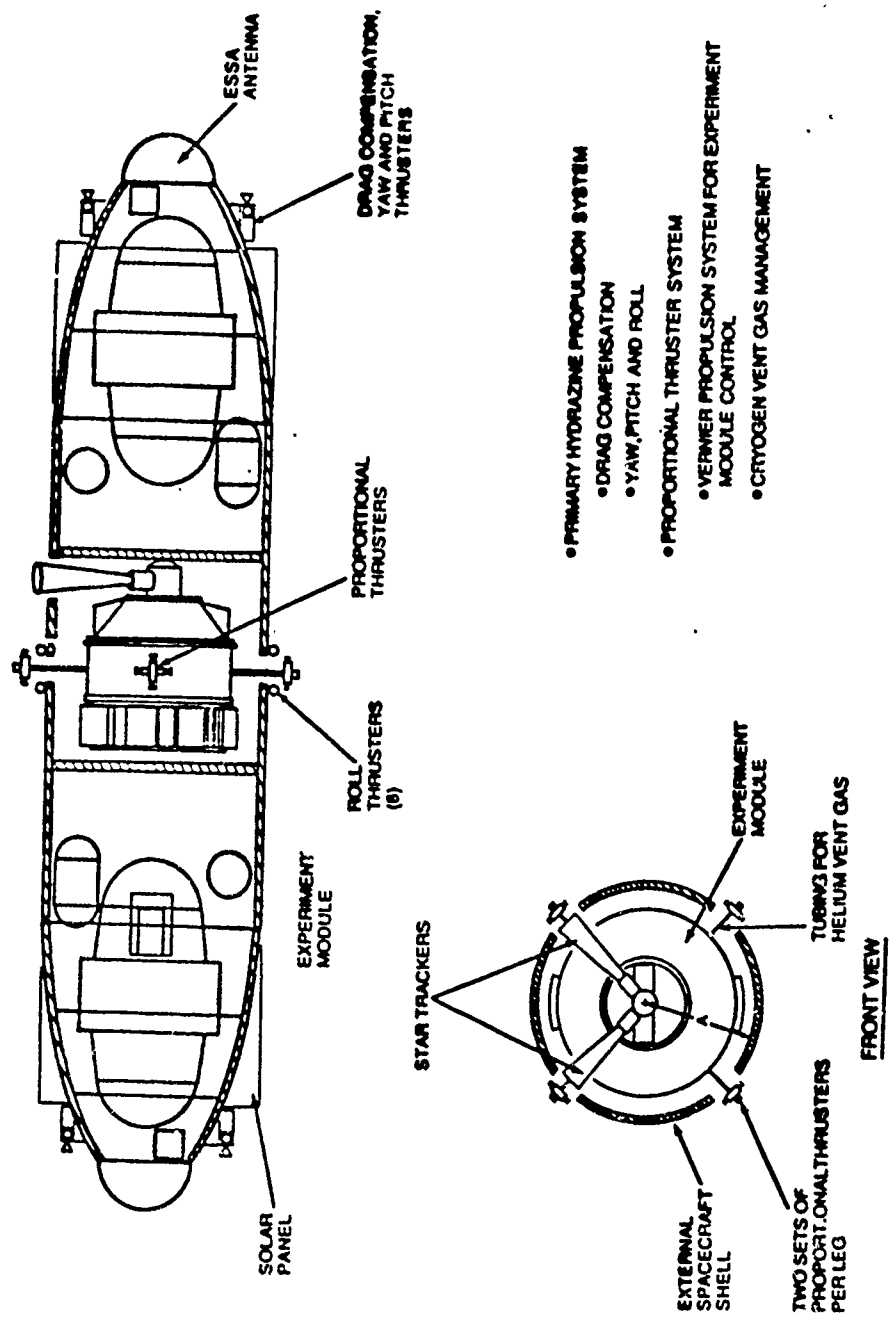


Fig. 8. SGGM Spacecraft

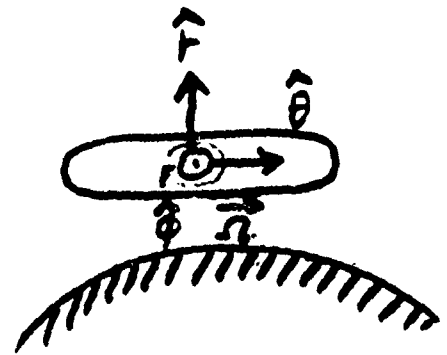
Removal of centrifugal acceleration error

$$\delta \Gamma \cong 2\Omega_0 \delta \Omega$$

For Earth-fixed orientation, $\Omega_0 = 1.2 \times 10^{-3} \text{ rad/sec}$.

$$\delta \Omega \leq \frac{10^{-13} \text{ sec}^{-2} \text{ Hz}^{-1/2}}{2 \times 1.2 \times 10^{-3} \text{ rad/sec}} = \underline{4 \times 10^{-11} \text{ rad sec}^{-1} \text{ Hz}^{-1/2}}$$

Fortunately, gradiometer itself can be used to detect and remove this error to the first order.



$$\Gamma'_{ij} = \begin{pmatrix} \Gamma_{rr} + \Omega_0^2 + 2\Omega_0 \delta \Omega_\phi & \Gamma_{r\theta} & \Gamma_{r\phi} - \Omega_0 \delta \Omega_r \\ \Gamma_{r\theta} & \Gamma_{\theta\theta} + \Omega_0^2 + 2\Omega_0 \delta \Omega_\phi & \Gamma_{\theta\phi} - \Omega_0 \delta \Omega_\theta \\ \Gamma_{r\phi} - \Omega_0 \delta \Omega_r & \Gamma_{\theta\phi} - \Omega_0 \delta \Omega_\theta & \Gamma_{\phi\phi} \end{pmatrix}$$

$$\sum_i \Gamma'_{ii} = 0 + 2(\Omega_0^2 + 2\Omega_0 \delta \Omega_\phi) + O(\delta \Omega^2)$$

$$\Rightarrow \begin{cases} \Gamma_{rr} = \Gamma'_{rr} - \frac{1}{2} \sum_i \Gamma'_{ii} + O(\delta \Omega^2) \\ \Gamma_{\theta\theta} = \Gamma'_{\theta\theta} - \frac{1}{2} \sum_i \Gamma'_{ii} + O(\delta \Omega^2) \\ \Gamma_{\phi\phi} = \Gamma'_{\phi\phi} + O(\delta \Omega^2) \end{cases}$$

4. Development Schedule

- 1) Superconducting accelerometer (1970~1974)
 - Developed for cryogenic gravitational wave detector (Stanford U.).
 - Basic transducer for many GW detectors.
- 2) Prototype SGG's (1976-1980)
 - Design sensitivity : $1 \text{ E Hz}^{-1/2}$
 - Principle demonstrated (Stanford U.).
- 3) Model I SGG (1980-1984)
 - Design sensitivity : $0.03 \text{ E Hz}^{-1/2}$.
 - Single-axis diagonal.
 - Laboratory test of R^{-2} performed.
- 4) Model II SGG (1985-1989)
 - Design sensitivity : $3 \times 10^{-3} \text{ E Hz}^{-1/2}$.
 - Three-axis diagonal.
 - Improved circuit
- 5) Model III SGG (1989-)
 - Design sensitivity : $10^{-4} \text{ E Hz}^{-1/2}$.
 - Single-axis diagonal
 - Negative spring incorporated

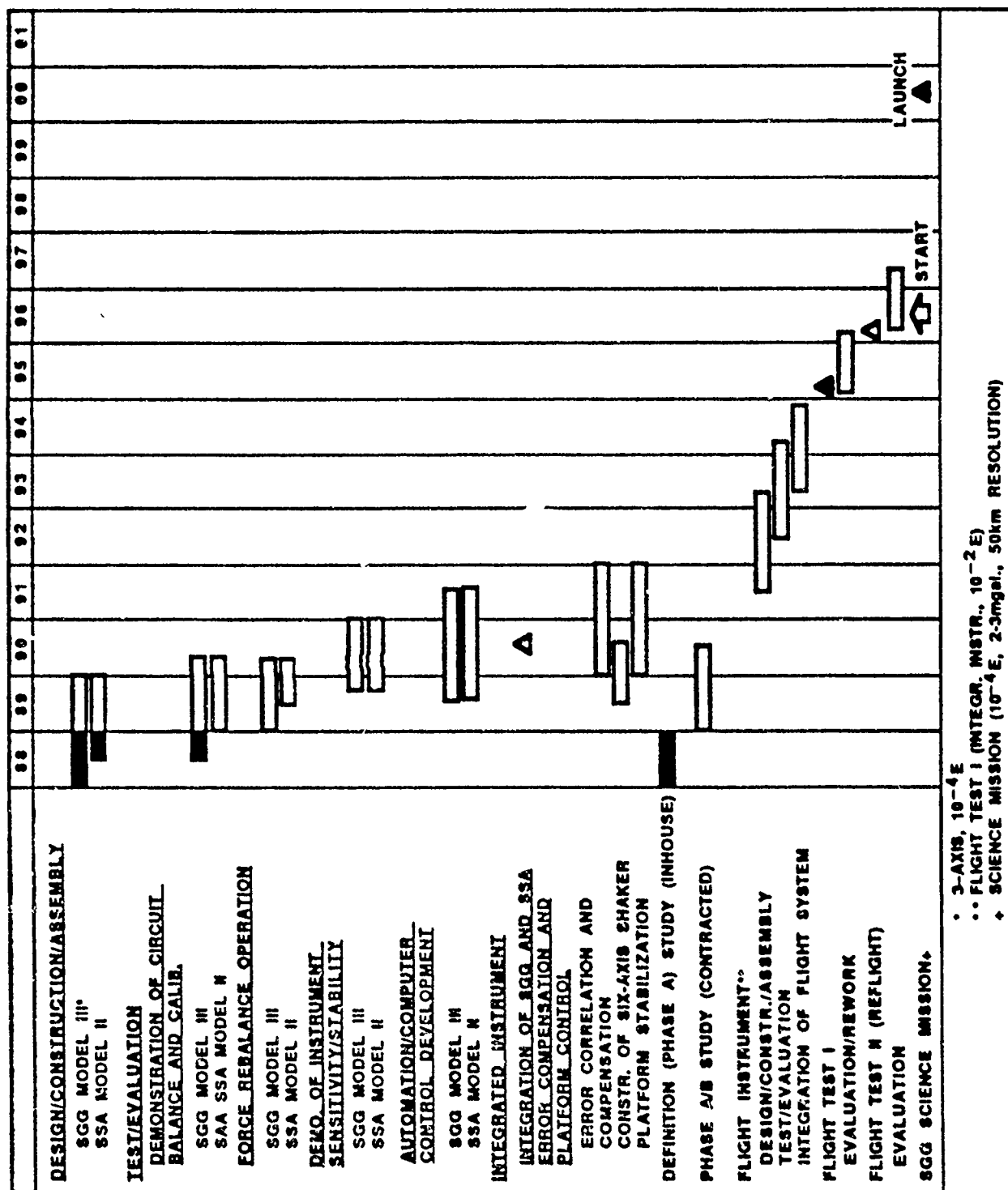


Figure 3-11. Superconducting gravity gradiometer development schedule.

5. Cryogenic Requirements

Temperature: 1.5 K

Temperature Stability: $10^{-4} \text{ K Hz}^{-1/2}$ at SGG.

Mission Lifetime: 6 months

Size of Instrument: 30 cm diameter, 100 kg

Volume of Cryogen: 300 l

Special Requirements: low-g ($10^{-8} g_E \text{ Hz}^{-1/2}$)

Boil-off gas to be used for
attitude control of dewar.

Self gravity fluctuation to be
minimized